SÍNTESIS Y CARACTERIZACIÓN DE NUEVAS FORMULACIONES BASADAS EN LA INCORPORACIÓN DE SORAFENIB EN NANOESTRUCTURAS FUNCIONALIZADAS CON MANOSA Y GALACTOSA PARA EL TRATAMIENTO DE CÉLULAS TUMORALES HEPÁTICAS

María Negrete González

Tesis Doctoral

Sevilla

DIRECTORES: Jordi Muntané Relat y Noureddine Khiar

TUTOR: Francisco Javier Padillo Ruiz

Cirugía oncológica. Terapia celular y trasplante de órganos

Síntesis y caracterización de nuevas formulaciones basadas en la incorporación de sorafenib en nanoestructuras funcionalizadas con manosa y galactosa para el tratamiento de células tumorales hepáticas

TESIS DOCTORAL

María Negrete González

Sevilla, 2021

Cirugía oncológica. Terapia celular y trasplante de órganos

Síntesis y caracterización de nuevas formulaciones basadas en la incorporación de sorafenib en nanoestructuras funcionalizadas con manosa y galactosa para el tratamiento de células tumorales hepáticas

Memoria presentada por la
Graduada María Negrete González
para optar al título de Doctora por la Universidad de Sevilla

El presente trabajo ha sido realizado por la Graduada en Química María Negrete González, con DNI 77809716-A, en el grupo de Mecanismos moleculares del hepatocarcinoma y sus estrategias terapéuticas (CTS-1098) en el Instituto de Biomedicina de Sevilla, bajo la dirección del Dr. Jordi Muntané Relat y el Dr. Noureddine Khiar.

Los directores del trabajo:

Fdo. Jordi Muntané Relat

Fdo. Noureddine Khiar

AGRADECIMIENTOS

Afrontarse a un reto como este siempre da miedo. Pones en una balanza las cosas positivas frente a las negativas. Este proyecto siempre había formado parte de mis pensamientos, pero nunca hubiera imaginado hacerlo realidad sin el apoyo de todas las personas que han estado detrás todo este tiempo.

Además de una experiencia que me ha hecho madurar a nivel científico, este proyecto también me ha hecho madurar a nivel personal. Y todo esto ha sido posible gracias a los mensajes de apoyo, palabras de comprensión y la confianza dada de todas las personas que han estado a mi lado.

En primer lugar, quiero expresar mi más sentido agradecimiento a mi director de tesis, Jordi Muntané, por haberme dado la oportunidad de realizar este proyecto. Gracias por tu confianza a lo largo de todo este camino, a pesar de que me faltaba mucho por aprender, y por toda tu ayuda ofrecida, el tiempo dedicado y las enseñanzas que me has mostrado a lo largo de estos años.

También agradecer a mi codirector de tesis, Noureddine Khiar, quien me ha mostrado la química más pura. Gracias por la confianza y por el tiempo dedicado.

Gracias también al Dr. Javier Padillo por su tutela en esta tesis.

A mis compañeros de laboratorio, a los que estaré eternamente agradecida. Sin ellos, este camino no hubiera sido el mismo. Habéis sido un apoyo fundamental a lo largo de estos años, ya no solo por la ayuda ofrecida en el laboratorio si no por el cariño y los ánimos cuando estaba a punto de tirar la toalla.

Por ello muchísimas gracias a María Ángeles y Elena, quienes desde el primer momento me enseñaron con paciencia y cariño todo lo necesario: western blot, aislamiento de hepatocitos… ¡Ay esas guardias, como nos traían de cabeza! Gracias por ser un apoyo indispensable en esos largos "jueves locos" y por vuestra alegría y buena actitud en todo momento. Y por supuesto, sin olvidarme de Álvaro, quien nos ha hecho siempre más amena todas las mañanas, tardes y noches con la alegría que te caracteriza. Gracias por tu predisposición siempre para ayudar en todo lo que pudieras. Y por supuesto a Patri, quien me ha enseñado a lo largo de estos años muchísimas cosas. Gracias por el apoyo ofrecido en este camino. Eres un ejemplo a seguir por tu esfuerzo y constancia.

Y por supuesto dar las gracias también a Sheila, Paloma, Laura, Fran, Paula, Yaiza…

Por último, quiero darle las gracias a Raúl González, quien formó parte de mis primeros pasos en el laboratorio y confió en mi desde primera hora. Gracias por enseñarme tanto.

Gracias por haber sido un pilar fundamental a lo largo de estos años. Siempre me acordaré de todos los buenos momentos vividos: desayunos, almuerzos, comidas de Navidad, Feria… Ha sido un placer trabajar con vosotros. Sois ejemplo de compañerismo y profesionalidad. Todos vosotros formáis un equipo de imparables. En definitiva, gracias por todo.

Agradecer también a todo el grupo del Dr. Noureddine Khiar por todo el apoyo ofrecido. Sobre todo, a Elena, por estar siempre atenta y a disposición. Gracias por toda tu ayuda ofrecida y por todo lo que me has enseñado durante los meses que estuve con vosotros.

A lo largo de estos años, mis directores y tutor de tesis me han brindado la oportunidad de poder colaborar con diferentes grupos de investigación. Estas experiencias han hecho que madure aún más como investigadora. En primer lugar, gracias a la Dra. Alicia Gutiérrez-Valencia, por enseñarme tanto sobre cromatografía líquida y por la confianza aportada en mí desde el primer momento. Me llevo todas tus enseñanzas para toda mi trayectoria profesional. Agradecer también al grupo de la Dra. Eva-Alés, quien me ha acogido como un más en su departamento. Gracias por los consejos y el apoyo, y por la atención y el cariño con el que siempre me has tratado.

A mis amigas y compañeras de fatigas químicas, Isa y Ainara. Gracias por todo vuestro apoyo desde el minuto uno que decidí comenzar esta aventura. Recordaré todos los momentos vividos los cuatro años de carrera, tanto los buenos como los malos que,

aunque la química nos ha dado muchas alegrías también nos ha dado muchos disgustos. Gracias por aparecer en mi vida y permanecer en ella, sois pura luz.

No me puedo olvidar de mencionar a todas mis amigas, especialmente a María C., María M. y a mi comadre. Gracias por tanto apoyo estos años. Por aguantar mis agobios e intentar calmarme cuando me creía que el día tenía 48 horas. Gracias porque sin vuestro apoyo, probablemente hoy no estaría cerrando esta etapa. Siempre os estaré agradecida por comprender mis ausencias, pero también celebrar mis éxitos como si fueran vuestros. Y por supuesto, agradecer todos los buenos momentos que me habéis hecho pasar para despejarme. Infinitas gracias.

Y por último quiero darle mi más profundo agradecimiento a mi familia. En primer lugar, a mis padres, gracias por inculcarme los valores que hoy en día tengo, por enseñarme que todo esfuerzo tiene su recompensa y por no dejarme nunca caer. Gracias por mostrarme la importancia de la responsabilidad, pero también la importancia de ser feliz. Habéis dejado atrás vuestros intereses para interponerlos por los míos. Siempre he obtenido de vosotros un abrazo o una sonrisa que me ha ayudado a seguir adelante. Hemos madrugado, llorado juntos durante todos estos años, pero también hemos reído y celebrado. Sin duda, gran parte de esta tesis es mérito vuestro. Gracias por confiar siempre en mí, a pesar de mis agobios que siempre venían acompañados de mi mal humor. Con vosotros todo es mucho más sencillo. Os quiero mucho.

Gracias infinitas a mi hermano, la alegría de mi casa y el mayor regalo que mis padres me pudieron hacer cuando tenía 5 años. ¡Qué suerte tenemos los que te tenemos cerca! Siento tanta admiración por ti, por tu forma de ver la vida, de superar obstáculos. Gracias por tener siempre una sonrisa y un abrazo que regalarme. A pesar de que eres el pequeño de la casa, me quedan millones de cosas por aprender de ti. A tu lado la vida se ve de otra forma, y que alegría me da saber que siempre te tendré cerca. Te quiero infinito.

Gracias también al resto de mi familia, a mis cuatro abuelos, tíos, primos. A todos gracias de corazón, sois un apoyo incondicional. Me siento muy afortunada de poder teneros cerca. Especialmente, darle las gracias a mi tía Inma, quien es para mí como una hermana. Gracias aconsejarme en todo, por cuidarme y quererme tanto. Desde que tengo uso de razón has sido mi modelo para seguir. Te quiero mucho.

Gracias también a Jose Manuel, quien ha recorrido todo este trayecto a mi lado. La vida te puso a mi lado justo en el momento que más lo necesitaba. Me siento tan afortunada

de tenerte en mi vida. Gracias por tranquilizarme y apoyarme en los momentos más duros de esta etapa. Por la confía que has tenido en mi desde el primer momento. Porque en los momentos de bajón y negatividad, has estado ahí para demostrarme que podía. Gracias porque a tu lado me siento más segura y feliz. Te quiero mucho.

No me puedo olvidar de mencionar a mi otra familia, mi familia política, Manolo, Mari Carmen y Javier, gracias por vuestro apoyo y cariño.

Gracias a cada uno de vosotros, porque de una forma u otra me habéis ayudado a llegar hasta aquí.

“Investigar es ver lo que todo el mundo ha visto,

y pensar lo que nadie más ha pensado”.

Albert Szent-Györgyi

A mis padres

RESUMEN

El carcinoma hepatocelular (HCC) representa el 80% de las neoplasias hepáticas primarias que aparecen principalmente en el contexto de la cirrosis hepática crónica. Es la sexta neoplasia más frecuente, la tercera causa de muerte por cáncer y el 7% de las neoplasias registradas. Algunos de los factores de riesgos mas importantes para el desarrollo del HCC son: diversos aspectos demográficos, alteraciones inmunológicas, VHB o la infección crónica por VHC.

El tratamiento para esta enfermedad depende del estadio en el que se encuentre el paciente. Sorafenib (Nexavar®, Bayer) es la terapia molecular de primera línea para pacientes que se encuentran en estadio avanzado de HCC. Diversos estudios han concluido que los pacientes que tomaron Sorafenib sobrevivieron un promedio de 10,7 meses, en comparación con los 7,9 meses que sobrevivieron quienes tomaron placebo. Se ha demostrado que Sorafenib induce la muerte celular y reduce la proliferación celular en el rango µmolar en las células de cáncer de hígado. Sin embargo, su administración está asociada a varias complicaciones que son consecuencia de su falta de especificidad celular y las elevadas dosis requeridas debida a su hidrofobicidad intrínseca con el objetivo de mantener la efectividad del tratamiento. Los efectos secundarios más frecuentes de Nexavar son diarrea, erupciones cutáneas, alopecia, infección, «reacción de

mano-pie» y fatiga. Aunque menos frecuentes, existen otros riesgos como puede ser ataque cardiaco o perforación gastrointestinal (un agujero que se desarrolla en la parte interna del intestino).

La búsqueda de enfoques no invasivos que permitan el uso de sorafenib para tratar el HCC, con efectos tóxicos mínimos o nulos, es un área de interés permanente en la oncología moderna. El advenimiento de la nanomedicina, cuyo objetivo último es transportar una cantidad suficiente de sustancias activas a través de las barreras fisiológicas y alcanzar, de forma selectiva, los tejidos afectados por la enfermedad, ha tenido un impacto significativo en este campo.

A lo largo de este estudio se ha desarrollado dos estrategias de direccionamiento activo del sorafenib de gliconanomicelas independientes con sorafenib basadas en su funcionalización hacía los receptores de manosa (pMicMan) o asialoglicoproteína (pMicGal), utilizando gliconanomicelas útiles para inducir la apoptosis y reducir la proliferación celular en células de HCC (HepG2 y Huh7).

El estudio mostró que sorafenib, en un rango nanomolar, (10-20 nM) incluido en el vector pMicMan dirigido al receptor de manosa, pero no el fármaco libre ni su encapsulación en pMicGal dirigido al receptor de la asialoglicoproteína, inducía apoptosis y reducía la proliferación celular en células HepG2 y Huh7. Este efecto se relacionó con una mayor incorporación vía endosomal de pMicMan que pMicGal a las células. El procesamiento vía lisosomal reduce la actividad del fármaco en células tumorales hepáticas. Se observó que las dichos nanovectores funcionalizados cargados con Sorafenib, realizaban una liberación controlada en el tiempo, siendo estas del 35% y del 39% de su contenido a las 24 horas en pMicMan y pMicGal respectivamente.

Por lo tanto, se concluye que, aunque ambos nanovectores funcionalizados, pMicMan y pMicGal, son útiles para la encapsulación de sorafenib, su presentación en pMicMan promovió una mayor incorporación vía endosomal que la observada con pMicGal lo que permitió bajar la dosis de tratamiento hasta 1.000 veces en células tumorales hepáticas (10 nM). La confirmación de este hallazgo in vivo permitiría reducir los efectos secundarios asociados a su uso.

ÍNDICE

ÍNDICE DE FIGURAS

Tabla 3. Apoptosis de células Huh7 e incorporación intracelular de nanomicelas con sorafenib incorporado. Inducción de caspasa-3.

Figura 11. (a) Incorporación endosomal de **pMicMan** y **pMicGal** por inmunofluorescencia usando nanomicelas que contienen FM 1-43. (b) La incorporación endosomal se inhibió preincubando las células durante 10 minutos con dynasore (80 µM) o citocalasina D (8 µM).

Figura 12. Tráfico de **pMicMan** y **pMicGal**. El rojo del Nilo se utilizó para proporcionar información sobre el procesamiento endosómico y lisosómico. La incubación de las células a 4ºC bloqueó la incorporación de nanomicelas. La presencia de nanopartículas en diferentes compartimentos celulares se evaluó utilizando marcadores endosomales, lisosomales y autofagosomas mediante procedimiento de colocalización por inmunofluorescencia. El procedimiento para la incorporación de la sonda y la inmunofluorescencia se describe en la parte experimental. Aumentos x60

Figura 13. Impacto del procesamiento lisosomal de **pMicMan** y **pMicGal** en la actividad caspasa-3 (a) y proliferación celular (b) en células HepG2. Las células se incubaron con cloroquina (50 µM) y 3-metiladenina (3Me-A) (5 µM) 2 horas antes de la administración de **pMicMan** y **pMicGal** que contenían sorafenib (20 nM), y de dynasore (80 µM) y citocalasina D (8 µM) administrados 10 min antes de la administración de los fármacos. La actividad caspasa-3 y la incorporación de BrdU se determinaron según se describe en la sección de Material y Métodos.

ABREVIATURAS

3-metiladenina, 3Me-A

Ablación por radiofrecuencia, RFA

Ácido desoxirribonucleico, ADN

Ácido etilendiaminotetracético, EDTA

Ácido poli(láctico-glicolico), PLGA

Ácido pentacasadiinoico, PCDA

Adenosín trifosfato, ATP

Agua deuterada, D_2O

Albúmina bovina sérica, BSA

Antígeno de superficie del virus de la hepatitis B, HbsAg

Antígeno e del virus de la hepatitis B, HbeAg

Arginina-glicina-ácido aspártico, RGD

Barcelona Clinic Liver Cancer, BCLC

Bromodeoxiuridina, BrdU

Carcinoma hepatocelular, HCC

Carga del fármaco, DL

Cirrosis biliar primaria, CBP

Cóctel Inhibidor de Proteasas, CIP

Colangiocarcinoma humano, HuCC

Concentración micelar crítica, CMC

Crecimiento de hepatocitos, HGF

Cromatografía en capa fina, TLC

Cromatografía líquida-espectrometría de masas en tándem, LC-

Dimetilsulfóxido, DMSO

Dipalmitoilfosfatidilcolina, DPPC

Dispersión dinámica de la luz, DLS

Dominio 2 de homología del factor de crecimiento epidérmico, TIE2

Efecto de permeabilización y retención, EPR

Eficiencia de encapsulación, EE

Enfermedad hepática por depósito de grasa, EGNA

Especies reactivas del oxígeno, ROS

Esteatohepatitis no alcohólica, EHNA o NASH

Factor de crecimiento derivado de plaquetas, PDGFR

Factor de crecimiento endotelial vascular, VEGFR

Factor de crecimiento epidérmico, EGF

Factor de crecimiento de fibroblastos 19, FGF19

Factor de crecimiento de hepatocitos, HGF

Factor de crecimiento de insulina 2, IGF2

Fluorescencia del infrarrojo cercano, NIRF

Fluoruro de fenilmetanosulfonilo, PMSF

Food and Drug Administration, FDA

Función hepática conservada, Child Pugh A

Galactosa, Gal

Guanosina trifosfato, GTP

Índice de polidispersión, PDI

Inhibidor de apoptosis ligado a X, XIAP

Inhibidor de la quinasa dependiente de ciclina 2A, CDK2A

Inyección percutánea de etanol, PEI

Leucemia de células mieloides, Mcl-1

Microscopía electrónica de transmisión, TEM

N-acetilgalactosamina, GalNAc

N,N-dimetilformamida, DMF

N,N-diisopropiletilamina, DIPEA

Nanoparticulas Solidas de Lípidos, SLN

Performance Status, PS

Polidiacetileno, PDA

Polietilenglicol, PEG

Polifluoruro de vinilideno, PVDF

Protein kinase RNA-like ER kinase, PERK

Quimioembolización, TACE

Quitosano modificado, HMC

Receptor de asialoglicoproteína receptor, ASGPR

Receptor de manosa, MR

Retículo endoplasmático, ER

Resonancia magnética nuclear, RMN

Supervivencia Global Media, OS

Tampón fosfato salino (Phosphate-buffered saline), PBS

Tetraetilenglicol, TEC

Tetrahidrofurano, THF

Transcriptasa inversa de telomerasa, TERT

Ultravioleta, UV

Virus de la hepatitis A, VHA

Virus de la hepatitis B, VHB

Virus de la hepatitis C, VHC

INTRODUCCIÓN

Cáncer primario de hígado

El carcinoma hepatocelular o hepatocarcinoma (HCC), es el cáncer primario de hígado más frecuente (90%) que representa la sexta neoplasia maligna más común en todo el mundo y la tercera causa de muerte relacionada con cáncer por detrás del cáncer de pulmón y de mama (1). Alrededor de 700.000 personas mueren cada año debido a HCC, y en países como Estados Unidos y Canadá sigue incrementándose su incidencia y mortalidad (2).

El análisis epidemiológico de la enfermedad indica que no presenta una distribución geográfica homogénea, y esto se debe a la heterogénea distribución de los factores de riesgo que están implicados en la aparición del cáncer hepático como el virus de la hepatitis B (HBV) que es más frecuente en Asia y África, y C (HCV) más frecuente en Europa, Norte América y Japón, alcoholismo, obesidad y diabetes de tipo II (3). Existe una distribución geográfica de manera que la incidencia es elevada en países en vías de desarrollo como los del sudeste asiático y el África subsahariana; intermedia en Japón y países europeos del área mediterránea, e inferior en el norte de Europa y Estados Unidos (4).

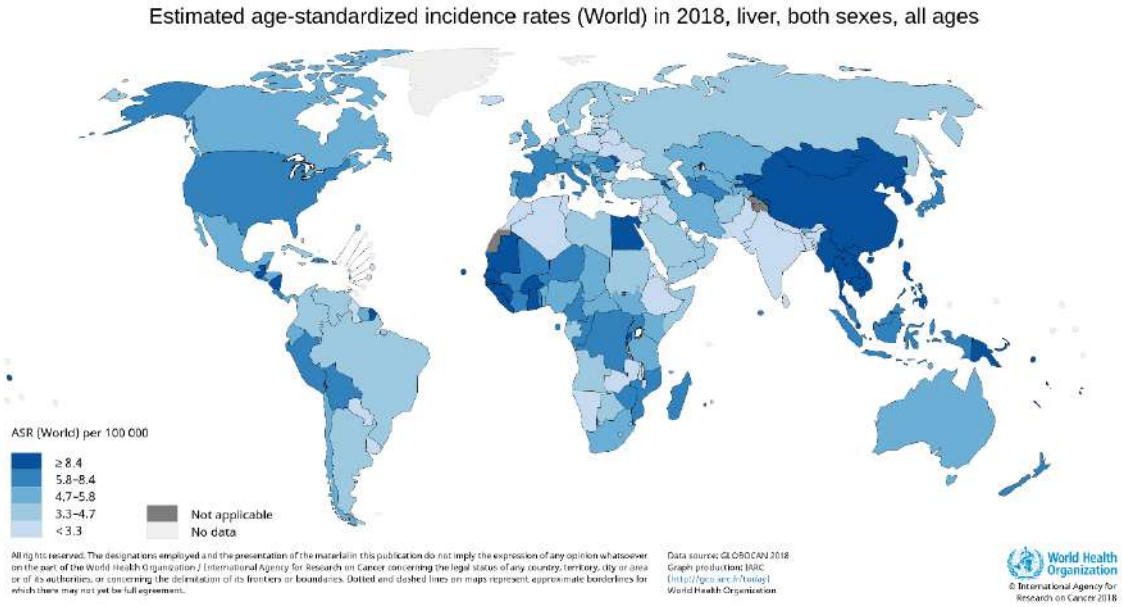

Figura 1. Mapa de la incidencia del cáncer de hígado en el mundo.

En la mayor parte de pacientes (90%) el HCC se desarrolla en un contexto de enfermedad hepática crónica con presencia de cirrosis hepática relacionado con diversas etiologías. La mortalidad del HCC es muy elevada, con una tasa de supervivencia a los 5 años del 5-6%. En nuestro entorno, el estadiaje, pronóstico de la enfermedad y propuestas terapéuticas, se rigen con el sistema Barcelona Clinic Liver Cancer (BCLC). La mayor parte de pacientes (70%) se diagnostican en la fase intermedia (BCLC B) y avanzada (BCLC C) de la enfermedad en donde solo son posibles tratamientos paliativos como quimioembolizacion y tratamiento sistémico (5). En las fases iniciales (BCLC 0 y A) son posibles tratamientos locorregionales y quirúrgicos con intención curativa mejorando así la tasa de supervivencia. (6)

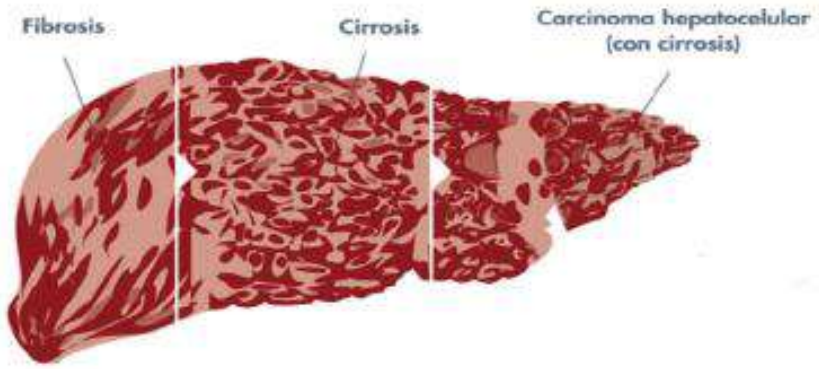

Figura 2. Esquema de la evolución desde un hígado sano hasta el desarrollo de un carcinoma hepatocelular

Los factores de riesgo más importantes para el desarrollo de HCC son (7,8):

1. Diversos aspectos demográficos como la edad del paciente y género masculino, asociado a una mayor exposición a los distintos factores de riesgo (9), mayor índice de masa corporal, niveles elevados de andrógenos y disminuidos de estradiol.

2. Alteraciones inmunológicas (trastornos relacionados con las hepatitis autoinmunes). Su incidencia es baja y aparece más frecuentemente en el sexo femenino.
3. El 90% de los HCC aparecen en hígados cirróticos o con fibrosis avanzada con etiologías que promueven más rápidamente la generación de HCC como cuando es de origen viral en comparación con la cirrosis biliar primaria (CBP) (10). La incidencia de HCC sobre hígado no cirrótico es del 10-20% pero se ha observado que, aunque no presentan una cirrosis confirmada mediante biopsia, aparece cierto grado de fibrosis, esteatosis o displasia celular.
4. VHB: se ha estimado que 40 millones de personas son portadoras de este virus especialmente en Asia Oriental y África subsahariana (zona endémica de VHB), y con mayor riesgo relativo de desarrollar un HCC en los portadores crónicos de HbsAg positivo y aún mayor en los portadores HbeAg positivo de forma concomitante. Aunque también influyen factores como la carga del VHB en sangre y la edad del paciente. Por el contrario, el tratamiento del VHB con interferón o análogos de los nucleótidos reduce el riesgo de desarrollar HCC de forma significativa. Las campañas de vacunación en áreas de alta incidencia de HVB como Taiwán han permitido una disminución de la incidencia de HCC hasta el 60% (11,12).
5. La infección crónica por el VHC es la causa más frecuente en las zonas de baja e intermedia prevalencia como Estados Unidos, Europa y el área mediterránea. En los países orientales más del 70% de los pacientes con HCC presentan anticuerpos anti-HVC en suero. El riesgo relativo de desarrollar un HCC es mucho más alto en los pacientes positivos para VHC afectos de cirrosis o fibrosis

avanzada y la media de aparición desde la infección por VHC es 30 años. Sin embargo, también puede ocurrir en portadores sanos del virus (13–15).

6. La hemocromatosis se caracteriza por la absorción aumentada de hierro que a su vez incrementa las reacciones asociadas con la inducción de estrés oxidativo celular. Es aún controvertido si el riesgo de desarrollo de HCC es mayor en estos pacientes que en otros con cirrosis de etiología diferente. Una vez que aparece la cirrosis el riesgo anual de aparición de HCC es del 5%. También se asocia, al igual que con otros factores, a la presencia de diabetes mellitus tipo 2 (16).
7. Las toxinas ambientales como la micotoxina aflatoxina B1 que se acumula en cereales, legumbres y frutos secos como el maíz, la soja y los cacahuetes almacenados en condiciones insalubres se relacionan con la aparición de mutaciones en p53 y desarrollo de HCC en zonas rurales de Asia oriental y África. La toxina procedente de algas azul verdosas (microcystin) que contaminan el agua se ha relacionado también con la aparición de HCC (17).
8. El consumo elevado (más de 50-70 gramos al día) y sostenido en el tiempo de alcohol ha demostrado ser una causa directa de desarrollo de HCC. En Asia contribuye a un 10% de los HCC y al doble, en el caso de Europa. A pesar de que la ingesta alcohólica está relacionada con el riesgo de desarrollar cirrosis y HCC, la relación existente entre la cantidad y la duración del hábito enólico con el desarrollo del proceso maligno no están claramente determinadas. La coexistencia de infección crónica por VHC y VHB, y la ingesta de alcohol potencia el riesgo de desarrollar HCC (18).
9. La esteatohepatitis no alcohólica (EHNA o NASH) es una de las enfermedades que subyace a la presencia de HCC con rápida progresión en nuestro entorno geográfico. La EHNA evoluciona desde una esteatosis o enfermedad hepáticas

por depósito de grasa (EGNA) que progresa hacía fases más avanzadas de la enfermedad como la esteatosis que se asocia con presencia de formas de balonización celular, respuesta inflamatoria y fibrosis característico de la cirrosis hepática. La EHNA se asocia estrechamente con la diabetes mellitus de tipo 2 y la obesidad, como parte del síndrome metabólico. Se estima que hasta el 70% de pacientes diabéticos presentan esteatosis hepática, ascendiendo al 9% en el caso de pacientes obesos (19).

10. Enfermedades metabólicas: déficit de α1-antitripsina, porfiria cutánea parda, tirosinemia, hipercitrulinemia, glucogenosis grado IV, intolerancia hereditaria a la fructosa y la enfermedad de Wilson son considerados factores de bajo riesgo de HCC (20).
11. Los adenomas asociados a glucogenosis grado IV, a andrógenos o a anabolizantes pueden transformarse en HCC incluso en hígados no cirróticos. La enfermedad de Fanconi también es un factor de riesgo sobre todo si se trata con esteroides. El riesgo de malignización de adenomas por la toma de anticonceptivos es menor al 10%. Esta transformación es más frecuente en nódulos mayores de 5 cm, en el género masculino y se relaciona a su vez con mutaciones a nivel de las β-cateninas (21).

La génesis del HCC se asocia con un proceso inflamatorio crónico del tejido hepático cirrótico (vía indirecta) que conlleva regularmente a las condiciones de estrés oxidativo y nitrosativo asociado a un incremento de la inestabilidad genética de los hepatocitos inducida por mutaciones promotoras del cáncer (*drivers*) (vía directa). En general, la infección crónica por VHC se relaciona con reacción inflamatoria, estrés oxidativo por especies reactivas de oxígeno (ROS), daño y muerte hepatocelular (22).

Estadiaje de los pacientes y tratamientos recomendados

El tratamiento para esta enfermedad depende del estadio en el que se encuentre el paciente. La identificación del estadiaje, pronóstico y los tratamientos recomendados para los pacientes con HCC se toman mayoritariamente en base a la clasificación de BCLC cuya toma de decisión depende del número y tamaño de tumores, presencia de invasión vascular en el tumor y existencia de metástasis extrahepáticas, independencia del paciente y función hepática (2) (Figura 3).

El estadio 0 se define como enfermedad en estadio muy temprano, que se caracteriza por un solo nódulo ≤ 2 cm sin invasión tumoral y función hepática conservada (Child Pugh A). En el estadio A, o enfermedad temprana se incluyen pacientes con HCC constituido por hasta 3 nódulos ≤3 cm, asintomáticos (Performance Status o PS igual a 0) con Child-Pugh A o B. Las etapas 0 y A pueden ser tratadas de manera efectiva con las intervenciones curativas como las intervenciones locorregionales o métodos de ablación percutánea, como la inyección percutánea de etanol (PEI) o con radiofrecuencia (RFA), y los procedimientos quirúrgicos como la resección hepática y el trasplante hepático ortotópico. Debido a la ausencia de programas activos de seguimiento, los tratamientos curativos se pueden realizar solo en el 30-40% de los pacientes, con una supervivencia global media (OS) mayor a 60 meses, y de 5 años en el 50-80% de los pacientes (5).

Los pacientes en estadio intermedio o BCLC B presentan un tumor multinodular, sin invasión macrovascular o diseminación extrahepática, en pacientes asintomáticos con función hepática bien conservada y sin alteración de la independencia funcional (PS=0). Este subgrupo de pacientes puede ser tratado con quimioembolización (TACE) con una supervivencia global 26 meses (5).

Los pacientes con presencia de tumores extrahepáticos, invasión portal, Child-Pugh A-B y PS 1-2 se encuentran en el estadio avanzado o BCLC C. Estos pacientes se tratan con tratamiento sistémico. Actualmente, los tratamientos basados en la regulación de la respuesta inmune (anti-PD-1/anti-PD-L1; anti-cytotoxic T lymphocyte-associated protein 4 o anti-CTLA4) que se han añadido a los antiangiogénicos e inhibidores de tirosina quinasa han aumentado el número de posibilidades de terapéuticas y la supervivencia de estos pacientes por encima de 17 meses (2,23).

Los pacientes con síntomas de cáncer con insuficiencia hepática avanzada, crecimiento tumoral con afectación vascular, deterioro físico (PS> 2) se clasifican como estadio D o enfermedad en etapa terminal. La supervivencia en este estadio es inferior a 3 meses.

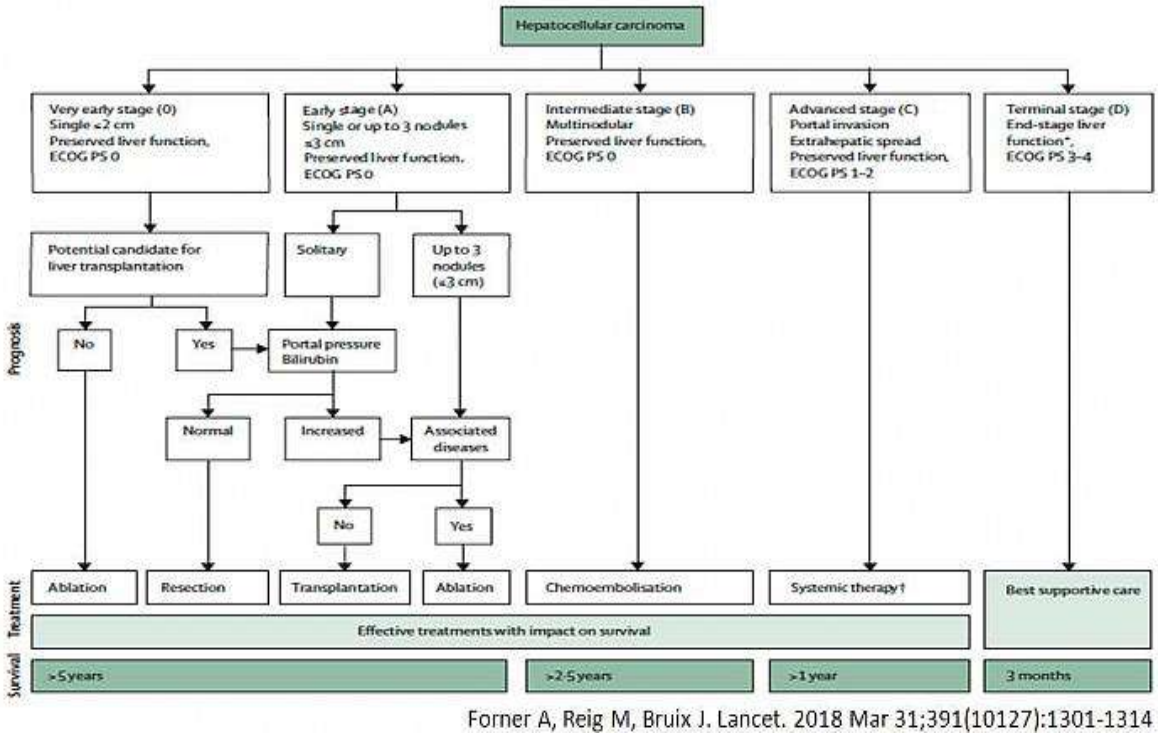

Figura 3. Clasificación del grupo Barcelona Clinic Liver Cancer (BCLC).

En nuestro entorno asistencial el inhibidor tirosina quinasa sorafenib (Nexavar®, Bayer) continúa siendo el tratamiento de elección de los pacientes en estadio BCLC C en la práctica clínica diaria. sorafenib es un inhibidor multiquinasa que reduce la proliferación celular y la angiogénesis del tumor, e incrementa el índice de apoptosis. La actividad de sorafenib se demostró en el ensayo clínico SHARP en pacientes con HCC avanzado y buena función hepática que permitió su aprobación en 2007 por la FDA (24). sorafenib inhibe VEGFR, PDGFR-β, Flt3 y c-Kit, así como a diversos componentes moleculares de la vía de señalización Raf/MEK/ERK (25,26). Sorafenib induce disfunción mitocondrial con generación de ROS y reducción de la fosforilación oxidativa o producción de ATP en las células cancerosas (34-37).

La administración de sorafenib aumenta los marcadores de estrés del retículo endoplásmico (ER), incluidos IRE1α, eIF2α y BiP/Grp78 en tejido hepático de pacientes sometidos a resección hepática por HCC (31). Además, la administración de sorafenib (10 μM) se ha relacionado con la liberación de Ca^{2+}, estrés oxidativo mitocondrial y apoptosis en células de leucemia humana (32). Sorafenib puede inducir la apoptosis de las células cancerosas mediante la regulación de múltiples factores proapoptóticos y antiapoptóticos, incluidos Bad, Bax, Bim, leucemia de células mieloides-1 (Mcl-1) e inhibidor de la apoptosis ligado a X (XIAP) (33). La expresión de estos factores puede regularse a niveles transcripcionales, traduccionales o postraduccionales y puede involucrar mecanismos independientes de la actividad ERK. La inhibición de la expresión de factor antiapoptótico Mcl-1 se encontró independiente de la inhibición de Raf/MEK/ERK por el fármaco (34). Recientemente, se ha identificado al factor proapoptótico Bim como relevante en la apoptosis inducida por sorafenib (35). De hecho, el aumento progresivo del estrés ER y la expresión de C/EBP homologous protein (CHOP) dependiente de (Protein Kinase RNA-like ER Kinase) PERK, y la reducción de

Thr308Akt/Akt y Ser473Akt/Akt se asociaron con la reducción del flujo autofágico y una regulación adicional de la expresión de BimEL y la actividad de caspasa-3 (36). Nuestro grupo ha demostrado que la administración de sorafenib es más eficaz en células tumorales hepáticas con significativa función mitocondrial y con p53 no mutado, y que la resistencia a sorafenib por dosis subterapéuticas de sorafenib se relaciona con reprogramación metabólica había la ruta glucolítica con riesgo de resistencia celular (37).

El tratamiento con inhibidores tirosina quinasa se asocia con la aparición de resistencias y recurrencia tumoral, probablemente como consecuencia de la reactivación de nuevas señales de supervivencia celular. Además, el uso de este fármaco conlleva diversos efectos secundarios como son reacciones cutáneas, diarrea, hipertensión, fatiga, alopecia, anorexia, síndrome de manos-pies, etc (38).

Lenvatinib (Lenvima®, Eisai) ha demostrado una respuesta no inferior a sorafenib en el tratamiento de los pacientes en estadio avanzado por lo que se utiliza como alternativa y en primera línea (39). Lenvatinib es un inhibidor de quinasas como son VEGFR1, VEGFR2 y VEGFR3 y eficaz en otros cánceres. Las fichas técnicas de los tratamientos a base de inhibidores tirosina quinasas y anticuerpos monoclonales advierten de los riesgos de aparición de efectos secundarios relacionados con la toxicidad dermatológica, problemas digestivos graves, hipertensión y un mayor riesgo de hemorragias (40,41).

Actualmente existen tratamientos en segunda línea que pueden mejorar la supervivencia del paciente y la progresión del tumor. Uno de los más destacados es regorafenib (Stivarga®, Bayer) en pacientes no respondedores a sorafenib o con efectos adversos relevantes (42). Regorafenib (Stivarga, BAY 73-4506; Bayer Pharma AG, Berlín, Alemania) tiene una estructura similar al sorafenib que se diferencia solo en el flúor en el anillo de fenilo. Esta diferencia da como resultado un mayor efecto inhibidor

sobre los receptores relacionados con la angiogénesis, incluyendo VEGFR2 y el receptor 1 del factor de crecimiento de fibroblastos (FGFR1). Regorafenib también inhibe VEGFR1, VEGFR3, RAF, TIE2 (dominio 2 de homología del factor de crecimiento epidérmico), KIT, RET y BRAF. Por lo tanto, regorafenib se dirige a una amplia gama de factores angiogénicos, el microambiente tumoral y las quinasas oncogénicas (43).

Otro tratamiento en segunda línea es cabozantinib (Cabometyx®, Ipsen) que ha demostrado ser un inhibidor de tirosina quinasas como VEGFR 1-3, MET y AXL (42). Este fármaco ha mostrado al compararse con resultados con placebo una mejor supervivencia y un mejor resultado en cuanto a tiempo libre de progresión del tumor.

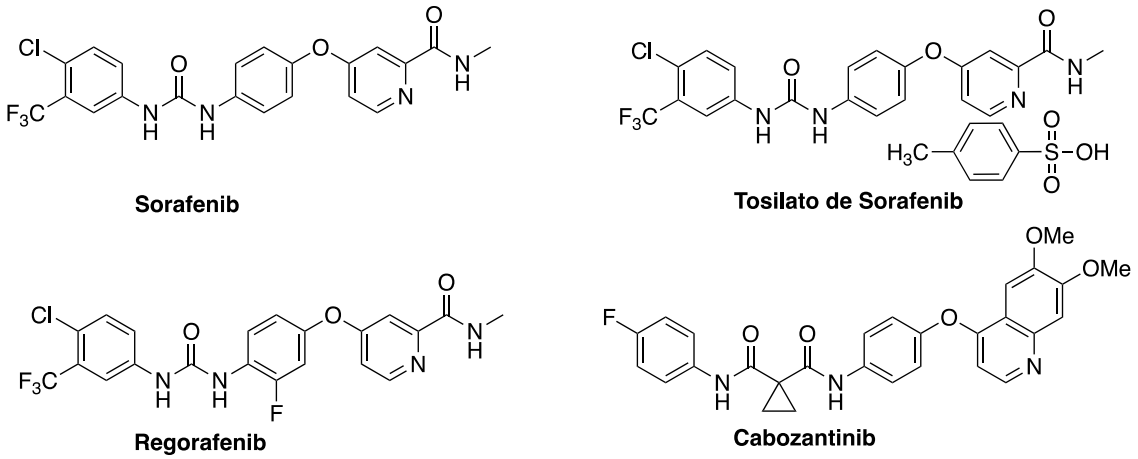

Figura 4. Estructura química del sorafenib, Tosilato de sorafenib, Regorafenib y Cabozatinib.

Alteraciones moleculares en el HCC y vías de señalización

Se han detectado varias alteraciones genéticas que afectan a diversas rutas de señalización celular y que son relevantes en el desarrollo del HCC. Entre ellas cabe citar las mutaciones en los genes CTNNB1 (β-catenina), dominio de interacción rico en AT 1A (ARID1A), ARID1B, AXIN, transcriptasa inversa de telomerasa (TERT), c-MYC, factor de crecimiento epidérmico (EGF), crecimiento de hepatocitos (HGF), así como mutaciones en RAS y TP53, amplificación del factor de crecimiento de fibroblastos 19

(FGF19), inhibidor de la quinasa dependiente de ciclina 2A (CDK2A) y sobreexpresión del factor de crecimiento de insulina 2 (IGF2) debido a modificaciones epigenéticas (44).

El HCC resulta de la acumulación media de 50 mutaciones somáticas lo que genera una importante multitud de clones relacionados pero molecularmente diferentes en el tumor lo que conlleva a la aparición de una elevada heterogeneidad molecular inter tumoral observada en el HCC (45,46). Existen varios subtipos moleculares de HCC, que presentan diferentes aberraciones moleculares relacionadas con un potencial replicativo ilimitado, reducción de la apoptosis celular, cambios en el metabolismo celular, estrés celular, inestabilidad cromosómica y deficiencia en la reparación del ADN celular que reduce las posibilidades terapéuticas por la aparición de numerosas resistencias a los tratamientos (22). Varios componentes de las vías de señalización, como Ras/Raf/Mek/Erk, PI3K/Akt/mTOR, VEGF/VEGFR, EGF/EGFR, etc. son objetivos prometedores en el HCC (44,47).

HCC expresa un alto nivel de VEGFA, un regulador crucial de la vascularización del tumor. Varias isoformas de VEGFA (en particular VEGFA-165) se han relacionado con la invasividad vascular, el estado de la enfermedad y el desarrollo de HCC (48–50). Uno de los factores más importantes en la hepatocarcinogénesis es la modulación de las vías de señalización oncogénicas y del desarrollo implicadas en la patogénesis del HCC, como las vías de transducción de señales clave Wnt/β-catenina, EGFR-Ras-MAPKK, c-Met, señalización de IGF, señalización Akt/mTOR y cascadas de señalización VEGF y PDGFR (51)

Nanomedicina

La búsqueda de enfoques no invasivos que permitan el uso de sorafenib para tratar el HCC, con efectos tóxicos mínimos o nulos, es un área de interés permanente en la

oncología moderna. El advenimiento de la nanomedicina, cuyo objetivo último es transportar una cantidad suficiente de sustancias activas a través de las barreras fisiológicas y alcanzar, de forma selectiva, los tejidos afectados por la enfermedad, ha tenido un impacto significativo en este campo (52–54). En esta área, el uso de nanopartículas solubles en agua como vectores para la liberación selectiva de compuestos citotóxicos a los tejidos tumorales ha mostrado resultados muy prometedores (55). De hecho, la reducción de efectos secundarios, el aumento de la solubilidad y el tiempo de circulación y la acumulación preferencial en el tejido tumoral debido al efecto de permeabilización y retención (EPR) de los quimioterapéuticos de molécula pequeña notoriamente tóxicos se pueden lograr mediante el direccionamiento de fármacos, ya sea pasivo o activo, utilizando nanopartículas (55). Los tumores sólidos pueden presentar un aumento de la vascularización y la permeabilidad, lo que da como resultado una mayor acumulación de nanopartículas en el espacio tumoral intersticial en comparación con el tejido normal o sano, junto con un drenaje linfático deficiente (56). Sin embargo, la heterogeneidad de los tumores sólidos puede limitar la eficacia de las terapias de nanopartículas basadas en EPR en humanos (57). Se están desarrollando una serie de enfoques basados en nanopartículas y micropartículas para dirigir el sorafenib al HCC.

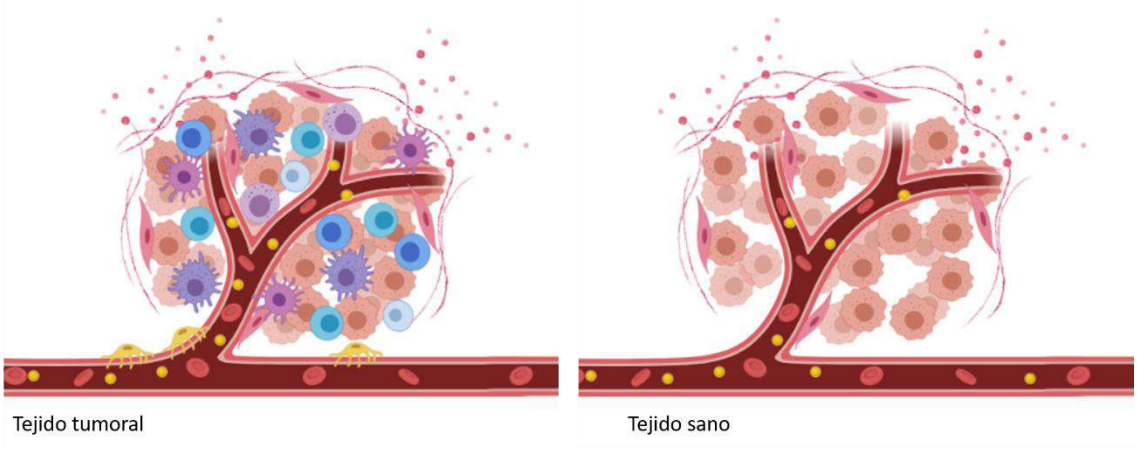

Figura 5. Efecto EPR aumentado en el tejido tumoral con respecto al tejido sano.

Estos incluyen liposomas (58), nanopartículas poliméricas (59,60), nanopartículas mesoporosas (61–63), microcápsulas núcleo-capa (64,65), nanopartículas cristalinas líquidas (66), nanopartículas de lípidos sólidos (67–70), y neutrales nanocompuestos anfifílicos basados en ciclodextrina (71). Sin embargo, aún no se ha investigado el desarrollo de nanovectores funcionalizados cargados con sorafenib. Además, si bien la mayoría de los enfoques informados se basan en el direccionamiento pasivo, recientemente se ha demostrado que es menos adecuado para reducir los efectos secundarios de los compuestos antitumorales en comparación con el direccionamiento activo, que se basa en la programación de nanopartículas al unirse a un ligando, que interactúa selectivamente. con receptores de superficie celular (72). Por ello, encontrar dianas biológicas nuevas, específicas, sobreexpresadas con respecto a las células normales, con alta eficiencia endocítica y poca tendencia a sufrir mutaciones es de suma importancia en nanomedicina.

Uno de los principales receptores para tal dirección es el ASGPR (73,74) que se encuentra predominantemente en los hepatocitos, HCC y en menor proporción en células no hepáticas (75). En particular, ASGPR pertenece al grupo de receptores con reciclado

constitutivo cada 15 minutos con o sin ligandos (76). La función principal de ASGPR es mantener la homeostasis de las glicoproteínas séricas mediando el reconocimiento y endocitosis de una amplia gama de glicoproteínas desialiladas que transportan residuos terminales de galactosa (Gal) o N-acetilgalactosamina (GalNAc) (77). Además, ASGPR juega un papel en las enfermedades infecciosas, ya que se demostró que el VHA y VHB, así como el virus de Marburg, se unen a él, lo que facilita las infecciones hepáticas. Otro receptor importante presente en las células hepáticas es el MR, pero cuya importancia en la patología del cáncer de hígado es poco conocida. El MR, también una lectina de tipo C, se expresa en la superficie de los macrófagos y algunos subconjuntos de células dendríticas inmaduras (78). MR participa en la presentación de antígenos, endocitosis de macrófagos y se considera un sello distintivo de los macrófagos asociados a tumores (79). Un estudio clínico reciente ha demostrado un aumento de la expresión de MR en muestras de cáncer de hígado en comparación con el tejido hepático adyacente sano y que la expresión de MR se asoció significativamente con el tamaño del tumor y la metástasis, lo que convierte a la MR en un receptor atractivo para dirigirse al HCC (80).

Las micelas, y más concretamente las micelas poliméricas, ocupan una posición privilegiada entre los sistemas de liberación de fármacos actualmente utilizados, con algunas formulaciones ya en el mercado o en estadios clínicos avanzados, lo que las hace muy atractivas para la implementación de sistemas de glicogestión (81). Entre los inconvenientes que han limitado el uso de micelas en general, y los derivados anfifílicos de bajo peso molecular en particular, como portadores de fármacos está su alta sensibilidad a la dilución. Las aproximaciones que superen este abrumador problema son muy necesarias para la aplicación de estos prometedores sistemas en medicina. En este sentido, los anfífilos diacetileno son muy adecuados, ya que pueden sufrir una fotopolimerización limpia mediante una reacción de adición 1,4 tras irradiación UV o

estímulos térmicos. De esta forma, se obtienen nanomateriales funcionales de polidiacetileno (PDA), (82) incluidas las micelas, (83) con mayor estabilidad y propiedades cromáticas interesantes (84).

OBJETIVOS

Este trabajo tiene como objetivo principal la caracterización y evaluación de la efectividad terapéutica de micelas diseñadas para acceder al MR y ASGPR para la encapsulación de sorafenib en el cultivo de células HepG2 y Huh7, con el objetivo final de verificar si dichas micelas son vehículos idóneos para este fármaco en HCC. Para ello se han abordado los siguientes objetivos parciales:

1. **Síntesis y caracterización de las dos formulaciones**
    a. Síntesis y purificación de los precursores micelares
    b. Caracterización de los precursores micelares
    c. Encapsulación de sorafenib en las nanomicelas

2. **Evaluar la expresión de los receptores en estudio**
    a. Estudiar la expresión de ASGPR en células HepG2 y Huh7
    b. Estudiar la expresión de MR en células HepG2 y Huh7

3. **Determinar el tráfico intracelular de estos nanotransportadores en células HepG2**
    a. Incorporación de Rojo del Nilo a las nanomicelas

4. **Cuantificar la concentración intracelular de sorafenib en las nanomicelas**
    a. Cuantificar la liberación de sorafenib encapsulado en las nanomicelas

5. **Valorar la inducción de la apoptosis y reducción de la proliferación celular por sorafenib por las dos formulaciones de micelas realizadas en comparación con el fármaco sin vehiculizar en HepG2 y Huh7**

MATERIALES Y MÉTODOS

Líneas celulares y condiciones de cultivo

La línea celular HepG2 (HB-8065^{TM}, American Type Culture Collection o ATCC; LGC Standards, S.L.U., Barcelona, Spain) y Huh7 (Apath LCC) no presentaron contaminación con micoplasma. Las células se usaron hasta el pase 30 para evitar la progresiva desdiferenciación y/o acumulación de nuevas mutaciones. Las células fueron mantenidas en Medio Mínimo Esencial con Sales de Earl (MEM/EBSS) (Ge Healthcare HyClone, Boston, US) suplementado con L-glutamina (2 mM) (E15-825, PAA), suero bovino fetal (FBS) (10 %) (F7524, Sigma-Aldrich, Lot No: 022M3395, endotoxina <0.2 EU/ml), Piruvato sódico (1 mM) (S11-003, PAA), aminoácidos no esenciales piruvato sódico (1 mM), aminoácidos no esenciales (M11-003, PAA), penicilina (100 U/ml) y estreptomicina (100 μg/ml) (P11-010, PAA), a 37ºC en un incubador humificado con 5% CO_2.

Las células fueron cultivadas con una densidad de 100.000 células/cm^2. Sorafenib (Nexavar®, Bayer, Suiza) se administró en un rango de dosis de 10 nM y 20 nM tras 24 horas de estabilización en el cultivo, obteniéndose los correspondientes lisados celulares a diferentes tiempos. Los lisados celulares fueron obtenidos rutinariamente en 50 mM HEPES (Ref. A1069.0250, Applichem, Darmstadt, Alemania) pH 7.5, 5 mM ácido etilendiaminotetraacético (EDTA) (A3234.0500, Applichem, Darmstadt, Alemania), 150 mM NaCl (A114.1000, Applichem, Darmstadt, Alemania), 1 % NP-40 (IGEPAL) (A1694.0250, Applichem, Darmstadt, Alemania), cocktail inhibidor de proteasas (Ref. P8340, Sigma-Aldrich, Misuri, USA), 1 mM fluoruro de fenilmetanosulfonilo (PMSF) (A0999.0025, Applichem, Darmstadt, Alemania), 1 mM NaF (A0547.0500, Applichem, Darmstadt, Alemania), y 1 mM Na_3VO_4 (A2196.0010, Applichem, Darmstadt, Alemania), mantenidos en hielo y aplicando vortex durante 15 segundos en cuatro

intervalos de cinco minutos. Las muestras fueron centrifugadas a 13.000 rpm a 4ºC. El sobrenadante fue recogido para la cuantificación de proteína y diversos análisis.

La medición de proteínas en el lisado celular se realizó mediante el kit comercial DC Protein Assay Reagents Package (5000116, Bio-Rad, California, USA). Los patrones, muestras y reactivos se depositaron en una placa de titulación no estéril (167008, Costar, Washington, USA). Por cada muestra, se necesitan 25 µl de mezcla de reactivos A+S y 200 µl del reactivo B por pocillo. La mezcla A+S se prepara con 980 µl serían de reactivo A se mezclan con 20 µl de reactivo S. Se deja en incubación durante 15 minutos a temperatura ambiente. La absorbancia de las muestras a 750 nm se midió en un lector de placa TECAN Infinitive 200 Pro (Männedorf, Suiza).

Aislamiento de hepatocitos primarios

El aislamiento de hepatocitos primarios se realizó usando en un primer lugar, HEPES pH 7,2 (10 mM HEPES ácido (A1069, Applichem, Darmstadt, Alemania), 136 mM NaCl (S5886, Applichem, Darmstadt, Alemania), 5 mM KCl (A1362, Applichem, Darmstadt, Alemania) 0.5% Glucosa (G7021, Applichem, Darmstadt, Alemania) y EGTA (0.5 mM EGTA (E4378 Applichem, Darmstadt, Alemania), 10 mM HEPES ácido (A1069, Applichem, Darmstadt, Alemania), 136 mM NaCl (S5886, Applichem, Darmstadt, Alemania), 5 mM KCl (A1362, Applichem, Darmstadt, Alemania), 0.5% Glucosa (G7021, Applichem, Darmstadt, Alemania) que se complementan con antioxidantes (1 ml/L; 100 mM Sorbitol (S1876, Applichem, Darmstadt, Alemania), 100 mM Manitol (M4125, Applichem, Darmstadt, Alemania), 100 mM GSH (G4251, Applichem, Darmstadt, Alemania)) y antibióticos/fungizona (10 ml/L). El tejido se lava secuencialmente con HEPES (500 ml), EGTA (500 ml) y HEPES (500 ml) a un flujo de 70 ml/min mediante una bomba de perfusión.

Seguidamente, se realizar una perfusión con colagenasa (0,05%; 0,5 mg/ml, C5138, Sigma Aldrich) y BSA (0,5%)-HEPES a 37ºC. La solución de colagenasa se prepara a relación de 250 mg de colagenasa en 500 ml HEPES complementado, a la que se le añaden 5 ml de 70 mM $CaCl_2$ (141221, Applichem, Darmstadt, Alemania). La perfusión se realiza a un flujo de 50 ml/min. Es necesario realizar la re-circulación de la solución de colagenasa aproximadamente durante 45 min dependiendo del grado de digestión del órgano. Una vez que se observa que el tejido está muy blando liberando hepatocitos por disgregación del parénquima hepático, se procede transferir la suspensión a un matraz y se filtra a través de una membrana de nylon 250 µ y posteriormente de 70 µ utilizando un embudo estéril. La suspensión celular se lava 3x con BSA (0,5%)-HEPES a 50g durante 5 min. Tras cada lavado se descarta el sobrenadante (células de kupffer, Ito cells y células endoteliales) y el precipitado celular se resuspende con 50 ml de solución de BSA (0,5%)-HEPES. Se prepara el medio de cultivo Dulbecco´s Modified Eagle´s Medium (DME; D2906, Sigma Aldrich)+Ham´s Nutrient Mixture F-12/Williams E (W4125, Sigma Aldrich) que se complementa con los 38 ml de la solución de aditivos (glutamina, glucosa, piruvato sódico, dexametasona, transferrina, etanolamina, glucagón, insulina y ácido linoleico), 2 ml de vitamina C (50 mg), 50 ml SBF descomplementado y antibióticos/fungizona (10 ml). El medio se mantiene a 37ºC hasta su utilización tras los lavados de la suspensión celular. El precipitado celular final se resuspende en un volumen de medio de cultivo complementado para su contaje.

Por último, se realiza el contaje celular mediante una cámara de Neubauer.

Las células se dispensan en los pocillos a una concentración de 10^6/ml y se distribuyen homogéneamente mediante agitación suave en varias direcciones. Las células se mantienen en atmósfera húmeda de aire/5% CO2 a 37ºC. El medio de cultivo se cambia a las 24 h.

Expresión del MR y ASGPR

La expresión del MR y ASGPR se determinó en geles de electroforesis desnaturalizante tipo Any kD™ Criterion™ TGX Stain-Free™ (#5678124; BioRad, Hercules, CA) transfiriéndose las proteínas a una membrana de polifluoruro de vinilideno (PVDF), que tras bloquear los sitios inespecíficos con una solución de albúmina bovina sérica (BSA) al 5 % durante 1 hora, se incubaron con los anticuerpos primarios para el MR (1:1000) (ab125028, Abcam, Cambridge, Reino Unido) y para ASGPR (1:200) (sc-52623, Santa Cruz Biotechnology, Inc., Dallas, Texas, Estados Unidos) durante 12 horas a 4ºC, y posteriormente se incubó con los anticuerpos secundarios correspondientes obtenidos de cabra frente a los anticuerpos de conejo IgG-HRP (1:10000) (sc-2004, Santa cruz, Dallas, Texas, USA) y obtenidos de cabra frente a los anticuerpos de ratón (1:10000) (sc-2005, Santa cruz, Dallas, Texas, Estados Unidos) preparados solución de BSA al 1% en PBS-T con el 0,1% de Tween durante 1 hora a temperatura ambiente. La membrana fue revelada mediante el ensayo quimioluminiscente Clarity™ Western ECL substrate (Ref 170-5061; Bio-Rad, Hercules, Estados Unidos). Las imágenes fueron adquiridas en un Sistema ChemiDoc™ Touch Imaging y fueron analizadas con Image Lab software. La expresión de la proteína fue normalizada con el contenido total de proteína siguiendo la tecnología Stain-Free. Entre las muestras se incluyó un marcador de peso molecular (Ref. 161-0374, Bio-Rad, California, Estados Unidos) que tiene un rango entre 10-250 kDa que nos permite identificar el peso de nuestras proteínas y delimitar el frente de carga. El peso molecular incluye dos proteínas de color rosa de 25 y 75 kDa para facilitar su identificación.

Síntesis, purificación y caracterización de los nanovectores

En este trabajo se han utilizado dos nanomicelas (**pMicMan** y **pMicGal**) a partir de manopiranosil y galactopiranosil neoglicolípidos respectivamente. La estructura y el tamaño de los gliconanoportadores obtenidos se han investigado mediante resonancia magnética nuclear (RMN), microscopía electrónica de transmisión (TEM) y dispersión dinámica de luz (DLS). Estas nanomicelas han sido utilizadas para la encapsulación de sorafenib, con el fin de estudiar la actividad antitumoral en células de HCC, así como el Rojo del Nilo para el estudio de su tráfico intracelular.

Todas las reacciones se llevaron a cabo bajo una atmósfera inerte usando material de vidrio secado previamente en la estufa y disolventes recién destilados y secos. El tetrahidrofurano (THF) y el dietil éter (Et_2O) se desecaron mediante reflujo y posterior destilación sobre Na/benzofenona, bajo atmósfera de nitrógeno. Para los otros disolventes [dimetilformamida (DMF), diclorometano (CH_2Cl_2) y tolueno], se hizo uso de un sistema de deshidratación por paso del disolvente a través de columnas de secado de la empresa *Innovative technology* (Newburyport, MA, USA)

La **cromatografía analítica en capa fina (c.c.f.)**, se ha realizado empleando cromatoplacas de gel de sílice soportada sobre aluminio *Alufram®Sil.G/V245 Merck* de 0.25 nm, revelado las placas eluidas y secas con ácido fosfomolíbdico o ácido sulfúrico. Para la purificación llevada a cabo, generalmente en columna cromatográfica bajo presión, se utilizó como fase estacionaria gel de sílice Merck 60 A (tamaño de poro 40-63 μm). La composición del eluyente empleado se detalla para cada compuesto

Los **poderes rotatorios** $[\alpha]^{20}_D$ se han determinado a temperatura ambiente, utilizando una celda de 10 cm de longitud. El polarímetro utilizado fue de la marca *Perkin Elmer 341MC* empleando la línea de emisión de sodio (λ= 589 nm) como fuente de luz.

Los **espectros de Resonancia Magnética Nuclear** (^{1}H-RMN, ^{13}C-RMN) se han registrado espectrómetros *Bruker DRX-300* (300 MHz), *DPX-400* (400 MHz) y *DRX-500* (500 MHz) del Instituto de Investigaciones Químicas. Los espectros se han registrado a partir de muestras en disolución en el disolvente deuterado que se indica entre paréntesis. Los desplazamientos químicos se expresan en ppm (δ), usando como referencia la señal residual del disolvente no deuterado. Para la asignación de las estructuras más complejas se han utilizado experimentos bidimensionales de correlación protón-protón (COSY) y protón-carbono (HETCOR) usando secuencias de pulsos estándar.

Los **espectros de masas (EM)** se obtuvieron empleando la técnica de ionización por electrospray (ESI) en un espectrómetro *Bruker Esquire6000*. Para ello se emplearon disoluciones de las muestras en CH_2Cl_2, MeOH, o sus mezclas, a concentración en el rango μM. Las muestras se introdujeron mediante inyección directa usando una jeringa *Cole-Palmer* a un flujo de 120 μL/h.

Los **espectros de masas de alta resolución (EMAR)** fueron realizados por el Servicio de Espectrometría de Masas de la Universidad de Sevilla en un espectrómetro *Kratos MS-80-RFA* y en un espectrómetro de masas *Micromass* modelo *AutoSpec*.

Los **espectros de UV-Vis** se registraron en un espectrómetro *UV/Vis Perkin Elmer Lambda 12* del Instituto de Investigaciones Químicas, utilizando como disolvente agua milli-Q (18 μΩ).

Los **espectros de fluorescencia** fueron realizados en el Instituto de Ciencia de Materiales de Sevilla (ICMS) en un *Jobin Yvon FLUOROLOG FL3-11*

fluorimeter equipado con dos monocromadores, a una longitud de onda de excitación 345 nm.

Las micrografías obtenidas del **microscopio electrónico de transmisión (TEM)** se obtuvieron en microscopios Philips CM10 trabajando a 80 kV, éste último en los Servicios Generales de Investigación de la Universidad de Sevilla (CITIUS). Para la preparación de las muestras se colocaron 15 μL de disolución objeto de estudio y 15 μL de una disolución de acetato de uranilo (2%) como agente de tinción, ambos sobre una rejilla de cobre recubierta con una película de carbono. Tras 2 minutos se eliminó el exceso de muestra y aditivo por absorción en un papel de filtro.

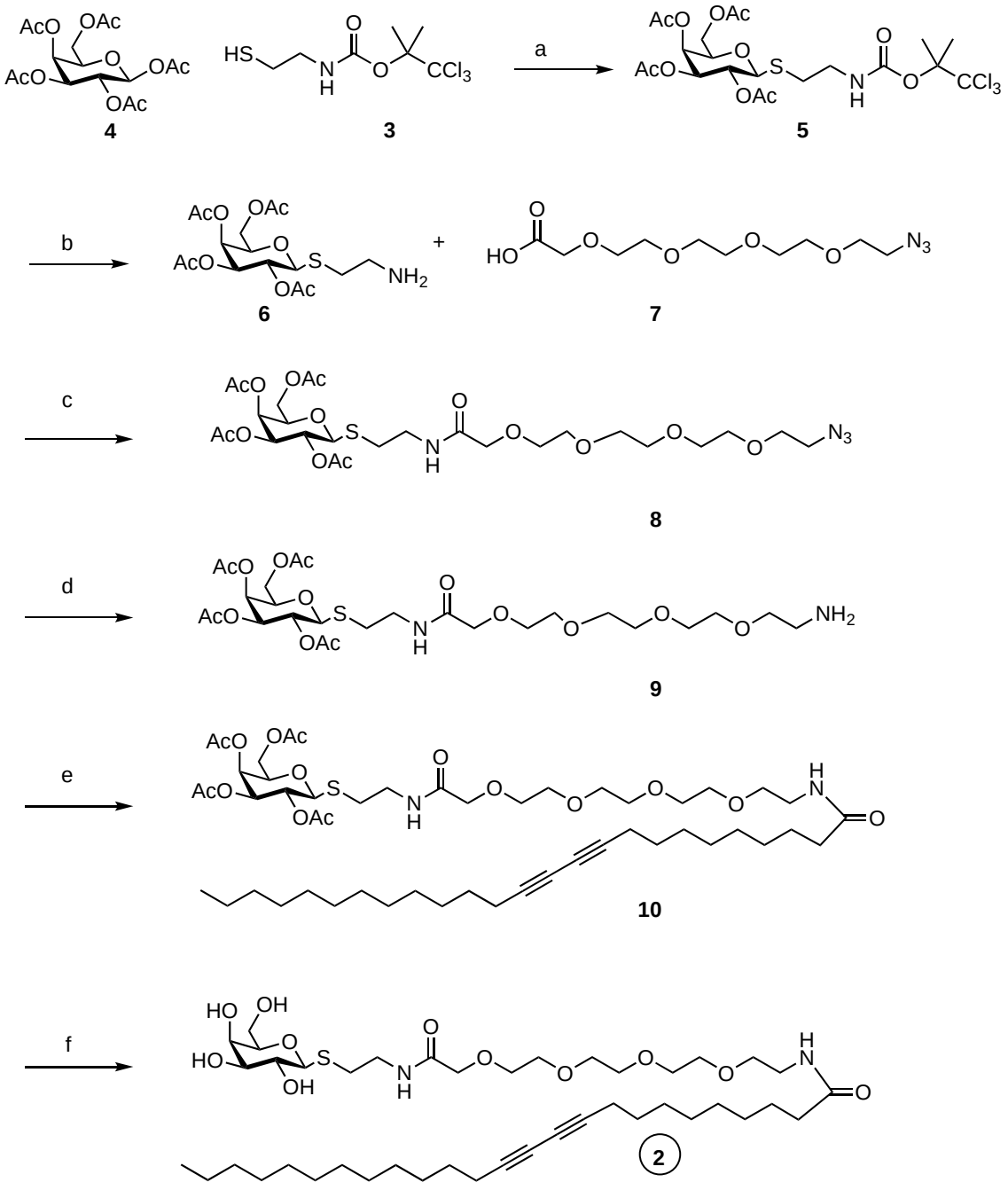

Esquema 1. Síntesis del neoglicolípido autoasociativa derivado de galactosa 2 a partir del tetraacetato de galactosa 3 (a) BF3 · Et2O, CH2Cl2, 70%; (b) AcOH, Zn, CH2Cl2, 72% (c) DIPEA, TBTU, DMF, 92%; (d) SnCl2, PhSH, Et3N, THF, 52%; (e) PCDA, DIPEA, TBTU, DMF, 62%; (f) MeONa, MeOH, Amberlite IR 120 H+, rend, cuant.

Compuesto 2 Tiogalactopiranósido	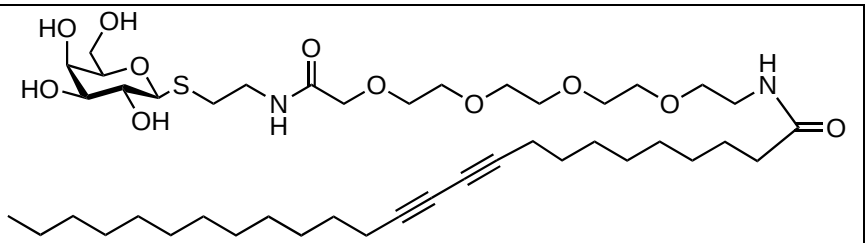
Compuesto 3	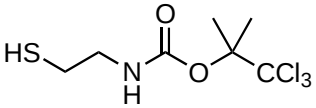
Compuesto 4 Galactosa peracetilada	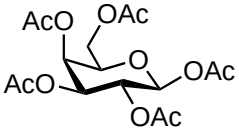
Compuesto 5	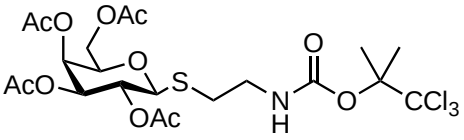
Compuesto 6 Derivado de aminoetiltiogalactopiranósido	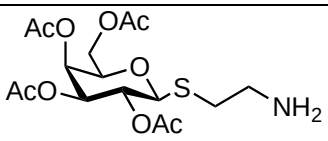
Compuesto 7 Espaciador bifuncional 5	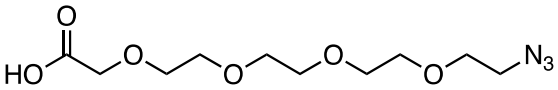
Compuesto 8 Azido derivado	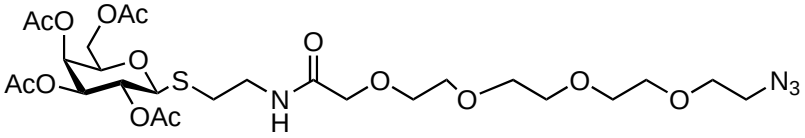
Compuesto 9	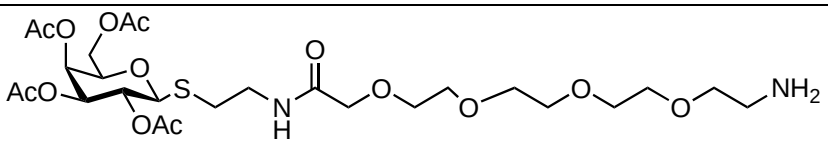

Compuesto 10 Monómero final peracetilado	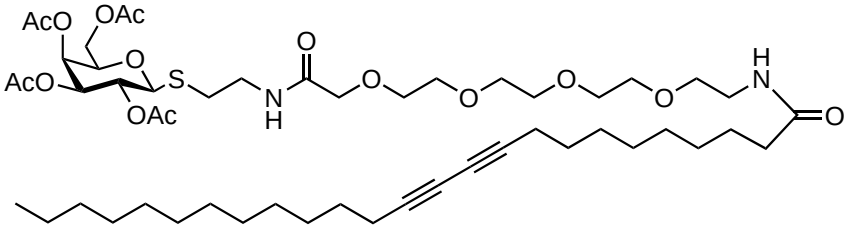

Tabla. 1. Compuestos sintetizados a lo largo de la síntesis del monómero anfífilo de galactosa autoasociativo 2

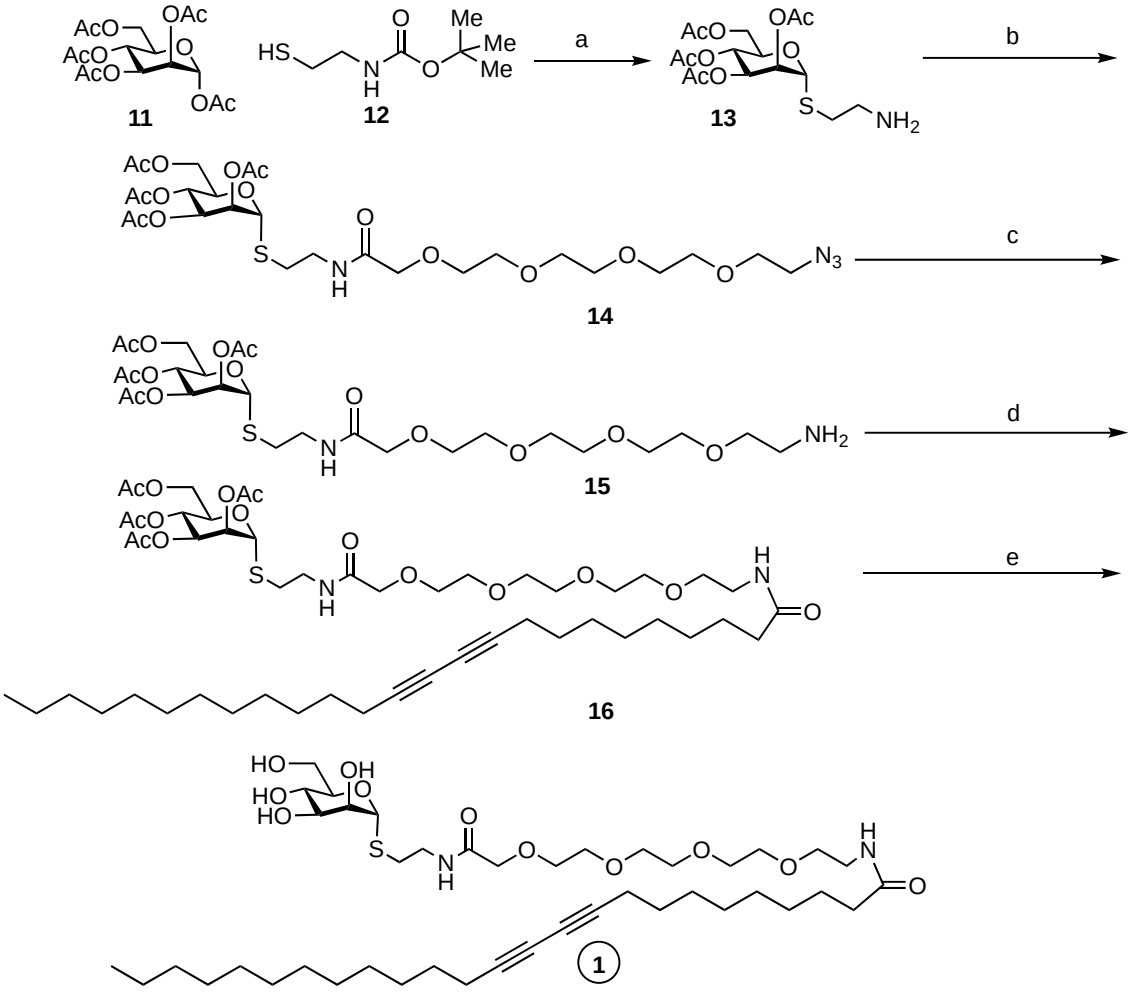

Esquema 2. Síntesis del neoglicolípido autoasociativa derivado de manosa 1 a partir del tetraacetato de manosa 11 (a) BF3 · Et2O, CH2Cl2, 50%; (b) 7, DMT-MM, 4-metil-morfolina, THF, 68%; (c) SnCl2, PhSH, Et3N, THF, 65%; (e) PCDA, DMT-MM, 4-metil-morfolina, THF, 60% (f) MeONa, MeOH, Amberlite IR 120 H+, 98%.

Compuesto 2 Tiogalactopiranósido	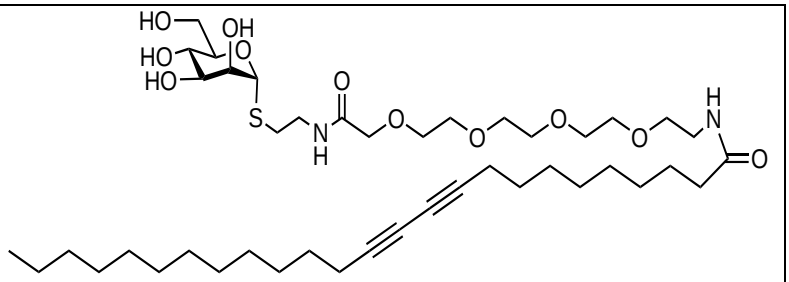
Compuesto 11 Manosa peracetilada	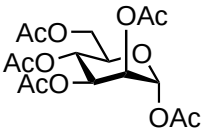
Compuesto 12 Boc-Cisteamina	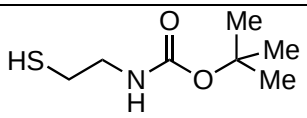
Compuesto 13 Derivado de aminoetiltiomanopiranósido	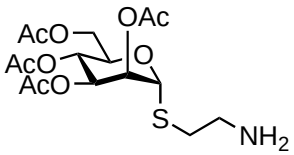
Compuesto 14	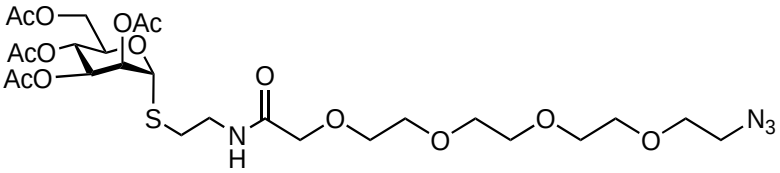
Compuesto 15	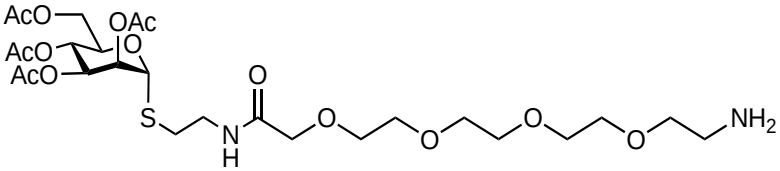
Compuesto 16 Monnómero final **1** peracetilado	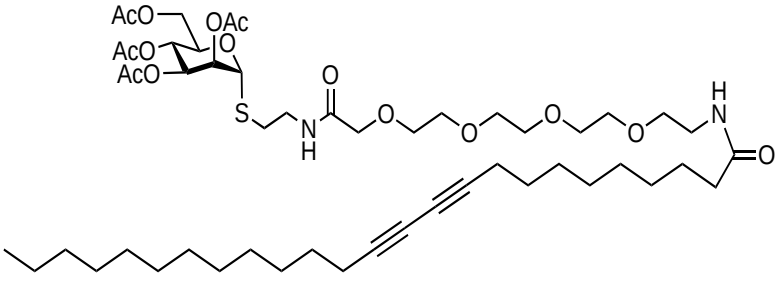

Tabla 2. Compuestos sintetizados a lo largo de la síntesis del monómero anfífilo de galactosa autoasociativo 1

La síntesis de los dos monómeros ha sido realizada siguiendo 2 rutas diferentes. Para la síntesis del monómero 1, Esquema 2, se ha seguido una ruta previamente desarrollada en el grupo de Síntesis asimétrica y Nanosistemas Funcionales. Esta ruta que utiliza como producto de partida la manos peracetilada 11, se basa en una reacción de "one-pot" de tiglicosidación desprotección del grupo terc-butiloxicarbonilo en una sola etapa reacción. Debido a problemas de separación de los anómeros a y b formados en la reacción de tioglicosidación, se ha desarrollado una nueva aproximación para la síntesis del monómero autoasociativo 2, Esquema 1. En esta aproximación se utiliza como donador de glicosilo la galactosa peracetililada , y la cisteamina tricloroBOC 3 como aceptor de glicosilo, siguiendo el protocolo desarrolado por el grupo de Gildersleeve.

3.3.1 Síntesis de (2-Aminoetil) 2,3,4,6-tetra-*O*-acetil-α-D-tiomanopiranósido (13)

A partir de la manosa acetilada **12** (1 g, 1 eq) en CH_2Cl_2 anhidro, bajo atmósfera de argón y en agitación, se le añaden 2-(Boc-amino)etanotiol **13** (1.5 eq) y $BF_3{\cdot}Et_2O$ (10 eq). La reacción se calienta a reflujo (45 ºC) durante 24 horas, observándose por c.c.f. un nuevo producto con un R_f menor que el producto de partida. El crudo se neutraliza con una disolución acuosa de $NaHCO_3$, se extrajo la fase orgánica con CH_2Cl_2. Se secó con Na_2SO_4 anhidro, se filtró y se evaporó el disolvente a vacío, obteniéndose el compuesto **13** (0.5 g, 1.23 moles) con un rendimiento del 50% mediante columna cromatográfica en CH_2Cl_2 /MeOH (30:1).

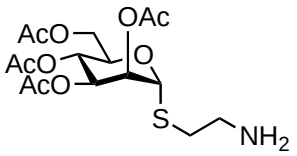

13

^{1}H RMN (400 MHz, $CDCl_3$): δ 5.46 (sa, 2H, NH_2), 5.42-5.15 (m, 3H, H-1, H-4, H-2), 5.09 (dd, 1H, $J_{3,4}$ = 10.2 Hz, $J_{3,2}$ = 2.7 Hz, H-3), 4.29-4.23 (m, 1H, H-5), 4.17 (dd, 1H, $J_{6a,6b}$ = 12.5 Hz, $J_{6a,5}$ = 5.1 Hz, H-6a), 4.00 (d, 1H, J = 12.6 Hz, H-6b), 2.95 (sa, 2H, $C\underline{H}_2NH_2$), 2.84-2.67 (m, 2H, SCH_2), 2.04 (s, 3H, CH_3COO), 1.98 (s, 3H, CH_3COO), 1.94 (s, 3H, CH_3COO), 1.87 (s, 3H, CH_3COO).

^{13}C RMN (125.7 MHz, $CDCl_3$): δ 170.5 (CO), 169.8 (CO), 169.7 (CO), 169.6 (CO), 82.3 (C1), 70.8 (C4), 69.3 (C3), 69.2 (C5), 66.0 (C2), 62.3 (C6), 39.8 (CH_2NH_2), 32.1 (SCH_2), 20.7 (CH_3), 20.6 (CH_3), 20.5 ($2CH_3$).

EMAR: Calculado para $C_{16}H_{25}NO_9S$ 408.1328 $[M+H]^+$, encontrado 408.1326.

3.3.2 Síntesis de (17-Azido-4-oxo-6,9,12,15-tetraoxa-3-azaheptadecanil) 2,3,4,6 tetra-*O*-acetil-α-D- tiomanopiranósido (14)

A una disolución del espaciador **7** (320 mg,) en THF (25 mL) se añadió DMT-MM (320mg, 1.15 mmol). Tras 5 minutos de agitación se enfrío la mezcla a 0ºC y se añadió una disolución del amino derivado **13** y 4-metilmorfolina (126 μL, 1.1eq). La reacción se agita a temperatura ambiente durante 24 horas, se evapora el disolvente a sequedad y se purificó el producto por cromatografía en columna usando como eluyente una mezcla de CH_2Cl_2:MeOH (20:1), obteniéndose el compuesto **14** con un rendimiento del 68%.

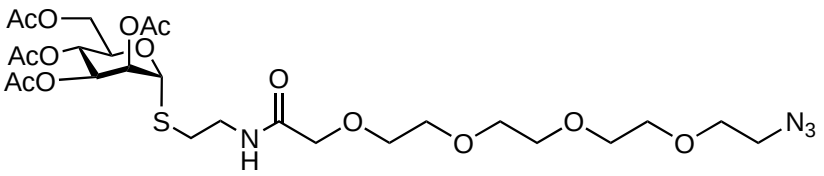

14

^{1}H RMN (400 MHz, $CDCl_3$): δ 7.31 (t, 1H, J = 6.5 Hz, NHCO), 5.25-5.20 (m, 3H, H-1,

H-4, H-2), 5.15 (dd, 1H, $J_{3,4}$ = 10.4 Hz, $J_{3,2}$ = 3.2 Hz, H-3), 4.32-4.29 (m, 1H, H-5), 4.23 (dd, 1H, $J_{6a,6b}$ = 12.2 Hz, $J_{6a,5}$ = 5.9 Hz, H- 6a), 4.03 (dd, 1H, $J_{6b,6a}$ = 12.5 Hz, $J_{6b,5}$ = 1.9 Hz, H-6b), 3.91 (s, 2H, $COCH_2O$), 3.60-3.56 (m, 14H, 7 CH_2O), 3.48-3.44 (m, 2H, $C\underline{H}_2NH$), 3.31 (t, 2H, J = 5.2 Hz, CH_2N_3), 2.80-2.68 (m, 2H, SCH_2), 2.08 (s, 3H, CH_3COO), 2.01 (s, 3H, CH_3COO), 1.98 (s, 3H, CH_3COO), 1.91 (s, 3H, CH_3COO).

^{13}C RMN (125.7 MHz,$CDCl_3$): δ 170.5 (CO), 170.1 (CO), 169.8 (CO), 169.7 (CO), 169.6 (CO), 82.4 (C1), 70.9 (C4), 70.8, 70.6, 70.5, 70.4, 70.3, 70.1, 69.9, 69.3 (C3), 69.1 (C5), 66.2 (C2), 62.4 (C6), 50.6 (CN_3), 38.1 (CH_2NH), 31.0 (SCH_2), 20.8 (CH_3), 20.6 (CH_3), 20.5 (CH_3).

EMAR: Calculado para $C_{26}H_{42}N_4O_{14}SNa$ 689.2316 $[M+Na]^+$, encontrado 689.2289.

3.3.3 Síntesis de (17-Amino-4-oxo-6,9,12,15-tetraoxa-3-azaheptadecanil) 2,3,4,6-tetra-*O*-acetil-α-D- tiomanopiranósido (15)

Sobre una disolución de cloruro de estaño (170 mg, 0,9 mmol) en THF (15 mL), se adicionó tiofenol (370 μL, 3,6mmol) y Et_3N (370 μL, 2,76 mmol). Seguidamente, se añadió el compuesto **14** (400mg, 0,6mmol) disuelto en THF (10 mL). Se dejó agitando durante 30 min a temperatura ambiente. La reacción se llevó a cabo bajo atmosfera de argón y se siguió por cromatografía en capa fina (DCM:MeOH 9:1). La mezcla de la reacción se neutralizó con bicarbonato sólido, se filtró y se concentró hasta sequedad. Se purificó el crudo de reacción obtenido mediante cromatografía en columna utilizando como eluyente una mezcla de CH_2Cl_2:MeOH 9:1, obteniéndose el compuesto **15** como un aceite de color amarillo y con un rendimiento del 65%.

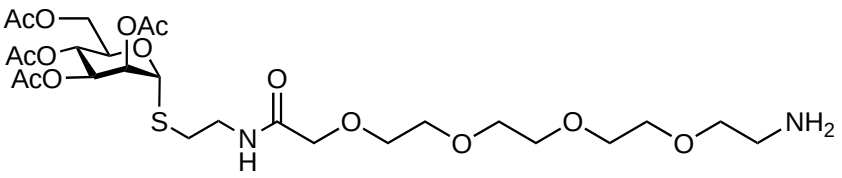

15

^{1}H RMN (400 MHz, $CDCl_3$): δ 7.83 (t, 1H, *J* = 5.0 Hz, NHCO), 5.29-5.22 (m, 3H, H-1, H-4, H-2), 5.15 (dd, 1H, $J_{3,4}$ = 10.0 Hz, $J_{3,2}$ = 3.4 Hz, H-3), 4.32-4.31 (m, 1H, H-5), 4.24 (dd, 1H, $J_{6a,6b}$ = 12.0 Hz, $J_{6a,5}$ = 5.2 Hz, H- 6a), 4.07 (d, 1H, *J* = 2.0 Hz, H-6b), 4.04 (s, 2H, $COCH_2O$), 3.80 (t, 2H, *J* = 4.4 Hz, $OC\underline{H}_2CH_2NH_2$), 3.66-3.59 (m, 12H, 6 CH_2O), 3.48-3.44 (m, 2H, $C\underline{H}_2NHCO$), 3.14 (t, 2H, *J* = 4.5 Hz, $C\underline{H}_2NH_2$), 2.83-2.72 (m, 2H, SCH_2), 2.10 (s, 3H, CH_3COO), 2.03 (s, 3H, CH_3COO), 1.99 (s, 3H, CH_3COO), 1.92 (s, 3H, CH_3COO).

^{13}C RMN (125.7 MHz, $CDCl_3$): δ 170.6 (CO), 170.5 (CO), 169.9 (CO), 169.8 (CO), 169.6 (CO), 82.3 (C1), 70.8, 70.6 (C4), 70.2, 70.1, 70.0, 69.9, 69.6, 69.4 (C3), 69.1 (C5), 66.7 (C2), 66.2, 62.4 (C6), 39.6 (CNH_2), 38.2 (CH_2NH), 30.9 (SCH_2), 20.9 (CH_3), 20.7 (CH_3), 20.6 (CH_3).

EMAR: Calculado para $C_{26}H_{44}N_2O_{14}SNa$ 640.2516 $[M+Na]^+$, encontrado 640.2489.

3.3.4 Síntesis de (4,19-Dioxo-6,9,12,15-tetraoxa-3,18-diaza-28,30-tritetracontadiinil) 2,3,4,6-tetra-*O*-acetil- *α*-D-tiomanopiranósido (16)

A una disolución de ácido 10,12-pentacosadiinoico (154 mg, 0,412 mmol) y DMT-MM (114 mg, 0,375 mmol) en THF se añade el compuesto **15** (240 mg, 0, 375 mmol). Posteriormente, se adicionó gota a gota 4-metilmorfolina (41 μl, 0,375mmol) y se mantuvo agitando durante 24 h a temperatura ambiente. Se concentra el crudo de reacción

hasta sequedad y se purifica por columna cromatográfica usando como eluyente DCM:MeOH 30:1, obteniéndose el compuesto **16** con un rendimiento del 60 %.

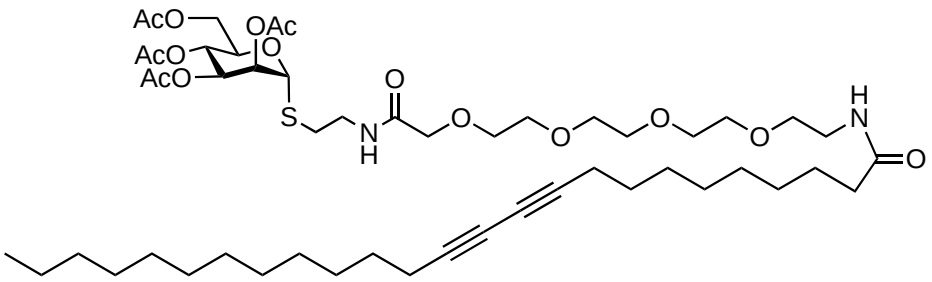

16

^{1}H RMN (400 MHz, $CDCl_3$): δ 7.31 (t, 1H, *J* = 5.7 Hz, NHCO), 6.18 (t, 1H, *J* = 5.7 Hz, NHCO), 5.30-5.24 (m, 3H, H-1, H-4, H-2), 5.19 (dd, 1H, $J_{3,4}$ = 10.0 Hz, $J_{3,2}$ = 3.3 Hz, H-3), 4.35-4.32 (m, 1H, H-5), 4.27 (dd, 1H, $J_{6a,6b}$ = 12.2 Hz, $J_{6a,5}$= 5.2 Hz, H-6a), 4.07 (dd, 1H, $J_{6b,6a}$ = 12.2 Hz, $J_{6b,5}$ = 2.1 Hz, H-6b), 3.97 (s, 2H, $COCH_2O$), 3.67- 3.48 (m, 16H, $7CH_2O$, $OCH_2C\underline{H}_2NH$), 3.41-3.38 (m, 2H, $SCH_2C\underline{H}_2NH$), 2.84-2.71 (m, 2H, SCH_2), 2.20 (t, 4H, *J* = 7.1 Hz, 2 $CH_2C{\equiv}C$), 2.14-2.11 (m, 5H, $COC\underline{H}_2CH_2$, CH_3COO), 2.05 (s, 3H, CH_3COO), 2.02 (s, 3H, CH_3COO), 1.95 (s, 3H, CH_3COO), 1.59-1.56 (m, 2H, $COCH_2C\underline{H}_2$), 1.48-1.45 (m, 4H, 2 $C\underline{H}_2CH_2C{\equiv}C$), 1.33-1.22 (m, 26H, 13 CH_2), 0.84 (t, 3H, *J* = 6.8 Hz, $C\underline{H}_3CH_2$).

^{13}C RMN (125.7 MHz, $CDCl_3$): δ 173.2 (CO), 170.5 (CO), 170.1 (CO), 169.8 (CO), 169.7 (CO), 169.6 (CO), 82.4 (C1), 77.5 ($CH_2C{\equiv}\underline{C}$), 77.3 ($CH_2C{\equiv}\underline{C}$), 70.9, 70.8 (C4), 70.5, 70.4, 70.2, 70.0, 69.4 (C3), 69.1 (C5), 67.2, 66.2 (C2), 65.3 ($CH_2\underline{C}{\equiv}C$), 65.2 ($CH_2\underline{C}{\equiv}C$), 62.4 (C6), 39.1 ($CH_2NH$), 38.1 ($SCH_2\underline{C}H_2$), 36.6 ($NHCO\underline{C}H_2CH_2$), 31.9 ($\underline{C}H_2CH_2CH_3$), 31.1 ($SCH_2$), 29.6, 29.5, 29.4, 29.3, 29.2, 29.0, 28.9, 28.8, 28.7, 28.3, 25.6 ($COCH_2\underline{C}H_2CH_2$), 22.6 ($\underline{C}H_2CH_3$), 20.8 ($CH_3$), 20.6 ($2CH_3$), 19.1 (2 $\underline{C}H_2C{\equiv}C$), 14.1 ($\underline{C}H_3CH_2$).

EMAR: Calculado para $C_{51}H_{84}N_2O_{15}SNa$ 1019.5490 $[M+Na]^+$, encontrado 1019.5484.

3.3.5 Síntesis de (4,19-Dioxo-6,9,12,15-tetraoxa-3,18-diaza-28,30-tritetracontadiinil) α-D-tiomanopiranósido (1)

A una disolución del compuesto **16** (210 mg, 0.211 mmol) en MeOH (3 mL) se le adicionó una disolución 0.84 M de metóxido sódico en metanol (0.1 mL, 0.084 mmol) y se agitó durante 30 minutos a temperatura ambiente. La reacción se siguió por ccf obteniéndose un producto con Rf menor. La mezcla se neutralizó con resina ácida, se filtró y se concentró hasta sequedad. Se obtuvo el compuesto **1** como un sólido amarillo con un rendimiento del 98 %.

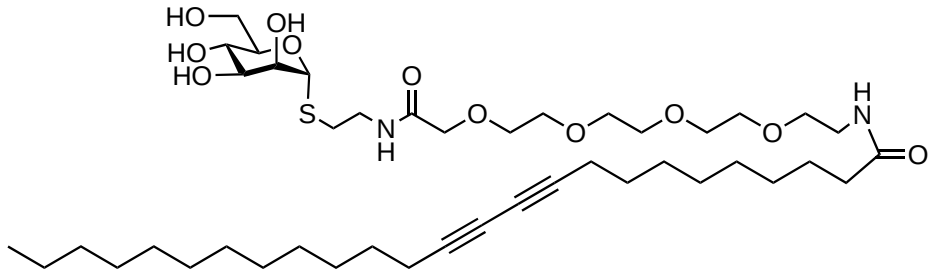

1

^{1}H RMN (400 MHz, $CDCl_3$): δ 8.12 (t, 1H, *J* = 6.3 Hz, NHCO), 7.97 (t, 1H, *J* = 6.3 Hz, NHCO), 5.33 (s, 1H, H-1), 4.03 (s, 2H, $COCH_2O$), 3.94-3.90 (m, 2H, H-4, H-2), 3.88 (dd, 1H, $J_{3,4}$ = 11.7 Hz, $J_{3,2}$ = 2.4 Hz, H-3), 3.77-3.64 (m, 15H, H-5, H-6, 6 CH_2O), 3.56 (t, 2H, *J* = 5.4 Hz, $OC\underline{H}_2CH_2NH$), 3.40-3.37 (m, 4H, $2C\underline{H}_2NH$), 2.92-2.74 (m, 2H, SCH_2), 2.27 (t, 4H, *J* = 7.2 Hz, 2 $CH_2C{\equiv}C$), 2.22 (t, 2H, *J* = 7.4 Hz, $COC\underline{H}_2CH_2$), 1.65-1.63 (m, 2H, $COCH_2C\underline{H}_2$), 1.56- 1.50 (m, 4H, 2 $C\underline{H}_2CH_2C{\equiv}C$), 1.42-1.32 (m, 26H, 13 CH_2), 0.93 (t, 3H, *J* = 7.4 Hz, CH_3).

^{13}C RMN (125.7 MHz, $CDCl_3$): δ 175.0 (CO), 171.5 (CO), 85.2 (C1), 76.6 ($CH_2C{\equiv}\underline{C}$), 76.5 ($CH_2C{\equiv}\underline{C}$), 73.9 (C4), 72.3 (C3), 71.8 (C5), 70.6, 70.2, 70.1, 69.9, 69.3, 67.5 (C2), 65.2 (2 $CH_2C{\equiv}\underline{C}$), 61.5 (C6), 39.0 ($CH_2NH$), 38.3 ($CH_2NH$), 35.7 ($NHCO\underline{C}H_2CH_2$), 31.8 ($\underline{C}H_2CH_2CH_3$), 30.1 ($SCH_2$), 29.5, 29.4, 29.3, 29.2, 29.1, 29.0, 28.9, 28.8, 28.7, 28.6, 28.5, 28.2, 25.6 ($COCH_2\underline{C}H_2$), 22.4 ($\underline{C}H_2CH_3$), 18.4 (2 $\underline{C}H_2C{\equiv}C$), 13.2 ($\underline{C}H_3CH_2$).

EMAR: Calculado para $C_{43}H_{76}N_2O_{11}SNa$ 851.5068 $[M+Na]^+$, encontrado 851.5036

3.3.6. Síntesis del compuesto 3

A una solución de $NaHCO_3$ (7,14 g, 85 mmol) en 75 ml de agua se le añadió una mezcla de hidrocloruro de 2-aminoetanotiol (3,2 g, 28,2 mmol) en Et_2O bajo atmósfera de argón a -10°C con fuerte agitación. Después de 35 min, se añadió gota a gota una solución de 2,2,2-tricloro-1,1-dimetil etilcloroformato (10 g; 41,6 mmol) en 150 ml de Et_2O durante 45 min. Luego, se retiró el baño de hielo y se dejó agitar durante 6 h hasta que se alcanzó la temperatura ambiente. Se separó la fase orgánica, lavando con una solución de HCl (2 M). El extracto orgánico se secó sobre Na_2SO_4 anhidro, se filtró y se concentró al vacío. La purificación se realizó mediante columna cromatográfica utilizando como mezcla de eluyentes Hex/AcOEt (4: 1), obteniendo así el compuesto 3 con un rendimiento del 65% (5,13 g). RMN 1H (500 MHz, CDCl3): δ 5,21 (sa , 1H, NHCO), 3.37 (q, J = 6.4 Hz, 2H, CH2NH), 2.71 (m, 2H, SHCH2), 1.92 (s, 6H, COOC (C2H6CCl3)), 1.39 (t, J = 8.4 Hz, 1H, SH). 13C RMN (125,7 MHz, CDCl3): δ 153,9 (NHCOO), 106,4 (CCl3), 88,1 C (C2H6CCl3)), 43,7 (CH2NH), 24,7 (SHCH2), 21,71 C (C2H6CCl3)), 21,60 C (C2H6CCl3). HRMS: Calc. para C7H13NO2SCl3 279,9732 [M + H] +, encontrado 279,9740.

3.3.7. Síntesis del compuesto 5

A una solución de galactosa peracetilada (2,56 mmol, 1 equivalente) y el compuesto 3 como aceptor (1,1 equivalentes), se añadió gota a gota $BF_3 \cdot Et_2O$ (10 equivalentes) en CH_2Cl_2 (9,7 ml) a 0ºC. Después de 24 h, se agregaron 100 mL de CH_2Cl_2 y se neutralizó con una solución acuosa de $NaHCO_3$ (2 x 150 mL). Después de secar con Na_2SO_4 anhidro, se filtró y se evaporó. La purificación se realizó mediante columna cromatográfica, utilizando una mezcla de eluyentes Éter/Hex (1:1). Así se obtuvo el compuesto 5 como una espuma blanca con un rendimiento del 70% y una relación α/β de (16/84). [α] 20D: -10,16 (c 0,64, CHCl3) RMN 1H (400 MHz, CDCl3): δ 5,45 (d, 1H, J4,3 = 3,75 Hz, H-4), 5,42 (t, 1H, NH), 5.25 (t, 1H, J2,3 = J2,1 = 10.2 Hz, H-2), 5.06 (dd, 1H, J3,2 = 10.0 Hz, J3,4 = 3.5 Hz, H-3), 4.52 (d, 1H, J1,2 = 10.0 Hz, H-1), 4.19-4.12 (m, 2H, H-6a, H-6b), 3.98 (t, 1H, J5-6a = J5-6b = 6.8, H-5), 3.48-3.37 (m, 2H, CH2NH), 2.99-2.74 (m, 2H, SCH2), 2.18 (s, 3H, CH3), 2.08 (s, 3H, CH3), 2.07 (s, 3H , CH3), 2,00 (s, 3H, CH3), 1,93 (d, 6H, J = 1,6 Hz, COOC (C2H6CCl3). 13C RMN (100 MHz, CDCl3): δ 171,4 (CO), 170,2 (CO), 170,7 (CO), 169,9 (CO), 154,0 (NHCOO), 106,5 (CCl3), 88,1 (C (C2H6CCl3)), 84,3 (C1), 74,6 (C5), 71,7 (C3), 67,2 (C4), 66,9 (C2), 61,5 (C6), 40,9 (CH2NH2), 30,7 (SCH2), 21,7 (C (C2H6CCl3)), 21,5 (C (C2H6CCl3)), 20,8 (CH3), 20,7 (2CH3), 20,6 (CH3). HRMS: Calculado para C16H25NO9SNa 632,0497 [M + Na] +, encontrado 632,0497.

3.3.8. Síntesis del compuesto 6

A una solución del compuesto 5 (0,837 mmol, 1 equivalente) en CH_2Cl_2 (30 ml) se le añadieron 12 ml de AcOH y polvo de zinc (396 mg). Después de 24 horas con

agitación, se añadieron 100 ml de CH_2Cl_2 y una solución acuosa saturada de $NaHCO_3$. La fase orgánica se secó con Na_2SO_4 anhidro. Después de filtrar y concentrar a presión reducida, el compuesto puro se aisló del crudo por columna cromatográfica, usando CH_2Cl_2/MeOH como mezcla de eluyentes (15:1), y el compuesto 6 se obtuvo como un sólido blanco con un rendimiento de 83 %. [α] 20D: -3,9 (c 0,64, CHCl3). RMN 1H (500 MHz, CDCl3): δ 5,48 (d, 1H, J4,3 = 3,0 Hz, H-4), 5,25 (t, 3H, J2,3 = J2,1 = 10,0 Hz, H-2, NH2), 5.09 (dd, 1H, J3,2 = 10.0 Hz, J3,4 = 3.0 Hz, H-3), 4.63 (d, 1H, J1,2 = 10.0 Hz, H-1), 4.25 (dd, 1H , J6a-5 = 6 Hz, J6a-6b = 12Hz, H6a), 4.17 (dd, 1H, J6b-5 = 6 Hz, J6b-6a = 12Hz, H6b), 4.08 (t, 1H, J5-6 = 6Hz , H-5), 3.39-3.20 (m, 2H, CH2NH2), 3.18-2.98 (m, 2H, SCH2), 2.21 (s, 3H, CH3), 2.11 (s, 3H, CH3), 2.10 (s, 3H, CH3), 2,01 (s, 3H, CH3). 13C RMN (125,7 MHz, CDCl3): δ 170,7 (CO), 170,2 (CO), 169,9 (CO), 169,7 (CO), 84,3 (C1), 74,9 (C5), 71,6 (C3), 67,3 (C4), 66,7 (C2), 61,7 (C6), 40,5 (CH2NH2), 30,4 (SCH2), 20,9 (CH3), 20,8 (2CH3), 20,7 (CH3). HRMS: Calc. para C16H25NO9SNa 430,1147 [M + Na] +, encontrado 430,1141.

3.3.9. Síntesis del compuesto 8

Se agitó una solución de espaciador bifuncional 5 (compuesto 7) (1 equivalente), TBTU (1 equivalente) y DIPEA (1,5 equivalente) en DMF seco (2,3 ml) bajo una atmósfera de argón a temperatura ambiente durante 15 min. Luego, se añadió una solución del derivado de aminoglucósido (compuesto 6) (0,49 mmol, 1 equivalente) y DIPEA (1,5 equivalentes) en DMF seco (5 ml) a temperatura ambiente. La mezcla se agitó durante 24 h, el disolvente se eliminó al vacío y luego se añadieron 50 ml de CH_2Cl_2 para procesar con una solución acuosa de HCl (1 M), NaHCO3 (saturado) y NaCl (saturado). Después de secar con Na_2SO_4 anhidro, se filtró, se evaporó y se purificó mediante cromatografía en columna ultrarrápida usando CH_2Cl_2/MeOH como una mezcla de eluyentes (30: 1). El

compuesto 8 se obtuvo como un almíbar amarillo con un rendimiento del 92%. [α] 20D: - 10,4 (c 0,64, CHCl3). RMN 1H (400 MHz, CDCl3): δ 7.29 (t, 1H, J = 6.5, NH) 5.43 (d, 1H, J4,3 = 3.3 Hz, H-4), 5.21 (t, 1H, J2,3 = J2,1 = 10.0 Hz, H-2), 5.04 (dd, 1H, J3,2 = 10.0 Hz, J3,4 = 3.3 Hz, H-3), 4.55 (d, 1H, J1,2 = 10.0 Hz, H-1), 4.19-4.07 (m, 2H, H-6a, H-6b), 3.99 (s, 2H, COCH2O), 3.96 (t, 1H, J5,6a = J5,6b = 6.8, H-5), 3.70-3.64 (m, 14H, 7 CH2O), 3.62-3.43 (m, 2H, CH2NH), 3.81 (t, 2H, J = 5.3 Hz, CH2N3), 2.97-2.71 (m, 2H, SCH2), 2,16 (s, 3H, CH3), 2,06 (s, 3H, CH3), 2,04 (s, 3H, CH3), 1,97 (s, 3H, CH3). 13C RMN (100 MHz, CDCl3): δ 170,3 (CO), 170,2 (CO), 170,1 (CO), 169,9 (CO), 169,6 (CO), 84,3 (C1), 74,8 (C5), 71,9 (C3), 70,9 (7CH2O), 70,3 (COCH2O), 67,2 (C4), 67,2 (C2), 61,6 (C6), 50,9 (CH2N3), 39,1 (CH2NH), 30,4 (SCH2), 20,8 (CH3), 20,7 (2CH3), 20,6 (CH3). HRMS: Calculado para C26H42N4O14SNa 689,2310 [M + Na] +, encontrado 689,2300.

3.3.10. Síntesis del compuesto 9

A una solución de $SnCl_2$ (1,5 equivalente) en THF seco (3 ml), se le añadieron PhSH (6 equivalente) y Et_3N (4,5 equivalente.). Luego se añadió el derivado de azida (compuesto 8) (0,15, 1 equivalente.) disuelto en THF (3 ml) y la reacción se agitó a temperatura ambiente hasta que el material de partida se consumió por completo (30 min). Después, la reacción se neutralizó con $NaHCO_3$ sólido, se agitó durante 5 min, se filtró y se disolvió en MeOH y se agitó durante 1 hora más. Finalmente, después de evaporar el disolvente en condiciones de vacío de presión reducida, el compuesto 9 se purificó mediante cromatografía en columna ultrarrápida con un rendimiento del 52%. [α] 20D: -4,8 (c 0,66, CHCl3). RMN 1H (400 MHz, CDCl3): δ 7.76 (t, 1H, J = 5.6, NH) 5.36 (d, 1H, J4,3 = 3.4 Hz, H-4), 5.12 (t, 1H, J2,3 = J2,1 = 10.0 Hz, H-2), 5.01 (dd, 1H, J3,2 = 10.0 Hz, J3,4 = 3.3 Hz, H-3), 4.59 (d, 1H, J1,2 = 10.0 Hz, H-1), 4.15-4.05 (m, 2H, H-6a,

H-6b), 4.04 (s, 2H, COCH2O), 4.00 (t, 1H, J5,6a = J5,6b = 6.8, H-5), 3,81 (t, 2H, J = 4,7 Hz, OCH2CH2NH2), 3,69-3,56 (m, 12H, 6 CH2O), 3,52-3,39 (m, 2H, CH2NH), 3,05-2,94 (m, 4H, CH2NH2, NH2), 2,92-2,67 (m, 2H, SCH2), 2,09 (s, 3H, CH3), 2,00 (s, 3H, CH3), 1,98 (s, 3H, CH3), 1,91 (s, 3H, CH3). 13C RMN (100 MHz, CDCl3): δ 170,5 (CO), 170,2 (CO), 170,0 (CO), 169,7 (CO), 84,3 (C1), 74,4 (C5), 71,9 (C3), 70,6-70,3 (CH2O), 69,6 (COCH2O), 67,2 (C4), 66,7 (C2), 61,4 (C6), 39,7 (CH2NH2), 39,1 (CH2NH) 30,2 (SCH2), 20,9 (CH3), 20,8 (CH3), 20,7 (CH3) 20,6 (CH3). HRMS: Calc. para C26H45N2O14S 641,2586 [M + H] +, encontrado 641,2576.

3.3.11. Síntesis del compuesto 10

Una solución de ácido 10,12-pentacosadiinoico (1 equivalente), TBTU (1 equivalente) y DIPEA (1,5 equivalentes) en DMF seco (1,6 ml) bajo una atmósfera de argón se agitó a temperatura ambiente durante 15 min. A continuación, se añadió una solución del derivado de aminoglucósido (compuesto 9) (0,16 mmol, 1 equivalente) y DIPEA (1,5 equivalentes) en DMF seca (0,8 ml) a temperatura ambiente. La mezcla de reacción se agitó durante 24 h, el disolvente se eliminó al vacío y la mezcla obtenida se purificó mediante cromatografía en columna ultrarrápida. [α] 20D: -7,1 (c 0,73, CHCl3). RMN 1H (400 MHz, CDCl3): δ 7.26 (t, 1H, J = 5.4, NHCO) 6.16 (t, 1H, J = 5.4, NHCO) 5.39 (d, 1H, J4,3 = 3.3 Hz, H-4), 5.18 (t, 1H, J2,3 = J2,1 = 10.0 Hz, H-2), 5.02 (dd, 1H, J3,2 = 10.0 Hz, J3,4 = 3.3 Hz, H-3), 4.53 (d, 1H, J1,2 = 10.0 Hz, H-1), 4.19-4.04 (m, 2H, H-6a, H-6b), 3.97 (s, 2H, COCH2O), 3.94 (t, 1H, J5 , 6a = J5,6b = 6.5, H-5), 3.69-3.54 (m, 12H, 6 CH2O), 3.54- 3.43 (m, 4H, OCH2CH2NH), 3.43-3.35 (m, 2H, SCH2CH2NH), 2.93- 2,68 (m, 2H, SCH2), 2,19 (t, 4H, J = 6,3 Hz, 2 CH2C≡C), 2,15-2,08 (m, 5H, COCH2CH2, CH3COO), 2,03 (s, 3H, CH3COO), 2,00 (s, 3H, CH3COO), 1,94 (s, 3H, CH3COO), 1,58 (t, 2H, J = 6,8 Hz, COCH2CH2), 1,51-1,40 (m, 4H, 2

CH2CH2C≡C), 1,36-1,29 (m, 26H, 13 CH2), 0,83 (t, 3H, J = 6,5 Hz, CH3CH2). 13C RMN (100 MHz, CDCl3): δ 173,2 (CO), 170,4 (CO), 170,1 (CO), 167,0 (CO), 169,9 (CO), 169,6 (CO), 84,2 (C1), 81,6 (CH2C≡C), 79,5 (CH2C≡C), 74,4 (C5), 71,7 (C3) 70,6-70,3 (CH2O), 69,9 (COCH2O), 67,2 (C4), 67,1 (C2), 65,3 (CH2C≡C), 65,2 (CH2C ≡C), 61,3 (C6), 39,1 (CH2NH), 38,9 (SCH2CH2), 36,6 (NHCOCH2CH2), 31,9 (CH2CH2CH3), 30,3 (SCH2), 29,6-28,3, (COCH2CH2CH2), 25,6 (NHCOCH2CH2) 22,6 (CH2CH3) , 20,7 (CH3), 20,6 (2CH3), 20,5 (CH3), 19,1 (2CH2C≡C), 14,1 (CH3CH2). HRMS: Calc. para C51H84N2O15SNa 1019,5485 [M + Na] +, encontrado 1019,5468.

3.3.12. Síntesis de anfifilo 2

El glucósido peracetilado (compuesto 10) disuelto en MeOH se trató con MeONa 1 M hasta que el pH alcanzó 8–9. Después de 30 min, la mezcla de reacción se neutralizó con una resina ácida (forma de hidrógeno Amberlites IR 120), se filtró y el disolvente se eliminó a presión reducida. El compuesto final (compuesto 2) se obtuvo con un rendimiento cuantitativo. [α] 20D: -10,8 (c 0,5, MeOH). RMN 1H (500 MHz, MeOD): δ 4,38 (d, 1H, J1,2 = 10 Hz, H-1), 4,03 (s, 2H, COCH2O), 3,79 (dd, 1H, J6a, 6b = 10 Hz, J6,5 = 6,8 Hz, H-6a), 3,75-3,62 (m, 14H, H-6b, H-4, 6 CH2O), 3,62-3,53 (m, 6H, OCH2CH2NH, SCH2CH2, H-2, H- 5), 3.50 (dd, 1H, J3,2 = 9.3 Hz, J3,4 = 3.8 Hz, H-3) 3.40-3.37 (t, 2H, J = 5.6 Hz, CH2NH), 2.92-2.74 (m, 2H , SCH2), 2.27 (t, 4H, J = 7 Hz, 2 CH2C≡C), 2.22 (t, 2H, J = 7.4 Hz, COCH2CH2), 1.63 (t, 2H, J = 6.3, COCH2CH2), 1.56- 1,48 (m, 4H, 2 CH2CH2C≡C), 1,47-1,27 (m, 26H, 13 CH2), 0,93 (t, 3H, J = 6,3 Hz, CH3). 13C RMN (125,7 MHz, MeOD): δ 175,0 (CO), 171,4 (CO), 86,3 (C1), 79,4 (CH2C≡C), 76,5 (CH2C≡C), 74,9 (C5), 70,6 (C3), 70,2 -69,9 (CH2O), 69,9 (COCH2O), 69,3 (C4), 69,1 (C2), 65,1 (CH2C≡C), 61,4 (C6), 39,0 (CH2NH), 38,3 (SCH2CH2), 35,7

(NHCOCH2CH2), 31,8 (CH2CH2CH3), 30,1 (SCH2), 29,8-28,2 (COCH2CH2), 25,6 (NHCOCH2CH2) 22,4 (CH2CH3), 20,7 (CH3), 20,6 (2CH3), 20,5 (CH3), 18,4 (2CH2C≡C), 13,2 (CH3CH2). HRMS: Calc. Para C43H76N2O11SNa 851.5062 [M + Na] +, encontrado 851.5049.

Síntesis de las nanomicelas pMicMan y pMicGal

El neoglicolípido (1 o 2 de la Figura 5) se disolvió en agua milli-Q por encima de su concentración micelar crítica determinada por el método del pireno. Brevemente, la solución transparente se sonicó durante 30 minutos en oscuridad. La solución coloidal obtenida se sometió a irradiación bajo una lámpara UV a 254 nm durante 1 hora, promoviendo así la fotopolimerización de las funcionalidades de diino en derivados poliméricos de poli (diacetileno).

Medida del tamaño de los nanovectores

El tamaño de partícula y la distribución de las micelas se midieron usando un sistema Zetasizer Nano ZS (Malvern Instruments). Se usó un rayo láser a una longitud de onda de 632,8 nm. El ángulo de dispersión se ajustó a 90º cuando se realizaron las mediciones. Los valores se presentan como el tamaño promedio de volumen ± la desviación estándar de tres valoraciones. El error en las mediciones se calculó como el ancho a la altura media del pico dividido por dos.

Determinación de CMC

La concentración micelar crítica (CMC) de las micelas se determinó utilizando pireno como sonda de fluorescencia extrínseca. La concentración de pireno se mantuvo constante (0.6 10-6M en THF), y la concentración de ambos compuestos varió de 1 x 10-

3 M a 0.5 x 10-6 M. Las mediciones de fluorescencia se llevaron a cabo a 25º C usando un espectrofluorómetro Eclipse Varian Cary. A la longitud de onda de excitación fija de 334 nm, los espectros de emisión se escanearon de 300 a 350 nm. Las relaciones de intensidad de fluorescencia de pireno a 339 y 335 nm (I339/I335, I1/I3) se calcularon y se representaron frente al logaritmo de concentración del neoglicolípido. El valor de CMC se determinó a partir de la intersección de las dos líneas tangentes.

Análisis TEM

Se depositaron 15 µl de una solución diluida de pMicMan y pMicGal en una rejilla de carbono. Luego se añadió 15 µl de una solución de acetato de uranilo al 2 % para teñir negativamente las micelas, y el exceso de líquido se eliminó con papel de filtro. Las imágenes TEM se registraron en aparatos Philips CM 10 o CM 200 con un voltaje de aceleración de 80 kV o 200 kV.

Encapsulación de fármacos en los nanovectores

La carga de sorafenib implicó la sonicación previa durante 30 minutos bajo oscuridad total a temperatura ambiente de los precursores micelares. Las micelas no polimerizadas se analizaron posteriormente por TEM y DLS y se mantuvieron durante 3 horas bajo luz ultravioleta (254 nm) para la polimerización. El precursor micelar está formado por un doble carbono que contiene dos triples enlaces que se polimeriza en contacto con la luz. Estos dobles enlaces triples forman enlaces covalentes entre sí, lo que da rigidez y consistencia a las micelas.

Sorafenib se cargó a baja y alta concentración en ambas nanomicelas. Las micelas cargadas con sorafenib a baja carga, corresponde con una proporción 1:2 de sorafenib con respecto a las micelas, es decir, se añade la mitad de sorafenib con respecto a las micelas.

En el caso de las micelas con carga alta, la proporción es de 1:1 con respecto a sorafenib. El fluoróforo, Rojo del Nilo, se añadió a baja carga. La cantidad conveniente de sorafenib o Rojo del Nilo se añadió a las micelas polimerizadas y se dejó durante 24 horas con agitación a 54 °C. Después de completar el procedimiento, el exceso del fármaco se eliminó de las micelas por centrifugación a 92 g durante 20 minutos repitiendo el proceso entre dos y tres veces. Se recogió el sobrenadante que contenía micelas cargadas, se liofilizó y se congeló a -80ºC.

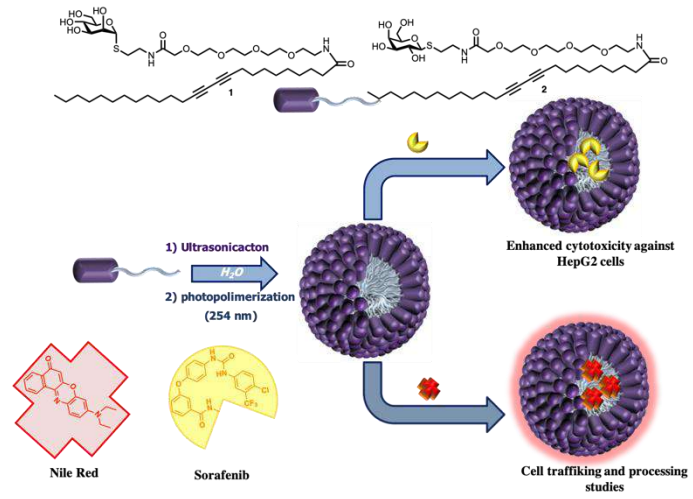

Figura 6. Representación esquemática de la formación de micelas fotopolimerizadas recubiertas de manosa y galactosa con la capacidad de dirigirse a receptores de manosa y asialoglicoproteína en las células del HCC.

Cuantificación de sorafenib mediante HPLC

Sorafenib se cuantificó utilizando el método de cromatografía líquida-espectrometría de masas en tándem (LC-MS/MS). La separación se realizó en una columna analítica Pursuit XRs Ultra C18 (2.8 µm, 100 mm × 2.0 mm) (Cat. 546695, Agilent Technologies, Santa Clara, EE. UU). La fase móvil consistió en una solución de acetonitrilo con ácido fórmico al 0.1% (Cat. 1.59002.2500, EMD Millipore Corporation,

Billerica, EE. UU.) (80/20 vol/vol orgánico/acuoso). Las curvas estándar fueron altamente lineales en el rango de 1–10.00 ng/mL.

Evaluación de la liberación espontánea de sorafenib a lo largo del tiempo de pMicMan y pMicGal

La liberación del fármaco a lo largo del tiempo de las nanomicelas que contienen sorafenib se llevó a cabo diluyendo estas en medio de cultivo y usando tubos de diálisis midi D-Tube TM (Cat. 71506-3, EMD Millipore Corporation, Billerica, Estados Unidos) La liberación se llevó a cabo a 37ºC para imitar condiciones experimentales *in vitro*. Las muestras fueron recogidas a diferentes tiempos 0, 15 min, 30 min, 60 min, 6 horas, 12 horas y 24 horas. El contenido restante del fármaco dentro de nanomicelas después de dichos tiempos se obtuvo rompiendo las micelas con DMSO. El fármaco se extrajo con una precipitación líquido/líquido con acetonitrilo.

Valoración de la incorporación celular de los nanovectores mediada por endosomas

La sonda de membrana FM 1-43 es un reactivo excelente para investigar los mecanismos de actividad endocítica. Las células se incubaron con FM1-43 (4 μM) (T3163, Thermo Fisher, Estados Unidos) durante 30 min. La inhibición de la actividad endocítica se realizó usando citocalasina D (8 μM) (C2618, Sigma-Aldrich) y dynasore (80 μM) (324410, Sigma-Aldrich) diluido en DMSO. Los inhibidores se añadieron 10 min antes que las nanomicelas. Los cubreobjetos se lavaron durante 5 minutos con una solución basal de Locke que contenía NaCl 140 mM, HEPES 10 mM, KOH 3 mM, $CaCl_2$ 2 mM, $MgCl_2$ 1 mM y glucosa 10 mM. El pH de la solución se ajustó a 7,3 con NaOH. Todos los productos químicos fueron adquiridos de Sigma. La fluorescencia se midió en un microscopio fluorescente invertido Axiovert 200 (Zeiss, Oberkochen, Alemania) equipado con un conjunto de filtros estándar para FM1-43 (XF115-2; Omega Optical). Las imágenes se capturaron con una cámara CCD ORCA-R2 (Hamamatsu

Photonics) controlada por el software HCImage (Hamamatsu Photonics, Hamamatsu, Japón). Las imágenes se adquirieron a una velocidad de 0,5 Hz, 1344×1024 píxeles (agrupadas 1 × 1), con un tiempo de exposición de 200 ms.

Medida del tráfico intracelular de pMicMan y pMicGal

El rojo del Nilo se ha utilizado principalmente para estudiar las gotas de lípidos. Sin embargo, también ha brindado información útil sobre el procesamiento endosomal y lisosomal. En este sentido, las nanomicelas se cargaron con rojo del Nilo (N3013, Sigma-Aldrich, Missouri, Estados Unidos). Rojo del Nilo se encontraba en las micelas en baja carga por lo que la cantidad de este marcador era la mitad del monómero. La presencia de nanopartículas en diferentes compartimentos celulares se evaluó utilizando un marcador endosomal (2 µg/ml) (anti-EEA1, E7659, Sigma-Aldrich, Missouri, Estados Unidos), lisosomal (10 µg/ml) (anti-Lamp1, L1418, Sigma-Aldrich) y de autofagosoma (1:50) (anti-BECN-1, sc-48341, Santa Cruz, Texas, Estados Unidos) mediante el procedimiento de tinción conjunta por inmunofluorescencia. Las células se incubaron con nanomicelas que contenían rojo del Nilo sobre un cubreobjeto durante 6 horas a 4ºC y 37ºC y en oscuridad. Tras la incubación, las células se lavaron dos veces con PBS (LO625-500, Biowest, Nuaillé, Francia) a 37ºC y se fijaron con 500 µl de formol (HT501128-4L, Misuri, Estados Unidos) durante 30 minutos a 4ºC. Antes del bloqueo se realizó los lavados correspondientes. Se realiza el bloqueo de sitios inespecíficos con una solución a base de BSA al 1% en PBS-T (250 µl) durante una hora a temperatura ambiente y en oscuridad. Se inició la incubación con los anticuerpos primarios en una solución de BSA al 5% en PBS-T en cámara húmeda en oscuridad y durante 12 horas. Tras la incubación con el anticuerpo primario y su posterior lavado, se inicia la incubación con el anticuerpo secundario en una solución de BSA al 5% en PBS-T durante 2 horas a temperatura ambiente y en oscuridad. Los cubreobjetos fueron colocados sobre

portaobjetos (J2800AMNZ, Thermo-Fisher, Massachusetts, USA). Se usó un medio de montaje que contenía DAPI para teñir el núcleo. Se utilizó un microscopio confocal de escaneo láser espectral Leica TCS-SP2 (Wetzlar, Alemania).

Impacto de la inhibición de la formación de autofagolisosomas en la actividad proapoptótica y antiproliferativa de sorafenib incorporado a pMicMan y pMicGal

El impacto del desarrollo de autofagolisosomas en presencia sorafenib contenido en las nanomicelas picMan y picGal en la apoptosis y la proliferación celular se evaluó utilizando cloroquina (50 μM), la cual previene la acidificación de los lisosomas, y 3-metiladenina (3Me-A) (5 μM) que inhibe la clase I y III PI3K y generación de autofagolisosoma. Los inhibidores se agregaron 2 horas antes de sorafenib. La inhibición de la actividad endocítica se realizó usando citocalasina D (8 μM) (Ref. C2618, Sigma-Aldrich) y dynasore (80 μM) (Ref. 324410, Sigma-Aldrich) diluido en DMSO. Los inhibidores se añadieron 10 min antes de las nanomicelas.

Ensayo de proliferación celular

La proliferación celular se midió como resultado de la incorporación de bromodeoxiuridina (BrdU) (11647229001; Roche Diagnostics, Indianápolis, Estados Unidos). Las células se sembraron y trataron en placas de 96 pocillos como se describió previamente. Se añadió BrdU (10 μM) 2 horas antes de la recolección de células para permitir su incorporación en el ADN. El ensayo incluye la desnaturalización de ADN con reactivo comercial FixDenat durante 30 minutos a temperatura ambiente para asegurar la unión adecuada del anticuerpo. Después las células se incubaron 90 minutos con un anticuerpo monoclonal anti-BrdU conjugado con peroxidasa de rábano. Las muestras se lavaron tres veces con solución salina tamponada con fosfato y se incubaron con una

solución de sustrato de peroxidasa que contenía peróxido de hidrógeno, luminol y 4-yodofenol durante 15 minutos a temperatura ambiente hasta el desarrollo del color. La absorbancia se midió a 370 nm usando 492 nm como longitud de onda de referencia usando un lector de microplacas Infinite 200 PRO (TECAN, Männedorf, Suiza).

Cuantificación de la muerte celular

La actividad de Caspasa-3/7 se determinó usando el ensayo Caspase-Glo® 3/7 (G8091, Promega, Madison, Estados Unidos). El ensayo proporciona un sustrato de caspasa luminogénica y Luciferasa UltraGlo™. El sustrato Caspase-Glo® 3/7 se agregó en el mismo volumen que lisados celulares que contienen proteínas totales, lo que resultó en la generación de una señal luminiscente de "tipo de brillo" que es directamente proporcional a la actividad de caspasa en la muestra. El volumen total se ajustó a 50 µl usando el tampón incluido en el ensayo.

Análisis estadístico

Todos los resultados se expresan como media±SEM de experimentos independientes (n=4-10). Los datos se compararon mediante el análisis de varianza (ANOVA) con la prueba de diferencia mínima significativa como análisis de comparación múltiple post hoc (homogeneidad de varianzas) o Games-Howell (no homogeneidad de varianzas). En el caso de que la prueba de Shapiro-Wilks mostrara una distribución no normal de los datos, se realizó la prueba Kruskal-Wallis no paramétrico acoplado al análisis post-hoc de U-Man-Whitney con la corrección de Finner. Los grupos significativamente diferentes ($p \leq 0.05$) se indicaron con letras diferentes (a, b, c, d, e o f).

RESULTADOS

Síntesis y caracterización de monómeros autoasociativos

La síntesis del tioglicósido autoassociativo derivado manosa **1** se ha realizado en 4 pasos sintéticos según el método publicado con anterioridad a partir de 2-aminoetil tiomanósido **13**, que se obtiene en un solo paso a partir de pentaacetato de manosa **11**. Para esta síntesis se siguió la síntesis ya descrita por el grupo del Dr. Khiar (Esquema 2) (85).

Para la síntesis de tiogalactopiranósido anfifilo **2**, se ha desarrollado una nueva ruta. Para asegurar la beta estereoselectividad necesaria, se siguió el método desarrollado por Gildersleeve, Dahmén (86), para el paso de tioglicosidación. La tioglicosilación catalizada por $BF_3.Et_2O$ usando 1,1-dimetil-2,2,2-tricloroetil N- (2-mercaptoetil) carbamato **3** como aceptor de glicosilo y galactosa pentaacetato **4** como donante de glicosilo, proporcionó el correspondiente β-tioglicósido **5** con un 70 % de rendimiento. A continuación, el tratamiento del derivado clorado **5** con zinc en presencia de ácido acético utilizando diclorometano como disolvente, da el 2-aminoetiltioglicósido **6** deseado, esquema 1. La formación del enlace amida con el espaciador bifuncional **7**, obtenido en tres pasos a partir de tetraetilenglicol (TEG), usando TBTU como agente de activación y DIPEA como base en DMF proporcionó el azido derivado **8** con un rendimiento del 92%. La reducción subsiguiente del grupo azido con tiofenol y cloruro de estaño, seguida por el acoplamiento de la amina resultante **9** con ácido pentacosadiinoico (PCDA) dio el neoglicolípido **10** con un buen rendimiento. Una desacetilación de Zemplen condujo al derivado de galactosa **2** con rendimiento cuantitativo (Esquema 1).

Síntesis y caracterización de micelas recubiertas de manosa y galactosa para la generación de los nanovectores pMicMan y pMicGal

Una vez obtenidos y caracterizados los monómeros 1 y 2 mediante espectroscopias de masas y RMN monodimensional (^{1}H, ^{13}C) y bidimensional (COSY y HETCOR), se determinaron por fluorescencia las concentraciones críticas micelar (CMC) correspondientes utilizando pireno como sonda (ver parte experimental) (86). La CMC del monómero **1** se determinó como 70±5 μM, mientras que la del monómero **2** fue 75 ± 5 μM.

Una vez determinadas las CMC se han realizado estudios sobre el autoensamblaje espontáneo de los monómeros **1** y **2** en agua para formar las micelas correspondientes y su posterior caracterización. En primer lugar, la formación de los sistemas nanomicelares dinámicos no polimerizados **MicMan** y **MicGal** se llevó a cabo mediante una simple dispersión del compuesto **1** y **2** en H_2O a una concentración superior a su CMC. Para minimizar la posible citotoxicidad de los monómeros diacetilénicos, los sistemas se dializaron con agua desionizada durante 48 horas. Posteriormente, las micelas dinámicas obtenidas (**MicMan**, **MicGal**, Figura 6a), se sometieron a irradiación UV (254 nm) durante 3 horas para la polimerización dando lugar a las micelas fotopolimerizadas finales (**pMicMan** y **pMicGal**). Cabe mencionar que, al entrar en contacto con el agua, los derivados diacetilenicos anfífilos se autoasocian espontáneamente de manera ordenada. En esta conformación, los grupos diino de moléculas adyacentes están dispuestos en una conformación y una distancia adecuadas, de modo que la reacción de polimerización tiene lugar por simple irradiación cuando la solución es sometida a una irradiación con luz UV a 254 nm. Esta polimerización que consiste en una reacción de adición 1,4 conduce a un polímero polidiacetilénico (PDA), con una alternancia de dobles y triples enlaces

conjugados que rigidfica el núcleo interno de las micelas, dando como resultado micelas polimerizadas estables, pMicMan-pMicGal (Figura 6a). Cabe señalar que esta polimerización procede sin el uso de un catalizador ni un iniciador de polimerización, lo que conduce directamente a nanosistemas puros sin la necesidad de ninguna etapa o etapas de purificación adicionales. El tamaño característico y las morfologías de las nanomicelas fotopolimerizadas **pMicMan** y **pMicGal** se determinaron mediante análisis de DLS y TEM (Figura 6b). El histograma de distribución de tamaño de las micelas polimerizadas en solución acuosa da una distribución multimodal con diámetros hidrodinámicos de 8 y 8,2 nm para **pMicMan** y **pMicGal** respectivamente, con una distribución de tamaño homogénea (índice de polidispersión, PDI, inferior a 0,3, Figura 6b). La morfología de las nanomicelas supramoleculares **pMicMan-pMicGal** visualizadas por TEM también se muestra en la Figura 2b. Los neoglicolípidos **1** y **2** se autoensamblan en solución acuosa en micelas esféricas y los diámetros observados en las micrografías TEM son similares a los obtenidos a partir de las mediciones de DLS. De manera interesante, estos resultados también indican que el tamaño de las micelas autoensambladas se corresponde al tamaño de los nanomateriales que se utilizan actualmente como nanovectores para la administración intracelular eficaz de fármacos.

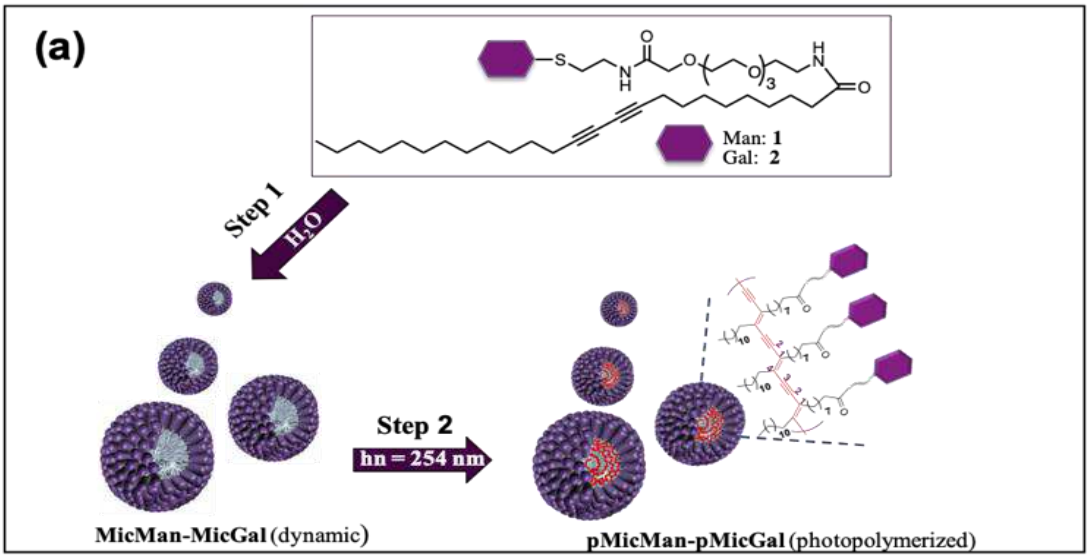
(a)
Man: 1
Gal: 2
Step 1
H2O
Step 2
hn = 254 nm
MicMan-MicGal (dynamic)
pMicMan-pMicGal (photopolymerized)

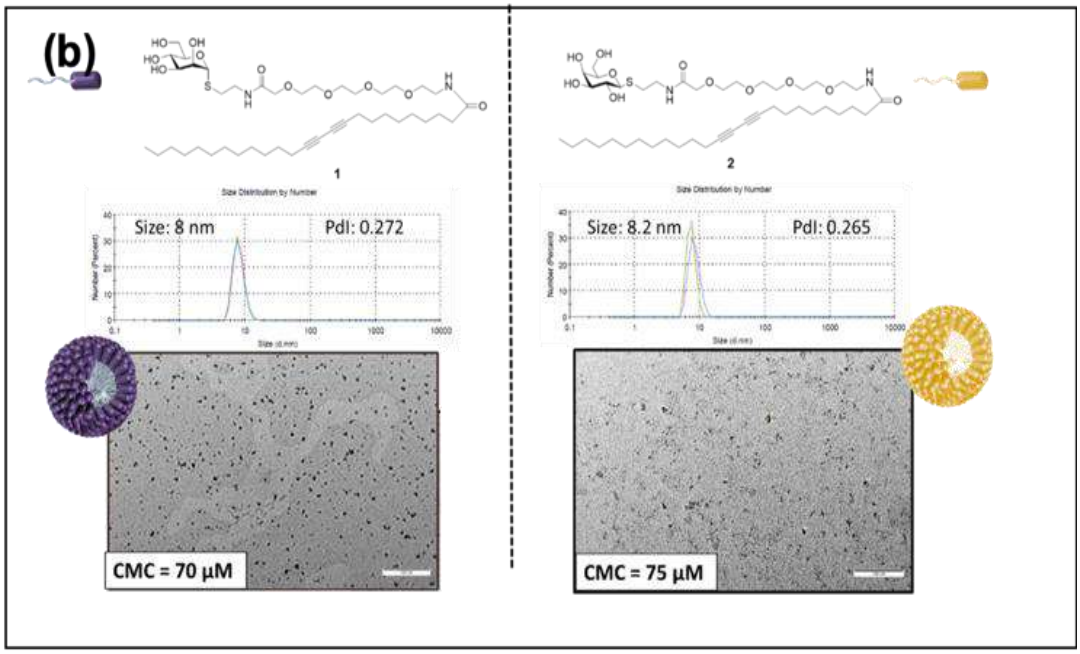
(b)
1
Size: 8 nm
PdI: 0.272
CMC = 70 µM
2
Size: 8.2 nm
PdI: 0.265
CMC = 75 µM

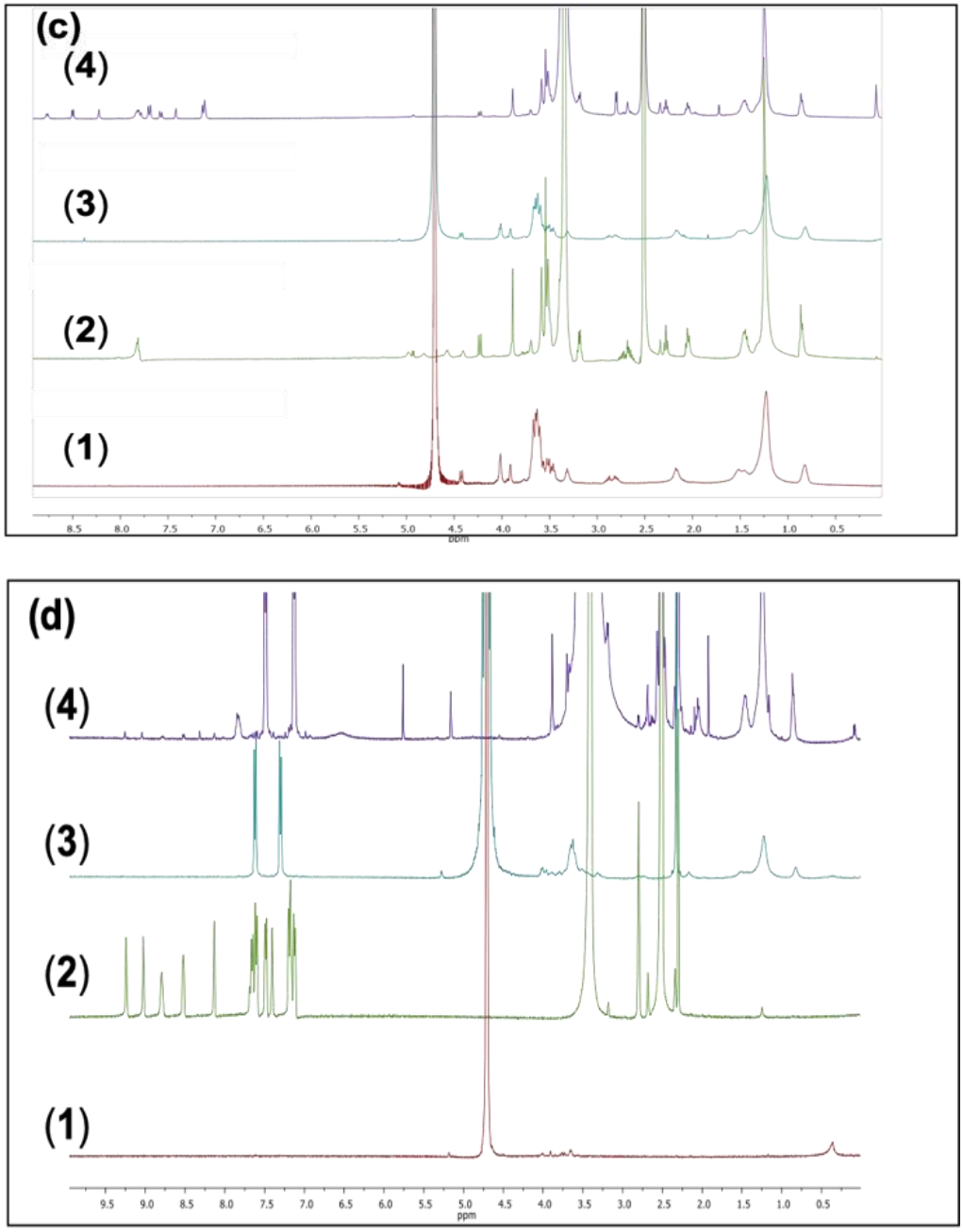

Figura 7 Síntesis y caracterización estructural y funcional de las micelas. (a) Procedimiento para la síntesis de nanomicelas dinámicas (**MicMan** y **MicGal**) y fotopolimerizadas (**pMicMan** y **pMicGal**). Paso 1) Autoensamblaje supramolecular en micelas dinámicas (**MicMa**n y **MicGal**), promovido por sonicación de los neoglicolípidos en agua. Paso 2) Fotopolimerización intermolecular del neoglicolípido y formación de micelas estáticas homogéneas (**pMicMan** y **pMicGal**). (b) Distribución de tamaño de las micelas estáticas **pMicMan** y **pMicGal** determinada por DLS y TEM, dentro de las imágenes TEM se indican la CMC de las micelas. (c) Estudio por RMN de protón de la inclusión de sorafenib dentro de la cavidad hidrófoba de **pMicGal**. (a) Espectro de **pMicGal** vacía registrado en D_2O, (2) Espectro de **pMicGal** registrado en DMSO-d_6 (3) Espectro del complejo de inclusión **pMicGal-Sorafenib** registrado en D_2O, (4) Espectro del

complejo de inclusión **pMicGal-Sorafenib** registrado en DMSO-d_6. (d) Estudio por RMN de protón de la inclusión del tosilato de Sorafenib dentro de la cavidad hidrofóbica de **pMicMan**. (1) Espectro del tosilato de sorafenib registrado en D_2O, (2) Espectro del tosilato de sorafenib registrados en DMSO-d_6 (3) Espectro del complejo de inclusión **pMicMan-tosilato de sorafenib** registrado en D_2O, (4) Complejo de inclusión **pMicMan-tosilato de sorafenib** registrado en DMSO-d_6

Carga de sorafenib y eficacia de encapsulación de las nanomicelas pMicMan y pMicGal

pMicMan y **pMicGal** presentan una cavidad interna hidrofóbica formada por la cola hodrocabonada del neoglicolípido, rodeada por restos de PEG y azúcar. El área hidrófoba interna de estas micelas puede albergar moléculas huésped hidrófobas como agentes citotóxicos, agentes de imagen, nanopartículas metálicas u otras biomoléculas [30]. Como tales, **pMicMan** y **pMicGal** pueden operar como nanovectores generales para fármacos o candidatos a fármacos poco hidrosolubles que, actualmente, representan el 40-70% de nuevas entidades químicas descubiertas mediante cribado de alto rendimiento. Para este estudio, se añadió sorafenib a una solución de micelas **pMicMan** o **pMicGal** en agua milliQ, y se agitó durante 24 h a 54 ° C. La mezcla así obtenida se centrifugó dos veces a 1500 rpm durante 20 minutos para eliminar el fármaco libre y el sobrenadante se liofilizó y se pesó.

La cantidad de droga incorporada se determinó mediante HPLC-LS tras la lisis con DMSO del nanovector cargado con fármaco, así como mediante la diferencia de masa entre la micela cargada y la micela vacia. El contenido de fármaco incoporado (DL) y la eficiencia de encapsulación (EE) se calcularon a partir de las siguientes ecuaciones (1) y (2).

$$EE(\%) = \frac{Carga\ actual\ de\ la\ droga}{Carga\ teórica} x100 \quad (1)$$

$$DL(\%) = \frac{Cantidad\ total\ de\ droga\ añadida}{PM\ del\ monómero\ 1 + PM\ de\ la\ micela} x100\ (2)$$

pMicMan presenta un contenido máximo de DL del 63% y un EE del 50% para sorafenib. Asimismo, **pMicGal** presenta una DL máxima del 42% y una EE del 43%. Sin embargo, hemos comprobado que, utilizando un contenido de carga más bajo, 18% para **pMicMan** y 13% para **pMicGal**, se puede lograr una liberación controlada sostenible. Se obtuvo una confirmación adicional de que los fármacos están realmente encapsulados por las micelas mediante el análisis de protón (^{1}HNMR), como se muestra en la figura 6 (c) utilizando **pMicGal** como nanoportador hidrófobo protegido. Los espectros ^{1}HNMR de micelas **pMicGal** vacías, micelas **pMicGal-sorafenib** y sorafenib libre se registraron en D_2O y en DMSO-d_6 (Figura 6c). Como se muestra en la Figura 6c1 y 6c2, los espectros de las micelas vacías en D_2O y DMSOd_6 contienen básicamente las señales, correspondientes al monómero **2**. El espectro de las micelas **pMicGal** cargadas con sorafenib registrado en D_2O es muy similar al de las micelas vacías (Figura 6c3), sin ninguna señal característica de sorafenib. Sin embargo, al registrar el espectro de las micelas cargadas con sorafenib en DMSOd_6 (Figura 6c4), se observan señales adicionales en la zona aromática que coinciden con el espectro de sorafenib junto con las señales de la micela.

Aún más indicativos de la capacidad de estas nanomicelas para encapsular sorafenib, son los experimentos llevados a cabo con el tosilato de sorafenib realizando la incorporación de este en ambos vectores. Como ejemplo ilustrativo, la figura 6d recopila los resultados con el nanovector **pMicMan** y todilato de sorafenib. La diferencia observada en este caso respecto a la inclusión de sorafenib en **pMicGal** es la aparición de un sistema AB en la zona aromática cuando se toma el espectro en agua deuterada

(compárese figura 6c3 y 6d3). Este sistema, que corresponde a los protones aromáticos del grupo tosilo, indica claramente que las micelas son capaces de disociar sorafenib del grupo tosilo y dejar encapsulado sorafenib sin el grupo tosilo.

Tomados en conjunto, estos resultados muestran claramente la capacidad de las micelas para funcionar como nanocontenedores para almacenar compuestos altamente hidrofóbicos dentro de su área hidrofóbica protegida.

Expresión del MR y ASGPR en células HepG2 y Huh7

Se ha demostrado que MR (87) y ASGPR (88) se expresan principalmente en la superficie de las células HepG2. Nuestro estudio confirmó que MR (Figura 7a) y ASGPR (Figura 7b) se expresan en hepatocitos humanos primarios, células HepG2 y Huh7. La expresión de MR es mayor que la expresión de ASGPR.

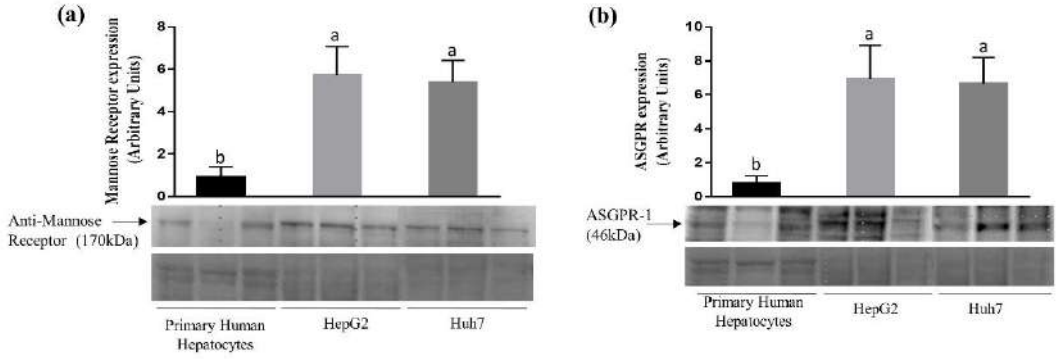

Figura 8. Expresión de MR (a) y ASGPR (b) en hepatocitos humanos primarios, células HepG2 y Huh7. Se utilizaron diferentes pases de HepG2 y Huh7. La expresión de MR y ASGPR se evaluó mediante análisis de Western-Blot descrito en Material y Métodos.

Liberación de sorafenib en pMicMan y pMicGal con baja y alta saturación de fármaco

En primer lugar, se determinó la estabilidad de nuestras preparaciones según el grado de saturación con sorafenib. La administración de sorafenib (10 µM) con saturación alta y baja de **pMicMan** con sorafenib liberó 76% y 35% de su contenido de fármaco al medio de cultivo (24 horas), respectivamente (Figura 8a). La administración de sorafenib (10 µM) con saturación de **pMicGal** con sorafenib alta y baja liberó 77% y 39% de su contenido al medio de cultivo (24 horas), respectivamente (Figura 8b). En consecuencia, se seleccionó un bajo grado de saturación de ambas nanomicelas para dilucidar sus actividades proapoptóticas y antiproliferativas.

También estudiamos la reducción del pH de 7,5 a 4,5 y observamos un aumento adicional en la liberación de sorafenib del 7% y el 24% para **pMicMan** y **pMicGal** (24 horas), respectivamente (Figura 8c y 8d).

(a)

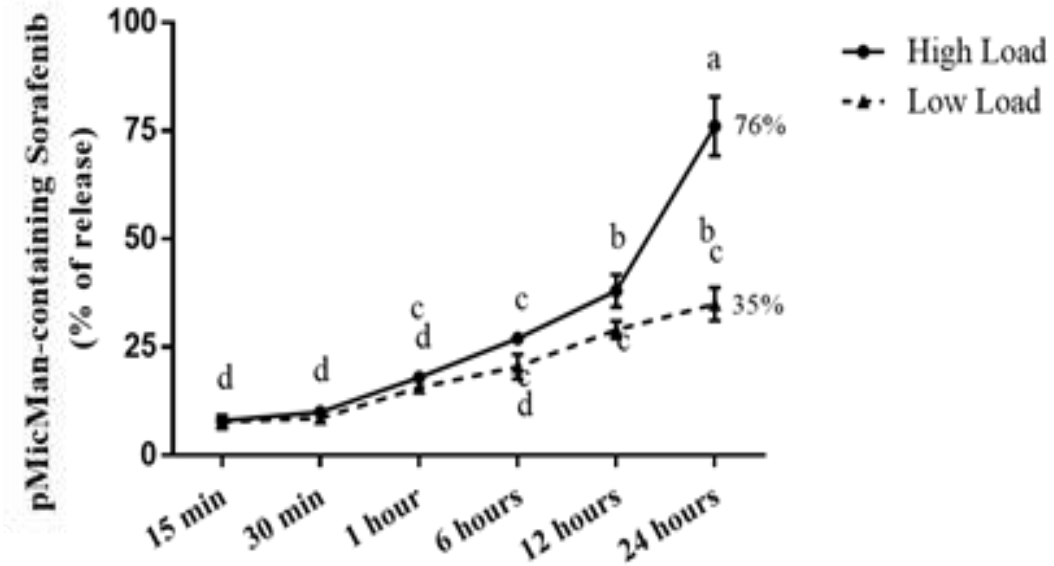
pMicMan-containing Sorafenib
(% of release)
100
75
50
25
0
15 min
30 min
1 hour
6 hours
12 hours
24 hours
High Load
Low Load
76%
35%

(b)

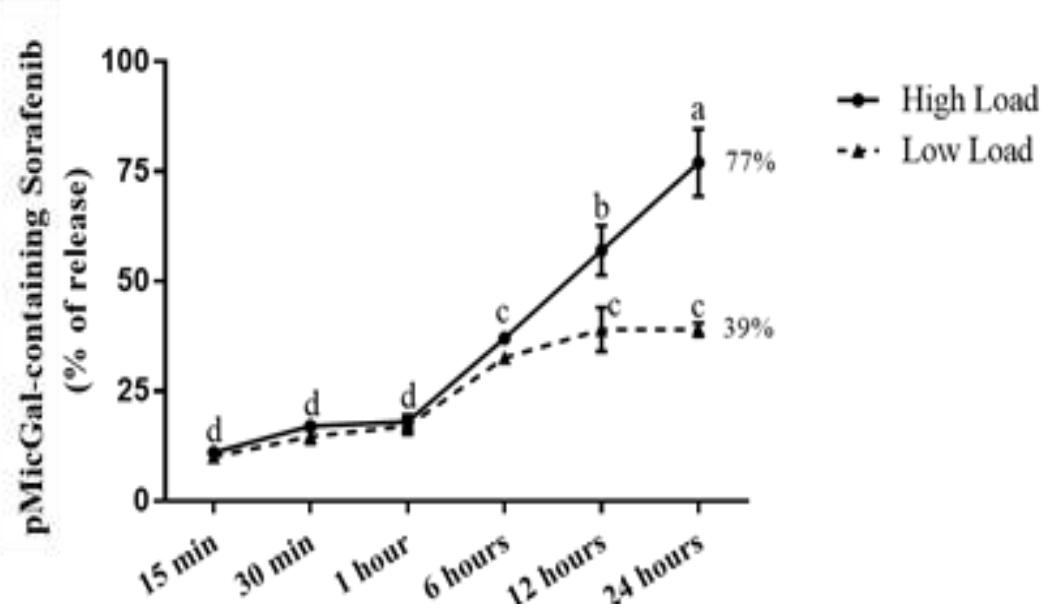
pMicGal-containing Sorafenib
(% of release)
100
75
50
25
0
15 min
30 min
1 hour
6 hours
12 hours
24 hours
High Load
Low Load
77%
39%

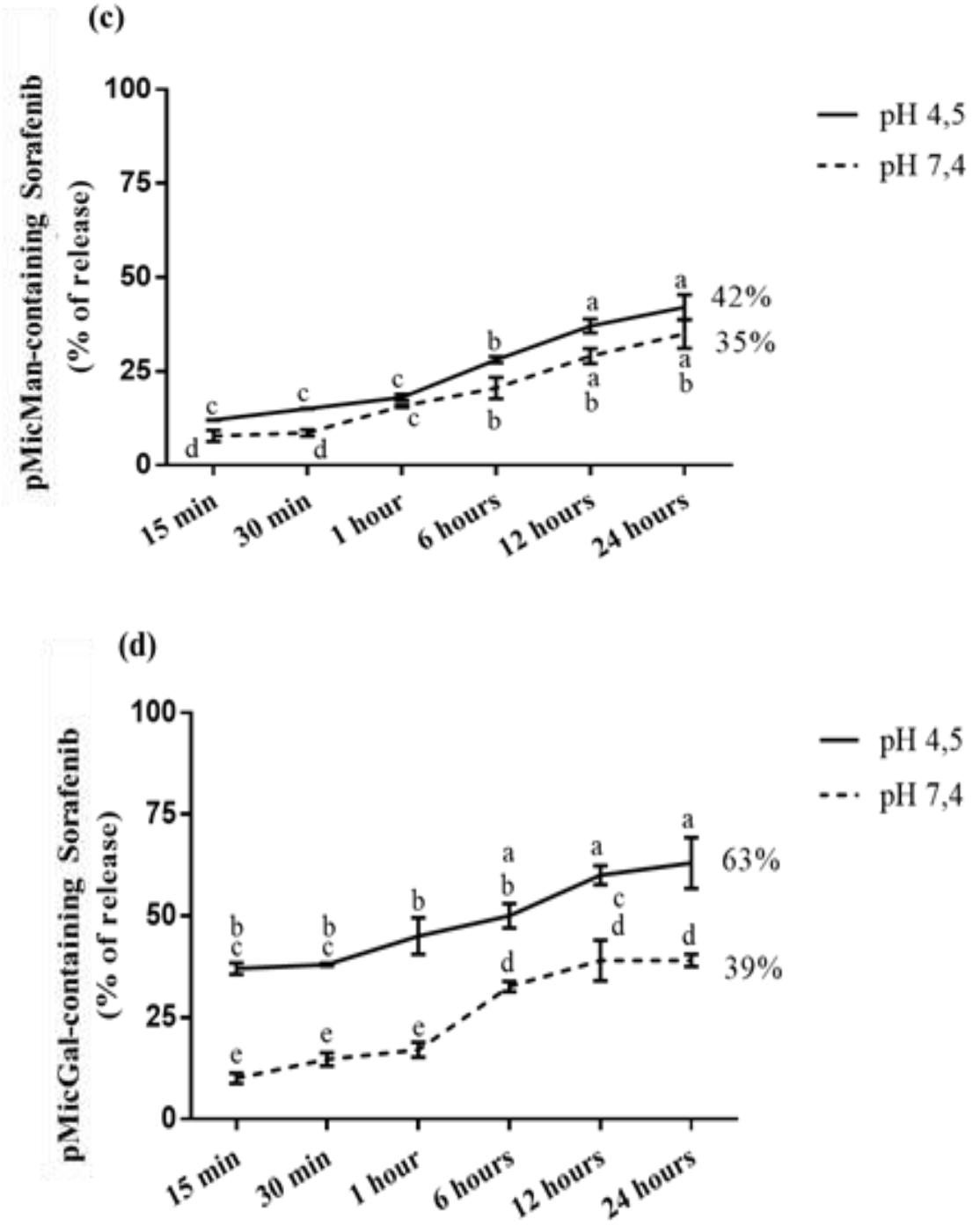

Figura 9. Cinética de liberación del sorafenib *in vitro* de sa carga alta y baja de **pMicMan** (a) y **pMicGal** (b). Una carga baja a pH 7,4 y 4,5 de **pMicMan** (c) y **pMicGal** (d). El sorafenib se midió usando cromatografía líquida-espectrometría de masas en tándem (LC-MS/MS).

Impacto de pMicMan y pMicGal cargado con sorafenib en la actividad de la caspasa-3 y la proliferación celular

Anteriormente nuestro grupo de investigación ha demostrado que la inducción de estrés ER por sorafenib (10 µM) indujo la apoptosis y redujo la proliferación celular en las células HepG2 (88). La administración de **pMicMan** con sorafenib (**pMicMan-sorafenib**) pero no pMicGal con sorafenib (**pMicGal-Sorafenib**) (10 y 20 nM) fue capaz de aumentar la caspasa-3 (Figura 9a) o reducir la proliferación celular (Figura 9b) en células HepG2 en comparación con las falta de actividad en las células tratadas con fármaco no vectorizadas correspondientes (24 horas) ($p \leq 0,05$).

Los valores de actividad caspasa-3 e incorporación de BrdU inducida por **pMicMan** y **pMicGal** con sorafenib se obtuvieron después de restar el valor correspondiente de nanomicelas vacías sin fármaco (Figura 9a y 9b, respectivamente).

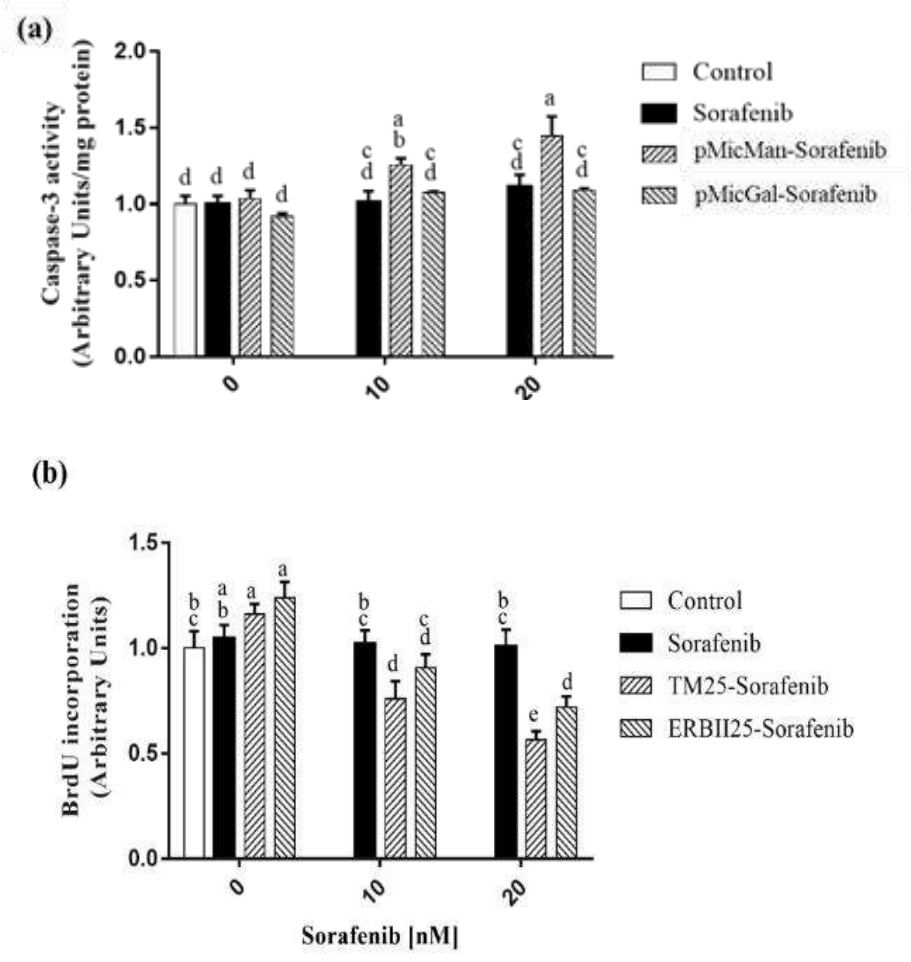

Figura 10. Inducción de caspasa-3 (a) y reducción de la proliferación celular (b) por sorafenib no vectorizado, sorafenib que contiene **pMicMan** y **pMicGal** en células HepG2. La actividad caspasa-3 y la incorporación de BrdU se determinaron según se describe en la sección de Material y Métodos.

La línea celular Huh7 fue tratada en las mismas condiciones de sorafenib. La administración de sorafenib a través de los vectores de transporte **pMicMan** y **pMicGal**, indujo un aumento en la caspasa-3 en comparación con el fármaco no vectorizado (Tabla 1).

Caspasa-3 (Arbitrary Units/mg protein)			
	0 nM	10 nM	20 nM
Control	1±0,19		
Sorafenib	1±0,18	1±0,10	1,03±0,08
pMicMan-Sorafenib	1,04±0,09	1,11±0,11	1,14±0,12
pMicGal-Sorafenib	1,06±0,14	1,07±0,10	1,09±0,11

Tabla 3. Actividad caspasa-3 inducida por sorafenib no encapsulado, pMicMan con sorafenib (**pMicMan-Sorafenib**) y pMicGal con sorafenib (**pMicGal-Sorafenib**) en células Huh7.

Tráfico de pMicMan y pMicGal en células HepG2

Se utilizó FM 1-43 para evaluar la internalización endosomal de **pMicMan** y **pMicGal** en células HepG2 (Figura 10a). Se utilizaron micelas vacías para estos experimentos. La inhibición de los mecanismos de internalización de la endocitosis se evaluó mediante dynasore y citocalasina D. **pMicMan** y **pMicGal** se incorporaron activamente a través de mecanismos endosomales, siendo su incorporación más afectada por la inhibición de dinamina usando dynasore que por la inhibición de la polimerización de actina usando citocalasina D (Figura 10b).

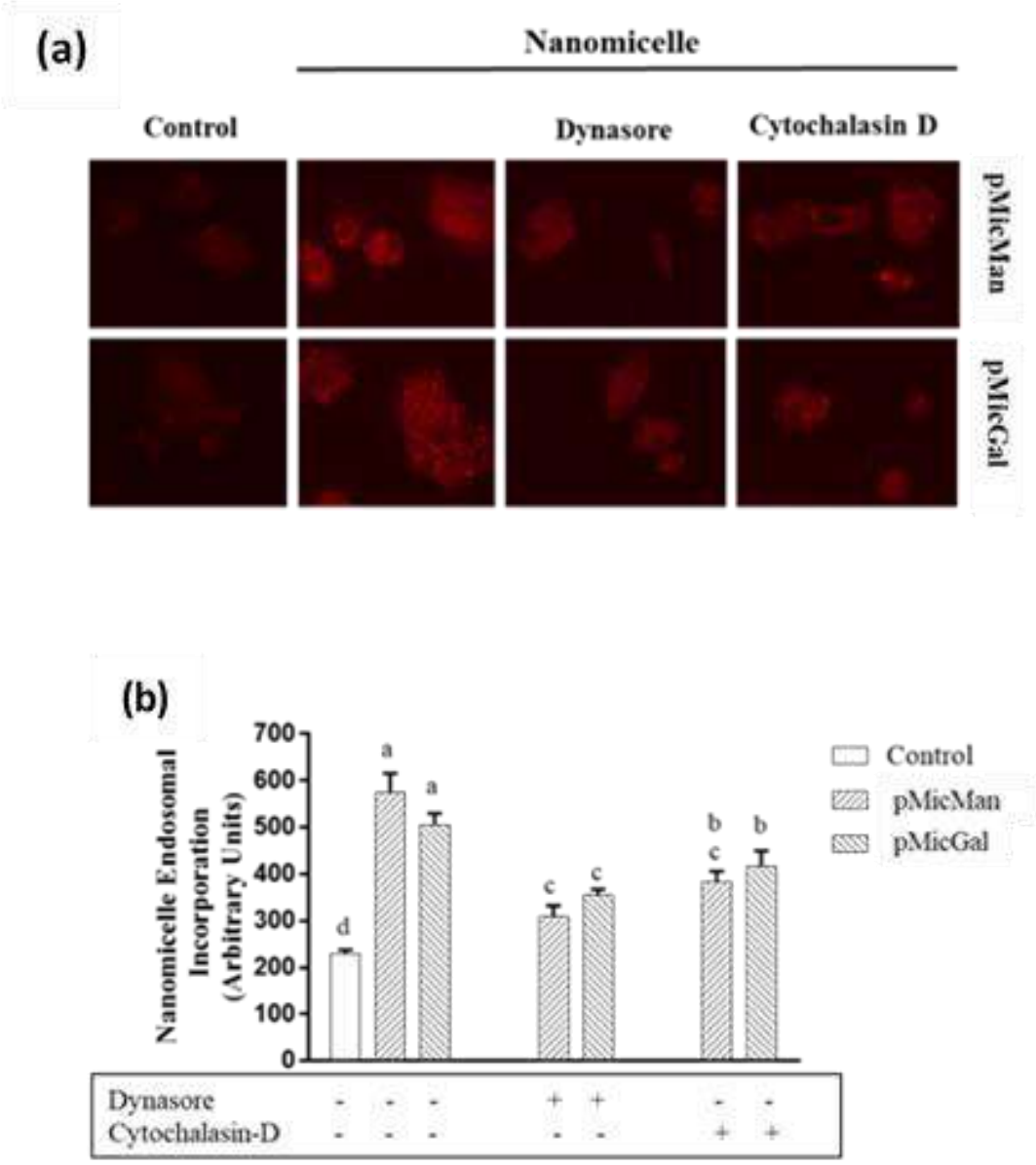

Figura 11.

(a) Incorporación endosomal de pMicMan y pMicGal por inmunofluorescencia usando nanomicelas que contienen FM 1-43. (b) La incorporación endosomal se inhibió preincubando las células durante 10 minutos con dynasore (80 µM) o citocalasina D (8 µM).

La incorporación de rojo del Nilo a nanomicelas permite valorar el grado de incorporación celular y tráfico a compartimentos específicos utilizando marcadores

endosomales (anti-EEA1), lisosomales (anti-Lamp1) y autofagosómicos (anti-BECN1) mediante inmunofluorescencia. La incorporación endosomal de **pMicMan** y **pMicGal** se inhibió a 4ºC en comparación con la observada a 37ºC (Figura 11a). Además, los resultados mostraron que **pMicMan** se colocalizó extensamente a nivel endosómico y lisosómico, mientras que **pMicGal** se colocalizó extensamente a nivel autofagolisosómico en relación con las contrapartes correspondientes (6 horas) en HepG2 (Figura 11b).

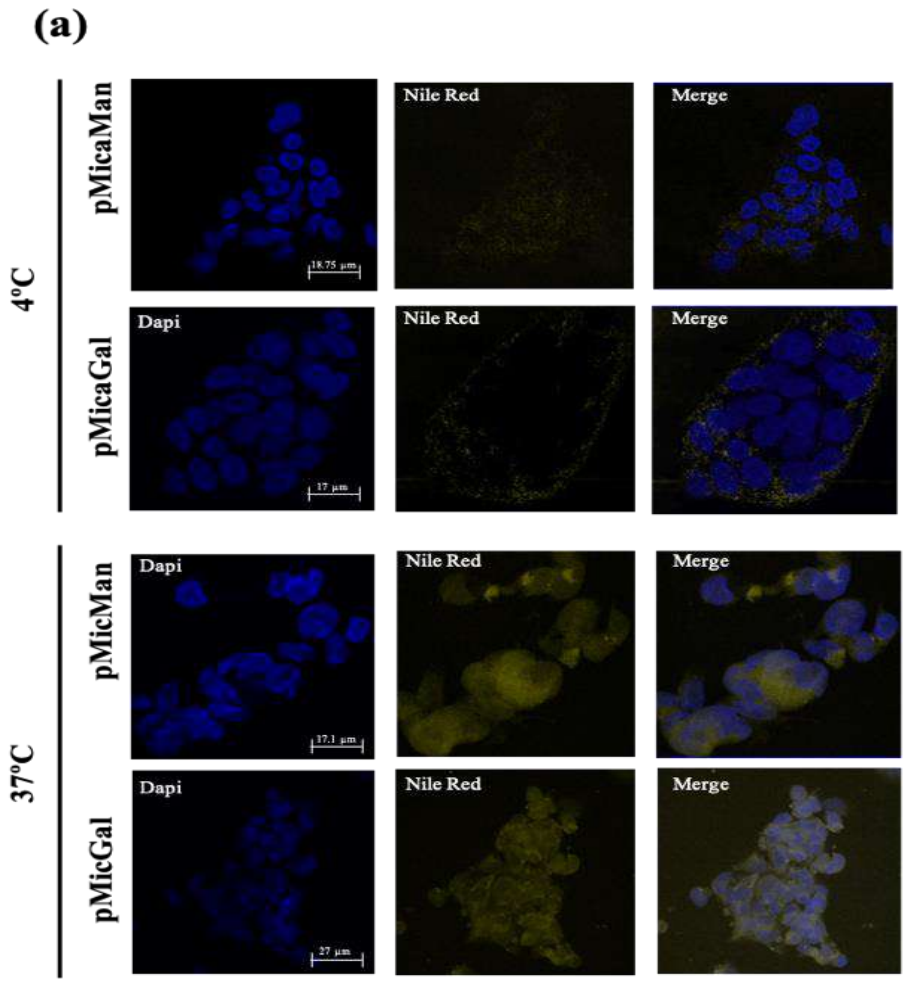

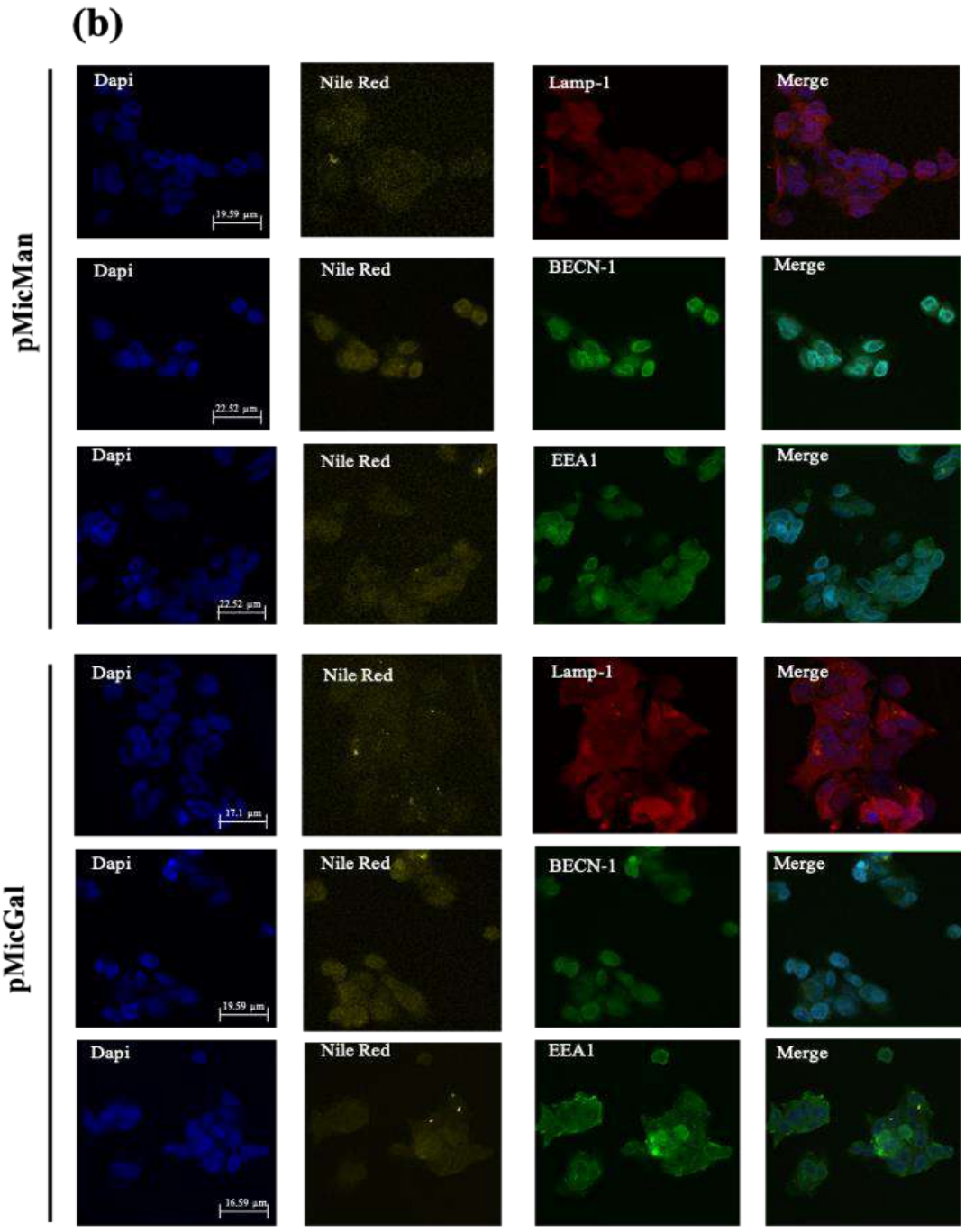

Figura 12. Tráfico de **pMicMan** y **pMicGal**. El rojo del Nilo se utilizó para proporcionar información sobre el procesamiento endosómico y lisosómico. La incubación de las células a 4ºC bloqueó la incorporación de nanomicelas. La presencia de nanopartículas en diferentes compartimentos celulares se evaluó utilizando marcadores endosomales, lisosomales y autofagosomas mediante procedimiento de colocalización por imunofluorescencia. El procedimiento para la incorporación de la sonda y la inmunofluorescencia se describe en la parte experimental. Aumentos x60

Impacto del procesamiento lisosomal de pMicMan y pMicGal cargados con Sorafenib en sus propiedades proapoptóticas y antiproliferativas

Los efectos de diferentes inhibidores implicados en la degradación de proteínas, como la cloroquina, 3-metiladenina (3Me-A), dynasore y citocalasina D sobre la actividad caspasa-3 y proliferación celular se ensayaron en nanomicelas que contienen sorafenib (20 nM) (Figura 12). La cloroquina previene la acidificación de los lisosomas y, en consecuencia, la degradación de las proteínas (89), lo que además puede implicar el bloqueo del último paso de la macroautofagia. De manera diferente, la 3Me-A es un inhibidor de la PI3K de clase I que afecta la supervivencia celular, pero también bloquea eficazmente una etapa temprana de la autofagia al inhibir la PI3K de clase III (18). Las células se vieron afectadas por la inhibición de dinamina usando dynasore y la citocalasina D inhibe la polimerización de actina. Los datos mostraron que la cloroquina, 3-MeA y citocalasina D aumentaron la caspasa-3 (Figura 12a) en las células tratadas con **pMicMan** y **pMicGal** cargadas con sorafenib. Cloroquina, 3-MeA, dynasore y citocalasina D redujeron la incorporación de BrdU (Figura 12b) en las células tratadas con **pMicMan** y **pMicGa**l cargadas con sorafenib.

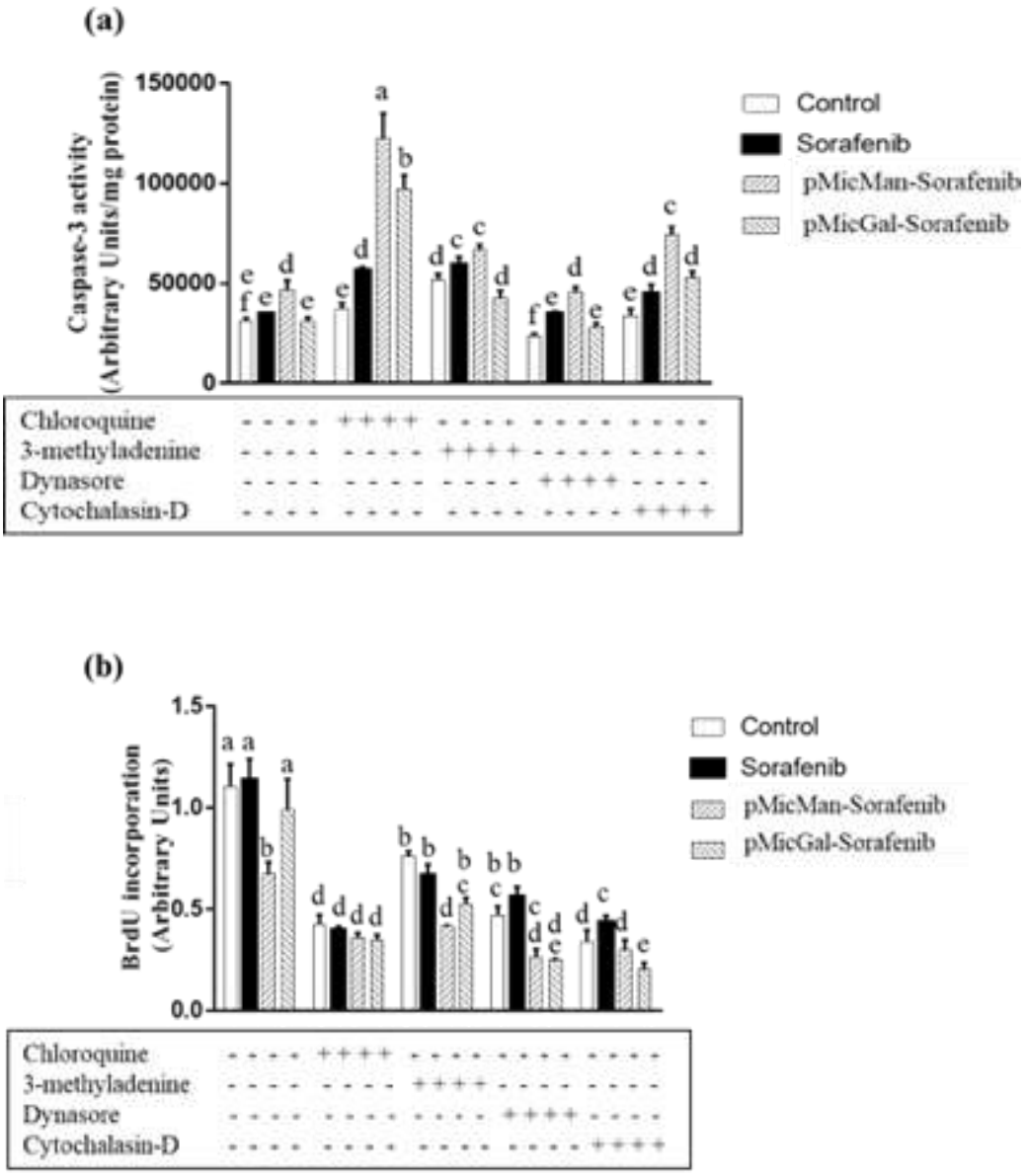

Figura 13. Impacto del procesamiento lisosomal de **pMicMan** y **pMicGal** en la actividad caspasa-3 (a) y proliferación celular (b) en células HepG2. Las células se incubaron con cloroquina (50 µM) y 3-metiladenina (3Me-A) (5 µM) 2 horas antes de la administración de pMicMan y pMicGal que contenían sorafenib (20 nM), y de dynasore (80 µM) y citocalasina D (8 µM) administrados 10 min antes de la administración de los fármacos. La actividad caspasa-3 y la incorporación de BrdU se determinaron según se describe en la sección de Material y Métodos.

DISCUSIÓN

Discusión

El HCC representa el 80% de las neoplasias hepáticas primarias que aparecen principalmente en el contexto de la cirrosis hepática crónica. Es la sexta neoplasia más frecuente (749.000 casos nuevos/año), la tercera causa de muerte por cáncer (692.000 casos nuevos/año) y el 7% de las neoplasias malignas registradas (5). Las infecciones virales por VHB y VHC, alcohol, aflatoxina B1, EHNA, tabaco, diabetes y enfermedades congénitas son factores de riesgo con incidencia geográfica variable que se han asociado con la inducción y progresión del HCC (90). Los tratamientos curativos (radiofrecuencia, resección hepática y trasplante hepático ortotópico) están indicados durante las primeras etapas de la enfermedad (BCLC 0-A) que resultan en una alta expectativa de supervivencia a 5 años (50-80%, 60 meses) (91). Hoy en día, sin embargo, dos tercios de los pacientes son diagnosticados en estadios más avanzados de la enfermedad (BCLC B-C) (89-92, 95). El sorafenib sigue siendo el único tratamiento sistémico aprobado para el HCC avanzado (BCLC C). Este fármaco se dirige a los receptores de tirosina quinasa y serina/treonina quinasas Raf involucradas en las vías de señalización de supervivencia celular (93). El sorafenib es el tratamiento estándar de primera línea para el estadio avanzado de HCC que ha demostrado un aumento de la tasa de supervivencia general en dos ensayos a gran escala, como el ensayo clínico SHARP, con una mediana de supervivencia general de 10,7 meses con sorafenib frente a 7,9 meses con placebo (riesgo cociente, 0,69; p<0,001) (94), y el ensayo clínico de Asia-Pacífico con una mediana de SG de 6,5 versus 4,2 meses, respectivamente (cociente de riesgo, 0,68; P = 0,014) (95).

La naturaleza hidrofóbica de sorafenib implica su baja biodisponibilidad (8,43%) y, en consecuencia, la necesidad de tratamiento con dosis altas (96) que, junto con la falta de especificidad celular, son responsables de la toxicidad sistémica y las complicaciones

que incluyen hipertensión, hemorragia y problemas gastrointestinales que implican la interrupción del tratamiento, pero generalmente se relacionan con la eficacia clínica (97).

La reducción del perfil de efectos secundarios se puede lograr mediante el uso de sistemas de administración de fármacos pasivos, capaces de aumentar la permeabilidad y el tiempo de circulación y la acumulación preferencial en el tejido tumoral a través del llamado efecto de permeación y retención (efecto EPR). Este efecto es una consecuencia del aumento de la vascularización, la arquitectura vascular defectuosa y el drenaje linfático deficiente. Diferentes terapias basadas en nanopartículas, incluidos liposomas, partículas basadas en albúmina, micelas poliméricas y nanopartículas poliméricas administradas a los pacientes, pueden mejorar la seguridad y eficacia de los fármacos (53,98,99). En este sentido, Jiu et al. han desarrollado y comparado varios modelos de nanopartículas biocompatibles cargadas con sorafenib, como los liposomas de ácido poli(láctico-co-glicólico) (PLGA), 1,2-dipalmitoil-sn-glicero-3-fosfocolina (DPPC), y liposomas hidrófobos de DPPC recubiertos con quitosano modificado (HMC) para optimizar la administración de fármacos y la inducción de la muerte celular en células de carcinoma de células renales con histología de células metastásicas humanas (100). El estudio mostró que las partículas de PLGA cargadas con sorafenib y los liposomas de DPPC recubiertos con HMC exhibieron una destrucción celular significativamente aumentada en comparación con sorafenib solo en concentraciones más bajas (100). Sin embargo, sorafenib incorporado a nanopartículas de dextrano y PLGA, así como al silicio poroso funcionalizado con el tripéptido arginina-glicina-ácido aspártico (RGD) como ligando, mostró una actividad antiproliferativa similar a la del sorafenib en el colangiocarcinoma humano [HuCC -T1] (101) y células endoteliales EA.hy926 (102), respectivamente. Otro estudio mostró que la estrategia basada en la incorporación de sorafenib en microesferas de PLGA co-encapsulando en nanopartículas ferromagnéticas

de óxido de hierro redujo la proliferación celular *in vitro* y redujo la densidad de microvasos y el área tumoral después de la infusión transcatéter en un modelo experimental basado en el ortotópico implantación de células de hepatoma de rata McA-RH7777 en ratas (103).

La generación de nanodiamante recubierto de lípidos anfifílicos, como una nueva nanopartícula derivada de carbono, que incorpora sorafenib demostró un aumento de la concentración de sorafenib de 14,95 veces en el tejido tumoral y un efecto de inhibición eficaz del crecimiento tumoral en modelos de xenoinjerto tumoral mediante inyección subcutánea de BGC-823 células de cáncer gástrico en ratones Balb c inmunodeprimidos (104). También se han desarrollado nanopartículas poliméricas duales cargadas con sorafenib. En este sentido, un núcleo de nanopartículas de polímero híbrido altamente complejo y multifuncional constituido por PLGA y funcionalizado con nanocristales de oro que sirven como andamios para que la doxorrubicina cargada sea recubierta adicionalmente con fosfolípidos ordinarios y fosfolípidos PEGilados (proporción 7/3) los cuales encapsulan sorafenib y PEG-etiquetado con fluoróforos Cy7 para obtener imágenes por fluorescencia del infrarrojo cercano (NIRF), da lugar a una viabilidad celular reducida en líneas celulares de cáncer de vena umbilical humana (HUVEC) (42%) y colon (LS174T) (72%) (24 horas), así como acumulación en el tumor derivado de LS174T en ratones desnudos (105). Otra nanopartícula combinada doble constituida por behenato de glicerilo, fosfatidilcolina de huevo y poloxámero 188 que incorporan sorafenib mostró un comportamiento farmacocinético satisfactorio tras la administración *in vivo* de acuerdo con la liberación sostenida del fármaco y la alta biodisponibilidad (106). De manera similar, la encapsulación de sorafenib en nanopartículas lipídicas sólidas utilizando palmitato de cetilo como matriz lipídica (6,35 μM) mostró un efecto citotóxico significativo del 40% después de 72 h de incubación en células HepG2 (89).

Una gran variedad de factores puede alterar el EPR y tener un efecto negativo sobre la acumulación de nanopartículas en tumores, como la vasculatura del tumor, la presión arterial y el tipo de tumor (lesión primaria frente a lesión metastásica) y ubicación. En consecuencia, el direccionamiento activo mediante la incoporación de un ligando de direccionamiento en las nanopartículas proporciona una terapia más eficaz. Diferentes estudios han desarrollado alternativas que involucran el direccionamiento específico hacía tumores de nanovectores utilizando anticuerpos, péptidos y ligandos con bajo peso molecular (107). Aunque la mayoría de los sistemas de administración de fármacos activos desarrollados para el tratamiento del HCC han utilizado el ASGPR como diana, (53,98) pocos se han utilizado para transportar sorafenib. Entre estos se encuentran las micelas poliméricas derivadas del conjugado polilactida-poliaminoácido galactosilado desarrollado por Craparo et al. (111). Los estudios de biodistribución en ratones demostraron, después de la administración oral de micelas recubiertas de galactosa cargadas con sorafenib, la acumulación preferencial de sorafenib en el hígado (112). Tunki et al (109), han utilizado nanopartículas sólidas de lípidos (SLN) unidas con polietilenglicol (PEGilado) recubiertos de galactosa como sistema de administración del fármaco. Estos sistemas llamados GAL-SSLN fueron cargados con sorafenib y mostraron una citotoxicidad y apoptosis superiores en HepG2 que el sorafenib solo (63). Guan et al (61), por su parte, utilizaron unas nanopartículas de sílice mesoporosas recubiertas con ácido lactobiónico como ligando las cuales se dirigen a ASGPR. Las nanopartículas sensibles al pH utilizadas han mostrado buenos resultados en la co-liberación de sorafenib y ácido ursólico y aumento de la apoptosis celular y regulan negativamente la expresión de proteínas EGFR y VEGFR2 relacionadas con la proliferación celular y la angiogénesis tumoral (113).

También se han utilizado otros ligandos para funcionalizar nanovectores hacía células de HCC, así como combinar sorafenib con otras moléculas citotóxicas. La combinación de doxorrubicina y sorafenib en nanopartículas estructuradas núcleo-capa híbridas de lípido-polímero funcionalizada con el tripéptido RGD (Arginina-Glicina-Asparagina) indicó una eficacia antitumoral mejorada en modelos de hepatocarcinogénesis *in vivo* con una biodisponibilidad mejorada y un tiempo de circulación más prolongado (114). Wang et al. han utilizado nanopartículas recubiertas de lípidos modificadas con RGD (Arginina-Glicina-Asparagina) para la administración conjunta de sorafenib y quercetina contra células de HCC. Estas nanopartículas modificadas con péptido RGD lograron el efecto de inhibición del crecimiento tumoral más significativo *in vitro* e *in vivo* (111). La sobreexpresión de los receptores de transferrina en las células de HCC ha permitido que puedan ser vías de funcionalización útiles para la vehiculización de fármacos (112). Malarvizhi et al (116) han desarrollado un nanovector de núcleo-capa funcionalizado a transferrina que encapsula doxorrubicina y sorafenib, y demostraron un efecto sinérgico en el HCC (113).

Otro receptor importante de tipo lectina es el MR que se encuentra expresado en macrófagos, células dendríticas y células endoteliales. Este receptor se ha utilizado para el transporte de fármacos manosilados, vectores de genes y antígenos. Aunque se ha demostrado que estos sistemas de transportes de fármacos son eficaces contra las células cancerosas de pulmón, colon y mama, no se ha demostrado la eficacia de los DDS manosilados contra las células del HCC.

Además, la incidencia del MR en las enfermedades hepáticas es generalmente poco conocida, lo que sugiere una expresión débil de este receptor en las células hepáticas. Nuestro estudio muestra, sin embargo, que el MR se expresa en los hepatocitos humanos primarios, y las células tumorales HepG2 y Huh7, sino que se expresa más que

el ASPGR, que se usa con frecuencia como diana para la administración de nanofármacos al hígado, lo que abre las puertas para su uso como vía de vehiculización de fármacos. Con el fin de revelar si esta característica estructural también es funcional y para validar MR como objetivo para los sistemas de administración de fármacos al HCC, utilizamos dos gliconanovectores **pMicMan** y **pMicGal** que exponen manosa y galactosa en su superficie. Estos nanovectores se obtuvieron mediante un enfoque ascendente (bottom-up) altamente convergente, en el que el paso clave es la fotopolimerización de monómeros autoasociados que refuerza la parte interna de las nanomicelas aumentando su estabilidad frente a la dilución. Todas las reacciones llevadas a cabo para realizar la síntesis de ambas micelas se han purificado posteriormente para aumentar la actividad de estas. En cada una de las reacciones se realizaron cromatografías de capa fina en gel de sílice, con las cuales controlamos la reacción, tal y como se describe en la metodología. Las micelas se caracterizaron adecuadamente a través de RMN, DLS y TEM.

Si bien estos nanovectores han mostrado una alta capacidad de carga de sorafenib, hemos seleccionado una carga baja de sorafenib para realizar nuestros estudios con el fin de minimizar el efecto de la liberación espontánea del fármaco antes de la incorporación a la célula (Figura 8). Curiosamente y en contraste con estudios previos en los que el sorafenib vectorizado era activo en el rango µmolar, la administración de pMicMan, pero no el fármaco incorporado a pMicGal, pudo aumentar la caspasa-3 o reducir la proliferación celular en el rango nanomolar (10-20 nM, 24 horas) en células HepG2 y Huh7 (Figura 9a y 9b). El sorafenib no vectorizado no aumentó la muerte celular ni alteró la proliferación celular en el rango nanomolar en las células HepG2 y Huh7 ($p \leq 0.05$). La principal actividad de sorafenib incorporado a **pMicMan** estaba relacionada con una mayor incorporación celular vía endosomal (Figura 10).

Las células pueden absorber macromoléculas del medio circundante por endocitosis, ya sea a través de endocitosis mediada por receptores en fosas recubiertas de clatrina, internalizadas y generando vesículas recubiertas de clatrina, o bien a través de vías de endocitosis independientes de clatrina basadas en las invaginaciones en caveolas. (114). La formación e internalización de fosas recubiertas de clatrina implica la participación del citoesqueleto de F-actina, (115) así como el proceso de formación de vesículas recubiertas de clatrina depende de la energía y requiere múltiples proteínas de unión a GTP como la dinamina (116).

El endosoma temprano permite la endocitosis de material que será posteriormente reciclado de nuevo a la membrana plasmática o secretado, así como degradado por fusión con el lisosoma en pasos posteriores. El uso de FM 1-43 nos permitió rastrear la incorporación endosomal de las nanomicelas. La incorporación endosomal de **pMicMan** y **pMicGal** se evitó a 4ºC en comparación con la incubación de las células a 37ºC (Figura 11). La incorporación de **pMicMan** y **pMicGal** en menor grado, si se ve muy afectada por el uso de dynasore y citocalasina D, lo que sugiere que vesículas recubiertas de clatrina está involucrado en el proceso de internalización de nanomicelas (Figura 10). La incorporación de rojo del Nilo a nanomicelas permitió la evaluación de su incorporación celular y tráfico a compartimentos específicos utilizando marcadores endosomales (anti-EEA1), lisosomales (anti-Lamp1) y autofagosómicos (anti-BECN1) que fueron valorados por inmunofluorescencia. **pMicMan** parecía estar colocalizado a nivel endosómico y lisosómico, mientras que **pMicGal** estaba colocalizado a nivel autofagolisosómico (Figura 11).

Curiosamente, el derivado de BODIPY, el cual se caracteriza por sus tres brazos conjugados con unidades de manosa co-ensambladas con Tween 80 para terapia fotodinámica dirigida, también ingresa a la célula a través de endocitosis mediada por

MR con acumulación preferencial en los lisosomas en el cáncer de mama MDA-MB-231 (117). En nuestras condiciones, la inhibición de la degradación lisosomal mediante cloroquina aumentó la actividad de caspasa-3 y redujo la proliferación celular con **pMicMan**, y en menor grado con **pMicGal**, en HepG2 (Figura 12). Estos datos sugieren que la degradación lisosomal impacta en la eficacia del fármaco en células HepG2. La reducción del pH de 7,4 a 4,5 indujo la liberación *in vitro* de sorafenib de los nanovectores **pMicMan** y **pMicGal** (Figura 8c y 8d). Se ha observado que la incorporación de fármacos en nanovectores que son captados por lisosomas perinucleares se liberar al espacio intracelular (118).

CONCLUSIONES

1) Los nanovectores dirigidos a MR (pMicMan) y ASGPR (pMicGal) son útiles para la encapsulación de sorafenib.
2) La incorporación de sorafenib (10 nM) a nanovectores dirigidos selectivamente a MR (pMicMan) induce apoptosis y reduce la proliferación celular
3) La mayor efectividad de **pMicMan** en relación con los nanovectores dirigidos a ASGPR (pMicGal) se relaciona con su mayor capacidad de incorporación celular vía endosomal.
4) La liberación de sorafenib se promueve en pH ácido compatible con las condiciones de lisosomas y los autogagolisosomas.

BIBLIOGRAFÍA

1. Dutta R, Mahato RI. Recent advances in hepatocellular carcinoma therapy. Vol. 173, Pharmacology and Therapeutics. Elsevier Inc.; 2017. p. 106–17.

2. Schwabe RF, Wiley JW, Bruix J, Reig M, Sherman M. Reviews in basic and clinical gastroenterology and hepatology Evidence-Based Diagnosis, Staging, and Treatment of Patients With Hepatocellular Carcinoma. 2016

3. Keating GM. Sorafenib: A Review in Hepatocellular Carcinoma. Vol. 12, Targeted Oncology. Springer-Verlag France; 2017. p. 243–53.

4. Altekruse SF, McGlynn KA, Reichman ME. Hepatocellular carcinoma incidence, mortality, and survival trends in the United States from 1975 to 2005. J Clin Oncol. 2009 Mar 20;27(9):1485–91.

5. Galle PR, Forner A, Llovet JM, Mazzaferro V, Piscaglia F, Raoul JL, et al. EASL Clinical Practice Guidelines: Management of hepatocellular carcinoma. J Hepatol. 2018 Jul 1;69(1):182–236.

6. Forner A, Llovet JM, Bruix J. Hepatocellular carcinoma. In: The Lancet. 2012. p. 1245–55.

7. Daza Carreño W, Dadán Muñoz S, Higuera Carrillo M. Infección recurrente por Clostridium difficile en pediatría. Reporte de dos casos y revisión de la literatura. Rev Colomb Gastroenterol. 2016 Mar 30;31(1):61.

8. Bosch FX, Ribes J, Borràs J. Epidemiology of primary liver cancer. Semin Liver Dis. 1999;19(3):271–85.

9. Hessheimer AJ, Forner A, Varela M, Bruix J. Metabolic risk factors are a major comorbidity in patients with cirrhosis independent of the presence of hepatocellular carcinoma. Eur J Gastroenterol Hepatol. 2010 Oct;22(10):1239–44.

10. Jones DE, Metcalf J V, Collier JD, Bassendine MF, James OF. Hepatocellular carcinoma in primary biliary cirrhosis and its impact on outcomes. Hepatology . 1997 Nov 1 ;26(5):1138–42.

11. Beasley RP. Hepatitis B virus. The major etiology of hepatocellular carcinoma. Cancer. 1988;61(10):1942–56.

12. Beasley RP, Lin CC, Hwang LY, Chien CS. Hepatocellular carcinoma and hepatitis B virus. A Prospective Study of 22 707 Men in Taiwan. Lancet. 1981 Nov 21;318(8256):1129–33.

13. Fattovich G, Giustina G, Degos F, Tremolada F, Diodati G, Almasio P, et al. Morbidity and mortality in compensated cirrhosis type C: A retrospective follow-up study of 384 patients. Gastroenterology. 1997;112(2):463–72.

14. Sun CA, Wu DM, Lin CC, Lu SN, You SL, Wang LY, Wu MH, Chen CJ. Incidence and cofactors of hepatitis C virus-related hepatocellular carcinoma: a prospective study of 12,008 men in Taiwan. Am J Epidemiol. 2003 Apr 15;157(8):674-82.

15. Lok AS, Seeff LB, Morgan TR, di Bisceglie AM, Sterling RK, Curto TM, et al. Incidence of Hepatocellular Carcinoma and Associated Risk Factors in Hepatitis C-Related Advanced

Liver Disease. Gastroenterology. 2009;136(1):138–48.

16. Jaskiewicz K, Banach L, Lancaster E. Hepatic siderosis, fibrosis and cirrhosis: the association with hepatocellular carcinoma in high-risk population. Anticancer Res. 1997 Sep-Oct;17(5B):3897-9.

17. Sun Z, Lu P, Gail MH, Pee D, Zhang Q, Ming L, et al. Increased risk of hepatocellular carcinoma in male hepatitis B surface antigen carriers with chronic hepatitis who have detectable urinary aflatoxin metabolite M1. Hepatology. 1999;30(2):379–83.

18. Klionsky DJ, Abdelmohsen K, Abe A, Abedin MJ, Abeliovich H, Arozena AA, et al. Guidelines for the use and interpretation of assays for monitoring autophagy (3rd edition) . Vol. 12, Autophagy. Taylor and Francis Inc.; 2016. p. 1–222.

19. Pérez-Aguilar F., Benlloch S., Berenguer M., Beltrán B., Berenguer J.. Esteatohepatitis no alcohólica: consideraciones fisiopatológicas, clínicas y terapéuticas. Rev. esp. enferm. dig. 2004 Sep ; 96(9): 628-648

20. Galle PR, Forner A, Llovet JM, Mazzaferro V, Piscaglia F, Raoul JL, et al. EASL Clinical Practice Guidelines: Management of hepatocellular carcinoma. J Hepatol. 2018 Jul 1;69(1):182–236.

21. Furuya K, Nakamura M, Yamamoto Y, Togei K, Otsuka H. Macroregenerative nodule of the liver. A clinicopathologic study of 345 autopsy cases of chronic liver disease. Cancer. 1988 Jan 1;61(1):99-105.

22. Cortes KC, Radkowski M. Oncogenesis of hepatocellular carcinoma. Exp Clin Hepatol. 2010;6(3–4):7–10.

23. Peck-Radosavljevic M. Drug therapy for advanced-stage liver cancer. Vol. 3, Liver Cancer. S. Karger AG; 2014. p. 125–31.

24. Llovet JM, Ricci S, Mazzaferro V, Hilgard P, Gane E, Blanc JF, de Oliveira AC, Santoro A, Raoul JL, Forner A, Schwartz M, Porta C, Zeuzem S, Bolondi L, Greten TF, Galle PR, Seitz JF, Borbath I, Häussinger D, Giannaris T, Shan M, Moscovici M, Voliotis D, Bruix J; SHARP Investigators Study Group. Sorafenib in advanced hepatocellular carcinoma. N Engl J Med. 2008 Jul 24;359(4):378-90. doi: 10.1056/NEJMoa0708857. PMID: 18650514.

25. Cervello M, Bachvarov D, Lampiasi N, Cusimano A, Azzolina A, McCubrey JA, et al. Molecular mechanisms of sorafenib action in liver cancer cells. Cell Cycle. 2012;11(15):2843–55.

26. Chen KF, Chen HL, Tai WT, Feng WC, Hsu CH, Chen PJ, et al. Activation of phosphatidylinositol 3-kinase/Akt signaling pathway mediates acquired resistance to sorafenib in hepatocellular carcinoma cells. J Pharmacol Exp Ther. 2011;337(1):155–61.

27. Tesori V, Piscaglia AC, Samengo D, Barba M, Bernardini C, Scatena R, et al. The multikinase inhibitor Sorafenib enhances glycolysis and synergizes with glycolysis blockade for cancer cell killing. Sci Rep. 2015 Mar 17;5.

28. Coriat R, Nicco C, Cheŕeau C, Mir O, Alexandre J, Ropert S, et al. Sorafenib-induced hepatocellular carcinoma cell death depends on reactive oxygen species production in vitro and in vivo. Mol Cancer Ther. 2012 Oct;11(10):2284–93.

29. French KJ, Coatney RW, Renninger JP, Hu CX, Gales TL, Zhao S, et al. Differences in effects on myocardium and mitochondria by angiogenic inhibitors suggest separate mechanisms of cardiotoxicity. Toxicol Pathol [Internet]. 2010 Aug 8];38(5):691–702.

30. Paech F, Mingard C, Grünig D, Abegg VF, Bouitbir J, Krähenbühl S. Mechanisms of mitochondrial toxicity of the kinase inhibitors ponatinib, regorafenib and sorafenib in human hepatic HepG2 cells. Toxicology. 2018 Feb 15;395:34–44.

31. Liu M, Zhou R, Wu X, Xu X, Su M, Yang B. Clinicopathologic characterization of sorafenib-induced endoplasmic reticulum stress in human liver cancer cells. J Physiol Pharmacol. 2018 Jan 1;69(4).

32. Rahmani M, Davis EM, Crabtree TR, Habibi JR, Nguyen TK, Dent P, et al. The Kinase Inhibitor Sorafenib Induces Cell Death through a Process Involving Induction of Endoplasmic Reticulum Stress. Mol Cell Biol. 2007 Aug 1;27(15):5499–513.

33. Zhang W, Konopleva M, Ruvolo VR, McQueen T, Evans RL, Bornmann WG, et al. Sorafenib induces apoptosis of AML cells via Bim-mediated activation of the intrinsic apoptotic pathway. Leukemia. 2008;22(4):808–18.

34. Yu C, Bruzek LM, Xue WM, Gores GJ, Carter CA, Kaufmann SH, et al. The role of Mcl-1 downregulation in the proapoptotic activity of the multikinase inhibitor BAY 43-9006. Oncogene. 2005 Oct 20;24(46):6861–9.

35. Rahmani M, Nguyen TK, Dent P, Grant S. The multikinase inhibitor sorafenib induces apoptosis in highly imatinib mesylate-resistant Bcr/Abl+ human leukemia cells in association with signal transducer and activator of transcription 5 inhibition and myeloid cell leukemia-1 down-regulation. Mol Pharmacol. 2007 Sep;72(3):788–95.

36. Rodríguez-Hernández MA, González R, de la Rosa ÁJ, Gallego P, Ordóñez R, Navarro-Villarán E, et al. Molecular characterization of autophagic and apoptotic signaling induced by sorafenib in liver cancer cells. J Cell Physiol. 2018 Jan 1;234(1):692–708.

37. Rodríguez-Hernández MA, Chapresto-Garzón R, Cadenas M, Navarro-Villarán E, Negrete M, Gómez-Bravo MA, et al. Differential effectiveness of tyrosine kinase inhibitors in 2D/3D culture according to cell differentiation, p53 status and mitochondrial respiration in liver cancer cells. Cell death & Dis. 2020;11(5).

38. Bondì ML, Botto C, Amore E, Emma MR, Augello G, Craparo EF, et al. Lipid nanocarriers containing sorafenib inhibit colonies formation in human hepatocarcinoma cells. Int J Pharm. 2015 Aug 1;493(1–2):75–85.

39. Kudo M, Finn RS, Qin S, Han K-H, Ikeda K, Piscaglia F, et al. Lenvatinib versus sorafenib in first-line treatment of patients with unresectable hepatocellular carcinoma: a randomised phase 3 non-inferiority trial. Lancet . 2018 Mar 24;391(10126):1163–73.

40. Galle PR, Forner A, Llovet JM, Mazzaferro V, Piscaglia F, Raoul J-L, et al. EASL Clinical Practice Guidelines: Management of hepatocellular carcinoma.. Vol. 69, Journal of Hepatology. 2018

41. Sasaki R, Kanda T, Fujisawa M, Matsumoto N, Masuzaki R, Ogawa M, et al. Different mechanisms of action of regorafenib and lenvatinib on toll-like receptor-signaling pathways in human hepatoma cell lines. Int J Mol Sci. 2020 May 1;21(9).

42. Llovet JM, Villanueva A, Marrero JA, Schwartz M, Meyer T, Galle PR, et al. Trial Design and Endpoints in Hepatocellular Carcinoma: AASLD Consensus Conference. Vol. 73, Hepatology. John Wiley and Sons Inc; 2021. p. 158–91.

43. Krishnamoorthy SK, Relias V, Sebastian S, Jayaraman V, Saif MW. Management of regorafenib-related toxicities: a review. Therap Adv Gastroenterol. 2015 Sep 7;8(5):285–97.

44. Llovet JM, Montal R, Sia D, Finn RS. Molecular therapies and precision medicine for hepatocellular carcinoma . Vol. 15, Nature Reviews Clinical Oncology. Nature Publishing Group; 2018. p. 599–616.

45. Ally A, Balasundaram M, Carlsen R, Chuah E, Clarke A, Dhalla N, et al. Comprehensive and Integrative Genomic Characterization of Hepatocellular Carcinoma. Cell 2017 Jun 15;169(7):1327-1341.e23.

46. Li L, Wang H. Heterogeneity of liver cancer and personalized therapy. Vol. 379, Cancer Letters. Elsevier Ireland Ltd; 2016. p. 191–7.

47. Cervello M, McCubrey JA, Cusimano A, Lampiasi N, Azzolina A, Montalto G. Targeted therapy for hepatocellular carcinoma: Novel agents on the horizon. Vol. 3, Oncotarget. Impact Journals LLC; 2012. p. 236–60.

48. Iavarone M, Lampertico P, Iannuzzi F, Manenti E, Donato MF, Arosio E, et al. Increased expression of vascular endothelial growth factor in small hepatocellular carcinoma. J Viral Hepat. 2007 Feb;14(2):133–9.

49. Sheen IS, Jeng KS, Shih SC, Kao CR, Chang WH, Wang HY, et al. Clinical significance of the expression of isoform 165 vascular endothelial growth factor mRNA in noncancerous liver remnants of patients with hepatocellular carcinoma. World J Gastroenterol. 2005 Jan 14;11(2):187–92.

50. Chesnokov MS, Khesina PA, Shavochkina DA, Kustova IF, Dyakov LM, Morozova O V., et al. Shift in VEGFA isoform balance towards more angiogenic variants is associated with tumor stage and differentiation of human hepatocellular carcinoma. PeerJ . 2018 Jun 5;2018(6):e4915.

51. Llovet JM, Bruix J. Molecular targeted therapies in hepatocellular carcinoma. Vol. 48, Hepatology. Hepatology; 2008. p. 1312–27.

52. Chew SA, Moscato S, George S, Azimi B, Danti S. Liver Cancer: Current and Future Trends Using Biomaterials. Cancers (Basel).. 2019 Dec 16;11(12):2026.

53. Sun Y, Ma W, Yang Y, He M, Li A, Bai L, et al. Cancer nanotechnology: Enhancing tumor cell response to chemotherapy for hepatocellular carcinoma therapy. Vol. 14, Asian Journal of Pharmaceutical Sciences. Shenyang Pharmaceutical University; 2019. p. 581–94.

54. Lu J, Wang J, Ling D. Surface Engineering of Nanoparticles for Targeted Delivery to Hepatocellular Carcinoma. Small . 2018 Feb 1;14(5):1702037.

55. Farjadian F, Ghasemi A, Gohari O, Roointan A, Karimi M, Hamblin MR. Nanopharmaceuticals and nanomedicines currently on the market: Challenges and opportunities. Vol. 14, Nanomedicine. Future Medicine Ltd.; 2019. p. 93–126.

56. Tanaka T, Shiramoto S, Miyashita M, Fujishima Y, Kaneo Y. Tumor targeting based on the effect of enhanced permeability and retention (EPR) and the mechanism of receptor-mediated endocytosis (RME). In: International Journal of Pharmaceutics. Int J Pharm; 2004. p. 39–61.

57. Golombek SK, May JN, Theek B, Appold L, Drude N, Kiessling F, et al. Tumor targeting via EPR: Strategies to enhance patient responses. Vol. 130, Advanced Drug Delivery Reviews. Elsevier B.V.; 2018. p. 17–38.

58. Liu J, Boonkaew B, Arora J, Mandava SH, Maddox MM, Chava S, et al. Comparison of

sorafenib-loaded poly (Lactic/Glycolic) acid and dppc liposome nanoparticles in the in vitro treatment of renal cell carcinoma. J Pharm Sci. 2015;104(3):1187–96. 59. Mieszawska AJ, Kim Y, Gianella A, Van Rooy I, Priem B, Labarre MP, et al. Synthesis of polymer-lipid nanoparticles for image-guided delivery of dual modality therapy. Bioconjug Chem. 2013 Sep 18;24(9):1429–34.

60. Kim DH, Kim MD, Choi CW, Chung CW, Ha SH, Kim CH, et al. Antitumor activity of sorafenib-incorporated nanoparticles of dextran/poly(DL-lactide-co-glycolide) block copolymer. Nanoscale Res Lett. 2012 Jan 27;7(1):91–91.

61. Guan Q, Guo R, Huang S, Zhang F, Liu J, Wang Z, et al. Mesoporous polydopamine carrying sorafenib and SPIO nanoparticles for MRI-guided ferroptosis cancer therapy. J Control Release. 2020 Apr 10;320:392–403.

62. Wang C-F, Mäkilä EM, Kaasalainen MH, Liu D, Sarparanta MP, Airaksinen AJ, et al. Copper-free azide–alkyne cycloaddition of targeting peptides to porous silicon nanoparticles for intracellular drug uptake. Biomaterials . 2014 Jan 7];35(4):1257–66.

63. Zhao R, Li T, Zheng G, Jiang K, Fan L, Shao J. Simultaneous inhibition of growth and metastasis of hepatocellular carcinoma by co-delivery of ursolic acid and sorafenib using lactobionic acid modified and pH-sensitive chitosan-conjugated mesoporous silica nanocomplex. Biomaterials. 2017 Oct 1;143:1–16.

64. Chen J, Sheu AY, Li W, Zhang Z, Kim DH, Lewandowski RJ, et al. Poly(lactide-co-glycolide) microspheres for MRI-monitored transcatheter delivery of sorafenib to liver tumors. J Control Release . 2014 Jun 28;184(1):10–7.

65. Paşcalău V, Tertis M, Pall E, Suciu M, Marinca T, Pustan M, et al. Bovine serum albumin gel/polyelectrolyte complex of hyaluronic acid and chitosan based microcarriers for Sorafenib targeted delivery. J Appl Polym Sci. 2020 Sep 10;137(34):49002.

66. Thapa RK, Choi JY, Poudel BK, Hiep TT, Pathak S, Gupta B, Choi HG, Yong CS, Kim JO. Multilayer-Coated Liquid Crystalline Nanoparticles for Effective Sorafenib Delivery to Hepatocellular Carcinoma. ACS Appl Mater Interfaces. 2015 Sep 16;7(36):20360-8.

67. Benizri S, Ferey L, Alies B, Mebarek N, Vacher G, Appavoo A, et al. Nucleoside-Lipid-Based Nanocarriers for Sorafenib Delivery. Nanoscale Res Lett . 2018 Dec 11;13(1):17.

68. Zhang H, Zhang FM, Yan SJ. Preparation, in vitro release, and pharmacokinetics in rabbits of lyophilized injection of sorafenib solid lipid nanoparticles. Int J Nanomedicine. 2012;7:2901–10.

69. Zhang Z, Niu B, Chen J, He X, Bao X, Zhu J, et al. The use of lipid-coated nanodiamond to improve bioavailability and efficacy of sorafenib in resisting metastasis of gastric cancer. Biomaterials . 2014;35(15):4565–72.

70. Grillone A, Riva ER, Mondini A, Forte C, Calucci L, Innocenti C, et al. Active Targeting of Sorafenib: Preparation, Characterization, and In Vitro Testing of Drug-Loaded Magnetic Solid Lipid Nanoparticles. Adv Healthc Mater . 2015 Aug 1 ;4(11):1681–90.

71. Bondì ML, Scala A, Sortino G, Amore E, Botto C, Azzolina A, et al. Nanoassemblies Based on Supramolecular Complexes of Nonionic Amphiphilic Cyclodextrin and Sorafenib as Effective Weapons to Kill Human HCC Cells. Biomacromolecules . 2015 Dec 14 ;16(12):3784–91.

72. Kamaly N, Xiao Z, Valencia PM, Radovic-Moreno AF, Farokhzad OC. Targeted polymeric therapeutic nanoparticles: Design, development and clinical translation. Chem Soc Rev.

2012 Mar 12 ;41(7):2971–3010.

73. Li Y, Huang G, Diakur J, Wiebe L. Targeted Delivery of Macromolecular Drugs: Asialoglycoprotein Receptor (ASGPR) Expression by Selected Hepatoma Cell Lines used in Antiviral Drug Development. Curr Drug Deliv . 2008 Oct 1;5(4):299–302.

74. D'Souza AA, Devarajan P V. Asialoglycoprotein receptor mediated hepatocyte targeting - Strategies and applications. Vol. 203, Journal of Controlled Release. Elsevier; 2015. p. 126–39.

75. Willoughby JLS, Chan A, Sehgal A, Butler JS, Nair JK, Racie T, et al. Evaluation of GalNAc-siRNA Conjugate Activity in Pre-clinical Animal Models with Reduced Asialoglycoprotein Receptor Expression. Mol Ther. 2018 Jan 3;26(1):105–14.

76. Ciechanover A, Schwartz AL, Lodish HF. Sorting and recycling of cell surface receptors and endocytosed ligands: The asialoglycoprotein and transferrin receptors. Vol. 23, Journal of Cellular Biochemistry. 1983. p. 107–30.

77. Mamidyala SK, Dutta S, Chrunyk BA, Préville C, Wang H, Withka JM, et al. Glycomimetic ligands for the human asialoglycoprotein receptor. J Am Chem Soc. 2012 Feb 1;134(4):1978–81.

78. Staines K, Hunt LG, Young JR, Butter C. Evolution of an Expanded Mannose Receptor Gene Family. Baker ML, editor. PLoS One. 2014 Nov 12;9(11):e110330.

79. Lee SH, Charmoy M, Romano A, Paun A, Chaves MM, Cope FO, et al. Mannose receptor high, M2 dermal macrophages mediate nonhealing Leishmania major infection in a Th1 immune environment. J Exp Med. 2018 Jan 1;215(1):357–75.

80. Fan W, Yang X, Huang F, Tong X, Zhu L, Wang S. Identification of CD206 as a potential biomarker of cancer stem-like cells and therapeutic agent in liver cancer. Oncol Lett. 2019 Sep 1;18(3):3218–26.

81. Cabral H, Miyata K, Osada K, Kataoka K. Block Copolymer Micelles in Nanomedicine Applications. Vol. 118, Chemical Reviews. American Chemical Society; 2018. p. 6844–92.

82. Assali M, Cid JJ, Fernández I, Khiar N. Supramolecular diversity through click chemistry: Switching from nanomicelles to 1D-nanotubes and tridimensional hydrogels. Chem Mater. 2013 Nov 12;25(21):4250–61.

83. Cid JJ, Assali M, Fernández-García E, Valdivia V, Sánchez-Fernández EM, Garcia Fernández JM, et al. Tuning of glyconanomaterial shape and size for selective bacterial cell agglutination. J Mater Chem B . 2016 Mar 21;4(11):2028–37.

84. Qian X, Städler B. Recent Developments in Polydiacetylene-Based Sensors. Vol. 31, Chemistry of Materials. American Chemical Society; 2019. p. 1196–222.

85. M. Pernía Leal, M. Assali, J. J. Cid, V. Valdivia, J. M. Franco, I. Fernández, D. Pozoc, N. Khiar. Synthesis of 1D-glyconanomaterials by a hybrid noncovalent–covalent functionalization of single wall carbon nanotubes: a study of their selective interactions with lectins and with live cells. Nanoscale, 2015,7, 19259-19272.

86. Cervello M, Emma MR, Augello G, Cusimano A, Giannitrapani L, Soresi M, et al. New landscapes and horizons in hepatocellular carcinoma therapy. Aging (Albany NY). 2020;12(3):3053–94.

87. Glickman JN, Kornfeld S. Mannose 6-phosphate-independent targeting of lysosomal

enzymes in I-cell disease B lymphoblasts. J Cell Biol . 1993;123(1):99–108.

88. Singh M, Ariatti M. Targeted gene delivery into HepG2 cells using complexes containing DNA, cationized asialoorosomucoid and activated cationic liposomes. J Control Release. 2003 Oct 30;92(3):383–94.

89. Ahlberg J, Berkenstam A, Henell F, Glausmann H. Degradation of short and long lived protein in isolated rat liver lysosomes. Effects of pH, temperature, and proteolytic inhibitors. The Journal of Biological Chemstry. 1984; 260 (9), 5847-5854.1985

90. Llovet JM, Burroughs A, Bruix J. Hepatocellular carcinoma. Lancet. Elsevier Limited; 2003. p. 1907–17.

91. Bruix J, Reig M, Sherman M. Evidence-Based Diagnosis, Staging, and Treatment of Patients with Hepatocellular Carcinoma . Vol. 150, Gastroenterology. W.B. Saunders; 2016. p. 835–53.

92. Giannini EG, Cucchetti A, Erroi V, Garuti F, Odaldi F, Trevisani F. Surveillance for early diagnosis of hepatocellular carcinoma: How best to do it? World J Gastroenterol. 2013 Dec 21;19(47):8808–21.

93. Wilhelm SM, Adnane L, Newell P, Villanueva A, Llovet JM, Lynch M. Preclinical overview of sorafenib, a multikinase inhibitor that targets both Raf and VEGF and PDGF receptor tyrosine kinase signaling. Vol. 7, Molecular Cancer Therapeutics. Mol Cancer Ther; 2008. p. 3129–40.

94. Llovet JM, Ricci S, Mazzaferro V, Hilgard P, Gane E, Blanc J-F, et al. Sorafenib in Advanced Hepatocellular Carcinoma. N Engl J Med . 2008 Jul 24 [;359(4):378–90.

95. Cheng AL, Kang YK, Chen Z, Tsao CJ, Qin S, Kim JS, et al. Efficacy and safety of sorafenib in patients in the Asia-Pacific region with advanced hepatocellular carcinoma: a phase III randomised, double-blind, placebo-controlled trial. Lancet Oncol 2009 Jan;10(1):25–34.

96. Wang XQ, Fan JM, Liu YO, Zhao B, Jia ZR, Zhang Q. Bioavailability and pharmacokinetics of sorafenib suspension, nanoparticles and nanomatrix for oral administration to rat. Int J Pharm. 2011 Oct 31;419(1–2):339–46.

97. Rimola J, Díaz-González Á, Darnell A, Varela M, Pons F, Hernandez-Guerra M, et al. Complete response under sorafenib in patients with hepatocellular carcinoma: Relationship with dermatologic adverse events. Hepatology. 2018 Feb 1;67(2):612–22.

98. Lu J, Wang J, Ling D. Surface Engineering of Nanoparticles for Targeted Delivery to Hepatocellular Carcinoma. Small. 2018 Feb 1;14(5):1702037.

99. Farjadian F, Ghasemi A, Gohari O, Roointan A, Karimi M, Hamblin MR. Nanopharmaceuticals and nanomedicines currently on the market: Challenges and opportunities. Vol. 14, Nanomedicine. Future Medicine Ltd.; 2019. p. 93–126.

100. Liu J, Boonkaew B, Arora J, Mandava SH, Maddox MM, Chava S, et al. Comparison of sorafenib-loaded poly (Lactic/Glycolic) acid and dppc liposome nanoparticles in the in vitro treatment of renal cell carcinoma. J Pharm Sci . 2015;104(3):1187–96.

101. Kim DH, Kim MD, Choi CW, Chung CW, Ha SH, Kim CH, et al. Antitumor activity of sorafenib-incorporated nanoparticles of dextran/poly(DL-lactide-co-glycolide) block copolymer. Nanoscale Res Lett. 2012 Jan 27;7(1):91–91.

102. Wang C-F, Mäkilä EM, Kaasalainen MH, Liu D, Sarparanta MP, Airaksinen AJ, et al.

Copper-free azide–alkyne cycloaddition of targeting peptides to porous silicon nanoparticles for intracellular drug uptake. Biomaterials. 2014 Jan 7;35(4):1257–66.

103. Chen J, Sheu AY, Li W, Zhang Z, Kim DH, Lewandowski RJ, et al. Poly(lactide-co-glycolide) microspheres for MRI-monitored transcatheter delivery of sorafenib to liver tumors. J Control Release . 2014 Jun 28;184(1):10–7.

104. Zhang Z, Niu B, Chen J, He X, Bao X, Zhu J, et al. The use of lipid-coated nanodiamond to improve bioavailability and efficacy of sorafenib in resisting metastasis of gastric cancer. Biomaterials. 2014;35(15):4565–72.

105. Mieszawska AJ, Kim Y, Gianella A, Van Rooy I, Priem B, Labarre MP, et al. Synthesis of polymer-lipid nanoparticles for image-guided delivery of dual modality therapy. Bioconjug Chem. 2013 Sep 1824(9):1429–34.

106. Zhang H, Zhang FM, Yan SJ. Preparation, in vitro release, and pharmacokinetics in rabbits of lyophilized injection of sorafenib solid lipid nanoparticles. Int J Nanomedicine. 2012;7:2901–10.

107. Kamaly N, Xiao Z, Valencia PM, Radovic-Moreno AF, Farokhzad OC. Targeted polymeric therapeutic nanoparticles: Design, development and clinical translation. Chem Soc Rev. 2012 Mar 12;41(7):2971–3010.

108. Craparo EF, Sardo C, Serio R, Zizzo MG, Bondì ML, Giammona G, et al. Galactosylated polymeric carriers for liver targeting of sorafenib. Int J Pharm. 2014 Mar 15;466(1–2):172–80.

109. Tunki L, Kulhari H, Vadithe LN, Kuncha M, Bhargava S, Pooja D, et al. Modulating the site-specific oral delivery of sorafenib using sugar-grafted nanoparticles for hepatocellular carcinoma treatment. Eur J Pharm Sci 2019 Sep 1 [;137.

110. Zhao R, Li T, Zheng G, Jiang K, Fan L, Shao J. Simultaneous inhibition of growth and metastasis of hepatocellular carcinoma by co-delivery of ursolic acid and sorafenib using lactobionic acid modified and pH-sensitive chitosan-conjugated mesoporous silica nanocomplex. Biomaterials. 2017 Oct 1;143:1–16.

111. Wang C, Su L, Wu C, Wu J, Zhu C, Yuan G. RGD peptide targeted lipid-coated nanoparticles for combinatorial delivery of sorafenib and quercetin against hepatocellular carcinoma. Drug Dev Ind Pharm. 2016 Dec 1;42(12):1938–44.

112. Zhang J, Hu J, Chan HF, Skibba M, Liang G, Chen M. iRGD decorated lipid-polymer hybrid nanoparticles for targeted co-delivery of doxorubicin and sorafenib to enhance anti-hepatocellular carcinoma efficacy. Nanomedicine Nanotechnology, Biol Med. 2016 Jul 1];12(5):1303–11.

113. Malarvizhi GL, Retnakumari AP, Nair S, Koyakutty M. Transferrin targeted core-shell nanomedicine for combinatorial delivery of doxorubicin and sorafenib against hepatocellular carcinoma. Nanomedicine Nanotechnology, Biol Med. 2014 Nov 1;10(8):1649–59.

114. SCIOT R, PATERSON AC, VAN EYKEN P, CALLEA F, KEW MC, DESMET VJ. Transferrin receptor expression in human hepatocellular carcinoma: an immunohistochemical study of 34 cases. Histopathology. 1988;12(1):53–63.

115. Yarar D, Waterman-Storer CM, Schmid SL. A dynamic actin cytoskeleton functions at multiple stages of clathrin-mediated endocytosis. Mol Biol Cell. 2005 Feb;16(2):964–75.

116. Damke H. Dynamin and receptor-mediated endocytosis. FEBS Lett . 1996 Jun 24;389(1):48–51.

117. Zhang Q, Cai Y, Li QY, Hao LN, Ma Z, Wang XJ, et al. Targeted Delivery of a Mannose-Conjugated BODIPY Photosensitizer by Nanomicelles for Photodynamic Breast Cancer Therapy. Chem - A Eur J. 2017 Oct 12;23(57):14307–15.

118. Guo W, Deng L, Yu J, Chen Z, Woo Y, Liu H, et al. Sericin nanomicelles with enhanced cellular uptake and ph-triggered release of doxorubicin reverse cancer drug resistance. Drug Deliv. 2018;25(1):1103–16.

PRODUCCIÓN CIENTIFICA

1. Navarro-Villarán E, de la Cruz-Ojeda P, Contreras L, González R, **Negrete M**, Rodríguez-Hernández MA, Marín-Gómez LM, Álamo-Martínez JM, Calvo A, Gómez-Bravo MA, de la Cruz J, Padillo J, Muntané J. Molecular Pathways Leading to Induction of Cell Death and Anti-Proliferative Properties by Tacrolimus and mTOR Inhibitors in Liver Cancer Cells. Cell Physiol Biochem. 2020 May 6;54(3):457-473. doi: 10.33594/000000230.

2. Rodríguez-Hernández MA, Chapresto-Garzón R, Cadenas M, Navarro-Villarán E, **Negrete M**, Gómez-Bravo MA, Victor VM, Padillo FJ, Muntané J. Differential effectiveness of tyrosine kinase inhibitors in 2D/3D culture according to cell differentiation, p53 status and mitochondrial respiration in liver cancer cells. Cell Death Dis. 2020 May 7;11(5):339. doi: 10.1038/s41419-020-2558-1.

3. González R, Rodríguez-Hernández MA, **Negrete M**, Ranguelova K, Rossin A, Choya-Foces C, Cruz-Ojeda P, Miranda-Vizuete A, Martínez-Ruiz A, Rius-Pérez S, Sastre J, Bárcena JA, Hueber AO, Padilla CA, Muntané J. Downregulation of thioredoxin-1-dependent CD95 S-nitrosation by Sorafenib reduces liver cancer.

Redox Biol. 2020 Jul;34:101528. doi: 10.1016/j.redox.2020.101528.

4. Rodríguez-Hernández MA, de la Cruz-Ojeda P, López-Grueso MJ, Navarro-Villarán E, Requejo-Aguilar R, Castejón-Vega B, **Negrete M**, Gallego P, Vega-Ochoa Á, Victor VM, Cordero MD, Del Campo JA, Bárcena JA, Padilla CA, Muntané J. Integrated molecular signaling involving mitochondrial dysfunction

and alteration of cell metabolism induced by tyrosine kinase inhibitors in cancer. Redox Biol. 2020 Sep;36:101510. doi: 10.1016/j.redox.2020.101510.

6. Negrete M, Romero-Ben E, Gutiérrez-Valencia A, Rosales-Barrios C, Alés E, Mena Barragán T, Castillejos MC, Flores J, de la Cruz-Ojeda P, Navarro-Villarán E, Cepeda-Franco C, Khiar N, **Muntané J.** PDA-Based Glyconanomicelles for Hepatocyte's Active Targeting via Mannose and Asialoglycoprotein Receptors. ACS Applied Bio Materials, aceptado 20 Mayo 2021

APORTACIONES A CONGRESOS

1. XII Reunión GERLI

Lugar de Celebración: Barcelona **Fecha:** 04-05/07/2019

Autores: María A. Rodríguez-Hernández, Elena Navarro-Villarán, Patricia de la Cruz, Raúl González, María Negrete, José M. Álamo, Francisco J. Padillo, Jordi Muntané

Título: Impacto antitumoral de los inhibidores tirosina quinasa y su relación con la disfuncional mitocondrial en el hepatocarcinoma

Tipo de participación: Ponencia Oral

2. HCC Summit 2019

Lugar de Celebración: Lisboa **Fecha:** 14-19/02/2019

Autores: Patricia de la Cruz-Ojeda, Raúl González, Elena Navarro-Villarán, María Negrete, María A. Rodríguez-Hernández, María I. Gómez-Espejo, Inés M. Fernández-Luque, Miguel A. Gómez-Bravo, Juan M. Praena-Fernández, María T. Ferrer, Francisco J. Padillo, Jordi Muntané

Título: Epigenetic signature of Sorafenib-responsiveness in patients with advanced hepatocellular carcinoma

Tipo de participación: Poster

3. VI International Workshop on "Nitric oxide in cancer and beyond"

Lugar de Celebración: New York **Fecha:** 20-22/09/2019

Autores: González R, Rodríguez-Hernández MA, Navarro-Villarán E, Staňková P, Negrete M, Ranguelova K, de la Cruz-Ojeda P, Kučera O, Červinková Z, Rossin A, Miranda-Vizuete A, Martínez-Ruiz A, Sastre J, Bárcena JA, Hueber AO, Padilla CA, Muntané J

Título: Evidences for the relevant role of oxidative and nitrosative stress in the mitochondrial dysfunction and cell death induced by Sorafenib in liver cancer cells

Tipo de participación: Comunicación Oral

4. Sociedad Española de Autofagia 2020

Lugar de Celebración: Cáceres **Fecha:** 04-06/03/2020

Autores: De la Cruz-Ojeda, P., González, R., Navarro-Villarán, E., Negrete, M., Rodriguez-Hernández, MA., Gómez-Espejo, MI., Fernandez-Luque, IM., Domínguez-Borrero, M., Gómez-Bravo, MA., Romero-González, Martín LM., Ferrer, MT., Praena Fernandez, JM., Padillo, FJ., Muntané, Jordi.

Título: Epigenetic signature involved in the therapeutic response of Sorafenib in advanced hepatocellular carcinoma

Tipo de participación: Comunicación Oral

5. 45 Congreso Anual de la Asociación Española para el Estudio del Hígado (AEEH)

Lugar de Celebración: Madrid **Fecha:** 12-14/02/2020

Autores: Patricia de la Cruz-Ojeda, Raúl González, Elena Navarro-Villarán,

María Negrete, María A. Rodríguez-Hernández, María I. Gómez-Espejo, Ángela Rojas, Inés M. Fernández-Luque, Manuela F. Domínguez-Borrero, Miguel Á. Gómez-Bravo, Manuel Romero-Gómez, Luis M. Marín, María T. Ferrer, Juan M. Praena-Fernández, Francisco J. Padillo, Jordi Muntané

Título: Firma epigenética de respuesta a Sorafenib en el hepatocarcinoma celular avanzado

Tipo de participación: Poster

6. **45 Congreso Anual de la Asociación Española para el Estudio del Hígado (AEEH)**

Lugar de Celebración: Madrid **Fecha:** 12-14/02/2020

Autores: Patricia de la Cruz-Ojeda, Elena Navarro-Villarán, María Negrete, María A. Rodríguez-Hernández, María I. Gómez-Espejo, Ángela Rojas, Inés M. Fernández-Luque, Manuela F. Domínguez-Borrero, Miguel Á. Gómez-Bravo, María J. Serrano, Manuel Romero-Gómez, Jose M. Álamo, María T. Ferrer, Juan M. Praena-Fernández, Francisco J. Padillo, Jordi Muntané

Título: Células tumorales circulantes como marcador predictivo de respuesta a la quimioembolización transarterial en el carcinoma hepatocelular

Tipo de participación: Poster

ANEXOS (ARTÍCULOS)

Cellular Physiology and Biochemistry

Cell Physiol Biochem 2020;54:457-473
DOI: 10.33594/000000230
Published online: 6 May 2020
Accepted: 29 March 2020

Original Paper

Molecular Pathways Leading to Induction of Cell Death and Anti-Proliferative Properties by Tacrolimus and mTOR Inhibitors in Liver Cancer Cells

Elena Navarro-Villarán[a,b] Patricia de la Cruz-Ojeda[a] Laura Contreras[a,c] Raúl González[a,b] María Negrete[a] María A. Rodríguez-Hernández[a,b] Luís M. Marín-Gómez[a,b,d] José M. Álamo-Martínez[a,b,d] Antonio Calvo[e] Miguel A. Gómez-Bravo[a,b,d] Jesús de la Cruz[a,c] Javier Padillo[a,b,d] Jordi Muntané[a,b,d]

[a]Institute of Biomedicine of Seville (IBiS), Hospital University "Virgen del Rocío"/CSIC/University of Seville, Seville, Spain, [b]Networked Biomedical Research Center Hepatic and Digestive Diseases (CIBEREHD o Ciberehd), Instituto de Salud Carlos III, Madrid, Spain, [c]Department of Genetics, University of Seville, Seville, Spain, [d]Department of General Surgery, Hospital University "Virgen del Rocío"/CSIC/University of Seville/IBiS, Seville, Spain, [e]Department of General Surgery, Hospital University of Puerto Real, Puerto Real, Spain

Key Words
Apoptosis • Autophagy • Endoplasmic reticulum stress • Immunosuppressants • Hepatocarcinoma

Abstract
Background/Aims: Orthotopic liver transplantation (OLT) is the recommended treatment for patients at early stages of hepatocarcinoma (HCC) with portal hypertension and/or increased bilirubinemia, but without vascular-associated diseases. Tumor recurrence, which is the main drawback for the survival of patients submitted to OLT for HCC, has been related to tumor-related variables and the immunosuppressive therapies. We have previously shown that Tacrolimus (FK506) exerts a more potent pro-apoptotic and anti-proliferative effects than the mammalian target of rapamycin (mTOR) inhibitors (Sirolimus and Everolimus) in liver cancer cells. This study identified the role of the immunosuppressant partners such as FK506-binding proteins (FKBPs) in the induction of cell death and arrest of cell proliferation by immunosuppressants in two representative liver cancer cells. ***Methods:*** The regulation of endoplasmic reticulum (ER) stress, apoptosis/autophagy, cell proliferation, and FKBPs expression was determined in Tacrolimus-, Sirolimus- and Everolimus-treated primary human hepatocytes, and hepatoma HepG2 and Huh7 cell lines. The functional repercussion of FKBPs on cell death and proliferation was also addressed using the siRNA technology. The assessed

R. González, M. Negrete and M. A. Rodríguez-Hernández contributed equally to this study.

Jordi Muntané Ph.D.
Instituto de Biomedicina de Sevilla (IBiS), Hospital Universitario "Virgen del Rocío"/CSIC/Universidad de Sevilla, Av. Manuel Siurot s/n, 41013-Seville (Spain)
Tel. +34-955923122, Fax +34-955923002, E-Mail jmuntane-ibis@us.es

antitumoral properties of the immunosuppressants were associated to microRNAs (miRNAs) pattern. ***Results:*** The enhanced pro-apoptotic and anti-proliferative properties of Tacrolimus *versus* mTOR inhibitors were associated with increased protein kinase RNA-like endoplasmic reticulum kinase (PERK)-related ER stress, ^{Ser15}P-p53/p53 ratio and p21 protein expression that may counterbalance the risk of proliferative upregulation caused by enhanced ^{Thr172}P-Cdk4/Cdk4 activation in liver cancer cells. The inhibition of the mTOR pathway by Sirolimus and Everolimus was related to an induction of autophagy; and at a high dose, these drugs impaired translation likely at a very early step of the elongation phase. Tacrolimus and mTOR inhibitors increased the protein expression of FKBP12 and FKBP51 that appeared to play pro-survival role. Interestingly, the administration of immunosuppressants yields a specific pattern of miRNAs. Tacrolimus and mTOR inhibitors decreased miR-92a-1-5p, miR-197-3p, miR-483-3p and miR-720, and increased miR-22-3p, miR-376a-3p, miR-663b, miR-886-5p, miR-1300 and miR-1303 expressions in HepG2 cells. ***Conclusion:*** The more potent pro-apoptotic and anti-proliferative properties of Tacrolimus *versus* mTOR inhibitors were associated with an increased activation of PERK and p53 signaling, and p21 protein expression. FKBP12 and FKBP51 appeared to be the most relevant partners of Tacrolimus and mTOR inhibitors exerting a pro-survival effect in HepG2 cells. The observed effects of immunosuppressants were related to a specific miRNA signature in liver cancer cells.

Introduction

Hepatocellular carcinoma (HCC) has been the sixth most common neoplasia in the world, and the fourth most common cause of cancer-related mortality worldwide during 2018 [1]. HCC is the main primary malignancy in the liver causing death in cirrhotic patients [2]. The performance status and hepatic function of the patient, number and size of the nodules, tumor vascular invasion, and the presence of extrahepatic metastasis, are actually used for the staging, prognosis as well as the therapeutic recommendation to the patients with HCC [3]. The curative treatments such as ablation, resection and orthotopic liver transplantation (OLT) are indicated at the very early stage (Barcelona Clinic Liver Cancer or BCLC 0) and early stage (BCLC A) of the disease characterized by the presence of 1-3 tumors less than or equal to 3 cm diameter, good liver function (Child-Pugh A-B), asymptomatic (Performance Status or PS 0), and absence of vascular invasion and extrahepatic metastases. OLT is indicated in patients with potential portal hypertension and/or bilirubinemia, but without vascular-associated diseases [3]. The patients subjected to OLT receive immunosuppressive therapy with Cyclosporin A, Tacrolimus (FK506) or mammalian target of rapamycin (mTOR) inhibitors (Rapamycin or Sirolimus, and Everolimus) to reduce graft rejection.

Immunophilins consist of a family of highly conserved proteins that binds to immunosuppressive drugs such as Cyclosporin A, Tacrolimus, and mTOR inhibitors. Cyclophilins and FK506-binding proteins (FKBPs) are the major immunophilins that binds to Cyclosporin A, or Tacrolimus and mTOR inhibitors, respectively [4]. FKBPs are involved in numerous cellular functions, such as protein folding, protein stability, kinase activity, receptor signaling, and protein trafficking, as well as play a role in cancer and chemoresistance [5]. Tacrolimus inhibits antigen receptor-dependent T cell proliferation through binding to the conserved active sites of the canonical FKBP members (FKBP12, FKBP51 and FKBP52), inhibiting its peptidylprolyl cis/trans isomerase (PPIase) activity [6], but also the phosphatase activity of Calcineurin, thereby preventing the calcium/calmodulin-dependent Calcineurin-related dephosphorylation of the nuclear factor of activated T cells (NFAT). The process downregulates the expression of IL-2, protooncogenes (H-RAS, c-MYC) and receptors for cytokines (IL-2 receptor) in T cells [7]. While binding to the same FKBP partners, Sirolimus and Everolimus exert their immunosuppressive properties by preventing IL-2-dependent T cell proliferation [8]. The immunosuppressive properties of the FKBP/Sirolimus complex are related to the interaction with the mTOR complex [9, 10].

The aim of the study was the identification of the role of FKBPs in the induction of cell death and anti-proliferative properties induced by immunosuppressants in liver cancer cells. The present study showed that the increased pro-apoptotic and anti-proliferative properties induced by Tacrolimus *versus* mTOR inhibitors were due to an enhanced protein kinase RNA-like endoplasmic reticulum kinase (PERK)-related endoplasmic reticulum (ER) stress. However, the administration of mTOR inhibitors increased autophagy markers compared to Tacrolimus treatment in HepG2 and Huh7 cell lines. We have also performed siRNA functional studies which showed that FKBP12 and FKBP51 mediate cell survival in immunosuppressive-treated HepG2 cells. We have observed a specific signature of microRNAs (miRNAs) expression upon treatment of HepG2 cells with Tacrolimus and mTOR inhibitors that was associated with the induction of apoptosis and anti-proliferative properties of the treatments.

Materials and Methods

Drugs

Tacrolimus (Ref AT23293, Carbosynth Limited, Berkshire, United Kingdom), Sirolimus (Ref 37094, Sigma-Aldrich, Sant Louis, Missouri, USA), and Everolimus (Ref FE23209, Carbosynth Limited) were dissolved in DMSO (95.8, 91.5 and 80.4 µg/µl, respectively) in order to obtain working solution useful for all the experimental work.

Primary human hepatocytes, cell lines and culture conditions

Human hepatocytes were prepared from healthy portions of liver resections obtained from three patients (two men and one woman, aged 63±5.2 years) submitted to surgical resection for liver metastasis from colorectal cancer. Isolation of human hepatocytes was based on a two-step collagenase procedure [11]. HepG2 (HB-8065™) cells were obtained from ATCC/LGC Standards (Barcelona, Spain). Huh7 cells were obtained from Apath LLC (New York, New York, USA). Both cells lines were negative for mycoplasma contamination. Cells (100000 cells/cm^2) were cultured in MEM with Earle's salts with L-glutamine (Ref E15-825, PAA Laboratories Inc, Toronto, Ontario, Canada) with 10 % FBS (F7524, Sigma-Aldrich, Lot No: 022M3395, endotoxin <0.2 EU/ml), sodium pyruvate (1 mM) (Ref S11-003, PAA Laboratories Inc), non-essential amino acids (Ref M11-003, PAA Laboratories Inc), Penicillin-Streptomycin solution (100 U/mL-100 µg/ml) (P11-010, PAA Laboratories Inc), at 37°C in a humidified incubator with 5 % CO_2. Drugs were added at a broad range of concentrations (0, 10 nM, 10 µM and 100 µM) 24 h after plating. Cell lysates were obtained at different time points according to the assays.

Measurement of apoptosis

Caspase-3-associated activity was determined using caspase-Glo® 3 assay systems (G8091, Promega, Fitchburg, Wisconsin, USA). Cells were treated with caspase-Glo® 3 reagent in an "add-mix-measure" format resulting in cell lysis, caspase-3-dependent cleavage of the substrate and generation of a "glow-type" luminescent signal. The signal generated is proportional to the amount of caspase-3 activity. The values are extrapolated into a calibration curve included in the assay. Chemiluminiscence was measured using an Infinite 200 PRO Microplate Reader (TECAN, Männedorf, Switzerland).

Evaluation of protein expression markers related to ER stress, autophagy, cell cycle, apoptosis and FKBPs

Cells were treated with lysis solution including 50 mM HEPES pH. 7.5, 5 mM EDTA, 150 mM NaCl, 1 % NP-40, commercial proteases inhibitor cocktail (P8340-5 ml, Sigma-Aldrich), 1 mM PMSF, 1 mM NaF and 1 mM Na_3VO_4. Protein expression was determined by SDS-PAGE coupled to Western-blot analysis. Proteins (50-100 µg) were separated by Any kD™ Criterion™ TGX Stain-Free™ Protein Gel, 18 well, 30 µl (#5678124, BioRad, Hercules, California, USA) and transferred to PVDF membranes. The membranes were incubated with the corresponding commercial primary and secondary antibodies coupled to horseradish peroxidase revealing protein content by Clarity™ Western ECL substrate (Ref 170-5061, BioRad) and analyzed in a ChemiDoc™ Touch Imaging System. Antibodies for Western-blot were obtained commercially and included 4E-BP1 (#9452), $^{Thr37/Thr46}$P-4E-BP1(#9459), Cdk4 (#12790), eIF2α (#5324), ^{Ser51}P-eIF2α (#9721)

and ^{Ser15}P-p53 (#9284) obtained from Cell Signaling Technology (Danvers, Massachusetts, USA); LC3 (PM036) purchased from MBL International (Woburn, Massachusetts, USA); GADD153 (C/EBP homologous protein or CHOP) (sc-575), Beclin (sc-48341), p21 (sc-397) and p53 (sc-6243) obtained from Santa Cruz Biotechnology (Dallas, Texas, USA); ^{Thr172}P-Cdk4 (PA5-64482) obtained from ThermoFisher (Waltham, Massachusetts, USA); FKBP12 (Ref NB300-508) and FKBP38 (Ref NBP1-77909) obtained from Novus Biologicals (Centennial, Colorado, USA); and FKBP51 (Ref MAB4094) and FKBP52 (Ref MAB4095) obtained from R&D Systems (Minneapolis, Minnesota, USA). The corresponding secondary antibodies anti-rabbit (sc-2004), anti-mouse (sc-2005) and anti-goat (sc-2768) IgG-HRP labelled were purchased from Santa Cruz. Densitometric analysis was performed using the software Image Lab 6.0 of BioRad.

Cell proliferation assay

The measurement of bromodeoxyuridine (BrdU) incorporation was used as marker of cell proliferation (Ref 11 647 229 001, Roche Diagnostics, Mannheim, Germany). Cells were seeded at low density (12500 cells/cm^2) at 37°C in a humidified incubator with 5 % CO_2. After 24 h of stabilization cells were treated with drugs including corresponding controls without BrdU. Two hours before evaluation of cell proliferation (12 h) 20 µl of BrdU (10 µM) was added to culture. DNA was denaturalized with 200 µl FixDenat solution included in the commercial assay for 30 min a room temperature. After removal, cells were incubated with 100 µl monoclonal anti-BrdU antibodies conjugated with horseradish peroxidase for 90 min at room temperature. Afterwards, cells were washed with phosphate buffer saline (PBS) (137 mM NaCl, 2.7 mM KCl, 4.3 mM Na_2HPO_4), and incubated with 100 µl revealing solution including hydrogen peroxide, luminol and 4-iodophenol for 15 min at room temperature. Absorbance was measured at 370 nm, using as reference wavelength 492 nm, and with an Infinite 200 PRO Microplate Reader (TECAN, Männedorf, Switzerland).

Assessment of protein translation

The protocol for polysome preparation of liver cancer cells was adapted from that we routinely employ for yeast cells [12]. Cells were grown up to 80 % confluency in 150 cm^2 dishes. Before cell harvesting, 200 µg/ml cycloheximide was added and incubated for 5 min at 37°C. Each dish was then placed on ice, the medium was collected, and the cultures washed twice with PBS without Ca^{2+} and Mg^{2+} containing 200 µg/ml cycloheximide. Then, 800 µl of lysis buffer (10 mM Tris-HCl, pH 7.4, 150 mM NaCl, 10 mM $MgCl_2$, 200 µg/ml cycloheximide, 200 µg/ml heparin, 2 mM DTT, 0.5 % NP40) was added to one dish, cells were scrapped, and transferred to the second dish. Cell lysate was incubated at 4°C with gentle end-over-end rotation for 10 min and then centrifuged at 12000 *g* for 8 min at 4°C in a refrigerated microfuge. The corresponding supernatants were recovered and the A_{260} measured using a NanoDrop ND-1000 Spectrophotometer (Thermo Fisher Scientific). About 10 absorption units of A_{260} were layered on top of 7-50 % (w/v) sucrose gradients prepared in 50 mM Tris-acetate, pH 7.5, 50 mM NH_4Cl, 12 mM $MgCl_2$, 1 mM DTT. The gradients were centrifuged at 260110 *g* (39000 rpm) in a Beckman SW41 rotor at 4°C for 2 h 45 min. The dissociation of the vacant 80S ribosomes was achieved by addition of high-salt (0.25 M NaCl) concentration within the gradients. Gradient analysis was performed with an ISCO UA-6 system (Isco, Inc. Lincoln, NE, USA) equipped to continuously monitor the A_{254}.

Regulation of FKBP expression by siRNA technology

Cells were seeded the day before the experimental intervention to reach 60 % confluency at the moment of cell transfection in 24 h. siRNA (25 nM) were mixed with the transfection reagent DharmaFECT 4 Transfection Reagent (77T-2004-02; GE Healthcare Dharmacon, Horizon-Discovery, Lafayette, Colorado, USA) for 20 min at room temperature and transferred to cell culture without antibiotic/antimycotic solution for 24 h. Afterwards, cells were maintained in fully complemented culture medium, and drugs were added 48 h after cell transfection. The siRNA of FKBP12 (on-target plus smart pool Human FKBP1A 2280 siRNA, ref L-009494), FKBP38 (on-target plus smart pool Human FKBP8 23770 siRNA, ref L-009673), FKBP51 (on-target plus smart pool Human FKBP4 2288 siRNA, ref L-006410) and FKBP52 (on-target plus smart pool Human FKBP5 2289 siRNA, ref L-004224), as well as non-targeting siRNA (on-target plus non-targeting siRNA pool, ref 77D-001810-10) used as negative control were also obtained from GE Healthcare Dharmacon.

Expression of miRNAs

Total RNA was extracted using the miRNeasy kit (Ref 217004, Qiagen, Hilden, Germany). Briefly, HepG2 cells and primary hepatocytes were lysed with QIAzol Lysis Reagent (Ref 79306, Qiagen). Chloroform was added to homogenates and these were centrifuged for 15 min at 12000 *g*. Upper aqueous phases containing RNA were transferred to clean tubes. After the addition of ethanol, RNA was bound RNeasy Mini spin column (Ref 74104, Qiagen) and washed in subsequent centrifugation steps. Eventually, RNA was eluted in 50 µl of RNase-free water. RNA was quantified using NanoDrop™ One/OneC Microvolume UV-Vis Spectrophotometer (Thermo Fisher Scientific). Quality control and RNA integrity assessment were performed with 2100 Bioanalyzer (Agilent Technologies, California, USA). All samples showed RIN higher than 8.

The miRNA expression profiling was obtained by qRT-PCR using the using the TaqMan® OpenArray® Human miRNA Panel (Ref 4470187, Life Technologies, Carlsbad, California, USA) and accessory kits (Applied Biosystems, Foster City, California, United States). Briefly, isolated miRNAs were reversed transcribed into cDNA using the TaqMan MicroRNA Reverse Transcription Kit (Ref 4366596, Life Technologies) and Megaplex RT Primers Human in a set of predefined pools A and B (Ref 4444750, Life Technologies). Prior to PCR, resulting cDNA was pre-amplified with Megaplex PreAmp Primers of gene-specific Human Pools A and B and the TaqMan PreAmp Master Mix (Ref 4391128, Life Technologies). The pre-amplified product was diluted 40 folds and mixed 1:1 v/v with the TaqMan OpenArray Real-Time PCR Master Mix (Ref 4462159, Life Technologies). Aliquots of the mixture were dispensed on a microfluidic OpenArray 384-well sample plate (Ref 4406947, Life Technologies). Next, TaqMan Open-Array Human MicroRNA Panels were loaded with the OpenArray AccuFill System and the PCR reactions were carried out with QuantStudio™ 12 K Flex OpenArray® Platform (QS12KFlex, Thermo Fisher, Waltham, Massachusetts, USA) following the manufacturer's instructions.

Thermo Fisher Cloud Relative Quantification software was used to obtain qPCR data. First, expression levels were calculated using the relative threshold cycle (Crt) method. TaqMan® OpenArray® Human miRNA Panel aims to obtain a total of 758 Crt values for each sample, which include 754 unique miRNAs, one negative control (ath-miR159a) and three endogenous positive controls (RNU48, RNU44 and U6). Crt values were normalized using the global mean strategy. Therefore, ΔCrt values were calculated as Crt miRNA-Crt global mean. Samples were clustered according to ΔCrt values of miRNAs expressed in all samples using the Pearson Correlation (uncentered) and average linkage methods with the Cluster (v 3.0) software. Dendogram illustration was created with Java TreeView software. Relative miRNA expression levels between control and experimental groups were calculated by using the ΔΔCrt method and exported for further analysis. Fold change values were calculated as 2-ΔΔCrt.

The bioinformatic analysis was also carried out based on significant differentially expressed miRNAs showing ≥2.0-fold or <0.5 fold changes, and with a *p*-value <0.05 that were used for in silico predictions. Target prediction was done using the TargetScan Database. Only highly conserved predicted targets with a cumulative weighted context score <-0.4 were selected. A gene regulatory network of differentially expressed miRNAs and their targets was constructed using Cytoscape (v3.6.0). In order to investigate the biological functions of miRNA targets, we carried Functional Annotation and Enrichment analysis of Gene Ontology (GO) terms and Kyoto Encyclopedia of Genes and Genomes (KEGG) pathways with the Database for Annotation, Visualization, and Integrated Discovery (DAVID) tool. Results were considered statistically significant when *p*-value <0.05 and False Discovery Rate (FDR) <0.05.

Statistical analysis

All results are expressed as mean ± SEM of independent experiments (n=3-8). Data were compared using the analysis of variance (ANOVA) with the Least Significant Difference's test as post-hoc multiple comparison analysis (homogeneity of variances) or Games-Howell (non-homogeneity of variances). If Shapiro-Wilks´s test showed non-normal distribution of data non-parametric Kruskal-Wallis coupled to U-Man-Whitney post-hoc analysis with Finner´s correction was done. The level of significance was set at *p≤0.05, **p≤0.01, ***p≤0.001. The groups significantly different (p≤0.05) were indicated with different letters.

Results

The differential pro-apoptotic and anti-proliferative properties of Tacrolimus and mTOR inhibitors were associated with PERK-dependent activation of ER stress in liver cancer cells

Our present data confirm previous study showing that Tacrolimus exerted a more potent pro-apoptotic and anti-proliferative properties than mTOR inhibitors [13]. The induction of apoptosis was inversely correlated to the reduction of cell proliferation by Tacrolimus and mTOR inhibitors in HepG2 (Fig. 1A and 1B, respectively) and Huh7 (Fig. 1C and 1D, respectively). Primary human hepatocytes were resistant to the pro-apoptotic and anti-proliferative effects of the treatments (Fig. 1E and 1F, respectively). The ER is responsible for protein folding and regulation of intracellular calcium concentrations through the tightly regulation of three ER transmembrane proteins: PERK, ATF6 and inositol-requiring enzyme 1 α (IRE1α) [14, 15]. Our data showed that Tacrolimus (100 μM), and to a lesser extent mTOR inhibitors (100 μM) strongly activated PERK as shown by the ^{Ser51}P-eIF2α/eIF2α ratio (Fig. 2A) and GADD153 (CHOP) protein expressions (Fig. 2B) in HepG2 cells. The impact of Tacrolimus and mTOR inhibitors in Huh7 cells followed the same pattern in ^{Ser51}P-eIF2α/eIF2α ratio and GADD153 protein expressions as that observed in HepG2 although at lower extend (Fig. 2C and 2D, respectively). The administration of the drugs does not alter ATF6- and IRE1α-dependent pathways in liver cancer cells (data not shown).

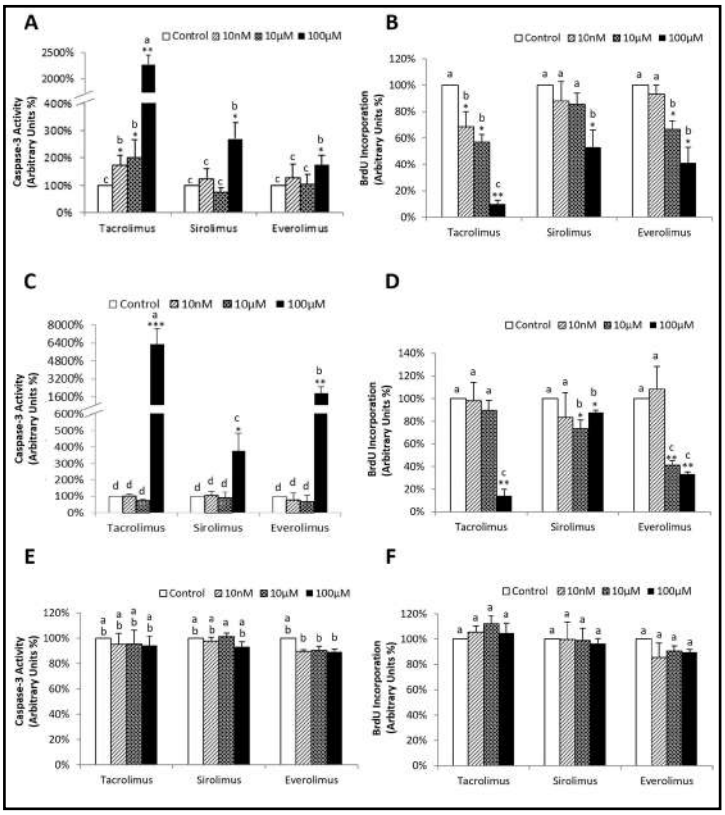

Fig. 1. Regulation of caspase-3 activity and BrdU incorporation in Tacrolimus-, Sirolimus- and Everolimus-treated HepG2 (A and B, respectively), Huh7 (C and D, respectively) and primary human hepatocytes (E and F, respectively). Apoptosis and cell proliferation were determined using commercial caspase-3 activity and BrdU incorporation assays respectively as described in Material and Methods. The variables were evaluated at 24 h after treatment administration (0, 10 nM, 10 μM, 100 μM). Results are expressed as mean ± SEM of five independent experiments. *p ≤ 0.05, **p ≤ 0.01 and ***p ≤ 0.001 between control and immunosuppressant-treated cells. The groups with different letters (a, b, c or d) were significantly different (p ≤ 0.05).

mTOR signaling appeared to be moderately downregulated in Huh7 than HepG2 cells

mTOR kinase activity induces 4E-BP1 phosphorylation, thus promoting CAP-dependent translation [16]. In agreement, the administration of high concentration of Tacrolimus (100 μM), and all tested concentrations of Sirolimus and Everolimus (10 nM, 10 μM and 100 μM) decreased $^{Thr37/Thr46}$P-4E-BP1/4E-BP1 ratio in HepG2 cells (Fig. 3A). The effect on this ratio was restricted to high drug concentration in Huh7 cells (Fig. 3B). However, the regulation of the $^{Thr37/Thr46}$P-4E-BP1/4E-BP1 ratio did not fully reflect the impact of polysome profile. As shown

in Supplementary Fig. 1A, doses of the drugs below 100 μM did not significantly alter the polysome profiles in HepG2 cells (for all supplemental material see www.cellphysiolbiochem.com). In contrast, both Tacrolimus and mTOR inhibitors administered at high concentration (100 μM) resulted in abnormal polysome profiles with a dramatic increase of the 80S peak and a reduction of actively translating polysomes in HepG2 (Fig. 4A) and Huh7 (Fig. 4B). This result is consistent with a reduction of global translation in treated cells. Interestingly, salt treatment was not able to dissociate the 80S peak from treated cells in 40S and 60S subunits, strongly suggesting that this peak does not correspond to 80S vacant ribosome but to monosomes, in clear contrast to the result found for control cells (Supplementary Fig. 1B). Altogether, these results suggest that immunosuppressive drugs at high concentration halts early translation elongation phase in HepG2 cells. Differently, in Huh7 cells the polysome profile appeared to be already slightly

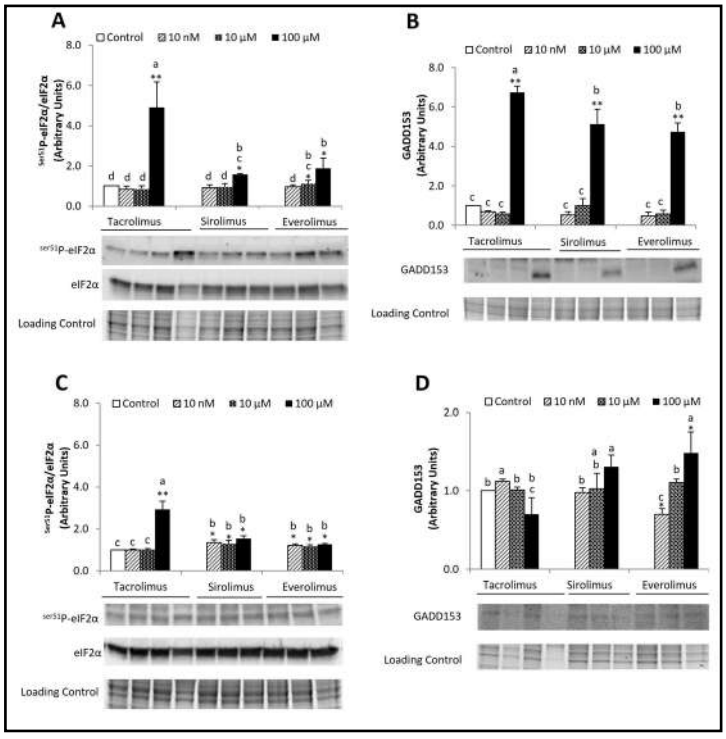

Fig. 2. ^{Ser51}P-eIF2α/eIF2α ratio and GADD153 protein expressions in Tacrolimus-, Sirolimus- and Everolimus-treated HepG2 (A and B, respectively) and Huh7 (C and D, respectively) cells. Treatments were administered at different concentrations (0, 10 nM, 10 μM, and 100 μM). The expression of ^{Ser51}P-eIF2α and eIF2α (3 h), and GADD153 (12 h) was evaluated by Western-blot analysis as described in Material and Methods. Results are expressed as mean ± SEM, and blots are representative of five independent experiments. *p ≤ 0.05 and **p ≤ 0.01 between control and immunosuppressant-treated cells. The groups with different letters (a, b, c or d) were significantly different (p ≤ 0.05).

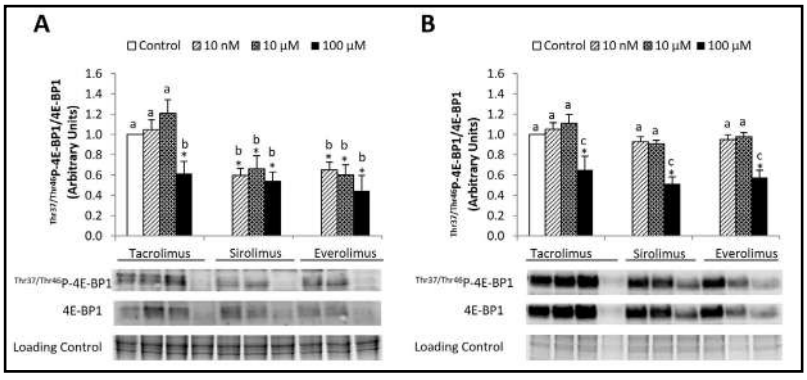

Fig. 3. $^{Thr37/Thr46}$P-4E-BP1/4E-BP1 ratio in Tacrolimus-, Sirolimus- and Everolimus-treated HepG2 (A) and Huh7 (B) cells. Treatments were administered at different concentrations (0, 10 nM, 10 μM, and 100 μM). The protein expression of $^{Thr37/Thr46}$P-4E-BP1/4E-BP1 (6 h) was determined by Western-blot analysis as described in Material and Methods. Results are expressed as mean ± SEM, and blots are representative of four independent experiments. *p ≤ 0.05 between control and immunosuppressant-treated cells. The groups with different letters (a, b or c) were significantly different (p ≤ 0.05).

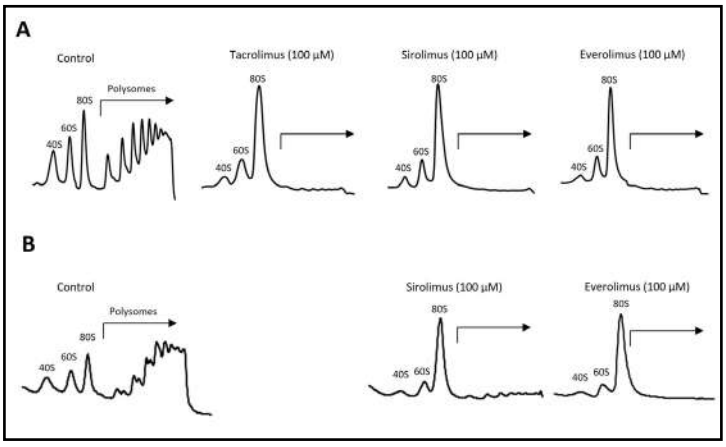

Fig. 4. Polysome profile in Tacrolimus-, Sirolimus- and Everolimus-treated HepG2 (A) and Huh7 (B) cells. Treatments were administered at 100 µM. Polysome profiles (12 h) were obtained following the procedure described in Material and Methods. No polysome profile was observed in Tacrolimus-treated Huh7 cells. Results are expressed as mean ± SEM of three to four independent experiments.

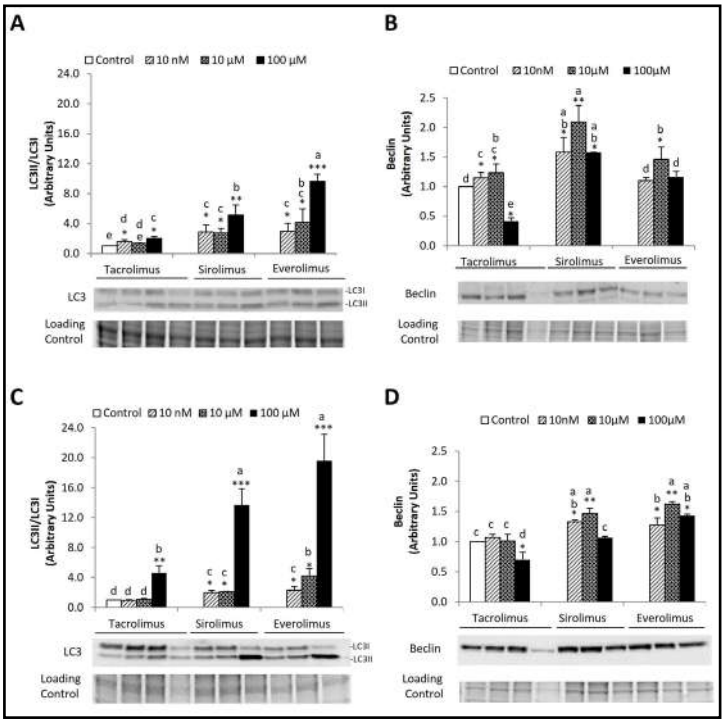

Fig. 5. LC3II/LC3I ratio and Beclin protein expressions in Tacrolimus-, Sirolimus- and Everolimus-treated HepG2 (A and B, respectively) and Huh7 (C and D, respectively) cells. Treatments were administered at different concentrations (0, 10 nM, 10 µM, and 100 µM). The protein expression of LC3II, LC3I and Beclin (6 h) was determined by Western-blot analysis described in Material and Methods. Results are expressed as mean ± SEM, and blots are representative of three to five independent experiments. *p ≤ 0.05, **p ≤ 0.01, and ***p ≤ 0.001 between control and immunosuppressant-treated cells. The groups with different letters (a, b, c, d, or e) were significantly different (p ≤ 0.05).

downregulated in the presence of low doses of mTOR inhibitors (10 µM) while still not altered at low doses of Tacrolimus (Supplementary Fig. 1C). No profile could be obtained for Huh7 cells treated with Tacrolimus at 100 µM concentration probably reflecting a relevant induction of cell death in these conditions (Fig. 4B).

The initiation of autophagy is controlled by the unc-51 like autophagy activating kinase 1 (ULK1)/ULK2 complex, which remains inhibited by mTOR, and is essential for the formation of the phagophore [17]. Thus, as a second readout of the mTOR pathway in hepatoma cells treated with Tacrolimus, Sirolimus and Everolimus, we determined the ratio of LC3II/LC3I and the levels of Beclin, two classical autophagy markers. The administration of mTOR inhibitors increased more significantly than Tacrolimus both parameters in HepG2 (Fig. 5A and 5B) and Huh7 (Fig. 5C and 5D). The LC3II/LC3I ratio appeared to be moderately increased in Huh7 (Fig. 5C) than that observed in HepG2 cells (Fig. 5A).

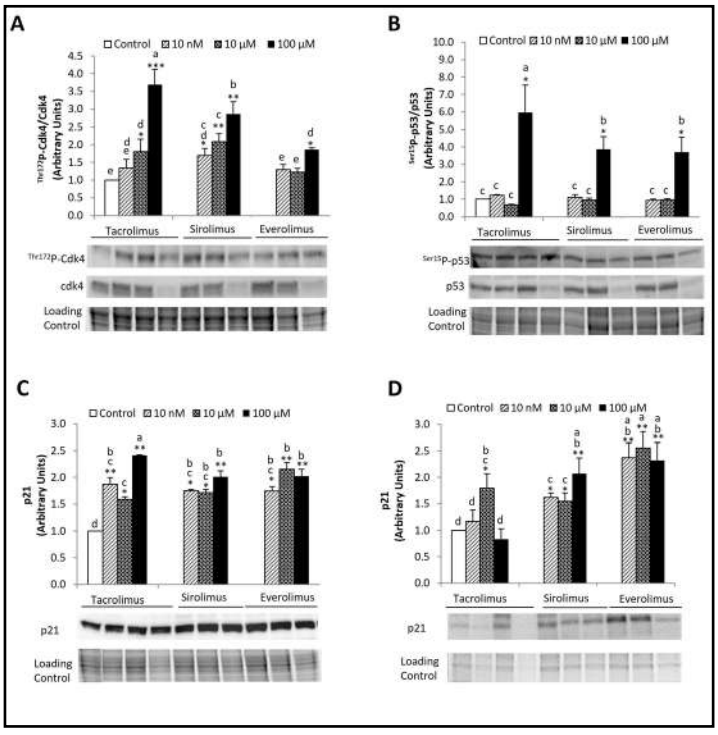

Fig. 6. ^{Thr172}P-Cdk4/Cdk4 (A) and ^{Ser15}P-p53/p53 (B) ratios in Tacrolimus-, Sirolimus- and Everolimus-treated HepG2 cells; as well as p21 protein expression in Tacrolimus-, Sirolimus- and Everolimus-treated HepG2 (C) and Huh7 (D). Treatments were administered at different concentrations (0, 10 nM, 10 µM, and 100 µM). The protein expression of ^{Thr172}P-Cdk4 and Cdk4 (6 h), ^{Ser15}P-p53 and p53 (12 h), and p21 (12 h) was determined by Western-blot analysis. Results are expressed as mean ± SEM, and blots are representative of three to five independent experiments. *p ≤ 0.05, **p ≤ 0.01 and ***p ≤ 0.001 between control and immunosuppressant-treated cells. The groups with different letters (a, b, c, d or e) were significantly different (p ≤ 0.05).

Regulation of cell cycle by Tacrolimus and mTOR inhibitors

We have previously shown that the anti-proliferative properties of Tacrolimus were related to a strong cell cycle arrest at G0/G1 phase in HepG2 cells [13]. The regulation of Cdk4/cyclin D complex and the phosphorylation of retinoblastoma protein (pRB) plays a fundamental role in activating E2F transcription factors, G1/S-phase gene expression and growth control [18, 19]. Calcineurin downregulates Cdk4 phosphorylation and its kinase activity [20]. The administration of Tacrolimus drastically upregulated the ^{Thr172}P-Cdk4/Cdk4 ratio in HepG2 cells (Fig. 6A). Sirolimus and Everolimus were also able to upregulate ^{Thr172}P-Cdk4/Cdk4 but to a lower extent than Tacrolimus (Fig. 6A). p53 is a key transcriptional factor involved in cell cycle arrest mainly through p21 upregulation leading to induction of apoptosis [21]. The expression of wild type p53 was lower in Huh7 compared to that observed in HepG2 cells (Supplementary Fig. 2). The activation of p53 involves its phosphorylation at Ser15. The ^{Ser15}P-p53/p53 ratio was increased after administration of the high concentrations of Tacrolimus and mTOR inhibitors in HepG2 cells (6- and 4-folds, respectively) (Fig. 6B). The pattern of inducibility of p21 by treatments were similar in HepG2 and Huh7 cells (Fig. 6C and 6D). The increase of ^{Ser15}P-p53/p53 ratio (Fig. 4B) and p21 (Fig. 4C) expression may counterbalance the potential pro-proliferative effect caused by ^{Thr172}P-Cdk4/Cdk4 upregulation (Fig. 4A) in HepG2 cells. The expression of p21 in Huh7 (Fig. 6D) was lower than that observed in HepG2 (Fig. 6C). However, a similar p21 pattern of expression upon treatments was observed in both liver cancer cell lines (Fig. 6C and 6D).

Role of FKBPs in the regulation of cell death and proliferation in drug-treated liver cancer cells

FKBPs play a relevant role in physiopathology, cancer and chemoresistance [5]. The administration of low (10 nM-10 µM) doses of Tacrolimus and mTOR inhibitors moderately but significantly increased the protein expression of FKBP12 (Fig. 7A) and FKBP51 (Fig. 7B) in HepG2 cells. However, FKBP12 (Fig. 7C) and FKBP51 (Fig. 7D) remained close to control levels upon the administration of low doses of Tacrolimus and mTOR inhibitor in Huh7 cells. The expression of FKBP38 and FKBP52 did not changed with the treatments (data not shown). In order to further identify the role of FKBP12 and FKBP51 in our system siRNA

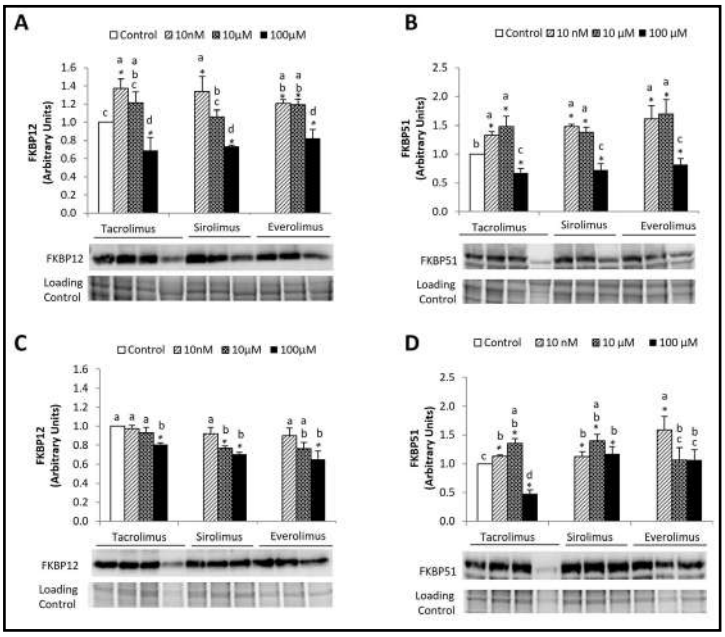

Fig. 7. FKBP12 and FKBP51 protein expressions in Tacrolimus-, Sirolimus- and Everolimus-treated HepG2 (A and B, respectively) and Huh7 (C and D, respectively) cells. Treatments were administered at different concentrations (0, 10 nM, 10 µM, and 100 µM). The protein expression of FKBP12 and FKBP51 was evaluated by Western-blot analysis as described in Material and Methods. Results are expressed as mean ± SEM, and blots are representative of four to six independent experiments. *p ≤ 0.05 between control and immunosuppressant-treated cells. The groups with different letters (a, b, c or d) were significantly different (p ≤ 0.05).

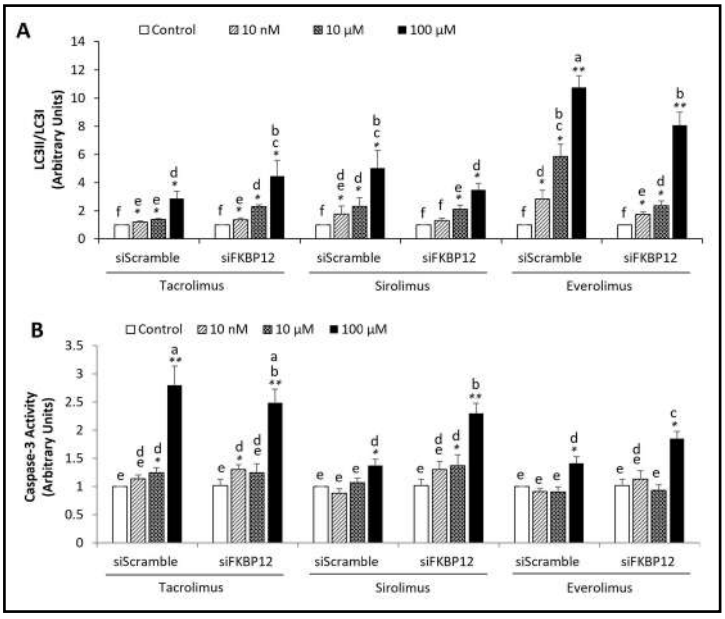

Fig. 8. Impact of FKBP12 downregulation on LC3II/LC3I ratio (A) and caspase-3 activity (B) in Tacrolimus-, Sirolimus- and Everolimus-treated HepG2 cells. The downregulation of FKBP12 was carried using siRNA technologies. Autophagy and apoptosis were determined using the measurement of LC3II/LC3I ratio and commercial caspase-3 activity assay, respectively as described in Materials and Methods. The protein expression of LC3II and LC3I was evaluated by Western-blot analysis as described in Material and Methods. Results are expressed as mean ± SEM of six independent experiments. *p ≤ 0.05 and **p ≤ 0.01 between control and immunosuppressant-treated cells. The groups with different letters (a, b, c, d, e or f) were significantly different (p ≤ 0.05).

technology was applied in HepG2 cells. Interestingly, the knockdown expression of FKBP12 by siRNA increased the LC3II/LC3I ratio (Fig. 8A) in Tacrolimus-treated HepG2 cells, while reduced this ratio and increased caspase-3 activity (Fig. 8B) in HepG2 cells treated with Sirolimus and Everolimus. The knockdown expression of FKBP51 by siRNA reduced BrdU incorporation (Fig. 9A) in control and drug-treated HepG2 cells, and increased caspase-3 activity (Fig. 9B) in drug-treated HepG2 cells. The application of siRNA strategies showed that FKBP12 and FKBP51 mediate cell survival in immunosuppressive-treated HepG2 cells.

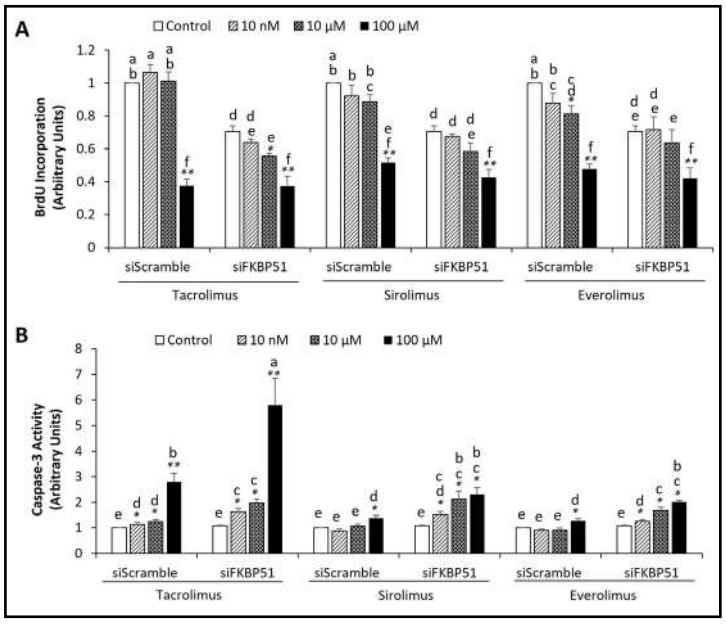

Fig. 9. Impact of FKBP51 downregulation on BrdU incorporation (A) and caspase-3 activity (B) in Tacrolimus-, Sirolimus- and Everolimus-treated HepG2 cells. The downregulation of FKBP51 was carried using siRNA technologies. Cell proliferation and apoptosis were determined using commercial BrdU incorporation and caspase-3 activity assays respectively as described in Material and Methods. Results are expressed as mean ± SEM of six independent experiments. *p ≤ 0.05 and **p ≤ 0.01 between control and immunosuppressant-treated cells. The groups with different letters (a, b, c, d, e or f) were significantly different (p ≤ 0.05).

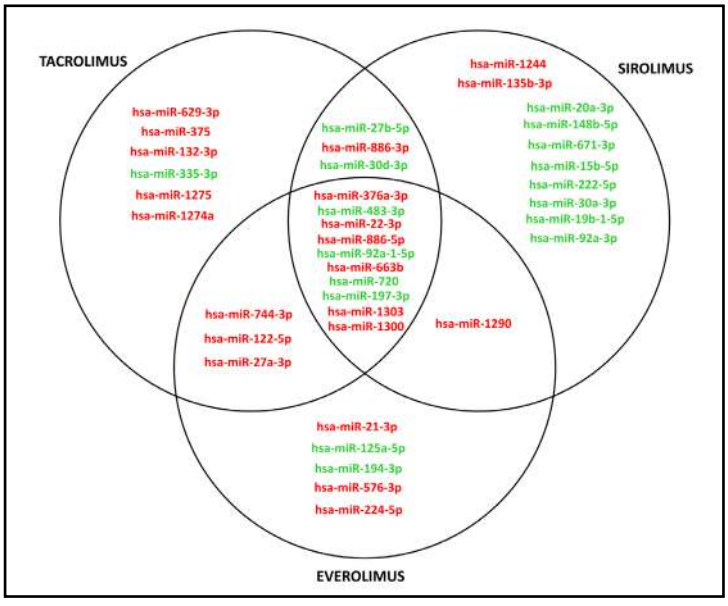

Fig. 10. Up- (red) and down-regulation (green) of miRNA expression in Tacrolimus-, Sirolimus- and Everolimus-treated HepG2 cells. Treatments were administered at 10 µM final concentration. The expression of miRNA was analysed using a commercial TaqMan® OpenArray® Human miRNA Panel as described in Material and Methods. miRNA data are obtained from three independent experiments.

The immunosuppressants drastically altered miRNA expression pattern in HepG2 cells but not in primary human hepatocytes

miRNAs are non-coding short RNA sequences that normally destabilize and/or prevent translation of complementary target mRNAs [22]. The level of expression and activity of critical components of miRNA biogenesis and miRNAs themselves are profoundly altered in all types of cancers [23]. We assessed whether Tacrolimus, Sirolimus and Everolimus were able to alter miRNA expression pattern in primary human hepatocytes and liver cancer cells. As shown in Fig. 10, the induction of apoptosis and reduction of cell proliferation by Tacrolimus, Sirolimus and Everolimus were associated with a decrease of miR-92a-1-5p, miR-197-3p, miR-483-3p and miR-720, and an increase of miR-22-3p, miR-376a-3p, miR-663b, miR-886-5p, miR-1300 and miR-1303 in HepG2 cells (Fig. 10 and Supplementary Table 1). Differently, primary human hepatocytes were highly unresponsiveness to alteration

of miRNA expression by the treatments. In this sense, Tacrolimus only downregulated miR-151a-5p expression (0.369 fold-change, $p \leq 0.042$), while Sirolimus upregulated miR-1291 expression (2.838 fold-change, $p \leq 0.038$) in primary human hepatocytes.

Discussion

HCC is the primary indication for OLT, and the tumor recurrence, which is estimated 8 %-20 % in different studies, is the main drawback for the survival of patients [24]. The administration of immunosuppression therapies, such as calcineurin inhibitors (Cyclosporin A and Tacrolimus) or mTOR inhibitors (Sirolimus and Everolimus), are required to avoid graft rejection in organ transplantation. Tumor-related variables appear to be widely related to recurrence [25]. However, controversial reports exist in relation to the involvement of immunosuppression regimes in tumor recurrence. Cyclosporine A and Tacrolimus have been suggested to be related to increased risk of tumor recurrence post-OLT [26, 27], in contrast to the immunosuppression based on mTOR inhibitors [28-32]. However, the five-year disease-free survival between two cohorts receiving or not Sirolimus regimes following OLT showed no differences in a prospective phase III multicenter randomized-controlled trial [33]. The induction of apoptosis and cell cycle arrest induced by drugs are key features for their antitumoral properties. In this sense, we [13], and others [34-37], have showed that Tacrolimus and mTOR inhibitors promote apoptosis and reduce cell proliferation in cancer cells. In concordance, the present study showed that the administration of Tacrolimus, and to a lesser extent of Sirolimus and Everolimus, greatly increased apoptosis and reduced cell proliferation in HepG2 and Huh7 cells (Fig. 1). Interestingly, this pro-apoptotic and anti-proliferative properties were limited to liver cancer cells, as primary human hepatocytes were unresponsiveness to the different immunosuppressant treatments (Fig. 1).

The ER is highly sensitive to alterations in cellular homeostasis and provides quality control program ensuring that only correctly folded proteins transit to the Golgi and unfolded or misfolded proteins are degraded. The selective upregulation of ER transmembrane proteins PERK, ATF6 or IRE1α induces the activation of unfolded protein response (UPR) that involves transcriptional recovery response, transcriptional induction response of ER chaperones, transcriptional induction response of amino acid transporter and activation of nuclear factor kappa light chain enhancer of activated B cells (NF-κB), and apoptotic response [38]. The main effector of PERK-mediated apoptosis is the transcription factor GADD153 (CHOP) which can be induced through all three ER branches [39]. In our conditions, the administration of Tacrolimus, and mTOR inhibitors to a lesser extent, induced a significant PERK activation measured by ATF4-dependent increase of ^{Ser51}P-eIF2α/eIF2α that led a potent upregulation of GADD153 in HepG2 cells (Fig. 2A and 2B, respectively). Huh7 cells showed a lower responsiveness to these drugs compared to that observed in HepG2 cells (Fig. 2C and 2D versus Fig. 2A and 2B, respectively). The increased upregulation of PERK activation of Tacrolimus versus mTOR inhibitors (Fig. 2) was related to the higher pro-apoptotic and anti-proliferative properties in HepG2 and Huh7 cells (Fig. 1).

FK506-binding domain (FKBD) of FKBP12 binds to Tacrolimus and mTOR inhibitors [6]. The complex generated upon the binding of Sirolimus and Everolimus to FKBP12 interacts with the FKBP-rapamycin binding domain in mTOR, adjacent to the catalytic kinase domain, and blocks its function [40]. The activation of mTOR induces phosphorylation of p70S6K1 and 4E-BP1, and promotes mRNA translation and cell cycle progression [41]. Although mTOR inhibitors reduced around 50 % control $^{Thr37/Thr46}$P-4E-BP1/4E-BP1 in HepG2 cells at any dose tested (Fig. 3A), the global mRNA translation visualized via the analysis of the polysome profiles was only altered at high concentration of the drugs (100 μM) (Fig. 4A) when apoptosis were sharply induced (Fig. 1A). In Huh7 cells, translation is already moderately impaired at a low concentration of mTOR inhibitors but not of Tacrolimus (Supplementary Fig. 1), despite the lack of inhibitory effect on the $^{Thr37/Thr46}$P-4E-BP1/4E-BP1 ratio (Fig. 3B). Interestingly, the negative effect of Tacrolimus or mTOR inhibitors on mRNA translation was characterized by

an increase of the 80S peak and a reduction of actively translating polysomes in HepG2 and Huh7 (Fig. 4A and 4B, respectively). The lack of effectiveness of salt treatment suggested the absence of vacant 80S ribosomes that it is compatible with the blockage of translation at early elongation phase instead of alteration within the initiation of the translation phase in drugs (100 μM)-treated HepG2 cells (Supplementary Fig. 1B). Altogether, these results strongly suggest that other mechanisms different than the activation of the 4E-BP1 repressor protein might be responsible of the impairment of translation.

mTOR inhibits the formation of the initial membrane nucleation of autophagic process through the regulation of a protein complex composed of ULK1, autophagy-related gene 13 (ATG13), and focal adhesion kinase family-interacting protein of 200 kDa (FIP200) [42-44]. The inhibition of mTOR by Sirolimus and Everolimus upregulated the expression of LC3II/LC3I ratio and Beclin in both HepG2 (Fig. 5A and 5B) and Huh7 (Fig. 5C and 5D) cell lines. Interestingly, Tacrolimus was also able to moderately increase autophagic markers which is consistent with the PERK/eIF2α activation signaling and ER-stress-induced autophagy in the two different hepatoma cells lines tested (Fig. 2 and Fig. 5) [45].

Tacrolimus, and to a lesser extent mTOR inhibitors, increased ^{Thr172}P-Cdk4/Cdk4 (Fig. 6A) that could be explained by the Calcineurin inhibition by the immunosuppressive agents [20]. This observation might highlights the potential common impact of Tacrolimus and mTOR inhibitors on Calcineurin activity in contrast to the previous observation in which it was suggested a relevant antagonism of Sirolimus and Everolimus on Tacrolimus-induced Calcineurin inhibition via saturation of FKBP12 in peripheral blood mononuclear cells [46]. The inhibition of Calcineurin-dependent phosphatase activity by Tacrolimus and Cyclosporine increased Cdk4-related activity and cell cycle progression in Jurkat cells [20]. In our experimental setting, the potential risk of pro-proliferative effect of Tacrolimus and mTOR inhibitors by upregulation of Cdk4 phosphorylation, can be counterbalance by the up-regulation of p21 protein expression in the both cell hepatoma cell lines tested (Fig. 6C and 6D). p21 is a universal Cdk inhibitor whose gene expression is upregulated by p53 [47]. It is worthy to mention that p21 expression was also upregulated in Huh7 (Fig. 6D) although a strong reduction of p53 expression was observed in Huh7 compared to that observed in HepG2 (Supplementary Fig. 2).

FKBPs are involved in relevant cellular functions, and play a role in cancer and chemoresistance [5]. The attenuation of NFAT transcriptional activity by Tacrolimus downregulates the expression of downstream target genes such as cyclooxygenase-2 and c-MYC, thus resulting in decreased cell viability/colony formation, cell migration/invasion, and increased apoptosis in bladder cancer cell lines [48]. Several reports have suggested that Sirolimus exerts potent anticancer effects in addition to is immunosuppressant activity [49, 50]. Our study showed that the expression of FKBP12 and FKBP51 was increased in HepG2 cells (Fig. 7A and 7B), but at lower extend in Huh7 (Fig. 7C and 7D), by the administration of low concentrations of the treatments. Tacrolimus and mTOR inhibitors can bind FKBP12 through FKBD [6]. The downregulation of FKBP12 by siRNA strategy increased autophagy in Tacrolimus-treated HepG2 cells, while reduced autophagy and increased apoptosis in mTOR inhibitor-treated HepG2 cells (Fig. 8). The downregulation of FKBP51 reduced cell proliferation in control and immunosuppressant-treated HepG2 cells, while increased apoptosis in immunosuppressant-treated HepG2 cells (Fig. 9). These results suggest that FKBP12 and FKBP51 play a general pro-survival role in liver cancer cells.

miRNAs are small non-coding RNAs of ~22-nucleotides which mediate destabilization and/or translational suppression of target mRNAs bearing partially complementary sequences [22]. The level of expression and activity of different components of the miRNA biogenesis pathway are often found to be dysregulated in cancer [23]. No reports exist in the literature identifying the alteration of miRNA expression caused by Tacrolimus and mTOR inhibitors. The induction of apoptosis and reduction of cell proliferation by Tacrolimus, Sirolimus and Everolimus (10 μM) were associated with a decrease in the expression of miR-92a-1-5p, miR-197-3p, miR-483-3p and miR-720 expressions, while an increase in the expression of miR-22-3p, miR-376a-3p, miR-663b, miR-886-5p, miR-1300 and miR-1303 expression in

HepG2 cells (Fig. 10 and Supplementary Table 1). Very few reports exist identifying the role of the above miRNAs in other settings. In this sense, miR-483-3p is an oncogenic miRNA that affects Wnt/β-catenin, TGF-β, and TP53 signaling pathways by targeting several genes as *CTNNB1*, *SMAD4*, *IGF1*, and *BBC3* in different tumor cells [51]. The downregulation of miR-483-3p by immunosuppressants might be relevant for its antitumoral properties. By contrast, the upregulation of miR-663b [52], miR-22-3p [52] and miR-1303 [53] has been related to oncogenic properties in non-hepatic tumor cells. More studies are required to understand the precise contribution of miRNAs in the cellular response observed upon the treatments with Tacrolimus and mTOR inhibitors in hepatoma cells.

Conclusion

Tacrolimus exerted a more potent pro-apoptotic and anti-proliferative properties than mTOR inhibitors that appeared to be associated with an increased PERK-related induction of ER stress and activation of the p53-p21 cell signaling. FKBP12 and FKBP51 appeared to be the most relevant FKBP partners of immunosuppressants being both related to pro-survival effect in HepG2 cells. FKBP12 and FKB51 appeared to be related to the regulation of cell death or cell proliferation, respectively. A pattern of miRNA expression was observed independently of the administered immunosuppressants in liver cancer cells.

Abbreviations

Autophagy-related gene 13 (ATG13); Barcelona Clinic Liver Cancer (BCLC); Bromodeoxyuridine (BrdU); C/EBP homologous protein (CHOP/GADD153); Endoplasmic reticulum (ER); FK506-binding domain (FKBD); FK506-binding protein (FKBP); Focal adhesion kinase family-interacting protein of 200 kDa (FIP200); Hepatocarcinoma (HCC); Inositol-requiring enzyme 1 α (IRE1α); Mammalian target of rapamycin (mTOR); MicroRNAs (miRNAs); Nuclear factor of activated T cells (NFAT); Nuclear factor kappa light chain enhancer of activated B cells (NF-κB); Ortothopic liver transplant (OLT); Peptidylprolyl cis/trans isomerase (PPIase); Performance status (PS); Protein kinase RNA-like endoplasmic reticulum kinase (PERK); Retinoblastoma protein (pRB); Unfolded protein response (UPR); Unc-51 like autophagy activating kinase 1 (ULK1).

Acknowledgements

The authors declare and ensure that all human samples have been used after obtaining patients's written consent. The study follows the ethical principles written down in the declaration of Helsinki. Furthermore, study protocols and experimental procedures must have been reviewed by the Ethical Committee of the Hospital University "Virgen del Rocío" (Seville, Spain).

We thank the Institute of Health Carlos III (ISCiii) cofinanced by the European Regional Development Fund "A way to achieve Europe" (ERDF) (PI13/00021, P16/00090 and PI19/01266), as well as the Andalusian Ministry of the Economy, Innovation, Science and Employment (CTS-6264) and Andalusian Ministry of Health (PI13/00025, PI16/0198, PIP-0215-2020 and PI-0216-2020) for their financial support to J.M. We also thank the Spanish Ministry of Economy and Competitiveness (MINECO) cofinanced by the ERDF (BFU2016-75352-P AEI/FEDER, EU) for their financial support to J.d.l.C. We thank Biomedical Research Network Center for Liver and Digestive Diseases (CIBERehd) founded by the ISCiii and cofinanced by the ERDF for their financial support. E.N-V. acknowledges IFI18/00014 fellowship from the ISCiii. P.d.l.C-O. acknowledges FPU17/00026 fellowship from the Spanish Ministry of Education (MEC). L.C. acknowledges FPU16/05127 fellowship from the MEC.

Disclosure Statement

The authors have no conflicts of interest to declare.

References

1 Bray F, Ferlay J, Soerjomataram I, Siegel RL, Torre LA, Jemal A: Global cancer statistics 2018: GLOBOCAN estimates of incidence and mortality worldwide for 36 cancers in 185 countries. CA Cancer J Clin 2018;68:394-424.
2 Sangiovanni A, Del Ninno E, Fasani P, De Fazio C, Ronchi G, Romeo R, Morabito A, De Franchis R, Colombo M: Increased survival of cirrhotic patients with a hepatocellular carcinoma detected during surveillance. Gastroenterology 2004;126:1005-1014.
3 Bruix J, Reig M, Sherman M: Evidence-Based Diagnosis, Staging, and Treatment of Patients With Hepatocellular Carcinoma. Gastroenterology 2016;150:835-853.
4 Galat A: Peptidylprolyl cis/trans isomerases (immunophilins): biological diversity--targets--functions. Curr Top Med Chem 2003;3:1315-1347.
5 Romano S, Sorrentino A, Di Pace AL, Nappo G, Mercogliano C, Romano MF: The emerging role of large immunophilin FK506 binding protein 51 in cancer. Curr Med Chem 2011;18:5424-5429.
6 Siekierka JJ, Hung SH, Poe M, Lin CS, Sigal NH: A cytosolic binding protein for the immunosuppressant FK506 has peptidyl-prolyl isomerase activity but is distinct from cyclophilin. Nature 1989;341:755-757.
7 Ke H, Huai Q: Structures of calcineurin and its complexes with immunophilins-immunosuppressants. Biochim Biophys Res Commun 2003;311:1095-1102.
8 Bierer BE, Mattila PS, Standaert RF, Herzenberg LA, Burakoff SJ, Crabtree G, Schreiber SL: Two distinct signal transmission pathways in T lymphocytes are inhibited by complexes formed between an immunophilin and either FK506 or rapamycin. Proc Natl Acad Sci U S A 1990;87:9231-9235.
9 Sharma VK, Li B, Khanna A, Sehajpal PK, Suthanthiran M: Which way for drug-mediated immunosuppression? Curr Opin Immunol 1994;6:784-790.
10 Sabers CJ, Martin MM, Brunn GJ, Williams JM, Dumont FJ, Wiederrecht G, Abraham RT: Isolation of a protein target of the FKBP12-rapamycin complex in mammalian cells. J Biol Chem 1995;270:815-822.
11 Pichard L, Raulet E, Fabre G, Ferrini JB, Ourlin JC, Maurel P: Human hepatocyte culture. Methods Mol Biol 2006;320:283-293.
12 Kressler D, de la Cruz J, Rojo M, Linder P: Fal1p is an essential DEAD-box protein involved in 40S-ribosomal-subunit biogenesis in Saccharomyces cerevisiae. Mol Cell Biol 1997;17:7283-7294.
13 Navarro-Villaran E, Tinoco J, Jimenez G, Pereira S, Wang J, Aliseda S, Rodriguez-Hernandez MA, Gonzalez R, Marin-Gomez LM, Gomez-Bravo MA, Padillo FJ, Alamo-Martinez JM, Muntane J: Differential Antitumoral Properties and Renal-Associated Tissue Damage Induced by Tacrolimus and Mammalian Target of Rapamycin Inhibitors in Hepatocarcinoma: *In vitro* and *In vivo* Studies. PLoS One 2016;11:e0160979.
14 Szegezdi E, Logue SE, Gorman AM, Samali A: Mediators of endoplasmic reticulum stress-induced apoptosis. EMBO Rep 2006;7:880-885.
15 Fribley A, Zhang K, Kaufman RJ: Regulation of apoptosis by the unfolded protein response. Methods Mol Biol 2009;559:191-204.
16 Gingras AC, Gygi SP, Raught B, Polakiewicz RD, Abraham RT, Hoekstra MF, Aebersold R, Sonenberg N: Regulation of 4E-BP1 phosphorylation: a novel two-step mechanism. Genes Dev 1999;13:1422-1437.
17 Mercer CA, Kaliappan A, Dennis PB: A novel, human Atg13 binding protein, Atg101, interacts with ULK1 and is essential for macroautophagy. Autophagy 2009;5:649-662.
18 Tamrakar S, Rubin E, Ludlow JW: Role of pRB dephosphorylation in cell cycle regulation. Front Biosci 2000;5:D121-137.
19 Dowdy SF, Hinds PW, Louie K, Reed SI, Arnold A, Weinberg RA: Physical interaction of the retinoblastoma protein with human D cyclins. Cell 1993;73:499-511.
20 Baksh S, DeCaprio JA, Burakoff SJ: Calcineurin regulation of the mammalian G0/G1 checkpoint element, cyclin dependent kinase 4. Oncogene 2000;19:2820-2827.
21 Harris SL, Levine AJ: The p53 pathway: positive and negative feedback loops. Oncogene 2005;24:2899-2908.

22 Patil VS, Zhou R, Rana TM: Gene regulation by non-coding RNAs. Crit Rev Biochem Mol Biol 2014;49:16-32.
23 Hata A, Lieberman J: Dysregulation of microRNA biogenesis and gene silencing in cancer. Sci Signal 2015;8:re3.
24 Silva MF, Sherman M: Criteria for liver transplantation for HCC: what should the limits be? J Hepatol 2011;55:1137-1147.
25 Santopaolo F, Lenci I, Milana M, Manzia TM, Baiocchi L: Liver transplantation for hepatocellular carcinoma: Where do we stand? World J Gastroenterol 2019;25:2591-2602.
26 Vivarelli M, Cucchetti A, La Barba G, Ravaioli M, Del Gaudio M, Lauro A, Grazi GL, Pinna AD: Liver transplantation for hepatocellular carcinoma under calcineurin inhibitors: reassessment of risk factors for tumor recurrence. Ann Surg 2008;248:857-862.
27 Rodriguez-Peralvarez M, Tsochatzis E, Naveas MC, Pieri G, Garcia-Caparros C, O'Beirne J, Poyato-Gonzalez A, Ferrin-Sanchez G, Montero-Alvarez JL, Patch D, Thorburn D, Briceno J, De la Mata M, Burroughs AK: Reduced exposure to calcineurin inhibitors early after liver transplantation prevents recurrence of hepatocellular carcinoma. J Hepatol 2013;59:1193-1199.
28 Tallon Aguilar L, Barrera Pulido L, Bernal Bellido C, Pareja Ciuro F, Suarez Artacho G, Alamo Martinez JM, Garcia Gonzalez I, Gomez Bravo MA, Bernardos Rodriguez A: Causes and predisposing factors of de novo tumors in our series of liver transplant recipients. Transplant Proc 2009;41:2453-2454.
29 Toso C, Patel S, Asthana S, Kawahara T, Girgis S, Kneteman NN, Shapiro AM, Bigam DL: The impact of sirolimus on hepatocyte proliferation after living donor liver transplantation. Clin Transplant 2010;24:695-700.
30 Ferreiro AO, Vazquez-Millan MA, Lopez FS, Gutierrez MG, Diaz SP, Patino MJ: Everolimus-based immunosuppression in patients with hepatocellular carcinoma at high risk of recurrence after liver transplantation: a case series. Transplant Proc 2014;46:3496-3501.
31 Zimmerman MA, Trotter JF, Wachs M, Bak T, Campsen J, Skibba A, Kam I: Sirolimus-based immunosuppression following liver transplantation for hepatocellular carcinoma. Liver Transpl 2008;14:633-638.
32 Angelico R, Parente A, Manzia TM: Using a weaning immunosuppression protocol in liver transplantation recipients with hepatocellular carcinoma: a compromise between the risk of recurrence and the risk of rejection? Transl Gastroenterol Hepatol 2017;2:74.
33 Geissler EK, Schnitzbauer AA, Zulke C, Lamby PE, Proneth A, Duvoux C, Burra P, Jauch KW, Rentsch M, Ganten TM, Schmidt J, Settmacher U, Heise M, Rossi G, Cillo U, Kneteman N, Adam R, van Hoek B, Bachellier P, Wolf P, et al.: Sirolimus use in liver transplant recipients with hepatocellular carcinoma: a randomized, multicenter, open-label phase 3 trial. Transplantation 2016;100:116-125.
34 Wang Z, Zhou J, Fan J, Tan CJ, Qiu SJ, Yu Y, Huang XW, Tang ZY: Sirolimus inhibits the growth and metastatic progression of hepatocellular carcinoma. J Cancer Res Oncol 2009;135:715-722.
35 Boulay A, Rudloff J, Ye J, Zumstein-Mecker S, O'Reilly T, Evans DB, Chen S, Lane HA: Dual inhibition of mTOR and estrogen receptor signaling *in vitro* induces cell death in models of breast cancer. Clin Cancer Res 2005;11:5319-5328.
36 Avellino R, Romano S, Parasole R, Bisogni R, Lamberti A, Poggi V, Venuta S, Romano MF: Rapamycin stimulates apoptosis of childhood acute lymphoblastic leukemia cells. Blood 2005;106:1400-1406.
37 Chung YW, Chung MW, Choi SK, Choi SJ, Choi SJN, Chung SY: Tacrolimus-induced apoptosis is mediated by endoplasmic reticulum-derived calcium-dependent caspases-3,-12 in Jurkat cells. Transplant Proc 2018;50:1172-1177.
38 Zhang K, Kaufman RJ: The unfolded protein response: a stress signaling pathway critical for health and disease. Neurology 2006;66:S102-109.
39 Verfaillie T, Salazar M, Velasco G, Agostinis P: Linking ER stress to autophagy: potential implications for cancer therapy. Int J Cell Biol 2010;2010:930509.
40 Choi J, Chen J, Schreiber SL, Clardy J: Structure of the FKBP12-rapamycin complex interacting with the binding domain of human FRAP. Science 1996;273:239-242.
41 Neuhaus P, Klupp J, Langrehr JM: mTOR inhibitors: an overview. Liver Transpl 2001;7:473-484.
42 Ganley IG, Lam du H, Wang J, Ding X, Chen S, Jiang X: ULK1.ATG13.FIP200 complex mediates mTOR signaling and is essential for autophagy. J Biol Chem 2009;284:12297-12305.

43 Hosokawa N, Hara T, Kaizuka T, Kishi C, Takamura A, Miura Y, Iemura S, Natsume T, Takehana K, Yamada N, Guan JL, Oshiro N, Mizushima N: Nutrient-dependent mTORC1 association with the ULK1-Atg13-FIP200 complex required for autophagy. Mol Biol Cell 2009;20:1981-1991.
44 Jung CH, Jun CB, Ro SH, Kim YM, Otto NM, Cao J, Kundu M, Kim DH: ULK-Atg13-FIP200 complexes mediate mTOR signaling to the autophagy machinery. Mol Biol Cell 2009;20:1992-2003.
45 Kouroku Y, Fujita E, Tanida I, Ueno T, Isoai A, Kumagai H, Ogawa S, Kaufman RJ, Kominami E, Momoi T: ER stress (PERK/eIF2alpha phosphorylation) mediates the polyglutamine-induced LC3 conversion, an essential step for autophagy formation. Cell Death Differ 2007;14:230-239.
46 van Rossum HH, Romijn FP, Smit NP, de Fijter JW, van Pelt J: Everolimus and sirolimus antagonize tacrolimus based calcineurin inhibition via competition for FK-binding protein 12. Biochem Pharmacol 2009;77:1206-1212.
47 Sherr CJ: G1 phase progression: cycling on cue. Cell 1994;79:551-555.
48 Kawahara T, Kashiwagi E, Ide H, Li Y, Zheng Y, Miyamoto Y, Netto GJ, Ishiguro H, Miyamoto H: Cyclosporine A and tacrolimus inhibit bladder cancer growth through down-regulation of NFATc1. Oncotarget 2015;6:1582-1593.
49 Periyasamy S, Hinds T, Jr., Shemshedini L, Shou W, Sanchez ER: FKBP51 and Cyp40 are positive regulators of androgen-dependent prostate cancer cell growth and the targets of FK506 and cyclosporin A. Oncogene 2010;29:1691-1701.
50 Cloughesy TF, Yoshimoto K, Nghiemphu P, Brown K, Dang J, Zhu S, Hsueh T, Chen Y, Wang W, Youngkin D, Liau L, Martin N, Becker D, Bergsneider M, Lai A, Green R, Oglesby T, Koleto M, Trent J, Horvath S, Mischel PS, Mellinghoff IK, Sawyers CL: Antitumor activity of rapamycin in a Phase I trial for patients with recurrent PTEN-deficient glioblastoma. PLoS Med 2008;5:e8.
51 Pepe F, Visone R, Veronese A: The glucose-regulated miR-483-3p influences key signaling pathways in cancer. Cancers (Basel) 2018;10:pii:E181.
52 Jiang H, Cheng L, Hu P, Liu R: MicroRNA663b mediates TAM resistance in breast cancer by modulating TP73 expression. Mol Med Rep 2018;18:1120-1126.
53 Li Z, Xu Z, Xie Q, Gao W, Xie J, Zhou L: miR-1303 promotes the proliferation of neuroblastoma cell SH-SY5Y by targeting GSK3beta and SFRP1. Biomed Pharmacother 2016;83:508-513.

Rodríguez-Hernández et al. *Cell Death and Disease* (2020)11:339
https://doi.org/10.1038/s41419-020-2558-1

Cell Death & Disease

ARTICLE Open Access

Differential effectiveness of tyrosine kinase inhibitors in 2D/3D culture according to cell differentiation, p53 status and mitochondrial respiration in liver cancer cells

María A. Rodríguez-Hernández[1,2], Raquel Chapresto-Garzón[1], Miryam Cadenas[1], Elena Navarro-Villarán[1,2], María Negrete[1], Miguel A. Gómez-Bravo[1,2,3], Victor M. Victor[2,4,5], Francisco J. Padillo[1,2,3] and Jordi Muntané[1,2,3]

Abstract

Sorafenib and Regorafenib are the recommended first- and second-line therapies in patients with advanced hepatocellular carcinoma (HCC). Lenvatinib and Cabozantinib have shown non-inferior antitumoral activities compared with the corresponding recommended therapies. The clinical trials have established recommended doses for each treatment that lead different blood concentrations in patients for Sorafenib (10 μM), Regorafenib (1 μM), Lenvatinib (0.1 μM), and Cabozantinib (1 μM). However, very low response rates are observed in patients attributed to intrinsic resistances or upregulation of survival signaling. The aim of the study was the comparative dose–response analysis of the drugs (0–100 μM) in well-differentiated (HepG2, Hep3B, and Huh7), moderately (SNU423), and poorly (SNU449) differentiated liver cancer cells in 2D/3D cultures. Cells harbors wild-type p53 (HepG2), non-sense p53 mutation (Hep3B), inframe p53 gene deletion (SNU423), and p53 point mutation (Huh7 and SNU449). The administration of regular used in vitro dose (10 μM) in 3D and 2D cultures, as well as the dose–response analysis in 2D cultures showed Sorafenib and Regorafenib were increasingly effective in reducing cell proliferation, and inducing apoptosis in well-differentiated and expressing wild-type p53 in HCC cells. Lenvatinib and Cabozantinib were particularly effective in moderately to poorly differentiated cells with mutated or lacking p53 that have lower basal oxygen consumption rate (OCR), ATP, and maximal respiration capacity than observed in differentiated HCC cells. Sorafenib and Regorafenib downregulated, and Lenvatinib and Cabozantinib upregulated epidermal growth factor receptor (EGFR) and mesenchymal–epithelial transition factor receptor (c-Met) in HepG2 cells. Conclusions: Sorafenib and Regorafenib were especially active in well-differentiated cells, with wild-type p53 and increased mitochondrial respiration. By contrast, Lenvatinib and Cabozantinib appeared more effective in moderately to poorly differentiated cells with mutated p53 and low mitochondrial respiration. The development of strategies that allow us to deliver increased doses in tumors might potentially enhance the effectiveness of the treatments.

Introduction

Liver cancer is the sixth most common cancer and the fourth most frequent cause of cancer-related death worldwide[1]. Sorafenib is the standard of care for patients in advanced hepatocellular carcinoma (HCC) stage[2,3]. Different phase III clinical trials showed Lenvatinib was statistically non-inferior to Sorafenib in overall median survival as first-line therapy[4], and Regorafenib was

Correspondence: Jordi Muntané (jmuntane-ibis@us.es)
[1]Institute of Biomedicine of Seville (IBiS), Hospital University "Virgen del Rocío"/CSIC/University of Seville, Seville, Spain
[2]Spanish Network for Biomedical Research in Hepatic and Digestive diseases (CIBERehd), Institute of Health Carlos III (ISCIII), Madrid, Spain
Full list of author information is available at the end of the article
Edited by U. Maurer

SPRINGER NATURE CDDpress

recommended as second-line therapy in patients non-responsive but tolerant to Sorafenib[5]. Cabozantinib has also showed positive results as a second-line treatment for advanced HCC[6].

Sorafenib is a multityrosine kinase inhibitor, and Raf-mitogen-activated protein kinase (MAPK)–extracellular signal-regulated kinase (ERK) signaling[7], with potent antiproliferative and proapoptotic properties in liver cancer cells[8,9]. The induction of cell death by Sorafenib has been related to a rise in PUMA and BIM, as well as a reduction in induced myeloid leukemia cell differentiation protein (Mcl-1) and survivin[9]. Sorafenib (10 μM) induced a sustained endoplasmic reticulum stress promoting a rise of Bim_{EL} expression that mediates the shift from survival autophagic pathway to apoptosis in HepG2[10]. Regorafenib, Lenvatinib, and Cabozantinib have also been shown to promote cell death and antiproliferative properties in vitro and in vivo, using different cancer cells lines[11–13].

The aim of the present study was to determine the impact of cell differentiation stage and p53 genetic status in the effectiveness of tyrosine kinase receptor inhibitors (TKIs) in liver cancer cells. A comparative dose–response analysis of the antiproliferative and proapoptotic effectiveness of Sorafenib, Regorafenib, Lenvatinib, and Cabozantinib was carried out in 2D and 3D cultured liver cancer cells. The study includes HCC cell lines in well- (HepG2, Hep3B, and Huh7), moderately (SNU423), and poorly (SNU449) differentiated stages, as well as expressing wild-type p53 (HepG2), non-sense p53 mutation (Hep3B), inframe p53 gene deletion (SNU423), and p53 point mutation (Huh7 and SNU449)[14,15].

Materials and methods

Drugs

Sorafenib (FS10808), Regorafenib (FR16116), Cabozantinib (FD59688), and Lenvatinib (FC75063) were obtained from Carbosynth Limited (Berkshire, UK). Drugs were solved in dimethyl sulfoxide as stock solution (100 mM).

Primary human hepatocytes, cell lines, and culture conditions

Human hepatocytes were prepared from liver biopsies obtained from two patients (one female and one man, aged 43 ± 6.0 years) submitted to surgical resection for liver tumors after obtaining patients' written consent. The study protocol was approved by the Ethical Committee of the Institution. The isolation of human hepatocytes was based on the two-step collagenase procedure, and cells were cultured as previously described[16]. HepG2 (HB-8065™, American Type Culture Collection (ATCC)/LGC Standards, SLU, Barcelona, Spain), Hep3B (HB-8064™, ATCC/LGC Standards), Huh7 (Apath LLC, Brooklyn, USA), SNU423 (CRL-2238, ATCC/LGC Standards), and SNU449 (CRL-2234, ATCC/LGC Standards) cell lines were cultured in supplemented Minimum Essential Medium with Earle's Balanced Salts (GE Healthcare HyClone, Boston, USA) at 37°C in a humidified incubator with 5% CO_2.

Multicellular spheroids were generated according to the liquid overlay technique (Supplementary Fig. 1)[17]. The spheroid area (μm^2), non-trypan and trypan blue-stained cells, Ki67- and TUNEL-positive cells, and caspase-3 activity were analyzed in spheroids (%, fold over control). Cells were also cultured in monolayer (100,000 cells/cm^2). Treatments (0–100 μM) were administrated 24 h after plating, and cell lysates obtained at different time points for measuring cell proliferation and apoptosis as previously described[10].

Cell proliferation

Cell proliferation was assessed in 3D and 2D cultured cells. Non-trypan blue-stained viable cells were quantified in trypsin-treated spheroids, as well as Ki67-positive cells were determined in 4% paraformaldehyde-fixed spheroid sections (5 μ) by immunocytochemistry as described previously[18]. Immunofluorescence analysis was performed using Olympus BX61 microscope. Fluorescence quantification was performed using Leica Application Suite Advanced Fluorescence software and ImageJ software. Cell proliferation rate was also measured by bromodeoxyuridine (BrdU) incorporation in 2D cultured cells using the recommendation included in the commercial assay (11647229001, Roche Diagnostics, Basel, Switzerland)[18]. Data are shown as the relative absorbance at 370 nm, using as reference wavelength 492 nm (Absorbance, %, fold over control) using an Infinite 200 PRO Microplate Reader (TECAN, Männedorf, Switzerland).

Measurement of cell death

Cell death was assessed either in trypsin-isolated cells with the measurement of trypan blue-stained non-viable cells in spheroids, or TUNEL-positive cells in 4% paraformaldehyde-fixed spheroid sections (5 μ) useful for DeadEnd™ Fluorometric TUNEL System (G3250, Promega, Madison, Wisconsin, USA). Caspase-3-associated activity was determined using Caspase-Glo® Assay Systems (G8091, Promega) in 3D and 2D cultured cells. Both, spheroids and cells were lysed as described above and treated with Caspase-Glo® Reagent in an "add-mix-measure" format, resulting in caspase-3-dependent cleavage of the substrate and generation of a "glow-type" luminescent signal. The signal generated is proportional to the amount of caspase activity. The values were extrapolated into a calibration curve included in the assay and the results are shown as the relative light units (RLU, %, fold over control).

Mitochondrial respiration

Mitochondrial respiration in intact adhered cells was assessed with the XFp Cell Mito Stress Test Kit in a XFp Extracellular Flux Analyzer (Seahorse Bioscience, Billerica, Massachusetts, USA). Oxygen consumption rate (OCR) was measured in cells 48 h after plating and data normalized to total protein content per well (pmol/min/μg protein) as previously described[19].

Expression of tyrosine kinase receptors

The expression of epidermal growth factor receptor (EGFR), vascular endothelial growth factor receptor (VEGFR), platelet-derived growth factor receptor (PDGFR), fibroblast growth factor receptor (FGFR), and mesenchymal–epithelial transition factor receptor (c-Met) was determined by SDS–PAGE electrophoresis coupled to western blot analysis. Proteins (50–100 μg)

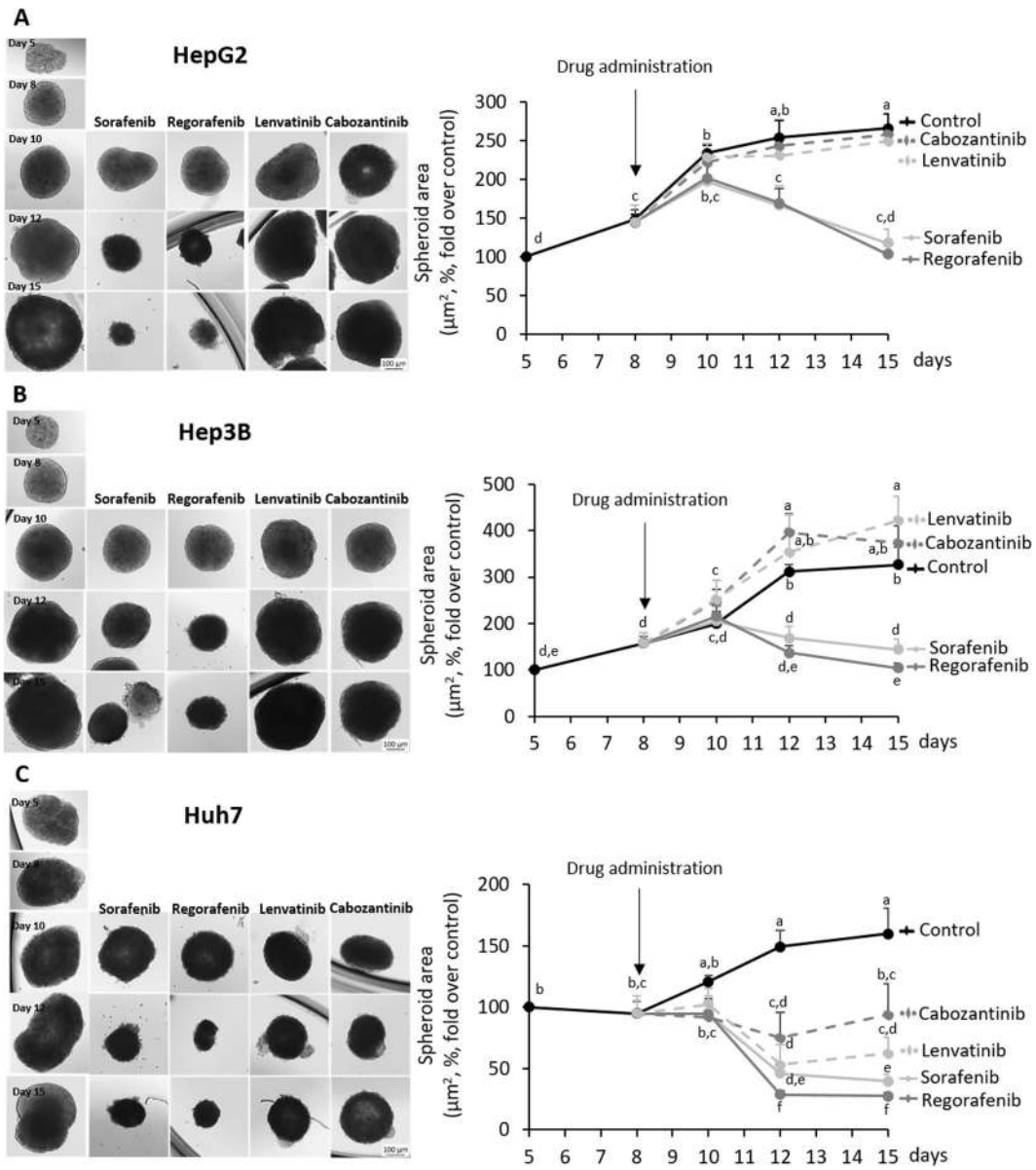

Fig. 1 Drug effectiveness in liver cancer cells cultured in spheroids. Effect of Sorafenib, Regorafenib, Lenvatinib, and Cabozantinib in the area of spheroids generated by HepG2 (**a**), Hep3B (**b**), and Huh7 (**c**) cells. Drugs (10μM) were administered at day 8th after spheroid establishment, and cultures were maintained up to day 15th as described in "Materials and methods" section. The area of the spheroids (μm², %, fold over control) were measured at days 8th, 10th, 12th, and 15th. All results are expressed as mean±SD of independent experiments ($n = 3$). The groups with statistically significant differences among them ($p \leq 0.05$) were indicated with different letters (a, b, c, d, e, or f). Magnification of images are ×10.

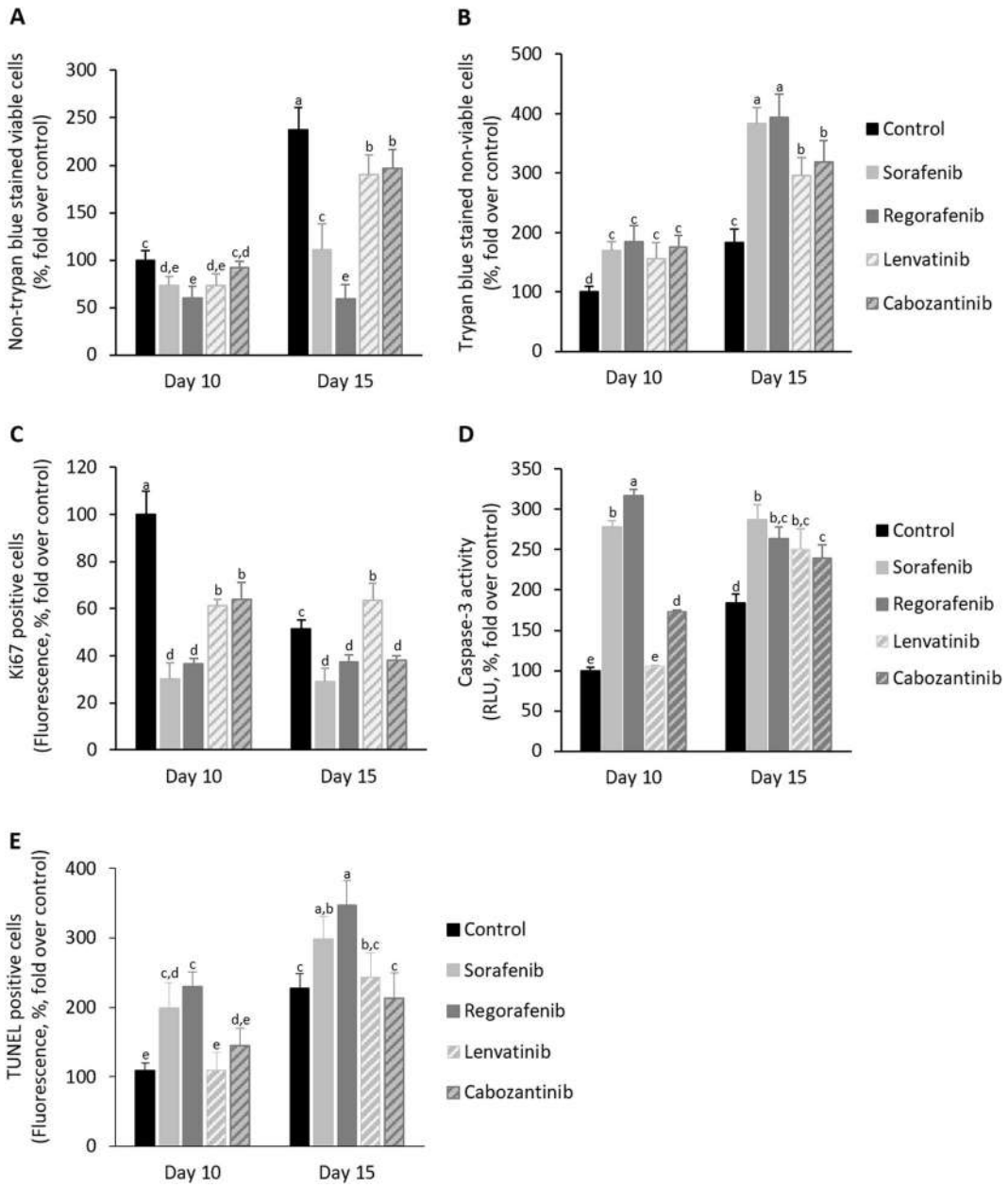

Fig. 2 Drug effectiveness in HepG2 cells cultured in spheroids. Effect of Sorafenib, Regorafenib, Lenvatinib, and Cabozantinib in non-trypan blue-stained viable cells **(a)**, trypan blue non-viable cells (**b**), Ki67-positive cells (**c**), caspase-3 activity (**d**), and TUNEL-positive cells (**e**) in spheroids generated by HepG2 cells. Drugs (10μM) were administered at day 8th after spheroid establishment, and cultures were maintained up to day 15th as described in "Material and methods" section. The parameters were measured at days 10th and 15th. Trypan blue staining in cells from trypsin-dissociated spheroids allowed the identification of viable and non-viable cells (%, fold over control). Ki67- and TUNEL-positive cells were determined by immunohistochemistry, and caspase-3 activity was assessed using commercial caspase-Glo® Assay Systems as described in "Materials and methods" section. Ki67- and TUNEL-positive cells were assessed by fluorescence methods (fluorescence, %, fold over control). Caspase-3 activity is shown as the RLU (%, fold over control). All results are expressed as mean±SD of independent experiments ($n = 3$). The groups with statistically significant differences among them ($p \leq 0.05$) were indicated with different letters (a, b, c, d, or e).

were separated by Any kD™ Criterion™ TGX Stain-Free™ Protein Gel, 18 well, 30 µl (#5678124, BioRad, Hercules, California, USA), and transferred to PVDF membranes. The system uses stain-free technology, which is a method that appears to be more reliable as a protein loading control than the measurement of housekeeping proteins[20]. The membranes were incubated with the corresponding commercial primary EGFR (#4267 S), VEGFR

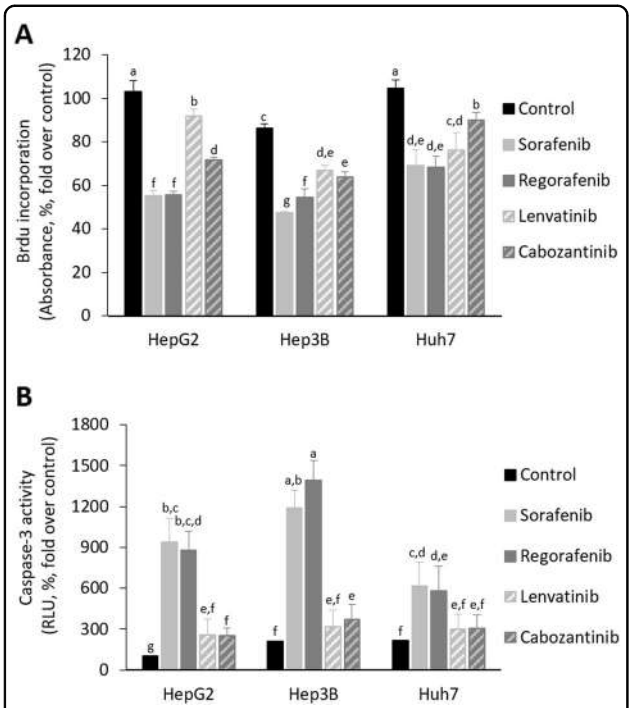

Fig. 3 Drug effectiveness in liver cancer cells cultured in monolayer. Effect of Sorafenib, Regorafenib, Lenvatinib, and Cabozantinib in BrdU incorporation (**a**) and caspase-3 activity (**b**) in HepG2, Hep3b, and Huh7 cells cultured in 2D system. Drugs (10μM) were administered at 24h after plating. BrdU incorporation and caspase-3 activity were determined 24h after drug administration using commercial colorimetric assay and caspase-Glo® Assay Systems as described in "Materials and methods" section, respectively. BrdU incorporation is shown as the absorbance at 370nm (reference wavelength: 492nm; absorbance, %, fold over control). Caspase-3 activity is shown as the RLU (%, fold over control). All results are expressed as mean ± SD of independent experiments ($n = 4$). The groups with statistically significant differences among them ($p \leq 0.05$) were indicated with different letters (a, b, c, d, e, f, or g).

(#2479 S), PDGFR (#3174 S), FGFR (#3472 S), and c-Met (#8198 S) obtained from Cell Signaling Technology (Danvers, Massachusetts, USA), and secondary anti-rabbit (sc-2004) IgG-HRP-labeled (Santa Cruz Biotechnology, Inc, Dallas, Texas, USA) antibodies revealing protein content by Clarity™ Western ECL substrate (170–5061, BioRad) and analyzed in a ChemiDoc™ Touch Imaging System. The densitometric analysis (Densitometry, %, fold over control) was performed using the software Image Lab 6.0 of BioRad.

Statistical analysis

All results are expressed as mean ± SD of independent experiments ($n = 2$–8). Data were compared using the analysis of variance with the Least Significant Difference's test as post hoc multiple comparison analysis (homogeneity of variances) or Games-Howell (non-homogeneity of variances). If Shapiro–Wilks's test showed non-normal distribution of data nonparametric Kruskal–Wallis coupled to Mann–Whitney *U* post hoc analysis with Finner's correction was done. The level of significance was set at $^{*}p \leq 0.05$, $^{**}p \leq 0.01$, and $^{***}p \leq 0.001$ between groups. The groups with statistically significant differences ($p \leq 0.05$) were also indicated with different letters. The sample size was determined using Granmo v7 software. All statistical analyses were performed using the IBM SPSS Statistics 19.0.0 (SPSS Inc., IBM, Armonk, New York, USA) software.

Results

Differential antiproliferative and proapoptotic properties of Sorafenib, Regorafenib, Lenvatinib, and Cabozantinib administered at a regular used in vitro dose (10 μM) in 3D and 2D cultured-differentiated HCC with different p53 status

The administration of Sorafenib and Regorafenib strongly reduced the area of spheroids generated from HepG2, Hep3B, and Huh7 cells (Fig. 1a–c, Supplementary Table 1). Lenvatinib and Cabozantinib appeared to be effective in Huh7 (Fig. 1c, Supplementary Table 1), but not in HepG2 and Hep3B cell lines (Fig. 1a, b, Supplementary Table 1). Sorafenib and Regorafenib reduced Ki67-positive cells (Fig. 2c), as well as increased caspase-3 activity (Fig. 2d) and TUNEL-positive cells (Fig. 2e) at day 10th, and while reduced non-trypan blue-stained viable cells (Fig. 2a) and increased trypan blue-stained non-viable cells (Fig. 2b) at day 15th in spheroids more strongly than Lenvatinib and Cabozantinib in cultured spheroids. The increased antiproliferative and proapoptotic effectiveness of Sorafenib and Regorafenib versus Lenvatinib and Cabozantinib (10 μM) in spheroids was further assessed in 2D cultured HepG2, Hep3B, and Huh7 cells (24 h, Fig. 3). BrdU incorporation (Fig. 3a) and caspase-3 activity (Fig. 3b) in 2D cultured HepG2, Hep3B, and Huh7 cell lines partially confirmed 3D data. Sorafenib and Regorafenib exerted potent antiproliferative and proapoptotic effects in decreasing order of effectiveness in HepG2 ≥ Hep3B ≥ Huh7 cultured in 2D system (Fig. 3a, b). Lenvatinib and Cabozantinib were also able to reduce cell proliferation (Fig. 3a), and at low extend increased caspase-3 activity in HepG2 cells (Fig. 3b), in HCC cells cultured in monolayer.

Dose–response antiproliferative and proapoptotic properties of Sorafenib, Regorafenib, Lenvatinib, and Cabozantinib in primary human hepatocytes and HCC cell lines according to differentiation and p53 status

Sorafenib (10 μM) exerted a potent antiproliferative activity at 24 h in all HCC cell lines (Fig. 4a). Regorafenib (10 μM) also exerted, but at lower extent than Sorafenib, antiproliferative activity in decreasing order HepG2 ≥ Hep3B ≥ SNU423 ≥ SNU449 ≥ Huh7. However,

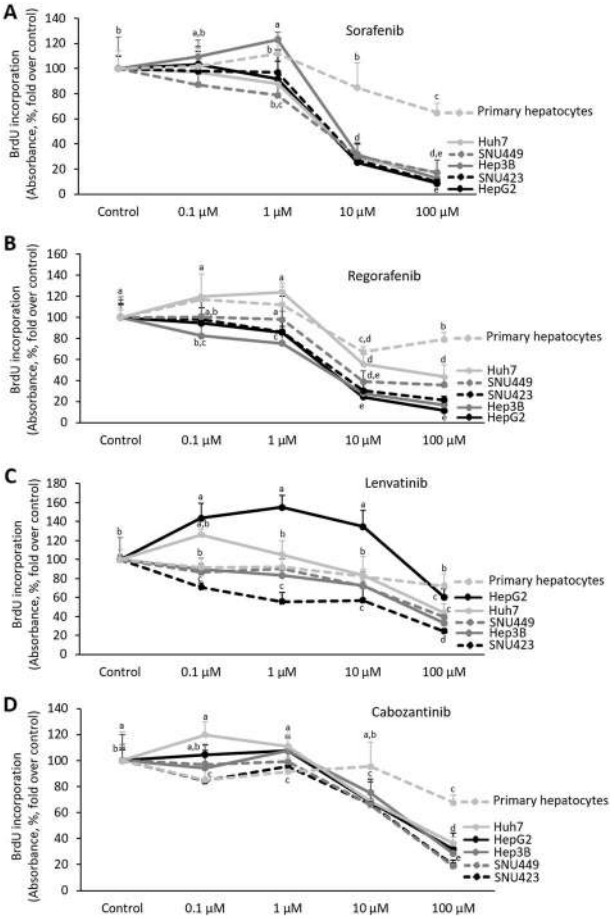

Fig. 4 Drug effectiveness on cell proliferation in liver cancer cells cultured in monolayer. Effect of Sorafenib (**a**), Regorafenib (**b**), Lenvatinib (**c**), and Cabozantinib (**d**) in BrdU incorporation in HepG2, Hep3b, Huh7, SNU423, SNU449, and primary human hepatocytes cultured in 2D system. Graphs are separated according to treatments. Drugs (0, 100nM, 1μM, 10μM, and 100μM) were administered at 24h after plating. BrdU was determined 24h after drug administration using a commercial colorimetric assay, as described in as described in "Materials and methods" section. BrdU incorporation is shown as the absorbance at 370nm (reference wavelength: 492nm; absorbance, %, fold over control). All results are expressed as mean±SD of independent experiments ($n = 6$). The groups with statistically significant differences among them ($p \leq 0.05$) were indicated with different letters (a, b, c, d, or e).

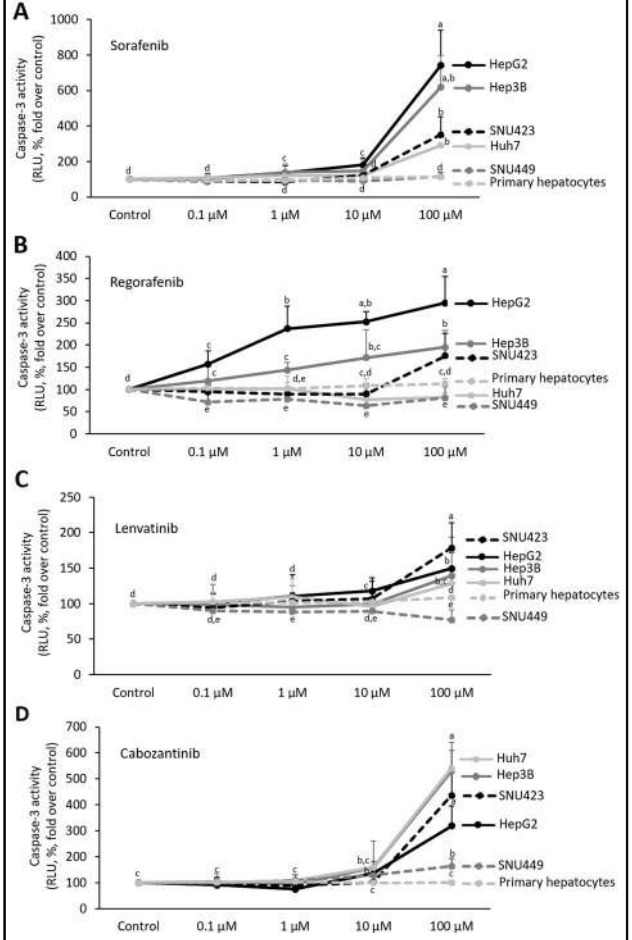

Fig. 5 Drug effectiveness on apoptosis in liver cancer cells cultured in monolayer. Effect of Sorafenib (**a**), Regorafenib (**b**), Lenvatinib (**c**), and Cabozantinib (**d**) in caspase-3 activity in HepG2, Hep3b, Huh7, SNU423, SNU449, and primary human hepatocytes cultured in 2D system. Graphs are separated according to treatments. Drugs (0, 100nM, 1μM, 10μM, and 100μM) were administered at 24h after plating. Caspase-3 activity was determined 24h after drug administration using a commercial caspase-Glo® Assay Systems as described in "Materials and methods" section. Caspase-3 activity is shown as the RLU (%, fold over control). All results are expressed as mean±SD of independent experiments ($n = 6$). The groups with statistically significant differences among them ($p \leq 0.05$) were indicated with different letters (a, b, c, d, or e).

Regorafenib at the recommended dose (1 μM) induced a moderate reduction of cell proliferation in HepG2 and Hep3B compared with untreated cells (Fig. 4b). Lenvatinib and Cabozantinib appeared to be more active in SNU423, SNU449, and Hep3B cells than HepG2 and Huh7 (Fig. 4c, d, respectively). In particular, Lenvatinib (0.1 μM) and Cabozantinib (1 μM) reduced cell proliferation in SNU423, as well as SNU423 and SNU449, cell lines (Fig. 4c, d, respectively).

Sorafenib (10 μM) induced caspase-3 activity in HepG2 and Hep3B (Fig. 5a). The highest dose of Sorafenib (100 μM) induced a significant rise of the downstream caspase activity in HepG2, Hep3B, SNU423, and Huh7 cells. Regorafenib (10 μM) also exerted, but at lower extent than Sorafenib, proapoptotic activity in decreasing order HepG2 ≥ Hep3B ≥ SNU423 ≥ Huh7 ≥ SNU449. Regorafenib (1 μM) induced caspase-3 activity in HepG2 and Hep3B compared with untreated cells (Fig. 5b). Although the dose–response study showed that the highest dose (100 μM) of Lenvatinib and Cabozantinib increased caspase-3 activity at variable extend in all cell lines; however, Lenvatinib (0,1 μM) and Cabozantinib

Table 1 Basal oxygen consumption rate (OCR), mitochondrial-dependent ATP generation, and maximal respiration capacity of HepG2, Huh7, Hep3B, SNU423, and SNU449 cell lines cultured in 2D system.

Cell lines	OCR	ATP generation	Maximal respiration capacity
HepG2	5.73 ± 0.429^{a}	3.86 ± 1.353^{a}	12.52 ± 0.801^{b}
Huh7	7.04 ± 0.728^{a}	3.45 ± 1.412^{a}	20.26 ± 1.312^{a}
Hep3B	5.50 ± 0.442^{a}	4.52 ± 0.624^{a}	$10.52 \pm 0.962^{b,c}$
SNU423	1.97 ± 0.366^{b}	1.43 ± 0.213^{b}	2.43 ± 0.620^{d}
SNU449	3.46 ± 1.061^{b}	0.45 ± 0.263^{c}	9.18 ± 1.103^{c}

The parameters were measured in cells 48 h after plating and expressed (pmol/min/μg protein) according to MitoStress kit protocol in a XFp Extracellular Flux Analyzer as described in "Materials and methods" section. All results are expressed as mean ± SD of independent experiments ($n = 6$). The groups with statistically significant differences ($p \le 0.05$) were indicated with different letters (a, b, c, or d).

(1 μM) were not able to induce caspase-3 in any cell lines tested (Fig. 5c, d, respectively).

Alteration of mitochondrial respiration in HCC cells

We have assessed OCR, mitochondrial-dependent ATP generation, and maximal respiration capacity at basal conditions in all cell lines. HepG2, Huh7, and Hep3B showed an increase in basal OCR and ATP generation than SNU423 and SNU449 cell lines (Table 1). HepG2 and Huh7, but not Hep3B, had higher maximal respiration capacity than SNU423 and SNU449 (Table 1).

Expression of tyrosine kinase receptor upon treatments in HCC cells

The administration of regular used in vitro dose (10 μM) of Sorafenib and Regorafenib reduced EGFR and c-Met protein expressions, while Lenvatinib and Cabozantinib increased EGFR and c-Met protein expressions (Fig. 6). The protein expression of VEGFR, PDGR, and FGFR was not altered by the treatments (data are not shown).

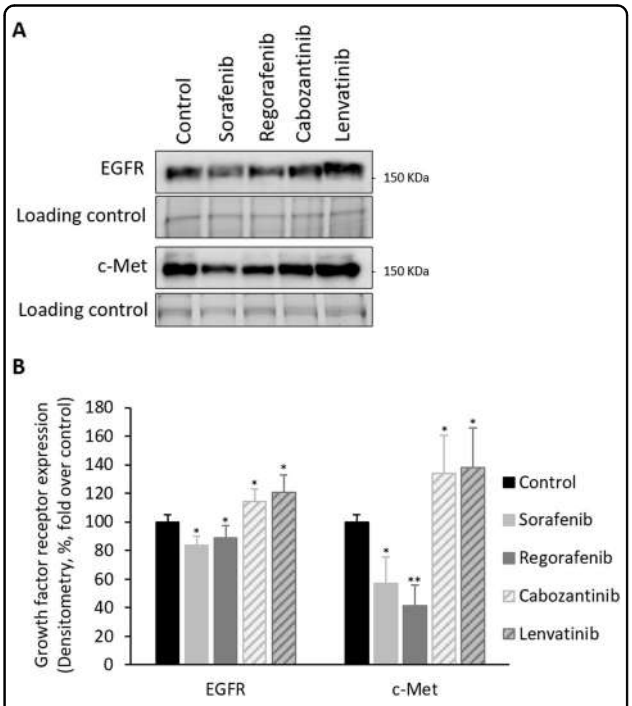

Fig. 6 Drug effectiveness on cell proliferation receptor protein expression in HepG2 cells cultured in monolayer. Effect of Sorafenib, Regorafenib, Lenvatinib, and Cabozantinib in the protein expression of EGFR and c-Met in HepG2 cells cultured in 2D system. Drugs (10μM) were administered at 24h after plating. The expression of tyrosine kinase receptors was assessed 24h after drug administration by SDS–PAGE electrophoresis coupled to western blot procedure as described in "Materials and methods" section. The values were obtained by densitometric analysis of the spots in relation to their loading control in the blots (densitometry, %, fold over control). All results are expressed as mean±SD of independent experiments ($n = 3$). The level of significance was set at $^{*}p \le 0.05$ and $^{**}p \le 0.01$ in comparison with their corresponding control.

Discussion

Two-thirds of patients with HCC are diagnosed in advanced stages receiving treatments as first- (Sorafenib and Lenvatinib) or second- (Regorafenib and Cabozantinib) line therapies[2–6]. However, drug resistance is widely observed and only a minor percentage of patients are effectively extending their survival after treatment[21].

Sorafenib and Regorafenib exerted a more potent relative beneficial properties than Lenvatinib and Cabozantinib in reducing spheroid area (Fig. 1, Supplementary Table 1), cell proliferation (Fig. 2a, c, as well as Fig. 3), and promoting cell death (Fig. 2b, d, e, as well as Fig. 3b) in 3D and 2D cultured-differentiated HCC cells. However, a detailed analysis showed differences in drug response in 3D and 2D cell culture models. The reduction of spheroid area by Sorafenib and Regorafenib was similar in all cell lines cultured in spheroids (Fig. 1, Supplementary Table 1); however, the increase of caspase-3 activity, and at lower extent the reduction of BrdU incorporation, showed a significant decreasing order of effectiveness of the drugs in HepG2 ≥ Hep3B ≥ Huh7 cells cultured in monolayer (Fig. 3). Lenvatinib and Cabozantinib that reduced spheroid area in 3D cultured Huh7, but not in HepG2 and

Hep3B (Fig. 1, Supplementary Table 1), appeared to reduce BrdU incorporation (Fig. 3a), and at low extent to increase caspase-3 activity (Fig. 3b), in all 2D cultured cell lines. These data might suggest that although a parallelism existed in drug response in 3D and 2D models, it can be feasible that the increased hypoxic environment in spheroids, which does not occur in cells cultured in monolayer, was inducing cell resistance to the antiproliferative and proapoptotic properties induced by the treatments. In fact, the enhanced expression of HIF-2alpha isoform causes a survival advantage in HepG2 cells cultured in spheroids[22].

An increase in non-trypan blue-stained viable cells (Fig. 2a), trypan blue-stained non-viable cells (Fig. 2b), caspase-3 activity (Fig. 2d), and TUNEL-positive cells (Fig. 2e), and reduction in Ki67-positive cells (Fig. 2c) at day 10th were observed compared to day 15th in spheroids from control HepG2 cells. These changes suggested the existence of active cell proliferation at day 10th that progressed, but also coexisted with cell cycle arrest and apoptosis, at day 15th in spheroids. The presence of released autocrine factors or physical constraint might occur in our experimental conditions at day 15th after spheroid establishment. In addition, the strong reduction of Ki67-positive cells (Fig. 2c), and the increase of caspase-3 activity (Fig. 2d) and TUNEL-positive cells (Fig. 2e) induced by Sorafenib and Regorafenib at day 10th were associated with the reduction of non-trypan blue-stained viable cells (Fig. 2a), and the increase of trypan blue-stained non-viable cells (Fig. 2b) at day 15th in HepG2. This situation showed that the early activation of cell death and blockage of cell proliferation by Sorafenib and Regorafenib observed at day 10th had an impact in the number of viable and dead cells at day 15th in spheroids.

p53, a tumor suppressor gene involved in cell cycle control, DNA repair, apoptosis, and cell differentiation, is one of the most mutated genes (up to 67% according to the different studies) in HCC although mutation prevalence varies greatly depending on etiology[23]. The expression of p53 and other p53-related components of the gene family are transcriptionally regulating the expression of cell death receptors and apoptosis[24,25]. An association appears between p53 mutations, and the degree of cell dedifferentiation and survival in patients with HCC[26,27]. The experiments suggested that Sorafenib and Regorafenib compared with Lenvatininb and Cabozantinib were especially effective in HepG2 with wild-type 53, while a relative decreasing antiproliferative and proapoptotic properties were observed in 2D cultured Hep3B and Huh7 cell lines (Fig. 3a, b, respectively). This pattern of action is in agreement with our previous study that showed a more potent proapoptotic and antiproliferative effects of Sorafenib in HepG2 cells than Hep3b and Huh7 cells[10]. Sorafenib has also been shown to upregulated p53 and promotes p53-dependent apoptosis[9,28]. The lack of functional p53 in most HCC cells have been proposed as a possible mechanism for Sorafenib resistance[28,29]. The overexpression of p53 renders Hep3B more sensitive to Sorafenib, while p53 knockdown from HepG2 cells increased their resistance[30].

The clinical trials have established recommended dose for Sorafenib (800 mg/24 h), Regorafenib (160 mg/24 h), Lenvatinib (<60 kg: 8 mg/24 h; ≥60 kg: 12 mg/24 h), and Cabozantinib (60 mg/24 h) in the treatment of patients in advanced stage of HCC. The dose–response analysis enclosed concentrations found in blood from advanced HCC-treated patients. Sorafenib (10 μM), and at lower extent Regorafenib (1 μM), exerted the strongest effects in cultured HepG2 cell line, while the response was lower in 2D cultured Huh7, SNU423, and SNU449 (Figs. 4 and 5). Although, Lenvatinib and Cabozantinib showed to exert moderate antiproliferative effects at their recommended dose in SNU423, and SNU423 and SNU449, respectively (Fig. 4c, d, respectively). However, our study also showed that Lenvatinib and Cabozanitib exerted increased activity at higher dose than those recommended (0.1 μM and 1 μM, respectively; Figs. 4 and 5).

The induction of cell death by Sorafenib and Regorafenib has been related to mitochondrial dysfunction in cultured hepatocytes and liver mitochondria fraction from rats[31,32]. We have observed that basal OCR and mitochondrial-dependent ATP generation of SNU423 and SNU449 were significantly lower than observed in HepG2, Huh7, and Hep3B (Table 1). In addition, HepG2 and Huh7, but not Hep3B cells, had higher maximal respiration capacity than SNU423 and SNU449 (Table 1). Hep3B and SNU449, which show increased number of mesenchymal phenotype markers than PLC/PRF/5 and Huh7, are associated with an increased expression of transforming growth factor β (TGF-β) and vimentin, as well as shunt glucose-6-phosphate to the pentose phosphate pathway (PPP), overall parallel with the reduction in E-cadherin expression and OCR[33]. The proapoptotic effectiveness of Sorafenib are associated with mitochondrial dysfunction and reduction of glycolysis in HepG2 cells[19]. In this study, the lack of effectiveness of low dose of Sorafenib (10 nM) compared with the recommended dose (10 μM) was associated with an increased mitochondrial function and glycolysis[19]. In concordance, Fiume et al.[34] showed that the reduced decline of cell viability in SNU449 compared with that observed in PLC/PRF/5 by Sorafenib (4 and 8 μM) was associated with resistance to mitochondrial respiration downregulation. All this data might suggest that Lenvatinib and Cabozantinib, differently to Sorafenib and Regorafenib, have a relative higher antitumoral activity in cells with reduced mitochondrial respiration, increased glycolytic and PPP

pathways that are associated with increased epithelial–mesenchymal transition (EMT) phenotype.

The resistance of HCC cells during Sorafenib administration has been related to the upregulation of survival cell signaling mediated through insulin growth factor receptor (IGFR)[35,36], c-Met[37], and FGFR[36]. c-Met phosphorylation and activation of mTOR are also related to resistance to Sorafenib in patient-derived HCC xenograft[37]. Tovar el al.[36] have shown Sorafenib (5 μM) reduces cell viability in Hep3B (55%) and Huh6 (29%). Huh6 cell line, which express wild-type p53, shows increased number of markers and morphology features of undifferentiated cells than Hep3B cell line[38]. The resistance of Hep3B and Huh6 to Sorafenib is associated with FGFR[36], and EGFR[39], or FGFR[36] upregulation, respectively. Linsitinib (5 μM), a dual TKI of IGF1R/IR, and the pan-FGFR inhibitor BGJ398, increased the effectiveness of Sorafenib in both resistant cell lines[36]. The increased effectiveness of Sorafenib and Regorafenib (Figs. 3–5), in comparison with Lenvatinib and Cabozantinib, was related to the downregulation of EGFR and c-Met protein expression (Fig. 6) in 2D cultured HepG2 cells.

Fernando et al.[9] have shown that Sorafenib sensitizes HCC cells to the apoptotic activity of TGF-β through the intrinsic pathway and tumor necrosis factor-α (TNF-α)-dependent extrinsic pathway. The proapoptotic activity of Sorafenib is associated with downregulation of S-nitrosylation in cell death receptors in liver cancer cells[40]. In concordance with our study, untransformed hepatocytes did not respond to Sorafenib-induced cell death[9]. Sorafenib, Regorafenib, Lenvatinib, and Cabozantinib exerted a minor effect in cell proliferation and death in primary human hepatocytes (Figs. 4 and 5).

Different reports have suggested an association between EMT and chemoresistance in liver tumor cells. SNU449, HLF, and HLE liver cancer cell lines that express mesenchymal markers (CD44, vimentin, and snail) are refractory to Sorafenib treatment compared to HepG2, Hep3B, PLC/PRF/5-expressing epithelial markers (E-cadherin and CK-18)[41,42]. Similar conclusions were obtained by Van Zijl et al.[43] using HCC cells derived from patients. In fact, factors turning back mesenchymal to epithelial phenotypes increase responsiveness of HCC cells to Sorafenib[44]. The expression of EMT markers appeared to be more relevant than upregulation of EGFR expression or downstream activation of ERK signaling for the sensitivity of tumor cells to EGFR inhibitors[45]. The EMT status also predicts HCC cell sensitivity to IGFR inhibitors in HCC cells[46]. A recent gene expression classification of HCC has identified a poor survival subclass termed S2 that express E-cadherin, c-myc, and FGFR3-4 protein expression[47]. Intriguingly, S2 gene signature that included Hep3B, HepG2, and HuH7, but not SNU423, cell lines that were highly susceptible to inhibition of cell proliferation by FGFR1-4 inhibitors[47]. In our conditions, Lenvatinib that targets FGFR3/4, showed lower antiproliferative and proapoptotic activities in HepG2, Hep3B, and HuH7 than SNU423 cell lines (Figs. 4–5).

In conclusion, the present study showed that although a parallelism existed in the effectiveness of drugs in well-differentiated cells cultured in 3D and 2D models, it might be that the hypoxic environment generated in spheroids would be responsible for the minor effectiveness of drugs in cells cultured in the 3D system in comparison with that observed in 2D cultured cells. The administration of regular used in vitro dose (10 μM) in 3D and 2D cultures, as well as the dose–response analysis in 2D cultures showed that Sorafenib and Regorafenib were increasingly effective reducing cell proliferation, and inducing apoptosis in well-differentiated and wild-type p53 HCC cells. Lenvatinib and Cabozantinib were more effective than Sorafenib and Regorafenib in moderately to poorly differentiated cells with mutated or lacking p53 HCC cells. The study also suggested that the highest effectiveness of Sorafenib and Regorafenib might be associated with high mitochondrial respiration, in comparison with Lenvatinib and Cabozantinib that appeared to be more active in cells with low basal OCR, mitochondrial-dependent ATP generation, and maximal respiration capacity.

Acknowledgements

We thank Dr. Bernhard Brüne (Institute of Biochemistry, Faculty of Medicine, Goethe-University Frankfurt, Frankfurt, Germany) for his technical assistance in developing 3D culture of liver cancer cells in spheroids. We thank the predoctoral i-PFIS IIS-enterprise contract in science and technologies in health granted by the Institute of Health Carlos III (ISCiii; IFI18/00014; to E.N.-V.); the ISCiii (PI16/00090 and PI19/01266), the Andalusian Ministry of Health (PI-0198-2016), the Biomedical Research Network Center for Liver and Digestive Diseases (CIBERehd) founded by the ISCiii and co-financed by European Development Regional Fund "A way to achieve Europe" (ERDF) (to J.M.), and ISCiii (PI19/00838) and Valencian Ministry of Education, Culture and Sports (PROMETEO/2019/027) (to V.M.V.) for their financial support.

Author details

[1]Institute of Biomedicine of Seville (IBiS), Hospital University "Virgen del Rocío"/CSIC/University of Seville, Seville, Spain. [2]Spanish Network for Biomedical Research in Hepatic and Digestive diseases (CIBERehd), Institute of Health Carlos III (ISCIII), Madrid, Spain. [3]Department of General Surgery, Hospital University "Virgen del Rocío"/CSIC/University of Seville/IBIS, Seville, Spain. [4]Service of Endocrinology, University Hospital Doctor Peset, Foundation for the Promotion of Health and Biomedical Research in the Valencian Region (FISABIO), Valencia, Spain. [5]Department of Physiology, University of Valencia, Valencia, Spain

Conflict of interest

The authors declare that they have no conflict of interest.

Supplementary Information accompanies this paper at (https://doi.org/10.1038/s41419-020-2558-1).

Received: 20 February 2020 Revised: 22 April 2020 Accepted: 23 April 2020
Published online: 07 May 2020

References

1. Bray, F. et al. Global cancer statistics 2018: GLOBOCAN estimates of incidence and mortality worldwide for 36 cancers in 185 countries. *CA Cancer J. Clin.* **68**, 394–424 (2018).
2. Llovet, J. M. et al. Sorafenib in advanced hepatocellular carcinoma. *N. Engl. J. Med.* **359**, 378–390 (2008).
3. Cheng, A. L. et al. Efficacy and safety of sorafenib in patients in the Asia-Pacific region with advanced hepatocellular carcinoma: a phase III randomised, double-blind, placebo-controlled trial. *Lancet Oncol.* **10**, 25–34 (2009).
4. Kudo, M. et al. Lenvatinib versus sorafenib in first-line treatment of patients with unresectable hepatocellular carcinoma: a randomised phase 3 non-inferiority trial. *Lancet* **391**, 1163–1173 (2018).
5. Bruix, J. et al. Regorafenib for patients with hepatocellular carcinoma who progressed on sorafenib treatment (RESORCE): a randomised, double-blind, placebo-controlled, phase 3 trial. *Lancet* **389**, 56–66 (2017).
6. Abou-Alfa, G. K. et al. Cabozantinib in patients with advanced and progressing hepatocellular carcinoma. *N. Engl. J. Med.* **379**, 54–63 (2018).
7. Cervello, M. et al. Targeted therapy for hepatocellular carcinoma: novel agents on the horizon. *Oncotarget* **3**, 236–260 (2012).
8. Ou, D. L. et al. Induction of DNA damage-inducible gene GADD45beta contributes to sorafenib-induced apoptosis in hepatocellular carcinoma cells. *Cancer Res.* **70**, 9309–9318 (2010).
9. Fernando, J. et al. Sorafenib sensitizes hepatocellular carcinoma cells to physiological apoptotic stimuli. *J. Cell. Physiol.* **227**, 1319–1325 (2012).
10. Rodriguez-Hernandez, M. A. et al. Molecular characterization of autophagic and apoptotic signaling induced by sorafenib in liver cancer cells. *J. Cell. Physiol.* **234**, 692–708 (2018).
11. Carr, B. I. et al. Fluoro-Sorafenib (Regorafenib) effects on hepatoma cells: growth inhibition, quiescence, and recovery. *J. Cell. Physiol.* **228**, 292–297 (2013).
12. Xiang, Q. et al. Cabozantinib suppresses tumor growth and metastasis in hepatocellular carcinoma by a dual blockade of VEGFR2 and MET. *Clin. Cancer Res.* **20**, 2959–2970 (2014).
13. Ferrari, S. M. et al. Antineoplastic effect of lenvatinib and vandetanib in primary anaplastic thyroid cancer cells obtained from biopsy or fine needle aspiration. *Front Endocrinol. (Lausanne)* **9**, 764 (2018).
14. Ku, J. L. & Park, J. G. Biology of SNU cell lines. *Cancer Res. Treat.* **37**, 1–19 (2005).
15. Bhardwaj, B., Bhardwaj, G. & Lau, J. Y. Expression of p21 and p27 in hepatoma cell lines with different p53 gene profile. *J. Hepatol.* **31**, 386 (1999).
16. Pichard, L. et al. Human hepatocyte culture. *Methods Mol. Biol.* **320**, 283–293 (2006).
17. Milke, L. et al. Depletion of tristetraprolin in breast cancer cells increases interleukin-16 expression and promotes tumor infiltration with monocytes/macrophages. *Carcinogenesis* **34**, 850–857 (2013).
18. Navarro-Villaran, E. et al. Differential antitumoral properties and renal-associated tissue damage induced by tacrolimus and mammalian target of rapamycin inhibitors in hepatocarcinoma: in vitro and in vivo studies. *PLoS ONE* **11**, e0160979 (2016).
19. Rodriguez-Hernandez, M. A. et al. Dose-dependent regulation of mitochondrial function and cell death pathway by sorafenib in liver cancer cells. *Biochem. Pharmacol.* 113902, https://doi.org/10.1016/j.bcp.2020.113902 (2020).
20. Colella, A. D. et al. Comparison of Stain-Free gels with traditional immunoblot loading control methodology. *Anal. Biochem* **430**, 108–110 (2012).
21. Villanueva, A. & Llovet, J. M. Second-line therapies in hepatocellular carcinoma: emergence of resistance to sorafenib. *Clin. Cancer Res.* **18**, 1824–1826 (2012).
22. Menrad, H. et al. Roles of hypoxia-inducible factor-1alpha (HIF-1alpha) versus HIF-2alpha in the survival of hepatocellular tumor spheroids. *Hepatology* **51**, 2183–2192 (2010).
23. Villanueva, A., Newell, P., Chiang, D. Y., Friedman, S. L. & Llovet, J. M. Genomics and signaling pathways in hepatocellular carcinoma. *Semin Liver Dis.* **27**, 55–76 (2007).
24. Gonzalez, R. et al. Role of p63 and p73 isoforms on the cell death in patients with hepatocellular carcinoma submitted to orthotopic liver transplantation. *PLoS One* **12**, e0174326 (2017).
25. Schilling, T. et al. Interference with the p53 family network contributes to the gain of oncogenic function of mutant p53 in hepatocellular carcinoma. *Biochem. Biophys. Res. Commun.* **394**, 817–823 (2010).
26. International Human Genome Sequencing, C. Finishing the euchromatic sequence of the human genome. *Nature* **431**, 931–945 (2004).
27. Honda, K. et al. p53 mutation is a poor prognostic indicator for survival in patients with hepatocellular carcinoma undergoing surgical tumour ablation. *Br. J. Cancer* **77**, 776–782 (1998).
28. Wei, J. C. et al. Sorafenib inhibits proliferation and invasion of human hepatocellular carcinoma cells via up-regulation of p53 and suppressing FoxM1. *Acta Pharm. Sin.* **36**, 241–251 (2015).
29. Brost, S. et al. The multikinase inhibitor sorafenib induces p53 family-dependent apoptosis in hepatocellular carcinoma. *Z. fur Gastroenterologie* **51**, K83 (2013).
30. Omar, H. A., Tolba, M. F., Hung, J. H. & Al-Tel, T. H. OSU-2S/Sorafenib synergistic antitumor combination against hepatocellular carcinoma: the role of PKCdelta/p53. *Front. Pharm.* **7**, 463 (2016).
31. Weng, Z. et al. Regorafenib impairs mitochondrial functions, activates AMP-activated protein kinase, induces autophagy, and causes rat hepatocyte necrosis. *Toxicology* **327**, 10–21 (2015).
32. Zhang, J. et al. Effects of 31 FDA approved small-molecule kinase inhibitors on isolated rat liver mitochondria. *Arch. Toxicol.* **91**, 2921–2938 (2017).
33. Soukupova, J. et al. Role of the Transforming Growth Factor-beta in regulating hepatocellular carcinoma oxidative metabolism. *Sci. Rep.* **7**, 12486, https://doi.org/10.1038/s41598-017-12837-y (2017).
34. Fiume, L., Manerba, M., Vettraino, M. & Di Stefano, G. Effect of sorafenib on the energy metabolism of hepatocellular carcinoma cells. *Eur. J. Pharm.* **670**, 39–43 (2011).
35. Huynh, H. AZD6244 (ARRY-142886) enhances the antitumor activity of rapamycin in mouse models of human hepatocellular carcinoma. *Cancer* **116**, 1315–1325 (2010).
36. Tovar, V. et al. Tumour initiating cells and IGF/FGF signalling contribute to sorafenib resistance in hepatocellular carcinoma. *Gut* **66**, 530–540 (2017).
37. Huynh, H. et al. Sorafenib and rapamycin induce growth suppression in mouse models of hepatocellular carcinoma. *J. Cell. Mol. Med.* **13**, 2673–2683 (2009).
38. Waldherr, M. et al. Use of HuH6 and other human-derived hepatoma lines for the detection of genotoxins: a new hope for laboratory animals? *Arch. Toxicol.* **92**, 921–934 (2018).
39. Blivet-Van Eggelpoel, M. J. et al. Epidermal growth factor receptor and HER-3 restrict cell response to sorafenib in hepatocellular carcinoma cells. *J. Hepatol.* **57**, 108–115 (2012).
40. Rodriguez-Hernandez, A. et al. Regulation of cell death receptor S-nitrosylation and apoptotic signaling by Sorafenib in hepatoblastoma cells. *Redox Biol.* **6**, 174–182 (2015).
41. Chen, X. et al. Epithelial mesenchymal transition and hedgehog signaling activation are associated with chemoresistance and invasion of hepatoma subpopulations. *J. Hepatol.* **55**, 838–845 (2011).
42. Fernando, J. et al. A mesenchymal-like phenotype and expression of CD44 predict lack of apoptotic response to sorafenib in liver tumor cells. *Int. J. Cancer* **136**, E161–E172 (2015).
43. van Zijl, F. et al. A human model of epithelial to mesenchymal transition to monitor drug efficacy in hepatocellular carcinoma progression. *Mol. Cancer Ther* **10**, 850–860 (2011).
44. Soukupova, J. et al. Resminostat induces changes in epithelial plasticity of hepatocellular carcinoma cells and sensitizes them to sorafenib-induced apoptosis. *Oncotarget* **8**, 110367–110379 (2017).
45. Fuchs, B. C. et al. Epithelial-to-mesenchymal transition and integrin-linked kinase mediate sensitivity to epidermal growth factor receptor inhibition in human hepatoma cells. *Cancer Res.* **68**, 2391–2399 (2008).
46. Zhao, H. et al. Epithelial-mesenchymal transition predicts sensitivity to the dual IGF-1R/IR inhibitor OSI-906 in hepatocellular carcinoma cell lines. *Mol. Cancer Ther.* **11**, 503–513 (2012).
47. Schmidt, B. et al. Molecular subclasses of hepatocellular carcinoma predict sensitivity to fibroblast growth factor receptor inhibition. *Int. J. Cancer* **138**, 1494–1505 (2016).

Redox Biology 34 (2020) 101528

Contents lists available at ScienceDirect

Redox Biology

journal homepage: www.elsevier.com/locate/redox

Research Paper

Downregulation of thioredoxin-1-dependent CD95 S-nitrosation by Sorafenib reduces liver cancer

Raúl González[a,j], María A. Rodríguez-Hernández[a,j,1], María Negrete[a,1], Kalina Ranguelova[b], Aurelie Rossin[c], Carmen Choya-Foces[d,e], Patricia de la Cruz-Ojeda[a], Antonio Miranda-Vizuete[a], Antonio Martínez-Ruiz[d,e], Sergio Rius-Pérez[f], Juan Sastre[f], José A. Bárcena[g,h], Anne-Odile Hueber[c], C. Alicia Padilla[g,h], Jordi Muntané[a,i,j,*]

[a] Institute of Biomedicine of Seville (IBiS), Hospital University "Virgen Del Rocío"/CSIC/University of Seville, Seville, Spain
[b] Bruker BioSpin Corporation, Billerica, MA, USA
[c] Université Côte D'Azur, CNRS, Inserm, iBV, Nice, France
[d] Research Unit, Hospital University "Santa Cristina", Health Research Institute "La Princesa" (IIS-IP), Madrid, Spain
[e] Biomedical Research Network Center for Cardiovascular Diseases (CIBERCV), Madrid, Spain
[f] Department of Physiology, Faculty of Pharmacy, University of Valencia. Burjassot, Valencia, Spain
[g] Department of Biochemistry and Molecular Biology, University of Cordoba, Cordoba, Spain
[h] Maimonides Institute for Biomedical Research of Cordoba (IMIBIC), Cordoba, Spain
[i] Department of General Surgery, Hospital University "Virgen del Rocío"/IBiS/CSIC/University of Seville, Seville, Spain
[j] Biomedical Research Network Center for Liver and Digestive Diseases (CIBERehd), Madrid, Spain

ARTICLE INFO

Keywords:
Apoptosis
Cell proliferation
CD95
GSNOR
Hepatocarcinoma
Nrf2
NOS3

ABSTRACT

Hepatocellular carcinoma (HCC) represents 80% of the primary hepatic neoplasms. It is the sixth most frequent neoplasm, the fourth cause of cancer-related death, and 7% of registered malignancies. Sorafenib is the first line molecular targeted therapy for patients in advanced stage of HCC. The present study shows that Sorafenib exerts free radical scavenging properties associated with the downregulation of nuclear factor E2-related factor 2 (Nrf2)-regulated thioredoxin 1 (Trx1) expression in liver cancer cells. The experimental downregulation and/or overexpression strategies showed that Trx1 induced activation of nitric oxide synthase (NOS) type 3 (NOS3) and S-nitrosation (SNO) of CD95 receptor leading to an increase of caspase-8 activity and cell proliferation, as well as reduction of caspase-3 activity in liver cancer cells. In addition, Sorafenib transiently increased mRNA expression and activity of S-nitrosoglutathione reductase (GSNOR) in HepG2 cells. Different experimental models of hepatocarcinogenesis based on the subcutaneous implantation of HepG2 cells in nude mice, as well as the induction of HCC by diethylnitrosamine (DEN) confirmed the relevance of Trx1 downregulation during the proapoptotic and antiproliferative properties induced by Sorafenib. In conclusion, the induction of apoptosis and antiproliferative properties by Sorafenib were related to Trx1 downregulation that appeared to play a relevant role on SNO of NOS3 and CD95 in HepG2 cells. The transient increase of GSNOR might also participate in the deactivation of CD95-dependent proliferative signaling in liver cancer cells.

1. Introduction

Hepatocellular carcinoma (HCC) is the most common type of liver cancer developed in the context of a cirrhotic liver (80–90%). Although major prevalent genetic mutations are related to telomerase (60%), Wnt-β-catenin (54%), PI3K-Akt-mTOR (51%), p53 (49%) and MAPK (43%) signaling, the alteration of redox regulatory mechanisms is also observed in a relevant proportion of patients (12%) [1]. Only one third of HCC patients are diagnosed at early stage (0 or A), according to the Barcelona Clinic Liver Cancer (BCLC) staging system, being eligible for potential curative therapies such as local ablation, resection or orthotopic liver transplantation with 5-years survival in 50–80% of patients [2]. Then, high proportion of patients are diagnosed at more advanced stages of the disease (BCLC B–C) [3]. Sorafenib is the recommended therapy for patients with locally advanced/metastatic disease (BCLC C) stage with mean overall survival around 11 months [4,5]. The

* Corresponding author. Instituto de Biomedicina de Sevilla (IBiS), Av. Manuel Siurot s/n, 41013, Sevilla, Spain.
E-mail address: jmuntane-ibis@us.es (J. Muntané).
[1] These authors contributed equally to this work.

https://doi.org/10.1016/j.redox.2020.101528
Received 25 March 2020; Accepted 27 March 2020
Available online 04 April 2020

List of abbreviations:

HCC	hepatocellular carcinoma
Nrf2	nuclear factor E2-related factor 2
Trx1	thioredoxin 1
SNO	S-nitrosation
ROS	reactive oxygen species
NOS3	nitric oxide synthase type 3
GSNOR	S-nitrosoglutathione reductase
DEN	diethylnitrosamine
BCLC	Barcelona Clinic Liver Cancer
c-MET	mesenchymal-epithelial transition factor receptor
IGFR	insulin growth factor receptor
FGFR	fibroblast growth factor receptor
VEGFR	vascular endothelial growth factor receptor
PDGFR-β	platelet-derived growth factor receptor-β
JNK	c-Jun N-terminal
MEK	mitogen-activated protein kinase kinase
ERK	extracellular signalregulatedkinase
AMPK	AMP-activated protein kinase
NF-κB	nuclear factor-κB
HIF-1	hypoxia inducible factor-1
TrxR	thioredoxin reductase
NO	nitric oxide
Trx	thioredoxin
VEGF	vascular endothelial growth factor
DMPO	5,5-dimethyl-1-pyrroline-N-oxide
CMH	cyclic hydroxylamine 1-hydroxy-3-methoxycarbonyl-2,2,5,5-tetramethyl-pyrrolidine
MitoSOX™	mitochondrial superoxide indicator
DHE	dihydroethidium
H_2DCFDA	2,7-dichloro dihydro-fluorescein diacetate
DAF-2	4,5-diaminofluorescein diacetate
SFN	sulforaphane
EPR	electron paramagnetic resonance
$O_2^{\cdot-}$	superoxide anion
BrdU	bromodeoxyuridine
ARE	antioxidant response elements
H_2O_2	hydrogen peroxide
$OH^{\cdot}$	hydroxyl radicals
OH	hydroxyl anion
GST	glutathione-S-transferase
TrxR1	thioredoxin reductase type 1
Gpx1	glutathione peroxidase type 1
NQO1	NADPH-quinone oxidoreductase 1
HO-1	heme oxygenase 1
GCLC	glutamate-cysteine ligase catalytic subunit
PKA	protein kinase type A
PKC	protein kinase C
AMPK	5′ adenosine monophosphate-activated protein kinase
ERK	extracellular signal-regulated kinase
SHP-1	SH2 domain-containing tyrosine phosphatase
STAT3	signal transducers and activators of transcription type 3
Mcl-1	induced myeloid leukemia cell differentiation protein-1
RNS	reactive nitrogen species

resistance of HCC cells to Sorafenib has been related to the activation of survival cell signaling related to insulin growth factor receptor (IGFR) [6,7], mesenchymal-epithelial transition factor receptor (c-MET) [8], and fibroblast growth factor receptor (FGFR) [7].

Sorafenib simultaneously inhibits tyrosine kinase receptors such as vascular endothelial growth factor receptor (VEGFR) 2, VEGFR 3, platelet-derived growth factor receptor-β (PDGFR-β), Flt3 and c-Kit, as well as molecular components of the Raf-mitogen-activated protein kinase kinase (MEK)-extracellular signalregulatedkinase (ERK) signaling pathway [9]. The early induction by Sorafenib of endoplasmic reticulum stress, upregulation of c-Jun N-terminal (JNK) and AMP-activated protein kinase (AMPK)-dependent signaling was related to the induction of survival autophagic processes [10]. The induction of apoptosis by Sorafenib was associated with a decrease in S-nitrosation (SNO) of cell death receptors in HepG2 cells [11].

Cancer cells activate an adaptive program leading to the upregulation of reactive oxygen species (ROS)-scavenging systems, inhibition of apoptosis, and promoting advanced transformation, metastasis and resistance to anticancer drugs [12]. The adaptive response involves upregulation of redox-sensitive transcription factors, such as nuclear factor-κB (NF-κB), nuclear factor E2-related factor 2 (Nrf2), c-jun and hypoxia inducible factor (HIF-1), which lead to the increased expression of antioxidant molecules such as SOD, catalase, thioredoxin 1 (Trx1) and the GSH antioxidant system, as well as survival factors such as Bcl-2 and induced myeloid leukemia cell differentiation protein-1 (Mcl-1) [13]. The thioredoxin (Trx) system, constituted by NADPH, FAD-containing thioredoxin reductase (TrxR) (EC 1.8.1.9) and Trx, plays a key role against oxidative stress regulating protein thiol/disulfide balance, supplying electrons to thiol-dependent peroxidases (peroxiredoxins), ribonucleotide reductase and methionine sulfoxide reductases, as well as regulating the activity of many redox-sensitive transcription factors, and selenium and nitric oxide (NO) metabolism [14]. The expression of Trx1 has been shown to be increased in HCC and cultured liver cancer cells [15,16]. The present study showed that the induction of apoptosis and antiproliferative properties by Sorafenib was related to Trx1 downregulation which played a relevant role in SNO of nitric oxide synthase (NOS) type 3 (NOS3) and CD95 in HepG2 cells. The regulation of SNO might be also influenced by the transient upregulation of GSNOR by Sorafenib in liver cancer cells.

2. Material and Methods

2.1. Chemical and cell lines

Sorafenib Tosylate was obtained from Carbosynth Limited (Berkshire, UK) (Supplementary Fig. 1). Xanthine oxidase (X2252), xanthine (X0626), 5,5-dimethyl-1-pyrroline-N-oxide (DMPO) and cyclic hydroxylamine 1-hydroxy-3-methoxycarbonyl-2,2,5,5-tetramethyl-pyrrolidine (CMH) were obtained from Sigma-Aldrich (Missouri, USA). Red Mitochondrial Superoxide Indicator (MitoSOX™) (M36008), dihydroethidium (DHE) (D-11347), 2,7-dichloro dihydro-fluorescein diacetat (H_2DCFDA) (D-399) and 4,5-diaminofluorescein diacetate (DAF-2) (D-23842) were obtained from Life Technologies (Thermo Fisher Scientific, Massachusetts, USA). Sulforaphane (SFN, Sigma-Aldrich) and vascular endothelial growth factor (VEGF, PrepoTech, New Jersey, USA) were used as inducers of Nrf2 activation.

HepG2 (HB-8065™) was obtained from ATCC/LGC Standards (Barcelona, Spain). JHH2, JHH-4, JHH-5 and Huh-1 were obtained from the Japanese Collection of Research Bioresources Cell Bank (Tokyo, Japan). SNU886 was obtained from the Korean Cell Lines Bank (Seoul, Korea). MHCC97H was obtained from Woodland Pharmaceuticals (Massachusetts, USA).

2.2. Measurement of reactive oxygen and nitrogen species

Cells were incubated with DHE (10 μM), MitoSOX™ (5 μM), H_2DCFDA (10 μM) and DAF-2 (2.5 μM) for 30 min in culture medium for measuring superoxide anion ($O_2^{\cdot-}$) in cytoplasm and mitochondria, hydrogen peroxide (H_2O_2) and NO, respectively. The production of NO was also measured by quantification of nitrite/nitrate in culture medium using the Griess reaction [17].

2.3. Evaluation of the scavenging properties of Sorafenib

The scavenging properties of Sorafenib were evaluated by electron paramagnetic resonance (EPR) using the spin probe CMH (100 μM) and spin trap DMPO (100 mM) to monitor $O_2^{\cdot-}$ formation. The xanthine (50 μM) and xanthine oxidase (5 mU/mL) system was used to generate ROS for 30 min. The formation of the radicals was monitored using bench-top EMXnano spectrometer (Bruker, Massachusetts, USA). Deferoxamine (25 μM) was added when required in order to prevent Fenton reaction.

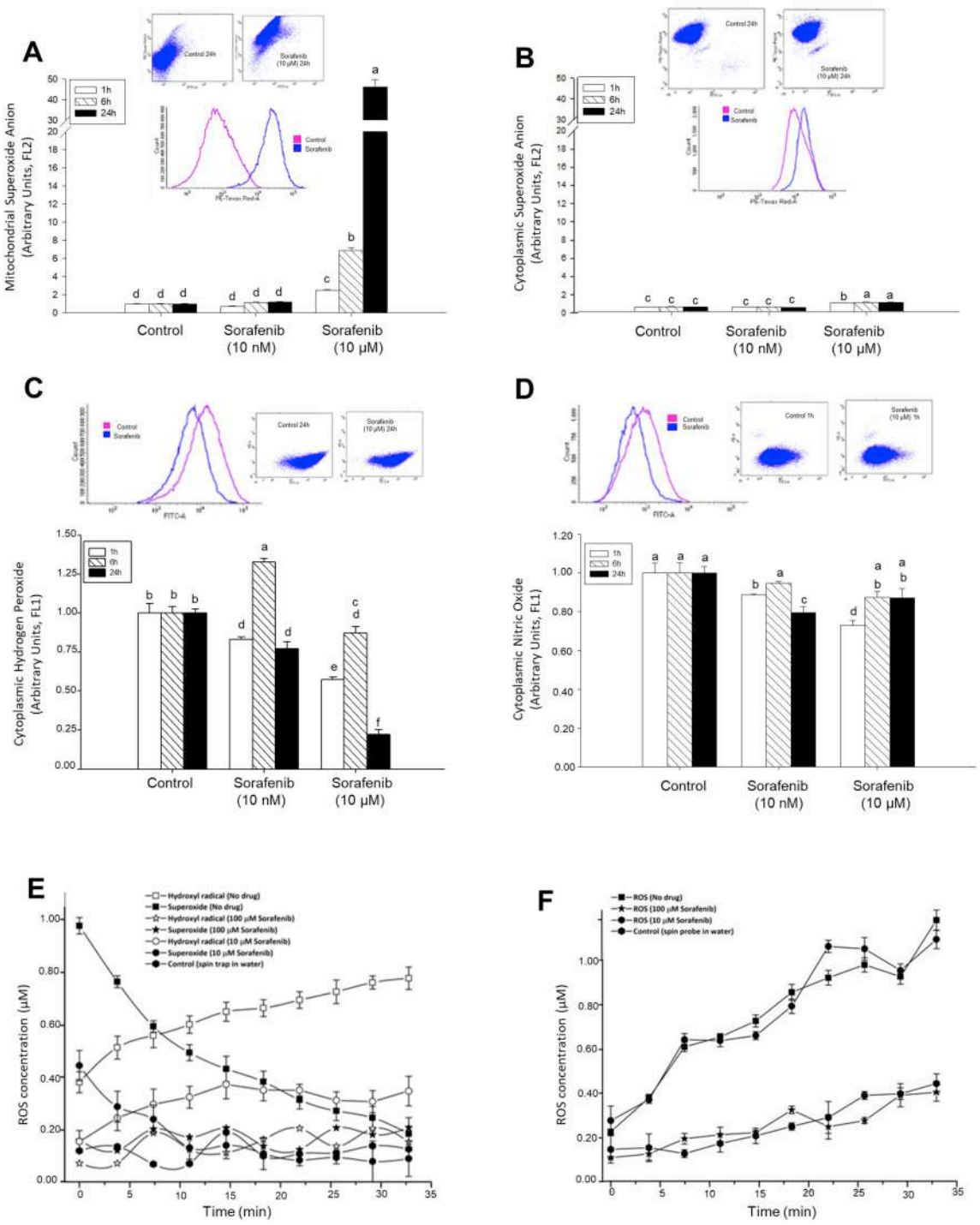

Fig. 1. Effect of Sorafenib on free radical generation. The effect of Sorafenib on the mitochondrial (A) and cytoplasmic (B) $O_2^{\cdot-}$, and cytoplasmic H_2O_2 (C) and NO (D) production in cultured HepG2, as well as *in vitro* scavenging properties of Sorafenib measured by spin trap (E) and spin probe (F) using a xanthine/xanthine oxidase system are shown. Mitochondrial and/or cytoplasmic ROS and reactive nitrogen species (RNS) were *in situ* determined using different fluorescent probes described in Material and Methods. The nitrone spin trap DMPO in presence of $O_2^{\cdot-}$ generating system promotes specific spin-adduct (DMPO-OOH) that rapidly decompose to DMPO-OH. $O_2^{\cdot}$ induces decomposition of H_2O_2 to hydroxil radical ($O^{\cdot}$) and hydroxyl anion (OH-) through the coupled Fenton and Haber-Weiss reaction in the presence of transition metal traces. This process explained the inversed relationship of detected $O_2^{\cdot-}$ and $OH^{\cdot}$ in the absence of drug over time (E). The spin probe CMH is oxidized by $O_2^{\cdot-}$ to the corresponding EPR active and stable nitroxides with coupled H_2O_2 generation (F). Data are expressed as mean ± SEM of 6–8 independent experiments. The groups with different letters (a, b, c, d, e or f) were significantly different ($p \leq 0.05$).

2.4. mRNA and protein expression

RT-PCR was performed in StepOnePlus RT-PCR System (Thermo Fisher Scientific, Waltham, USA). Reactions were performed in 96-well plates with optical sealing tape (Applied Biosystem, Foster City, California, USA) in 10 μL total volume containing SYBR Green MasterMix and corresponding cDNA (obtained with High capacity cDNA Reverse Transcription Kit, Applied Biosystems). The conditions for amplification were as follows: denaturation step of 95 °C for 10 min, followed by 40 cycles of 95 °C for 15 s, and 60 °C for 60 s. The melting temperature was fixed at 60 °C. All primers were designed using online Primer3 software.

Proteins were separated by Any kD™ Criterion™ TGX Stain-Free™ Protein Gel (BioRad) and transferred to PVDF membranes. The membranes were incubated with the corresponding commercial primary antibodies against Trx1 (Cat ATRX-04, IMCO Corporation Ltd, Stockholm, Sweden), NOS3 (sc-654), CD95 (sc-715) and caspase-8 (sc-7890) from Santa Cruz Biotechnology (Texas, USA); Nrf2 (#12721), Keap1 (#8047) obtained from Cell Signaling Technology (Massachusetts, USA).

The procedure for measuring SNO–NOS3 and SNO-CD95 was performed using biotin switch assay as previously described [18]. The

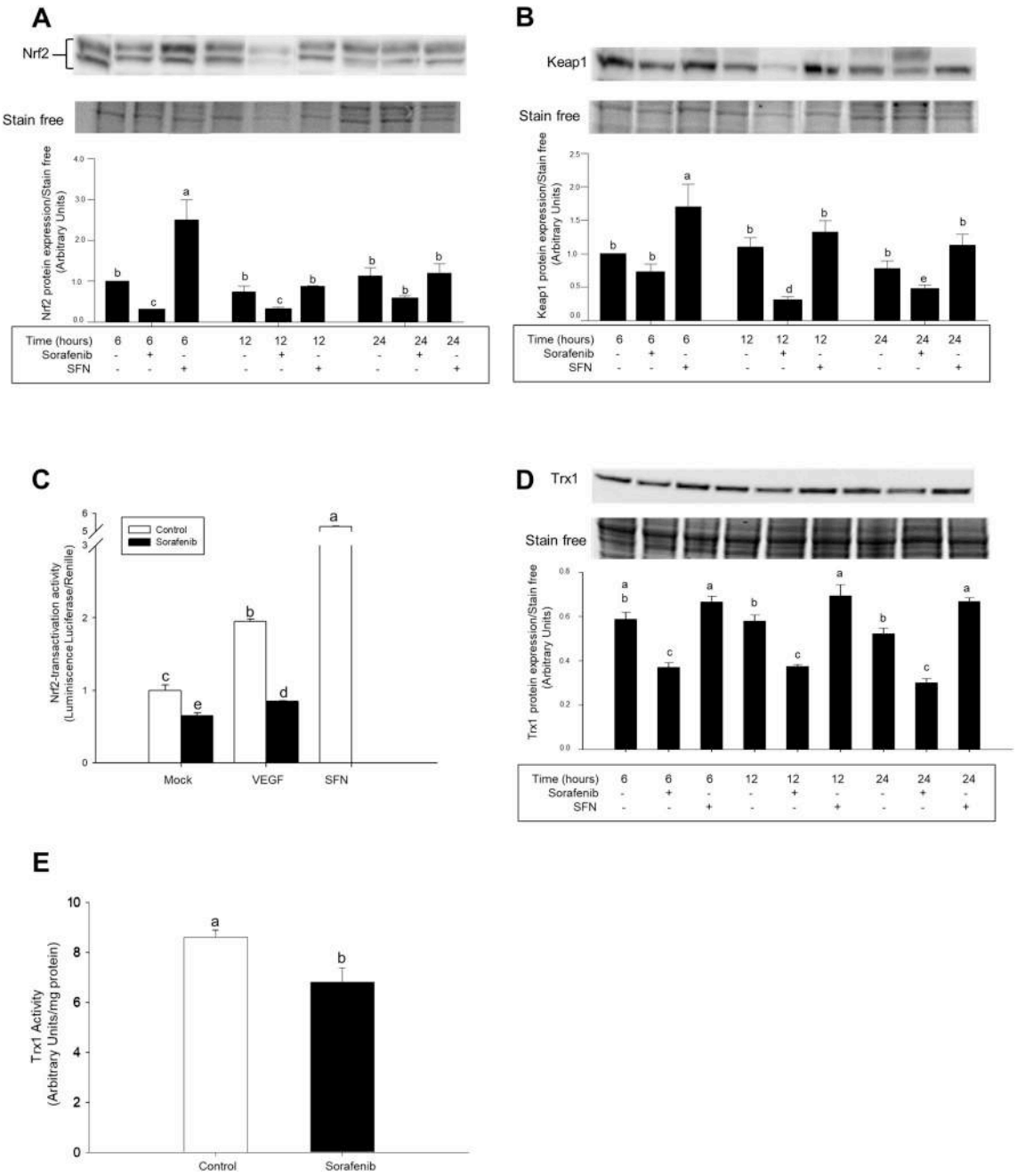

Fig. 2. Altered Nrf2-signaling pathway by Sorafenib in HepG2 cells. The reduction of Nrf2 (A) and Keap1 (B) expressions and Nrf2-transactivation activity (C) were associated with downregulation of Trx1 expression (D) and activity (E) in HepG2. Sorafenib (10 μM), VEGF (50 ng/ml) and SFN (10 μM) were administered 24 h after cell stabilization. The expression of Nrf2 and Keap1 in nuclear fraction, and Trx1 in cell lysate was measured by western-blot analysis as described in Material and Methods. Nrf2-transactivation activity was assessed using ARE-luc transfected HepG2 cells. pTK-Renilla was used as internal control vector. Trx1 activity was measured as detailed in Material and Methods. Data are expressed as mean ± SEM of 4 independent experiments. The groups with different letters (a, b, c, d or e) were significantly different ($p \leq 0.05$).

obtained SNO-biotinylated fractions were incubated with 45 μL Neutravidin Plus UltralinK resin (Pierce, Appleton, Wisconsin, USA) for 1 h in agitation, washed and assessed by Western Blot analysis.

2.5. GSNOR and Trx1 activities

S-nitrosoglutathione reductase (GSNOR) and Trx1 activities were measured as previously described [19,20].

2.6. Cell death and proliferation

Caspase-8 and -3-associated activities were determined using Caspase-Glo® 8 (G8201) and Caspase-Glo® 3 (G8091) Assay Systems (Promega, Madison, USA). Bromodeoxyuridine (BrdU) incorporation was used as marker of cell proliferation (Roche Diagnostics, Indianapolis, USA) in cultured HepG2 cells. Cell proliferation was also assessed in tumor sections by the measurement of Ki67 expression by immunohistochemistry procedure using antibodies against Ki67 (sc-23900, Santa Cruz Biotechnology).

2.7. Nrf2 signaling using a reporter gene vector

HepG2 cells were transiently transfected with Antioxidant Response Elements (ARE)-luciferase plasmid (Dr J. Alam, Department of Molecular Genetics, Ochsner Clinic Foundation, USA). Cells were lysed and assayed for luciferase activity by Dual-Luciferase® Reporter (DLR™) Assay System (Promega). pTK-Renilla was used as an internal control vector (Promega).

2.8. Trx1 knock-down and overexpression

Human Trx1 was down-regulated in HepG2 cells using siRNA (ref L-006340, Dharmacon, GE Healthcare Life Sciences). Trx1 overexpressing plasmid was obtained after amplification of human Trx1 by PCR from a cDNA library from human testis (Clonteck, Human Testis QUICK-CloneTM cDNA), and cloned into the pcDNA MYC plasmid at the EcoR1 and XhoI sites.

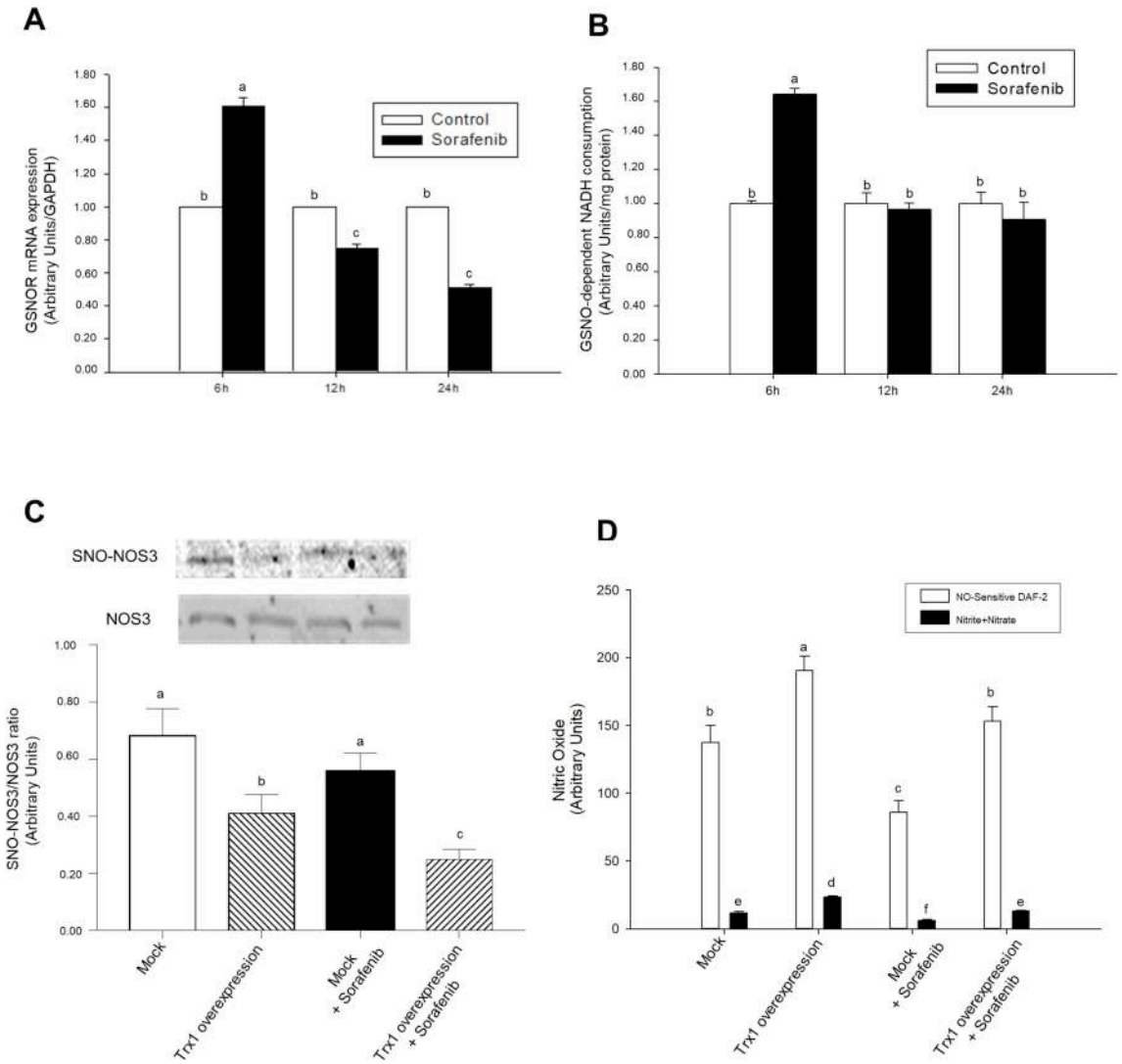

Fig. 3. Sorafenib transitory increased GSNOR expression and activity in HepG2. Trx1 overexpression reduced SNO–NOS3/NOS3 ratio and NO generation in HepG2 cells. Effect of Sorafenib in the mRNA expression (A) and activity (B) of GSNOR, as well as Trx1 overexpression on SNO–NOS3 (C), and NO *in situ* generation and NO-end products concentration in culture medium (D). Sorafenib (10 μM) was administered 24 h after cell stabilization. The SNO–NOS3 was determined by biotin-switch assay coupled to western-blot analysis as described in Material and Methods. NO generation was determined by the *in-situ* reaction with DAF-2, as well as nitrites + nitrates concentration in culture medium was determined by the Griess reagent as described in Material and Methods. Results are expressed as mean ± SEM of 4 independent experiments. The groups with different letters (a, b, c, d, e or f) were significantly different ($p \leq 0.05$).

2.9. Experimental models of liver cancer

Diethylnitrosamine (DEN, Sigma-Chemicals) (10 mg/kg day) was administered in drinking water (0.01% vol/vol) to Wistar rats (4 groups of 8 animals, n = 32; weighing 170-200 gr) for 15 weeks. Sorafenib (10 mg/kg day) was administered in edible hydrogel formulation 12 weeks after the initiation of DEN treatment and lasted until sacrifice of the animals at week 15th. The effect of Sorafenib was also evaluated in tumors-derived from subcutaneously implanted $10x10^6$ HepG2 cells, or HepG2 cells stably transfected with Trx1 overexpressing or empty pcDNA MYC (mock) vectors in Hsd:Athymic Nude-Foxn1^{nu} mice (Harlan Laboratories, Barcelona, Spain). When the tumors reached 5 mm, one group of animals received orally by gavage either Sorafenib (200 mg/kg) or solvent. The animals of each experimental group were sacrificed when tumor of animals from any experimental group reached 15 mm. All animal care and experimentation conformed to the Guide for the Care and Use of Laboratory Animals published by the National Academy of Sciences.

2.10. Statistical analysis

All results are expressed as mean ± SEM of independent experiments (n = 3–8). Data were compared using the analysis of variance (ANOVA) with the Least Significant Difference's test (homogeneity of variances) or Games-Howell (non-homogeneity of variances). If Shapiro-Wilks's test showed non-normal distribution of data non-parametric Kruskal-Wallis coupled to U-Man-Whitney post-hoc analysis with Finner's correction was done. All statistical analyses were performed using the IBM SPSS Statistics 19.0.0 (SPSS Inc., IBM, Armonk, NY, USA) software.

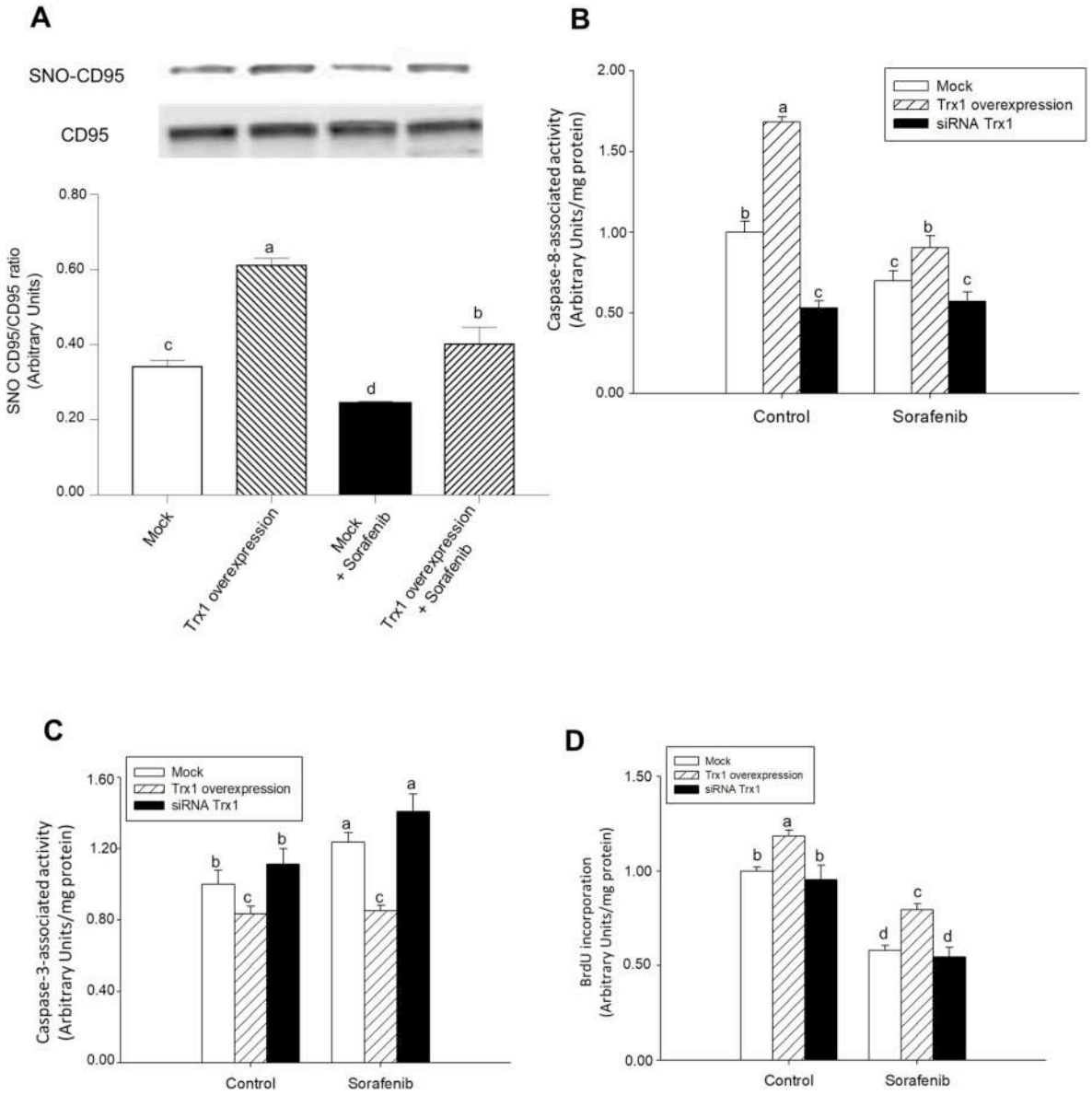

Fig. 4. Sorafenib reduced, but Trx1 had the opposite effect**, SNO-CD95/CD95 ratio, caspase-8 activity, and cell proliferation, while increased caspase-3 activity in HepG2.** Effect of Trx1 overexpression or siRNA Trx1 on SNO-CD95/CD95 ratio (A), caspase-8 activity (B), caspase-3 activity (C) and cell proliferation (D) in control and Sorafenib (10 μM)-treated hepG2 cells. Cell transfection using Trx1 overexpressing plasmid or siRNA Trx1, and Sorafenib administration were done as described in Material and Methods. The SNO-CD95 was determined by biotin-switch assay coupled to western-blot analysis, as well as caspase-8 and -3 activities and BrdU incorporation were measured at 24 h after Sorafenib administration as described in Material and Methods. Results are expressed as mean ± SEM of 4 independent experiments. The groups with different letters (a, b, c or d) were significantly different ($p \leq 0.05$).

3. Results

3.1. Sorafenib induced mitochondrial $O_2^{\cdot-}$ generation, but diminished cytoplasmic H_2O_2, $O_2^{\cdot-}$ and NO in HepG2

Coriat et al. [21] showed that Sorafenib increased intracellular generation of $O_2^{\cdot-}$, H_2O_2 and NO in HepG2. $O_2^{\cdot}$ was greatly and dose-dependently generated by Sorafenib at mitochondrial level (Fig. 1A) but was scarcely detected at cytoplasmic level (Fig. 1B). Sorafenib tended to decrease the intracellular concentration of H_2O_2 (Fig. 1C) and NO (1 h, Fig. 1D) in HepG2 cells. The scavenging properties of Sorafenib were assessed by EPR. The nitrone spin trap DMPO in presence of xanthine/xanthine oxidase generating system promotes specific spin-adduct (DMPO-OOH) that rapidly decomposes to DMPO-OH. $O_2^{\cdot}$ induces decomposition of H_2O_2 to hydroxyl radical ($OH^{\cdot}$) and hydroxyl anion (OH^-) through the coupled Fenton and Haber-Weiss reaction in the presence of transition metal traces. This process explained the inverse relationship among $O_2^{\cdot-}$ and $OH^{\cdot}$ generation in absence of drug over time (Fig. 1E). Sorafenib significantly lessened or abolished $O_2^{\cdot-}$ generation depending on the dose used (10 μM and 100 μM), respectively (Fig. 1E). The spin probe CMH is oxidized by $O_2^{\cdot-}$ to the corresponding EPR active and stable nitroxide with coupled H_2O_2 generation. In this case, Sorafenib (100 μM but not 10 μM) reduced $O_2^{\cdot-}$ production by xanthine/xanthine oxidase system for 30 min (Fig. 1F). The differences found in the DMPO and CMH experiments were probably due to their different kinetics, being the last one more reactive than DMPO against ROS and consequently higher competitor than Sorafenib. These results suggest that $O_2^{\cdot-}$ generation by Sorafenib (10 μM) in the mitochondria is scavenged in a dose-dependent manner by the drug at the cytoplasmic level.

3.2. Sorafenib downregulated Nrf2 signalling and Trx1 expression

Sorafenib reduced the expression of Nrf2 (Fig. 2A) and Keap1 (Fig. 2B) in nuclear fractions from HepG2 cells. The transcriptional factor Nrf2 positively regulates the expression of enzymes involved in phase I to III detoxification systems, GSH- and Trx-related antioxidant systems, carbohydrate and lipid metabolism, and heme and iron metabolism [22]. Sorafenib decreased Nrf2-transactivation activity in HepG2 cells transfected with ARE/Luc overexpressing vector (Fig. 2C). In agreement, the expression (Fig. 2D) and activity (Fig. 2E) of Trx1 were reduced in Sorafenib-treated HepG2 cells. Sorafenib also decreased mRNA expression of glutathione-S-transferase (GST), thioredoxin reductase type 1 (TrxR1), glutathione peroxidase type 1 (Gpx1), NADPH-quinone oxidoreductase 1 (NQO1), heme oxygenase 1 (HO-1) and glutamate-cysteine ligase catalytic subunit (GCLC) in HepG2 cells (Supplementary Figs. 2A–2F).

3.3. Sorafenib transiently upregulated GSNOR and reduced NOS3 activity. Role of Trx1

Thiol nitrosation (SNO) is a posttranslational modification that plays a critical role in health and disease [23]. GSNOR has been described as a highly conserved metabolizing enzyme involved in SNO homeostasis [24]. Intracellular GSNO exists in equilibrium with S-nitrosoproteins which are not substrates of GSNOR [24]. mRNA

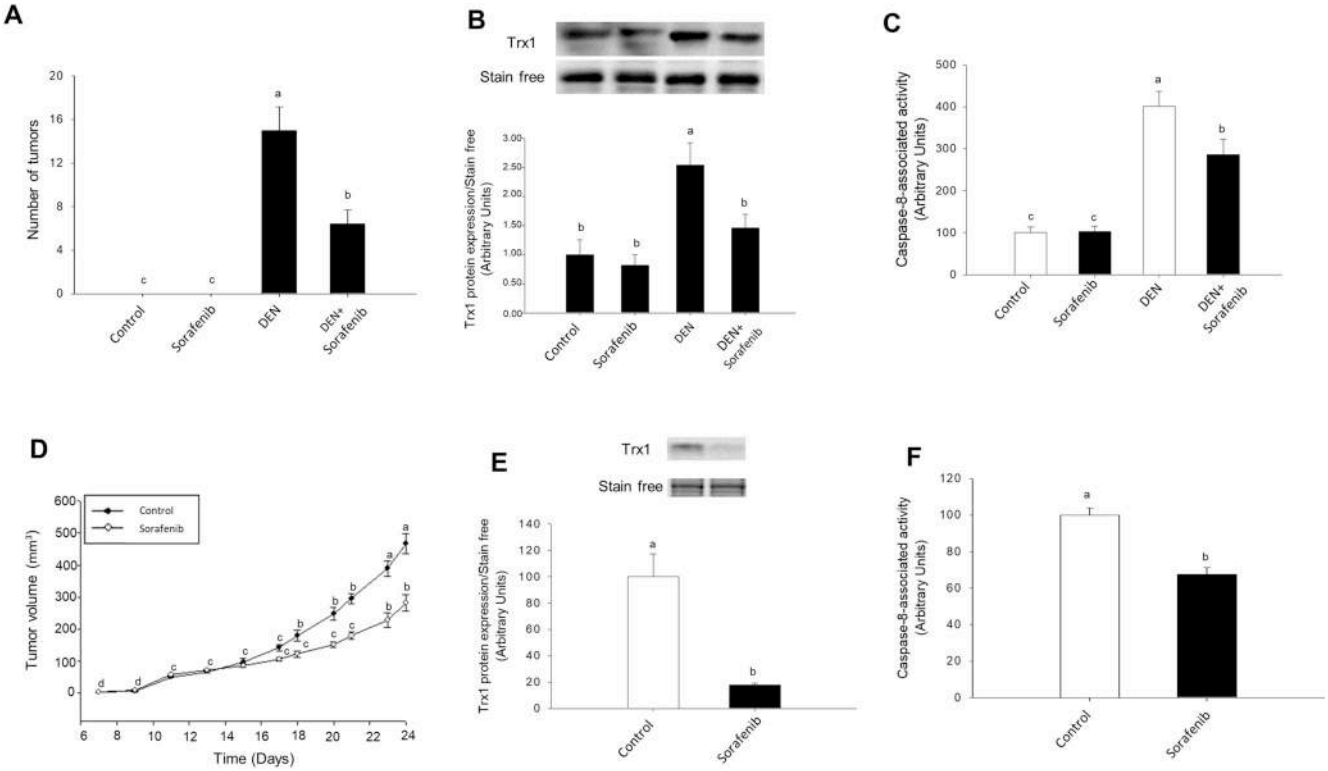

Fig. 5. The antitumoral properties of Sorafenib were associated with downregulation of Trx1 expression and caspase-8 activity in two xenograft mouse models. Effect of Sorafenib on the number of tumors induced by DEN (A) and tumor volume derived from subcutaneous HepG2 implantation (D), and their association with Trx1 expression (B and E, respectively) and caspase-8 activity (C and F, respectively). The administration of DEN (10 mg/kg day) was carried out during 17 weeks in Wistar rats (170 gr) in drinking water (0.01% vol/vol) or solvent. Sorafenib (10 mg/kg day) was administered 12 weeks after the initiation of DEN treatment DEN administration when liver nodules were evident (A, B and C). HepG2 cells (10×10^6) were subcutaneously implanted in male Hsd:Athymic Nude-Foxn1^{nu} mice. When the tumors reached 5 mm, one group of animals received orally by gavage either Sorafenib (200 mg/kg) or solvent (D, E and F). Trx1 expression and caspase-8 activity were measured as described in Material and Methods. Animals were sacrificed when tumors reached 15 mm. Results are expressed as mean ± SEM of six independent animals. The groups with different letters (a, b, c or d) were significantly different ($p \leq 0.05$).

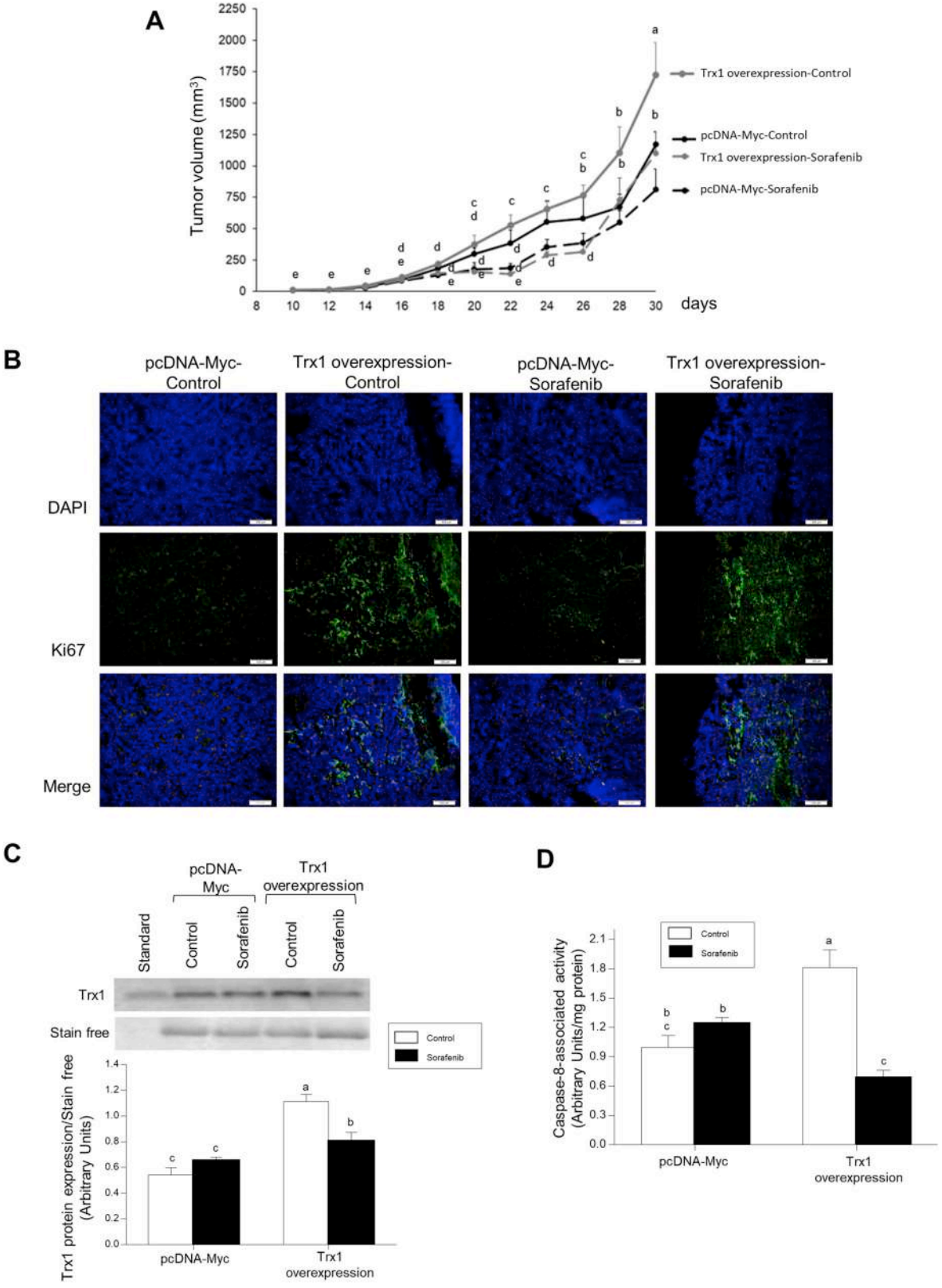

Fig. 6. The reduction of tumor volume by Sorafenib was associated with downregulation of cell proliferation, Trx1 expression and caspase-8 activity in Trx1 overexpressing HepG2 cells subcutaneously implanted in nude mice. Effect of Sorafenib in tumor volume (A), Ki67 (B) and Trx1 (C) expressions, and caspase-8 activity in tumors derived from subcutaneous implantation of HepG2 cells stably transfected with either Trx1 overexpressing or empty pcDNA Myc (mock) vectors in nude mice. HepG2 cells (10×10^6) were subcutaneously implanted in male Hsd:Athymic Nude-Foxn1^{nu} mice. When the tumors reached 5 mm, one group of animals received orally by gavage either Sorafenib (200 mg/kg) or solvent. Ki67 and Trx1 expressions, and caspase-8 activity were measured as described in Material and Methods. Animals were sacrificed when tumors reached 15 mm. Results are expressed as mean ± SEM of six independent animals. The groups with different letters (a, b, c, d or e) were significantly different ($p \leq 0.05$).

expression (Fig. 3A) and activity (Fig. 3B) of GSNOR were transiently increased after 6 h of Sorafenib treatment in HepG2 cells. NOS3 interacts with a variety of regulatory and structural proteins modulating its activity and traffic between plasma membrane, caveolae and intracellular membrane structures whose activity is tightly regulated by SNO [25]. Trx1 overexpression diminished SNO–NOS3 (Fig. 3C) and increased NO production (Fig. 3D) in both, control and Sorafenib-treated HepG2 cells. Sorafenib appeared to reduce NOS3 expression (Fig. 3C) and NO generation (Fig. 3D) in control and Sorafenib-treated HepG2 cells.

3.4. Sorafenib reduced SNO-CD95, caspase-8 activity and cell proliferation, and increased caspase-3 activity. Trx1 overexpression prevented the beneficial effect of Sorafenib in HepG2 cells

The induction of cell death by Sorafenib was related to a decrease in SNO-CD95 and a shift from caspase-8 to caspase-3 in HepG2 cells [11]. Sorafenib reduced SNO-CD95/CD95 ratio in control and Trx1-overexpressing HepG2 cells (Fig. 4A). Trx1 overexpression increased SNO-CD95 in control and Sorafenib-treated cells (Fig. 4A).

The increase in SNO-CD95 was directly related to caspase-8 activity (Fig. 4B) and cell proliferation (Fig. 4D), but inversely with caspase-3 activity (Fig. 4C). The overexpression of Trx1 increased caspase-8 activity (Fig. 4B) and cell proliferation (Fig. 4D) but decreased caspase-3 activity (Fig. 4C) in control and Sorafenib-treated cells. We addressed the question whether Trx1 downregulation by Sorafenib played a role during the induction of apoptosis and/or reduction of cell proliferation in HepG2 cells. The silencing of Trx1 by the siRNA strategy downregulated caspase-8 activity (Fig. 4B), but had no effect on caspase-3 activity (Fig. 4C) and cell proliferation (Fig. 4D) in control cells. The downregulation of Trx1 did not change these parameters in Sorafenib-treated HepG2 cells (Fig. 4B–D).

3.5. Role of Nrf2 in the proapoptotic properties of Sorafenib

The expression of Nrf2 and TrxR-Trx1 sytem has been related to resistance of cancer cells to chemotherapy [26–28]. The oxidative stress pathway is altered in a high number of HCC (12%) mainly related to KEAP1 mutations [1]. We tested whether HCC cells harboring inhibitory Keap1 mutations (JHH5, MHCC97H and Huh-1) altered the regulation of Trx1 expression, apoptosis and cell proliferation by Sorafenib in comparison with wild type Keap1 cancer cells (JHH2, JHH4 and SNU886). Sorafenib downregulated Nrf2 expression in Keap1 wild type HCC cell lines (JHH-2, JHH-4 and SNU886) (Supplementary Fig. 3A). Sorafenib downregulated the expression of Trx1 in all analyzed HCC cell lines (Supplementary Fig. 3B) that was related to increased caspase-3 (Supplementary Fig. 3C) and reduced cell proliferation (Supplementary Fig. 3D). Basal protein expression levels of Nrf2 appeared to be lower in Keap1-mutated cells than in cells with wild type Keap1 (Supplementary Fig. 3A) that were related to increased Sorafenib-dependent caspase-3 activation (Supplementary Fig. 3C).

3.6. The reduction of tumor growth by Sorafenib was related to decrease in Trx1 and SNO-CD95 expression, and caspase-8 activity in different experimental models of hepatocarcinogenesis

Sorafenib (200 mg/kg) reduced the number of tumor nodules (Fig. 5A), which was associated with a reduction of Trx1 expression (Fig. 5B), SNO-CD95 (Supplementary Fig. 4A) and caspase-8 activity (Fig. 5C) in animals treated with DEN for 17 weeks. The administration of Sorafenib (200 mg/kg) reduced tumor volume by 50% at 24 days after subcutaneous implantation of HepG2 cells (Fig. 5D). This effect was parallel to a decrease in the expression of Trx1 (Fig. 5E), SNO-CD95 (Supplementary Fig. 4B), and caspase-8 activity (Fig. 5F).

Trx1 overexpression increased tumor growth (Fig. 6A) and ki67 expression (Fig. 6B) in control and Sorafenib-treated animals. Sorafenib slowed tumor growth up to day 26th after implantation of Trx1 overexpressing HepG2 cells, while a strong relapse of tumor growth occurred from this time to the day of sacrifice (Fig. 6A). Sorafenib administration reduced Trx1 expression (Fig. 6C) and caspase-8 activity (Fig. 6D) in tumors derived from Trx1 overexpressing transfected HepG2 cells.

4. Discussion

Sorafenib has demonstrated a moderate but significant increase in median overall survival in patients with HCC and good liver function [29,30]. However, a proportion of patients (2%) are resistant to treatment [31] which has been related to the activation of cell survival IGFR [6,7], c-MET [8], and FGFR [7] signalings. The alteration of redox regulatory mechanisms mainly leading to Nrf2 activation by Keap1 mutation is observed in 12% of patients with HCC [1]. The induction of cell death by Sorafenib has been associated with the generation of oxidative stress in HepG2 cells [21]. In concordance with Rahmani et al. [32], Sorafenib induced $O_2^{\cdot-}$ generation in mitochondria and cytoplasm fractions, but we observed that the magnitude of this increase was much higher in the mitochondria than in the cytoplasm, which was accompanied with a decrease in cytoplasmic H_2O_2 and NO (Fig. 1A–D). The results are compatible with the active antioxidant properties of Sorafenib in cytoplasm. In fact, Sorafenib exerted dose-dependent ROS scavenging action *in vitro* (Fig. 1E and F). It is interesting to note that the clinical effectiveness of the drug has also been related to the lessening of oxidative stress in peripheral blood monocytic cells obtained from Sorafenib-responder HCC patients [33]. Sorafenib includes a trifluoromethylated or CF_3^- anion in its molecule that involves an increased antitumoral potency [34] (Supplementary Fig. 1). This CF_3^- group might be involved in the radical scavenger properties of Sorafenib through a nucleophilic mechanism based on the donation of one electron to the free radical ($O_2^{\cdot-}$ or $OH^{\cdot}$) [35].

Transcription factor Nrf2 is the master regulator of antioxidant response through ARE-dependent transcriptional activation of several genes involved in phase I to III detoxification systems, antioxidants, and transporters that protect cells from toxic and carcinogenic compounds [36]. The transactivation activity of Nrf2 is regulated by Keap1, which sequesters Nrf2 in the cytoplasm [37]. The generation of oxidative stress or pharmacological induction promotes oxidation of critical cysteines C273 and C288 of Keap1 that leads to Nrf2 escaping from Keap1 retention and allowing its translocation into the nucleus where it heterodimerizes with small Maf proteins and transactivates ARE driven gene expression [38]. The administration of Sorafenib reduced the nuclear translocation of Nrf2 in wild type Keap 1 cells such as HepG2 (Fig. 2) and JHH-2, JHH-4 and SNU886 (Supplementary Fig. 3). Nrf2 downregulation in nuclear fraction induced by Sorafenib was associated with reduced ARE-dependent Nrf2 transactivation capacity (Fig. 2C), Trx1 expression (Fig. 2D) and Trx1 activity (Fig. 2E), as well as the mRNA expression of GST, TrxR1, Gpx1, NQO1, HO-1 and GCLC in control and VEGF-stimulated HepG2 cells (Supplementary Fig. 2).

Redox modifications of protein cysteine thiols, and SNO in particular, is a posttranslational regulatory mechanism that plays an important role in the modulation of cellular processes by ROS and RNS with effects in health and disease [23]. Interestingly, mRNA expression and activity (Fig. 3A and B) of GSNOR were transiently increased in Sorafenib-treated HepG2 cells. The expression of NOS and NO generation within different cell types present in the tumor microenvironment, such as tumor, endothelial and inflammatory cells, as well as fibroblasts, regulate tumor growth, migration, invasion, survival, angiogenesis, and metastasis in cancer [39]. The expression of NOS2 has been related to poor prognosis in HCC [40].

NOS3 activity is tightly modulated by its phosphorylation state under control of protein kinase type A (PKA) and C (PKC), Akt, 5′ adenosine monophosphate-activated protein kinase (AMPK), Ca^{2+}/calmodulin-dependent kinase II, etc [41]. However, exposure of intact

endothelial cells, plasma membranes, or purified NOS to NO also reduces NOS catalytic activity [25] by inducing a change from dimeric (active) to monomeric (inactive) form [42]. NO donors induce SNO–NOS3 in multiple cysteines, such as those located at the positions 93 and 98 residues that are involved in its dimerization through the zinc tetrathiolate center [43]. Trx1 has two cysteines at its active site, Cys^{32}-Gly-Pro-Cys^{35}, that can catalytically reduce specific protein disulfide bonds and other oxidative cysteine modifications, and can serve as a denitrosylase towards specific SNO-proteins [44] (Fig. 7, Graphical Abstract). In addition, three structural Cys residues at positions 62, 69, and 73 are also present in Trx1. Cys^{73} displays transnitrosylating activity when the active site Cys^{32}/Cys^{35} is in the oxidized disulfide form and the reductase activity is blocked. The inhibition of caspase-3 activity by SNO has been shown to be mediated by Trx1 [44]. Sorafenib reduced NO generation probably though NOS3 downregulation moreover than altering SNO–NOS3 in control cells (Fig. 3D and C, respectively). Trx1 overexpression reduced SNO–NOS3 and increased NO generation (Fig. 3C and D, respectively).

Trx1 plays a key role against oxidative stress by regulating protein thiol/disulfide balance, supplying electrons to thiol-dependent peroxidases (peroxiredoxins), ribonucleotide reductase, methionine sulfoxide reductases, and regulating the activity of many redox-sensitive transcription factors, selenium and nitric oxide metabolism [14]. TrxR1, glutathione reductase and Nrf2-driven antioxidant systems attenuate potentially carcinogenic oxidative damage but also protect cancer cells from oxidative death. The expression of Nrf2 and TrxR-Trx1 system has been related to resistance of cancer cells to chemotherapy [26–28]. McLouglin et al. [45] showed that the frequency of DEN-induced cancer initiation decreased in TrxR1-null livers. Stable transfection of murine NIH 3T3 fibroblast-like cells and human MCF-7 breast cancer cells with cDNA encoding for human wild-type Trx increased cell proliferation, whereas redox-inactive mutant Trx acted in a dominant negative manner [46].

The induction of NO-related posttranslational modifications in components of cell death pathways promotes different outcomes in terms of cell death or survival [39]. In particular, the prevention of SNO-CD95 by mutation of Cys199 or Cys304 residues avoids its recruitment and activation, respectively [47]. Sorafenib reduced SNO-CD95 (Fig. 4A), caspase-8 (Fig. 4B), and cell proliferation (Fig. 4D) while increased caspase-3 (Fig. 4C). Although CD95 is a prototypical trigger of the extrinsic apoptotic pathway, it has also been shown to be required for optimal cell proliferation, motility and invasion in tumor cells [48].

The overexpression of Trx1 increased caspase-8 activity and cell proliferation, but decreased caspase-3 in control and Sorafenib-treated HepG2 cells (Fig. 4). The downregulation of Trx1 by siRNA strategy diminished caspase-8 activity (Fig. 4A), but had no effect on caspase-3 activity (Fig. 4C) and cell proliferation (Fig. 4D) in control cells. These results suggest that CD95-dependent caspase-8 activity might be the primary target of Trx1 downregulation. Silencing of Trx1 did not change these parameters in Sorafenib-treated HepG2 cells (Fig. 4B–D) that might suggest a critical role of Trx1 downregulation in the reduction of caspase-8 activity by Sorafenib in HepG2 cells (Fig. 4B). The inverse relationship between caspase-8 and caspase-3 during Sorafenib treatment has been previously shown in HepG2 cells [11].

Several tumorigenic signals such as NF-*k*B, ERK, and caspase-8 are downstream effectors of CD95 [49]. This protumorigenic phenotype has been related to tyrosine phosphorylation of caspase-8 by src-family kinases [50], as well as by oxidative stress-dependent YES activation of EGFR and CD95 tyrosine phosphorylation [51]. In addition, Chen et al. [52] showed that Sorafenib enhances TRAIL-induced cell death through SH2 domain-containing tyrosine phosphatase (SHP-1) dependent decrease in the phosphorylation of signal transducers and activators of transcription type 3 (STAT3) and downstream-regulated proteins such as Mcl-1, survivin, and cyclin D1 in hepatoma cells. STAT3 is a pro-survival transcription factor which is constitutively activated in human cancer cell lines. Tyrosine phosphorylation of STAT3 is dependent on the thiol redox state modulated by H_2O_2 and peroxiredoxin-2 levels and the Trx system activity [53]. We have recently shown that the treatment with Sorafenib induced thiol redox reductive changes in STAT3, and Trx1 downregulation counteracted this effect of the drug in HCC cell lines [16]. We are deeply investigating CD95-related downstream events leading to regulation by Sorafenib of cell proliferation in liver cancer cells.

The reduction of Trx1 expression and activity appears to be essential in the antitumoral action of Sorafenib. Two independent experimental models of HCC showed that the antitumoral properties of Sorafenib were related to a decrease in Trx1 expression, SNO-CD95 and caspase-8 activity (Fig. 5 and Supplementary Fig. 4). The *in vivo* experiment involving subcutaneous implantation of Trx1 overexpressing HepG2 cells further supports the relevant role of Trx1 in tumor growth. Sorafenib reduced tumor growth, Ki67 and Trx1 expressions and caspase-8 activity in tumors derived from Trx1-overexpressing HepG2 cells in nude mice (Fig. 6).

In conclusion, the antioxidant properties of Sorafenib might positively influence the downregulation of Nrf2-dependent Trx1 expression which plays a relevant role in the deactivation of NOS3 and CD95 through SNO. CD95 deactivation could also be achieved by transient upregulation of GSNOR and downregulation of CD95 by Sorafenib in HepG2 cells. Decreased expression of SNO-CD95 by Sorafenib involved reduction of caspase-8 activity and cell proliferation, and increased downstream caspase-3 activity in liver cancer cells (Fig. 7, Graphical Abstract). The mechanism supports the inverse relationship between caspase-8 and caspase-3 during Sorafenib treatment in HepG2 cells [11]. The relevance of Trx1, SNO-CD95 and caspase-8 downregulation in the antitumoral properties of Sorafenib was demonstrated in three independent experimental models of hepatocarcinogenesis.

Financial support

This study was funded by Institute of Health Carlos III (ISCIII) (PI13/00021, PI15/00107, PI16/00090 and PI19/01266), Spanish Ministry of Economy and Competitiveness (SAF2015-71208-R, BFU2016-8006-P, PGC2018-094276-B-I00 and RED2018-102576-T), Andalusian Ministry of Economy, Innovation, Science and Employment (BIO-216 and CTS-6264) and Andalusian Ministry of Equality, Health and Social Policies (PI-00025-2013 and PI-0198-2016). P de la C–O was supported by FPU predoctoral fellowship (FPU17/00026) from Ministry of Education, Culture and Sports. We thank the Biomedical Research Network Center for Cardiovascular Diseases (CIBERCV), and the Biomedical Research Network Center for Liver and Digestive Diseases (CIBERehd) founded by the ISCIII and co-financed by European Development Regional Fund “A way to achieve Europe” ERDF for their financial support.

Acknowledgments

We thank Prof. Jessica Zucman-Rossi and Dr. Sandra Rebouissou for supplying and providing information regarding the use of JHH2, JHH-4, JHH-5, Huh-1, SNU886 and MHCC97H cell lines.

Appendix A. Supplementary data

Supplementary data to this article can be found online at https://doi.org/10.1016/j.redox.2020.101528.

References

[1] K. Schulze, S. Imbeaud, E. Letouze, L.B. Alexandrov, J. Calderaro, S. Rebouissou, G. Couchy, et al., Exome sequencing of hepatocellular carcinomas identifies new mutational signatures and potential therapeutic targets, Nat. Genet. 47 (2015) 505–511.

[2] L. European Association For The Study Of The, R. European Organisation For, C. Treatment Of, EASL-EORTC clinical practice guidelines: management of hepatocellular carcinoma, J. Hepatol. 56 (2012) 908–943.
[3] R.T. Stravitz, D.M. Heuman, N. Chand, R.K. Sterling, M.L. Shiffman, V.A. Luketic, A.J. Sanyal, et al., Surveillance for hepatocellular carcinoma in patients with cirrhosis improves outcome, Am. J. Med. 121 (2008) 119–126.
[4] A. Forner, M. Reig, J. Bruix, Hepatocellular carcinoma, Lancet 391 (2018) 1301–1314.
[5] J. Bruix, M. Reig, M. Sherman, Evidence-based diagnosis, staging, and treatment of patients with hepatocellular carcinoma, Gastroenterology 150 (2016) 835–853.
[6] H. Huynh, AZD6244 (ARRY-142886) enhances the antitumor activity of rapamycin in mouse models of human hepatocellular carcinoma, Cancer 116 (2010) 1315–1325.
[7] V. Tovar, H. Cornella, A. Moeini, S. Vidal, Y. Hoshida, D. Sia, J. Peix, et al., Tumour initiating cells and IGF/FGF signalling contribute to sorafenib resistance in hepatocellular carcinoma, Gut 66 (2017) 530–540.
[8] H. Huynh, V.C. Ngo, H.N. Koong, D. Poon, S.P. Choo, C.H. Thng, P. Chow, et al., Sorafenib and rapamycin induce growth suppression in mouse models of hepatocellular carcinoma, J. Cell Mol. Med. 13 (2009) 2673–2683.
[9] M. Cervello, D. Bachvarov, N. Lampiasi, A. Cusimano, A. Azzolina, J.A. McCubrey, G. Montalto, Molecular mechanisms of sorafenib action in liver cancer cells, Cell Cycle 11 (2012) 2843–2855.
[10] M.A. Rodriguez-Hernandez, R. Gonzalez, A.J. de la Rosa, P. Gallego, R. Ordonez, E. Navarro-Villaran, L. Contreras, et al., Molecular characterization of autophagic and apoptotic signaling induced by sorafenib in liver cancer cells, J. Cell. Physiol. 234 (2018) 692–708.
[11] A. Rodriguez-Hernandez, E. Navarro-Villaran, R. Gonzalez, S. Pereira, L.B. Soriano-De Castro, A. Sarrias-Gimenez, L. Barrera-Pulido, et al., Regulation of cell death receptor S-nitrosylation and apoptotic signaling by Sorafenib in hepatoblastoma cells, Redox Biol. 6 (2015) 174–182.
[12] G. Martinez-Sanchez, A. Giuliani, Cellular redox status regulates hypoxia inducible factor-1 activity. Role in tumour development, J. Exp. Clin. Canc. Res. 26 (2007) 39–50.
[13] D. Trachootham, J. Alexandre, P. Huang, Targeting cancer cells by ROS-mediated mechanisms: a radical therapeutic approach? Nat. Rev. Drug Discov. 8 (2009) 579–591.
[14] J. Lu, A. Holmgren, The thioredoxin antioxidant system, Free Radic. Biol. Med. 66 (2014) 75–87.
[15] H. Nakamura, H. Masutani, Y. Tagaya, A. Yamauchi, T. Inamoto, Y. Nanbu, S. Fujii, et al., Expression and growth-promoting effect of adult T-cell leukemia-derived factor. A human thioredoxin homologue in hepatocellular carcinoma, Cancer 69 (1992) 2091–2097.
[16] M.J. López-Grueso, R. González, J. Muntané, J.A. Bárcena, C.A. Padilla, Thioredoxin downregulation enhances sorafenib effects in hepatocarcinoma cells, Antioxidants 8 (2019) 501-501.
[17] L.C. Green, D.A. Wagner, J. Glogowski, P.L. Skipper, J.S. Wishnok, S.R. Tannenbaum, Analysis of nitrate, nitrite, and [15N]nitrate in biological fluids, Anal. Biochem. 126 (1982) 131–138.
[18] A. Izquierdo-Álvarez, D. Tello, J.D. Cabrera-García, A. Martínez-Ruiz, Identification of S-nitrosylated and reversibly oxidized proteins by fluorescence switch and complementary techniques, Methods Mol. Biol. 1747 (2018) 73–87.
[19] L.M. Lopez-Sanchez, F.J. Corrales, R. Gonzalez, G. Ferrin, J.R. Munoz-Castaneda, I. Ranchal, A.B. Hidalgo, et al., Alteration of S-nitrosothiol homeostasis and targets for protein S-nitrosation in human hepatocytes, Proteomics 8 (2008) 4709–4720.
[20] A. Holmgren, Thioredoxin catalyzes the reduction of insulin disulfides by dithiothreitol and dihydrolipoamide, J. Biol. Chem. 254 (1979) 9627–9632.
[21] R. Coriat, C. Nicco, C. Chereau, O. Mir, J. Alexandre, S. Ropert, B. Weill, et al., Sorafenib-induced hepatocellular carcinoma cell death depends on reactive oxygen species production in vitro and in vivo, Mol. Canc. Therapeut. 11 (2012) 2284–2293.
[22] J.D. Hayes, A.T. Dinkova-Kostova, The Nrf2 regulatory network provides an interface between redox and intermediary metabolism, Trends Biochem. Sci. 39 (2014) 199–218.
[23] J.S. Stamler, S. Lamas, F.C. Fang, Nitrosylation. the prototypic redox-based signaling mechanism, Cell 106 (2001) 675–683.
[24] L. Liu, A. Hausladen, M. Zeng, L. Que, J. Heitman, J.S. Stamler, A metabolic enzyme for S-nitrosothiol conserved from bacteria to humans, Nature 410 (2001) 490–494.
[25] J.M. Patel, J. Zhang, E.R. Block, Nitric oxide-induced inhibition of lung endothelial cell nitric oxide synthase via interaction with allosteric thiols: role of thioredoxin in regulation of catalytic activity, Am. J. Respir. Cell Mol. Biol. 15 (1996) 410–419.
[26] X.J. Wang, Z. Sun, N.F. Villeneuve, S. Zhang, F. Zhao, Y. Li, W. Chen, et al., Nrf2 enhances resistance of cancer cells to chemotherapeutic drugs, the dark side of Nrf2, Carcinogenesis 29 (2008) 1235–1243.
[27] E.S.J. Arnér, Targeting the Selenoprotein Thioredoxin Reductase 1 for Anticancer Therapy, vol. 136, 2017, pp. 139–151.
[28] J.L. Roh, H. Jang, E.H. Kim, D. Shin, Targeting of the glutathione, thioredoxin, and Nrf2 antioxidant systems in head and neck cancer, Antioxidants Redox Signal. 27 (2017) 106–114.
[29] J.M. Llovet, S. Ricci, V. Mazzaferro, P. Hilgard, E. Gane, J.F. Blanc, A.C. de Oliveira, et al., Sorafenib in advanced hepatocellular carcinoma, N. Engl. J. Med. 359 (2008) 378–390.
[30] A.L. Cheng, Y.K. Kang, Z. Chen, C.J. Tsao, S. Qin, J.S. Kim, R. Luo, et al., Efficacy and safety of sorafenib in patients in the Asia-Pacific region with advanced hepatocellular carcinoma: a phase III randomised, double-blind, placebo-controlled trial, Lancet Oncol. 10 (2009) 25–34.
[31] A. Villanueva, J.M. Llovet, Second-line therapies in hepatocellular carcinoma: emergence of resistance to sorafenib, Clin. Canc. Res. 18 (2012) 1824–1826.
[32] J.F. Chiou, C.J. Tai, Y.H. Wang, T.Z. Liu, Y.M. Jen, C.Y. Shiau, Sorafenib induces preferential apoptotic killing of a drug- and radio-resistant Hep G2 cells through a mitochondria-dependent oxidative stress mechanism, Canc. Biol. Ther. 8 (2009) 1904–1913.
[33] M. Caraglia, G. Giuberti, M. Marra, R. Addeo, L. Montella, M. Murolo, P. Sperlongano, et al., Oxidative stress and ERK1/2 phosphorylation as predictors of outcome in hepatocellular carcinoma patients treated with sorafenib plus octreotide LAR, Cell Death Dis. 2 (2011) e150.
[34] Y. Zhou, J. Wang, Z. Gu, S. Wang, W. Zhu, J.L. Aceña, V.A. Soloshonok, et al., Next generation of fluorine-containing Pharmaceuticals, compounds currently in phase II–III clinical trials of major pharmaceutical companies: new structural trends and therapeutic areas, Chem. Rev. 116 (2016) 422–518.
[35] L. Chu, F.-L. Qing, Oxidative trifluoromethylation and trifluoromethylthiolation reactions using (Trifluoromethyl)trimethylsilane as a nucleophilic CF3 source, Acc. Chem. Res. 47 (2014) 1513–1522.
[36] M. Kobayashi, M. Yamamoto, Molecular mechanisms activating the Nrf2-Keap1 pathway of antioxidant gene regulation, Antioxidants Redox Signal. 7 (2005) 385–394.
[37] K. Itoh, N. Wakabayashi, Y. Katoh, T. Ishii, K. Igarashi, J.D. Engel, M. Yamamoto, Keap1 represses nuclear activation of antioxidant responsive elements by Nrf2 through binding to the amino-terminal Neh2 domain, Genes Dev. 13 (1999) 76–86.
[38] D.D. Zhang, M. Hannink, Distinct cysteine residues in Keap1 are required for Keap1-dependent ubiquitination of Nrf2 and for stabilization of Nrf2 by chemopreventive agents and oxidative stress, Mol. Cell Biol. 23 (2003) 8137–8151.
[39] R. Gonzalez, F.J. Molina-Ruiz, J.A. Barcena, C.A. Padilla, J. Muntane, Regulation of cell survival, apoptosis, and epithelial-to-mesenchymal transition by nitric oxide-dependent post-translational modifications, Antioxidants Redox Signal. 29 (13) (2018) 1312–1332, https://doi.org/10.1089/ars.2017.7072.
[40] M.A. Rahman, D.K. Dhar, E. Yamaguchi, S. Maruyama, T. Sato, H. Hayashi, T. Ono, et al., Coexpression of inducible nitric oxide synthase and COX-2 in hepatocellular carcinoma and surrounding liver: possible involvement of COX-2 in the angiogenesis of hepatitis C virus-positive cases, Clin. Canc. Res. 7 (2001) 1325–1332.
[41] Z. Hu, J. Chen, Q. Wei, Y. Xia, Bidirectional actions of hydrogen peroxide on endothelial nitric-oxide synthase phosphorylation and function: co-commitment and interplay of Akt and AMPK, J. Biol. Chem. 283 (2008) 25256–25263.
[42] K. Ravi, L.A. Brennan, S. Levic, P.A. Ross, S.M. Black, S-nitrosylation of endothelial nitric oxide synthase is associated with monomerization and decreased enzyme activity, Proc. Natl. Acad. Sci. U. S. A. 101 (2004) 2619–2624.
[43] M. Tummala, V. Ryzhov, K. Ravi, S.M. Black, Identification of the cysteine nitrosylation sites in human endothelial nitric oxide synthase, DNA Cell Biol. 27 (2008) 25–33.
[44] D.A. Mitchell, M.A. Marletta, Thioredoxin catalyzes the S-nitrosation of the caspase-3 active site cysteine, Nat. Chem. Biol. 1 (2005) 154–158.
[45] M.R. McLoughlin, D.J. Orlicky, J.R. Prigge, P. Krishna, E.A. Talago, I.R. Cavigli, S. Eriksson, et al., TrxR1, Gsr, and oxidative stress determine hepatocellular carcinoma malignancy, Proc. Natl. Acad. Sci. U. S. A. (2019).
[46] A. Gallegos, J.R. Gasdaska, C.W. Taylor, G.D. Paine-Murrieta, D. Goodman, P.Y. Gasdaska, M. Berggren, et al., Transfection with human thioredoxin increases cell proliferation and a dominant-negative mutant thioredoxin reverses the transformed phenotype of human breast cancer cells, Canc. Res. 56 (1996) 5765–5770.
[47] L. Leon-Bollotte, S. Subramaniam, O. Cauvard, S. Plenchette-Colas, C. Paul, C. Godard, A. Martinez-Ruiz, et al., S-nitrosylation of the death receptor fas promotes fas ligand-mediated apoptosis in cancer cells, Gastroenterology 140 (2011) 2009–2018 2018 e2001-2004.
[48] B.C. Barnhart, P. Legembre, E. Pietras, C. Bubici, G. Franzoso, M.E. Peter, CD95 ligand induces motility and invasiveness of apoptosis-resistant tumor cells, EMBO J. 23 (2004) 3175–3185.
[49] A. Martin-Villalba, E. Llorens-Bobadilla, D. Wollny, CD95 in cancer: tool or target? Trends Mol. Med. 19 (2013) 329–335.
[50] S. Barbero, A. Mielgo, V. Torres, T. Teitz, D.J. Shields, D. Mikolon, M. Bogyo, et al., Caspase-8 association with the focal adhesion complex promotes tumor cell migration and metastasis, Canc. Res. 69 (2009) 3755–3763.
[51] N.L. Ta, K. Chakrabandhu, S. Huault, A.O. Hueber, The tyrosine phosphorylated pro-survival form of Fas intensifies the EGF-induced signal in colorectal cancer cells through the nuclear EGFR/STAT3-mediated pathway, Sci. Rep. 8 (2018) 12424.
[52] K.F. Chen, W.T. Tai, T.H. Liu, H.P. Huang, Y.C. Lin, C.W. Shiau, P.K. Li, et al., Sorafenib overcomes TRAIL resistance of hepatocellular carcinoma cells through the inhibition of STAT3, Clin. Canc. Res. 16 (2010) 5189–5199.
[53] M.C. Sobotta, W. Liou, S. Stöcker, D. Talwar, M. Oehler, T. Ruppert, A.N.D. Scharf, et al., Peroxiredoxin-2 and STAT3 form a redox relay for H2O2 signaling, Nat. Chem. Biol. 11 (2015) 64–70.

Redox Biology 36 (2020) 101510

Contents lists available at ScienceDirect

Redox Biology

journal homepage: www.elsevier.com/locate/redox

Invited Review

Integrated molecular signaling involving mitochondrial dysfunction and alteration of cell metabolism induced by tyrosine kinase inhibitors in cancer

María A. Rodríguez-Hernández[a,b], Patricia de la Cruz-Ojeda[a], Mª José López-Grueso[c], Elena Navarro-Villarán[a,b], Raquel Requejo-Aguilar[c], Beatriz Castejón-Vega[d], María Negrete[a], Paloma Gallego[e], Álvaro Vega-Ochoa[a], Victor M. Victor[b,f,g], Mario D. Cordero[d,h], José A. Del Campo[e], J. Antonio Bárcena[c], C. Alicia Padilla[c], Jordi Muntané[a,b,i,*]

[a] Institute of Biomedicine of Seville (IBiS), IBiS/Hospital University "Virgen del Rocío"/CSIC/University of Seville, Seville, Spain
[b] Centro de Investigación Biomédica en red de Enfermedades Hepáticas y Digestivas (CIBEREHD), Madrid, Spain
[c] Department of Biochemistry and Molecular Biology, University of Cordoba, Maimonides Biomedical Research Institute of Cordoba (IMIBIC), Cordoba, Spain
[d] Research Laboratory, Oral Medicine Department, University of Seville, Seville, Spain
[e] Unit for the Clinical Management of Digestive Diseases, Hospital University "Nuestra Señora de Valme", Sevilla, Spain
[f] Service of Endocrinology and Nutrition, Hospital University "Doctor Peset", Foundation for the Promotion of Health and Biomedical Research in the Valencian Region (FISABIO), Valencia, Spain
[g] Department of Physiology, University of Valencia, Valencia, Spain
[h] Department of Physiology, Institute of Nutrition and Food Technology "José Mataix", Biomedical Research Center (CIBM), University of Granada, Armilla, Spain
[i] Department of General Surgery, Hospital University "Virgen del Rocío"/IBiS/CSIC/University of Seville, Seville, Spain

ARTICLE INFO

Keywords:
Autophagy
Cell death
Endoplasmic reticulum stress
mTOR
Redox status
PGC-1α

ABSTRACT

Cancer cells have unlimited replicative potential, insensitivity to growth-inhibitory signals, evasion of apoptosis, cellular stress, and sustained angiogenesis, invasiveness and metastatic potential. Cancer cells adequately adapt cell metabolism and integrate several intracellular and redox signaling to promote cell survival in an inflammatory and hypoxic microenvironment in order to maintain/expand tumor phenotype. The administration of tyrosine kinase inhibitor (TKI) constitutes the recommended therapeutic strategy in different malignancies at advanced stages.

There are important interrelationships between cell stress, redox status, mitochondrial function, metabolism and cellular signaling pathways leading to cell survival/death. The induction of apoptosis and cell cycle arrest widely related to the antitumoral properties of TKIs result from tightly controlled events involving different cellular compartments and signaling pathways. The aim of the present review is to update the most relevant studies dealing with the impact of TKI treatment on cell function. The induction of endoplasmic reticulum (ER) stress and Ca^{2+} disturbances, leading to alteration of mitochondrial function, redox status and phosphatidylinositol 3-kinase (PI3K)-protein kinase B (Akt)-mammalian target of rapamycin (mTOR) and AMP-activated protein kinase (AMPK) signaling pathways that involve cell metabolism reprogramming in cancer cells will be covered. Emphasis will be given to studies that identify key components of the integrated molecular pattern including receptor tyrosine kinase (RTK) downstream signaling, cell death and mitochondria-related events that appear to be involved in the resistance of cancer cells to TKI treatments.

1. TK inhibition in cancer treatment

The activation of receptor tyrosine kinase (RTK) and non-receptor tyrosine kinase (NRTK) transmits downstream signaling events related to cell proliferation, growth, migration, angiogenesis or cell dedifferentiation [1]. The genetic alterations of RTKs involve different molecular mechanisms such as gain-of-function mutation, genomic amplifications, chromosomal translocations and autocrine activation are related to transforming-related abilities in cancer and resistance to treatments [2].

Chemotherapy and radiotherapy exert their antitumoral activity using common mechanisms in normal and tumor cells leading to noxious side effects in the surrounding tissues. The traditional anti-cancer chemotherapy targets dividing cells inducing DNA damage that leads to

* Corresponding author. Institute of Biomedicine of Seville (IBiS), IBiS/Hospital University "Virgen del Rocío"/CSIC/University of Seville, Seville, Spain.
E-mail address: jmuntane-ibis@us.es (J. Muntané).

https://doi.org/10.1016/j.redox.2020.101510
Received 24 February 2020; Accepted 16 March 2020
Available online 23 May 2020

Abbreviations

AIF	Apoptosis-inducing factor
AML	Acute myeloid leukemia
ALL	Acute lymphocytic leukemia
AMPK	AMP-activated protein kinase
ALK	Anaplastic lymphoma kinase
APE1	Apurinic/apyrimidinic endonuclease 1
BNIP3	BCL2 Interacting Protein 3
BiP	Binding immunoglobulin protein
NIX	BNIP3-like
CAMKK2	Calcium/calmodulin-dependent protein kinase kinase 2
CHOP	C/EBP homologous protein
c-Met	Mesenchymal-epithelial transition factor receptor
CML	Chronic myeloid leukemia
CLL	Chronic lymphocytic leukemia
JNK	c-Jun N-terminal kinase
CSF-1R	CSF-1R Colony-stimulating factor receptor 1
CRC	Colon and rectum carcinoma
COX-2	Cyclooxygenase-2
ER	Endoplasmic reticulum
ENO2	Enolase 2
EGFR	Epidermal growth factor receptor
EMT	Epithelial-mesenchymal transition
ERK	Extracellular signal-regulated kinases
eIF2α	Eukaryotic Initiation Factor 2α
FGFR	Fibroblast growth factor receptor
Flt3	FMS-like tyrosine kinase 3
Grp78	Glucose-regulated protein 78
FoxM1	Forkhead Box M1
GIST	Gastrointestinal stromal tumor
GLUT1	Glucose transporter I
GLUT3	Glucose transporter 3
Grx1	Glutaredoxin 1
HNSCC	Head and neck squamous cell carcinoma
HCC	Hepatocellular carcinoma
HGF	Hepatocyte growth factor
HKII	Hexokinase II
H_2O_2	Hydrogen peroxide
HIF-1	Hypoxia-inducible factor-1
IRE1α	Inositol-requiring enzyme-1α, IRE1
JAK	Janus kinase
mTOR	Mammalian target of rapamycin
MMP	Matrix metalloproteinases
MITF	Melanocyte lineage-specification transcription factor
MAPK	Mitogen-activated protein kinase
MEK	MAPK/ERK
Mcl-1	Myeloid cell leukemia-1
SIRT1	NAD-dependent deacetylase sirtuin-1
NOX	NADPH oxidase
NRTK	Non-receptor tyrosine kinase
NSCLC	Non-small cell lung cancer
NF-kB	Nuclear factor kappa-light-chain-enhancer of activated B cells
Nrf2	Nuclear transcription factor erythroid 2-related factor 2
LDH	Lactate dehydrogenase
LKB1	Liver kinase B1
PUMA	p53 upregulated modulator of apoptosis
PPP	Pentose phosphate pathway
Prdx2	Peroxiredoxin 2
Prdx6	Peroxiredoxin 6
PGC-1α	Peroxisome proliferator-activated receptor-coactivator 1α
PI3K	Phosphatidylinositol 3-kinase
PTEN	Phosphatidylinositol 3,4,5-trisphosphate 3-phosphatase and tensin homolog
PFK1	6-Phosphofructo-1-kinase
PFKFB2	6-phosphofructo-2-kinase/fructose-2,6-biphosphatase 2
PDK-1	Phosphoinositide-dependent protein kinase-1
PDGFR	Platelet derived growth factor receptor
PARP-1	Poly (ADP-ribose) polymerase 1
PKA	Protein kinase A
Akt	Protein kinase B
PERK	Protein kinase RNA-like endoplasmic reticulum kinase
PPA2	Protein phosphatase A2
PTPB1	Protein tyrosine phosphatase B1
PDHA1	Pyruvate dehydrogenase E1 alpha 1
PKM2	Pyruvate kinase isoenzyme type M2
RHEB	Ras homolog enriched in brain
ROS	Reactive oxygen species
RTK	Receptor tyrosine kinase
RCC	Renal cell carcinoma
ROS1	ROS proto-oncogene 1
SWH	Salvador-Warts-Hippo
STAT3	Signal transducer and activator of transcription 3
S6K1	S6 kinase 1
SHP-1	Src homology region 2 domain-containing phosphatase-1
SREBP1	Sterol regulatory element-binding transcription factor 1
$O_2^{\cdot -}$	Superoxide anion
Trx1	Thioredoxin 1
TrxR1	Thioredoxin reductase 1
TGF-β	Transforming growth factor-β
TCA	Tricarboxylic acid
TK	Tyrosine kinase
TKI	Tyrosine kinase inhibitor
TSC	Tuberous sclerosis complex
ULK1/2	Unc51-like kinases
UPR	Unfolded protein response
VEGFR	Vascular endothelial growth factor receptor
XBP-1	X-Box binding protein 1
XIAP	X-linked inhibitor of apoptosis protein

DNA damage response, leading to potential activation of DNA repair mechanisms, suppression of global general translation, cell cycle arrest and, ultimately, either cell survival or cell death [3,4]. Tyrosine kinase inhibitors (TKIs) research has gradually been replacing these conventional anti-tumoral therapies in order to achieve more specific targets with the promise to enhance positive results. TKIs target specific oncogenic signaling in tumor cells minimizing side effects in healthy cells [5]. The degree of efficacy and selectivity is variable among TKI treatments, and they can be differentially beneficial depending on the target disease in terms of preventing tumor cell dedifferentiation, proliferation and oncogenic signaling. Some of the advantages of TKIs over traditional chemotherapy are their high selectivity, few side effects and good oral administration, with an absorption grade that differs among TKI molecules [6]. Currently, more than 20 TKI drugs have been approved both as first- and second-line therapies in clinical oncology for the treatment of different cancer diseases (Table 1). Even TKIs employment have resulted in a breakthrough in the area of cancer treatment, the acquired resistance of tumoral cells is still a crucial barrier that avoids better results in the cure of cancer [7].

TKIs are low-weight molecules that act as receptor antagonists through interfering with ATP-γ-phosphate for the ATP binding site within the kinase catalytic domain preventing the autophosphorylation, dimerization and activation of the downstream cascade, thereby reducing tyrosine kinase (TK) phosphorylation [1]. TKIs can also occupy an adjacent site to their ATP binding domain, allowing both the inhibitor and ATP to bind to the kinase [8]. There are various TKIs that vary in

Table 1
Tyrosine kinase inhibitors including targets, and their use as the recommended treatment in cancer. AML: Acute myeloid leukemia, ALL: Acute lymphocytic leukemia, CML: Chronic myeloid leukemia, CRC: Colon and rectum carcinoma, DTC: Differential thyroid carcinoma, GIST: Gastrointestinal stromal tumor, HCC: Hepatocellular carcinoma, MTC: Medullary thyroid carcinoma, c-Met: Mesenchymal-epithelial transition factor receptor, NSCLC: Non-small cell lung cancer, RCC: Renal cell carcinoma, STS: Soft tissue sarcoma.

TKI	Target	Diseases
Alectinib	ALK	NSCLC
Afatinib	EGFR	NSCLC
Axitinib	VEGFR, PDGFR, c-Kit	RCC
Brigatinib	ALK	NSCLC
Bosutinib	Abl, Src	CML, MTC
Cabozantinib	VEGFR, c-Met, RET, Flt3, c-Kit, Axl, Tie-2	HCC, MTC
Canertinib	EGFR	Breast cancer
Capmatinib	EGFR, c-Met	NSCLC
Ceritinib	ALK	NSCLC
Crizotinib	ALK, c-Met	NSCLC
Dasatinib	Abl, Src, PDGFR, c-Kit	CML
Dovitinib	VEGFR, FGFR, PDGFR, c-Kit, Flt3, CSF-1R	RCC
Erlotinib	EGFR	NSCLC
Gefitinib	EGFR	NSCLC
Herceptin	Her-2/neu	Breast Cancer
Imatinib	Abl, PDGFR, c-Kit	ALL, CML, CLL, GIST
Lapatinib	EGFR, ErbB2	Breast cancer
Leflunomide	PDGFR	Prostate cancer
Lenvatinib	VEGFR, PDGFR, FGFR, RET, c-Kit	DTC, HCC
Neratinib	HER2	Breast Cancer
Nilotinib	Bcr, Abl, PDGFR	CML
Osimertinib	EGFR	NSCLC
Pazopanib	VEGFR, PDGFR, FGFR, c-Kit	RCC, STS, NSCLC
Ponatinib	Bcr, Abl	CML, ALL
Regorafenib	VEGFR, PDGFR, FGFR, c-Kit, RET, Raf, Tie2	HCC, CCR, GIST
Ruxolitinib	JAK1, JAK2	Myelofibrosis
Semaxinib	VEGFR, c-Kit, Flt3	AML
Sorafenib	Raf, VEGFR, PDGFR, c-Kit, Flt3	RCC, HCC, Melanoma
Sunitinib	VEGFR, PDGFR, c-Kit, Flt3	GIST, RCC
Sutent	Flt3	AML
Vandetanib	VEGFR, EGFR	MTC
Vatalanib	VEGFR	CCR, Prostate cancer, RCC
Vemurafenib	B-Raf	Melanoma

their pharmacological effects, as well as in their side effects and target kinases, and the factors that define the effectiveness of inhibitors [9].

2. Alteration of ER stress and Ca^{2+} homeostasis by TKIs

The endoplasmic reticulum (ER) plays a crucial role in proteostasis, handling translocation during translation and folding of secretory proteins [10]. The accumulation of misfolded proteins in the lumen induces ER stress and triggers the unfolded protein response (UPR) to avoid cellular damage. Several situations including starvation, reduced glycosylation, drugs, alteration of redox status or mutant proteins might boost ER stress [11]. In mammals, inositol-requiring enzyme-1α (IRE1α), protein kinase RNA-like endoplasmic reticulum kinase (PERK) and ATF6 act as stress sensors governing restoration of homeostasis by attenuating translation, regulating ER lumen capacity and activating gene expression to reduce misfolding (Fig. 1).

2.1. Impact of TKI on ER stress

The administration of TKI induces ER stress with different functional repercussions in cancer cells. Sorafenib inhibits RTKs such as vascular endothelial growth factor receptor (VEGFR) and platelet-derived growth factor receptor (PDGFR), NRTK such as c-kit and FMS-like tyrosine kinase (Flt3), as well as serine-threonine Raf kinase (Table 1), which increases markers of ER stress, including IRE1α, eukaryotic initiation factor 2α (eIF2α) and binding immunoglobulin protein (BiP)/glucose-regulated protein 78 (BiP/Grp78) in hepatic tissue from patients submitted to liver resection for hepatocellular carcinoma (HCC) [12]. In addition, the administration of Sorafenib (10 μM) has been related to the induction of ER stress, Ca^{2+} release, generation of reactive oxygen species (ROS), and apoptosis in human leukemia cells [13]. In this study, cell death is related to the activation of PERK and subsequent phosphorylation of eIF2α, as well as induction of IRE1α and X-Box Binding Protein 1 (XBP-1) mRNA processing, independent of the Raf/mitogen-activated protein kinase (MAPK)/extracellular signal-regulated kinase (ERK) or MEK pathway [13]. We have recently showed that Sorafenib induces early (3–12 h) ER stress characterized by an increase of PERK and IRE1α signaling, but a decrease of ATF6 expression, temporally associated with the activation of c-Jun N-terminal kinase (JNK) and AMP-activated protein kinase (AMPK), and reduction of mammalian target of rapamycin (mTOR) and protein translation [14]. The downregulation of ER signaling using siRNA strategies has proved to reduce autophagy markers and increased apoptosis in Sorafenib-treated HepG2 cells [14]. The downregulation of ATF6 and autophagy mediated by Sorafenib [13,14] might be related to the disruption of the secretory pathway measured by Golgi fragmentation and phosphorylation of ATPase p97/VCP as the initiator of autophagy [15]. The induction of apoptosis by Sorafenib in renal cell carcinoma (RCC) has been related to the upregulation of PERK-related induction of ATF4, C/EBP homologous protein (CHOP) and p53 upregulated modulator of apoptosis (PUMA) [16].

Lenvatinib targets VEGFR, PDGFR, fibroblast growth factor receptor (FGFR), RET and c-Kit (Table 1), inducing an elevation of ER stress markers in nasopharyngeal cancer HK-1 cell line. Its combined treatment with iodine-131 potentiates ER stress and cell death, as well as reduces migration and invasiveness [17]. Differently, proapoptotic and antiproliferative properties induced by antiangiogenic drug Sunitinib with similar targets as Sorafenib (Table 1), are related to reduced expression of BiP/Grp78 and downregulation of PERK/eIF2α signaling in RCC [18]. The study supports the survival properties of ER stress in the model. In this sense, the knockdown of GRP78 inhibits cancer cell survival and induces apoptosis in cultured RCC [18]. Other study has shown that Sunitinib-related resistance is associated with IRE1α-dependent nuclear factor kappa-light-chain-enhancer of activated B cells (NF-κB) signaling pathway [19].

The administration of Dasatinib, another TKI that targets mutated Abl, Src, PDGFR and c-Kit (Table 1), induces AMPK activation, epidermal growth factor receptor (EGFR) degradation and ER stress downregulation that lead to apoptosis in sensitive Ca9-22 and HSC3 cell lines [20]. Combined treatment of Dasatinib with metformin has a synergistic effect by boosting AMPK activation, ER stress and EGFR downregulation in order to overcome resistance to Dasatinib in head and neck squamous cell carcinoma cells (HNSCC) [20]. The inhibition of protein translation induced by ER stress and AMPK-mTOR inhibition might be an important anti-tumor mechanism in Dasatinib and metformin [20]. Correlative evidence suggests that the upregulation of EGFR limits the effectiveness of TKIs in advanced non-small cell lung cancer cells (NSCLC) [21]. In fact, EGFR-TKIs acquired resistance limits therapy in advanced NSCLC. To overcome this resistance, a combined treatment based on EGFR targeted Gefinitib or Erlotinib (Table 1) and phosphoinositide-dependent protein kinase-1 (PDK-1) inhibitor OSU-03012 could reduce protein kinase B (Akt) and increased pro-apoptotic ER signaling through upregulation of CHOP, without concomitant induction of cytoprotective chaperones like BiP/Grp78 nor Grp94 [22]. As sustained treatment with Erlotinib promotes pro-survival autophagy signaling contributing to tumor cell resistance, the inhibition of the autophagic flux during Erlotinib therapy modulates ER response and contributes to cell death [23]. Ca^{2+} signaling might play a crucial role in the adaptive resistance to EGFR inhibitors. In this sense, Afatinib (Table 1), shows alterations in the proteome and phosphoproteome associated with increased Ca^{2+}-dependent adhesions and Ca^{2+}

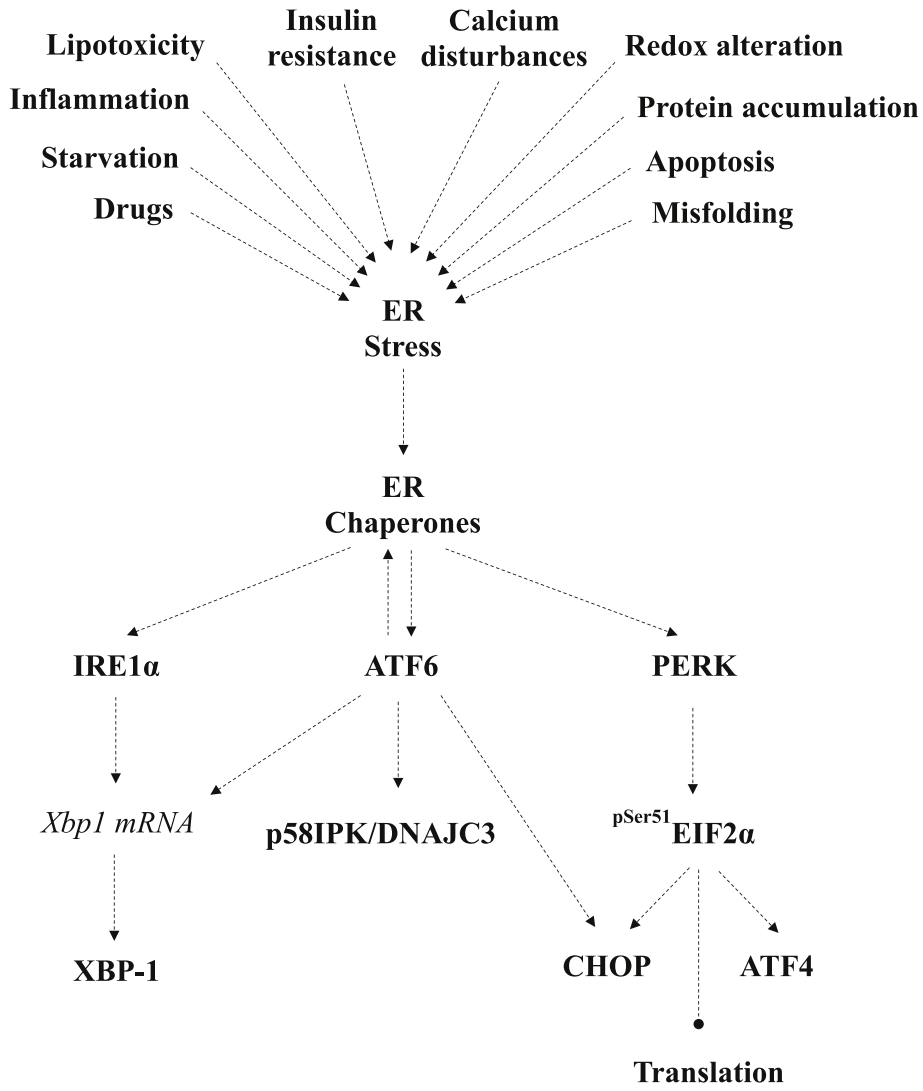

Fig. 1. Schematic representation of ER stress induction and downstream signaling events. Several factors might activate ER sensor chaperones inositol-requiring enzyme-1α (IRE1α), ATF6 and/or protein kinase RNA-like endoplasmic reticulum kinase (PERK), resulting in the inhibition of translation and induction of ER stress pathways. EIF2α: Eukaryotic initiation factor 2α, XBP-1: X-Box Binding Protein 1; CHOP: C/EBP homologous protein.

transporters in NSCLC PC9 cell line [24]. Ca^{+2} homeostasis could also be involved in resistant chronic myeloid leukemia (CML)-T1 cells to drugs that target Abl, PDGFR and c-Kit such as Imatinib (Table 1) [25].

3. Induction of mitochondrial dysfunction and ROS production by TKIs

ROS, mainly superoxide anion ($O_2^{\cdot-}$) and hydrogen peroxide (H_2O_2), are generated during normal mitochondrial function playing a relevant role in both physiological functions and tumor development [26]. Exacerbated ROS levels are widely associated with mitochondrial dysfunction, which can lead to damage of different cellular constituents like proteins, DNA and lipids. Unrepaired damage to mitochondrial DNA leads to defective complexes I or III which can result in increased electron uncoupling and translocation of electrons to oxygen leading $O_2^{\cdot-}$ generation [27].

The administration of TKIs has been reported to induce cytotoxicity in different cancer cell lines [28–30]. Mitochondrial damage is usually considered as a drug's "off-target" effect contributing to adverse reactions, and appears to be commonly shared by many drugs and toxins [31,32]. Ponatinib (Bcr-Abl), Sorafenib and Regorafenib (VEGFR, PDGFR, FGFR, c-Kit, RET, Raf, Tie2), but not Crizotinib (mesenchymal-epithelial transition factor receptor or c-Met, and anaplastic lymphoma kinase or ALK) and Pazopanib (VEGFR, PDGFR, FGFR and c-Kit), were able to induce relevant mitochondrial dysfunction, uncoupling components of electron transport chain and promoting ROS generation [28,29,33–35].

The mitochondrial dysfunction is also associated with the occurrence of several complications or side effects related to diarrhea, fatigue, hand-foot skin reaction and hypertension that have been related to effectiveness of the treatment in the case of patients in advanced stage of HCC [36]. In close connection with TKI-induced ROS generation and Ca^{2+} disturbances by TKI administration, generation of cardiotoxicity is a major health problem despite antitumor effectiveness [37,38]. Sorafenib induces mitochondrial dysfunction related to the impairment of complexes I, III and V in the electronic respiratory chain and mitochondrial membrane depolarization [28,35,39] (Fig. 2). The generation of ROS by Sorafenib has been observed in different studies [28,40]. In addition, the presence of oxidative stress and ERK down-regulation in peripheral blood mononuclear cells has been considered a good predictor of the evolution of patients with HCC treated with Sorafenib [41]. The induction of oxidative stress and depletion of antioxidant status by Sorafenib was related to Ca^{2+} disturbances that lead to its mitochondrial Ca^{2+} overload, which initiate lethal apoptotic

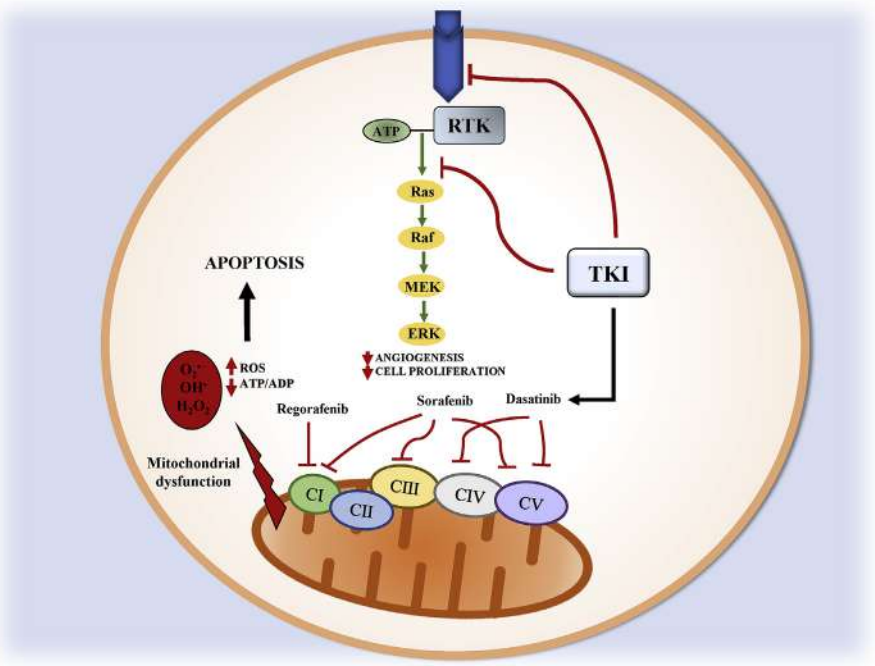

Fig. 2. Induction of mitochondrial dysfunction and reactive oxygen species (ROS) production by tyrosine kinase inhibitors (TKIs). TKIs act at the receptor tyrosine kinase (RTK), preventing Ras downstream events such as activation of mitogen-activated protein kinase (MAPK)/extracellular signal-regulated kinase (ERK) (MEK) and ERK phosphorylation that leads reduction of angiogenesis and tumor progression. TKIs might also induce mitochondrial dysfunction. Regorafenib impairs the activity of complex I of the respiratory chain. Dasatinib inhibits complexes IV and V. Sorafenib was demonstrated to behave as a mitochondrial uncoupler, and inhibits complexes I, III, V. The resulting ROS and products of the oxidative stress might be the cause and/or consequence of the mitochondrial dysfunction. Scheme extracted from elsewhere (190).

events [42]. Regorafenib also directly uncouples oxidative phosphorylation and promotes Ca^{2+} accumulation and swelling of mitochondria [34]. Moreover, Regorafenib produces impairment of the respiratory chain that affects the maximal capacity of complex I [28] (Fig. 2). In this context, Dasatinib inhibits complexes IV and V of the electron transport chain in H9c2 rat cardiomyoblasts [29] (Fig. 2). Interestingly, the antitumoral properties of the antiangiogenic Sunitinib are related to the reduction of kidney toxicity, recovery of GSH levels and lipid peroxidation reduction induced by cisplatin in subcutaneous implantation of Ehrlich ascites carcinoma cells in mice [43].

The antitumoral properties of Crizotinib, a TKI targeting ALK, ROS proto-oncogene 1 (ROS1) and c-Met [44], are related to cell death and ROS production in hepatocytes [45], cardiomyocytes [46], and alveolar rhabdomyosarcoma cells [47]. Gefitinib and Erlotinib, which target EGFR, have been also recently associated with the generation of oxidative stress [48]. The cytotoxicity of Erlotinib also involves NADPH oxidase (NOX) 4-induced oxidative stress in HNSCC cell lines [49]. The activity of Lapatinib, targeting a sub-class of EGFR 1 and/or 2 (ErbB1, ErbB2) [50], is also associated with ROS generation in inflammatory breast cancer models [51]. In concordance with the action of these TKIs, Imatinib that targets Abl, PDGFR and c-Kit [52], and is the recommended treatment for acute lymphocytic leukemia (ALL), chronic lymphocytic leukemia (CLL), CML and gastrointestinal stromal tumors (GIST), the induction of apoptosis is associated with ROS production and loss of the mitochondrial membrane potential [53].

4. Involvement of redox regulation in cancer

Oxidative stress, generated from ROS and antioxidant imbalance, is present in a large number of serious diseases including cancer [54]. A wide variety of stimuli derived from different signal molecules (growth factors, cytokines …) have been associated with H_2O_2 generation that can play a dual role, either in signaling or in oxidative stress, according to the local intracellular concentration attained [55]. During normal cell growth, levels of $O_2^{\cdot-}$ and H_2O_2 are kept under tight control by the intracellular redox regulatory mechanisms. In fact, several evidences support that the effect of intracellular ROS on oncogenesis is dependent on the ratio between intracellular $O_2^{\cdot-}$ and H_2O_2 in that a predominant increase in $O_2^{\cdot-}$ supports cell survival and promotes oncogenesis, and by contrast H_2O_2 prevents carcinogenesis by facilitating cell death signaling [56]. Alterations in redox regulatory mechanisms have been observed in different types of cancer together with the main prevalent genetic mutations related to telomerase, Wnt-β-catenin, PI3K/Akt/mTOR, p53 and MAPK signaling [57].

Despite the high production of ROS, cancer cells proliferate thanks to the induction of antioxidant defense systems through the activation of the nuclear transcription factor erythroid 2-related factor 2 (Nrf2) [58]. In these cells, the high rate of proliferation and apoptosis evasion may be achieved through the constitutive activation of redox-sensitive signal-transduction at the level of kinases such as MAPK family [59], phosphatidylinositol 3-kinase (PI3K)/Akt [60] and redox-sensitive transcription factors as NF-κB, Nrf2 and signal transducer and activator of transcription 3 (STAT3) [61], and inactivation of phosphatases as protein tyrosine phosphatase B1 (PTPB1) [62,63], protein phosphatase A2 (PPA2) [64] and phosphatidylinositol 3,4,5-trisphosphate 3-phosphatase and tensin homolog (PTEN) [65]. In this sense, and among other repercussions, the antitumoral activity of PPA2 [66] is reduced during oxidative and nitrosative stress when Tyr289 nitration within the B56ζ subunit of PP2A occurs, preventing the recruitment of its catalytic core, and consequently stabilizing the antiapoptotic properties of Bcl-2 [67].

A number of these signaling proteins that undergo redox changes are targets of redoxins, including thioredoxin 1 (Trx1) and glutaredoxin 1 (Grx1). In addition, it has been shown that peroxiredoxin 6 (Prdx6), Trx1 and thioredoxin reductase 1 (TrxR1) are often overexpressed in tumor cells and that high levels of Trx1 could be linked to drug resistance during cancer treatment [68,69]. As a matter of fact, it has been described that ROS production and NF-κB activation promote HCC progression [70] and that NF-κB DNA-binding activity is regulated by Trx1 [71,72].

STAT3 is an oncoprotein constitutively activated in several human cancers, what makes it a potential target for the development of cancer drugs [73]. STAT3 is activated by tyrosine phosphorylation which is influenced by its redox state. It has been described that STAT3 transcriptional activity can be modulated by S-glutathionylation [74] and it has also been found that its activity depends on its thiol redox state, which is influenced by H_2O_2 and peroxiredoxin 2 (Prdx2) levels and by the thioredoxin system activity [75]. The formation of Trx1-STAT3

disulfide exchange intermediates has been observed, suggesting that Trx1 may be a direct mediator of STAT3 disulfide reduction. Peroxiredoxin 6 (Prdx6) also promotes growth of lung tumors in mice through activation of Janus Kinase (JAK)2/STAT3 signaling [76].

Epithelial-mesenchymal transition (EMT) is an important de-differentiation process that occurs in normal development but also takes place in tumor cells and constitutes the first step towards metastasis during disease progression [77]. There are several proteins involved in EMT signaling pathways whose activity is ROS-dependent such as Smad, Snail, E-Cadherin, β-catenin and matrix metalloproteinases (MMP). It has also been described that transforming growth factor-β (TGFB) provokes an increase in the production of ROS, that results in the phosphorylation of Smad2, p38MAPK and ERK1/2 [78]. In addition, ROS may regulate EMT through a mechanism that involves NF-κB in close collaboration with hypoxia-inducible factor-1 (HIF-1) and cyclooxygenase-2 (COX-2) [79]. A critical molecular event of EMT is down-regulation of the cell adhesion molecule E-cadherin and its replacement by N-cadherin. It has been described by several authors that activation of Akt leads to a significant reduction in E-cadherin expression and nuclear localization of Snail, suggesting a role for the PI3K/Akt signaling pathway in the transient shift from E-cadherin to N-cadherin, and EMT progression in cancer [80]. The hyperactivation of PI3K/Akt signaling mediated by ROS and its relationship with tumor cell survival, apoptosis inhibition and resistance to chemotherapy has been described [81].

4.1. The role of redox in the resistance to TKIs

Given the role of redox status in tumorigenesis, we addressed how several studies have demonstrated a direct or indirect involvement of ROS in TKI-acquired resistance, usually through redox activation of the PI3K-Akt signaling pathways [1]. Akt is thought to be responsible for mediating the acquired resistance to Sorafenib via mTOR, but independent of PP2A, in HCC cells [82]. The overexpression of apurinic/apyrimidinic endonuclease 1 (APE1), a multifunctional enzyme that is involved in DNA repair and the redox regulation of transcription factors, significantly contributed to Gefitinib and Erlotinib resistance and Akt activation through a redox-dependent mechanism [83]. In addition, the combined treatment of Sorafenib and tetrandrine drastically increased apoptosis through ROS/Akt signaling in HCC cells [84].

The high basal levels of ROS found in TKI-resistant cancer cells are mainly due to elevated NOX expression [85] although mitochondrial ROS production cannot be discarded (Fig. 3). CML and glioblastoma cancer cell resistance to Imatinib and Dasatinib might be associated to overexpression of components of the NOX2/Egr-1/Fyn signaling axis, which prompts the search for inhibitors of p47phox, the organizer subunit of NOX2, to treat TKI-resistant cancers [85]. In Erlotinib-resistant NSCLC cells, effective cell death induction is achieved by combined treatment with Erlotinib and ampelopsin, concomitant with ROS accumulation through upregulation of NOX2 expression [86]. Recently, it has been found that TKI-resistant lung cancer cells exhibit poly (ADP-ribose) polymerase 1 (PARP-1) dependence for survival through restriction of NOX-mediated cytotoxic ROS production [87].

The combined treatment of Gefitinib- and Erlotinib-resistant k-Ras mutated NSCLC cells with Vorinostat has anti-proliferative and pro-apoptotic effects as well as increased ROS accumulation, Nrf2 down-regulation and Keap1 upregulation [88]. Dysfunctional mutations in Keap1 gene provoke constitutive activation of Nrf2 leading to TKI resistance in NSCLC cells [89]. From these studies, Nrf2, a transcriptional factor playing a pivotal role in cellular antioxidant defense, emerges as a candidate target for anticancer therapy (Fig. 3).

4.2. The effectiveness of combined treatment with TKI and redoxin inhibitors

Reversible redox modification of key Cys residues constitutes a regulatory mechanism of protein function [90]. H_2O_2 acting as a second messenger modulates signaling cascades by reversible oxidation of redox sensitive cysteine residues in receptors and transduction proteins, including those using tyrosine phosphorylation signals like EGFR, MAPKs, PTEN, PI3K/Akt and STAT3 [91,92]. In particular, oxidation of Cys797 at the tyrosine kinase active site of EGFR enhances its activity [93] and coincidentally, mutation of C797S in EGFR has been described as a novel mechanism of acquired resistance to third-generation TKIs [94]. Peroxiredoxins may catalyze the oxidative modification of these cysteines while Trx and Grx are responsible for their reduction, as

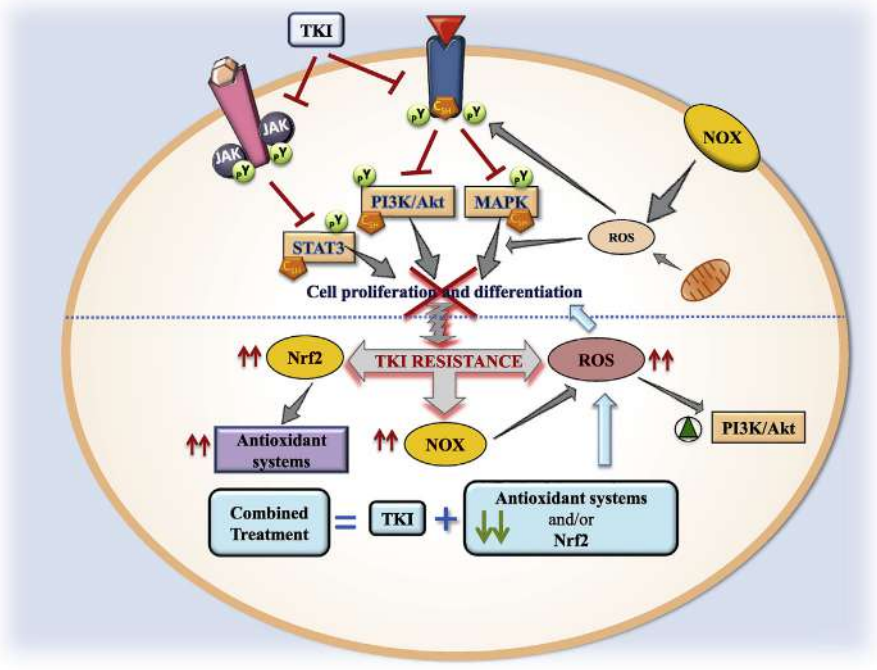

Fig. 3. Redox regulation by tyrosine kinase inhibitors (TKIs). Two receptor tyrosine kinase (RTK) are drawn inserted in the cell membrane with their respective bound ligands. The phosphorylated Tyr (pY) sites are also shown in RTK including redox sensitive intermediates (C_{SH}, redox sensitive Cys in reduced state). The pathways inhibited by TKI are indicated with a red crossed line. Reactive oxygen species (ROS) generation by NADPH oxidase (NOX) and mitochondria impacts on redox sensitive sites in different targets showed with straight grey arrows. Transition from TKI-induced inhibition of cell proliferation and differentiation to resistance to TKI is indicated by a curly grey arrow and doted blue line. Events that accompany TKI resistance are displayed with vertical fine red arrows showing increased levels of nuclear transcription factor erythroid 2-related factor 2 (Nrf2)-dependent rise of antioxidant status, NOX and ROS, and activation of phosphatidylinositol 3-kinase (PI3K)/protein Kinase B (Akt) (green triangle inside a green circle). Grey arrows indicate an action. The lower part of the illustration reflects the contention that a combination of TKI treatment and down-regulation of antioxidant systems could counteract the development of TKI resistance in cancer cells (blue arrows). Janus kinase, JAK. (For interpretation of the references to color in this figure legend, the reader is referred to the Web version of this article.)

mentioned above. Hence, a role for redoxins in regulating cell signaling is to be expected.

Combination of TKI with down-regulation or inhibition of Grx/GSH or Trx/TrxR systems has been explored to treat TKI resistance. In a study carried out in Gefitinib-resistant NSCLC cells, Grx1 was upregulated and its inhibition enhanced the effects of Gefitinib on apoptosis an cell cycle arrest via the EGFR/Forkhead Box M1 (FoxM1) signaling pathway [95]. Trx1 has been shown to be overexpressed in a wide variety of cancers and its expression is associated with aggressive tumor growth, resistance to standard therapy and therefore decreased patient survival [96]. Recently, treatment with TKI has been combined with Trx1 inhibitors or downregulation of its levels to increase the effectiveness in TKI-resistant cancer cells [97]. In this study [97], the resistance of breast cancer cells to Trastuzumab, an antibody against Her2, appears to be related to the high levels of reduced Trx1 affecting the activity of the PTEN inhibitor. The combined treatment of Trastuzumab and a Trx1-inhibitor reduced cell viability, Akt phosphorylation and Bcl2 levels, as well as increased the levels of ROS, phosphorylated JNK, G1 arrest and apoptosis [97]. The downregulation of Trx1 could be a promising approach to improve the response to chemotherapy in HCC [98]. Our group has studied the role of Trx1 system in the sensitivity of three HCC cell lines (HepG2, SNU423 and SNU475) with different degrees of EMT to Sorafenib treatment. Basal Trx1/TrxR1 levels are markedly higher in poorly-differentiated SNU475 cells [99]. In these cells, Sorafenib treatment combined with Trx1 down-regulation using siRNA strategies dramatically induces inactivation of TGFβ and activation of tumor-suppressor Salvador-Warts-Hippo (SWH) signaling, as well as thiol oxidative changes in STAT3 [99]. In another study, the combination of Sorafenib with metformin decreases tumor invasiveness and cell motility associated with Trx1 downregulation [100]. Therefore, combination of Sorafenib with Trx1 inhibitors should be a good approach in the design of anticancer therapies. The panorama is not clear so far regarding the mechanisms of TKI resistance with the involvement of a varied panoply of signaling elements in different types of cancers. However, redox imbalance appears as a recurrent phenomenon in the majority, if not all cases studied so far. Consequently, combined therapy with TKI and other treatments aimed at either weakening the antioxidant defenses or stimulating ROS producing mechanisms can be envisaged as a promising therapeutic approach (Fig. 3).

5. Regulation of AMPK and mTOR during treatment with TKIs

The PI3K/Akt/mTOR pathway is one of the key pathways altered in cancer cells regulating relevant processes such as protein synthesis, cell growth, cell survival and, motility, as well as autophagy or angiogenesis. Several genes, such as PIK3K gene, are either overexpressed by amplification or activated by somatic point mutations in cancer [101]. The oncosuppressor PTEN is also frequently mutated [102] that leads to downstream Akt activation which, in turn, is often found to be somatically overexpressed and mutated [103]. The hyperactivation of PI3K/Akt/mTOR signaling is usually associated with resistance to different targeted-mediated therapies [104]. In this sense, mTOR can be regulated by different routes, being of special interest its inhibition by the AMPK, an energy sensor that regulates cellular metabolism while maintaining homeostasis, and which is involved in autophagy activation [105]. AMPK is activated in situations involving a rise of the AMP/ATP ratio, that might occur in stress induced by glucose deprivation, hypoxia, tissue ischemia, or during exercise. Thus, AMPK exerts stimulatory effects on glucose uptake, glycolysis, and fatty acid oxidation, while inhibits ATP-consuming cellular events, such as protein synthesis or fatty acid synthesis [106]. Liver kinase B1 (LKB1) is the upstream kinase activating AMPK by phosphorylating its Thr172 site, whereas calcium/calmodulin-dependent protein kinase kinase 2 (CAMKK2) activates AMPK in response to calcium increase [107]. Although AMPK has been shown to promote ^{Ser15}p53 phosphorylation inducing cell cycle arrest, AMPKβ1 subunit is also upregulated by two downstream targets of p53 sestrin 1 and sestrin 2 [108]. The antitumoral properties of AMPK activation and mTOR inhibition have been related to antiproliferative and proapoptotic properties in leukemia [109]. Moreover, anti-apoptotic effects of AMPK have also been observed in other malignancies [110].

Autophagy is a highly conserved catabolic process that functions as a quality control system, facilitating the degradation of organelles and other damaged intracellular components in situations of metabolic stress. mTOR complex 1 works as a negative regulator of autophagy, exerting its inhibitory action by phosphorylating and inactivating Unc51-like kinases (ULK1/2) and Atg13 [111]. AMPK activation can

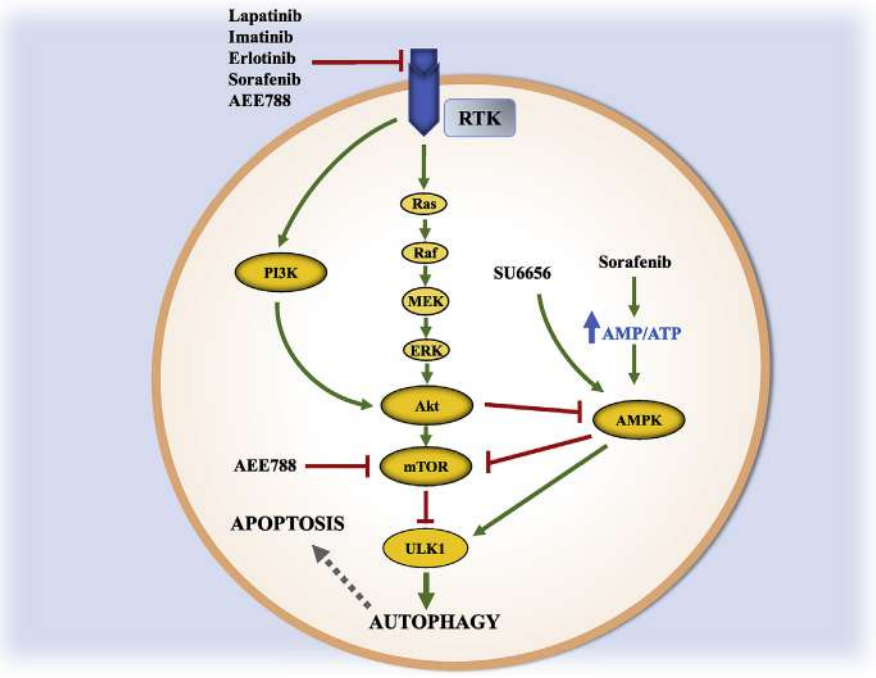

Fig. 4. Regulation of AMP-activated protein kinase (AMPK) and mammalian target of rapamycin (mTOR) during the treatment with tyrosine kinase inhibitors (TKIs). Regulation of cell proliferation, differentiation, angiogenesis and tumorigenesis signaling pathways by TKIs are closely related to the regulation of AMPK and mTOR. The binding of a mitogen to a receptor tyrosine kinase (RTK) stimulates the Ras/Raf/mitogen-activated protein kinase (MAPK)/extracellular signal-regulated kinases (ERK) (MEK) and phosphatidylinositol 3-kinase (PI3K)/protein kinase B (Akt) signaling that target mTOR pathways. Among other downstream events, mTOR phosphorylates Unc51-like kinase (ULK) and inhibits autophagy. Akt negatively regulates AMPK, a protein involved in mTOR inhibition and ULK phosphorylation that promotes autophagy. Different TKIs are able to activate (green line) or inhibit (red line) specific pathways involved in downregulation of survival pathways. The activation of AMPK and inhibition of mTOR by TKIs induce autophagy and/or apoptosis that leads to the blockage of tumorigenesis and cell proliferation processes. (For interpretation of the references to color in this figure legend, the reader is referred to the Web version of this article.)

subsequently trigger tuberous sclerosis complex (TSC)2 to repress mTOR complex 1 and, therefore, upregulates autophagy [112]. AMPK could also directly phosphorylate multiple sites in ULK1 that promotes autophagy [113] (Fig. 4).

Controversial reports exist on the antitumoral properties of autophagy during TKI treatments. It has been suggested that normalization of autophagy may be relevant to avoid cellular resistance to cancer drugs [114]. However, the baseline apoptotic priming is a key determinant of the reliable cell killing during TKI treatment [115]. It appears that response to targeted therapies can be predicted with the dynamic BH3 profiling technique to measure early changes in net pro-apoptotic signaling at the mitochondrion ('priming') [116]. Autophagy has been considered to be the mechanism regulating the proximity of tumor cells to apoptotic cliff during drug administration. In this sense, the inhibition of autophagy by drugs, that downregulates the expression of pro-apoptotic transcription regulators such as Foxo3a, reduces the threshold to the initiation of apoptosis [117].

Sorafenib and Regorafenib have been extensively demonstrated to induce autophagy [118]. We have recently observed that the early Sorafenib-induced ER stress and transitory upregulation of JNK and AMPK-dependent signaling are associated with the inhibition of mTOR and activation of autophagy [14]. The activation of AMPK by Sorafenib is related to inhibition of mitochondrial metabolism, and increase of AMP/ADP and ADP/ATP ratios [119]. The inhibition of PERK, IRE1α and ATF6 branches of ER stress reduces autophagy, which played a survival role in Sorafenib-treated HepG2 cells [14].

Imatinib induces AMPK activation and suppression of S6 kinase 1 (S6K1) and mTOR, that appears to be related to sensitization of CML cells [120]. However, it is known that activation of AMPK has antileukemic effects, since even being an autophagy activator, it can lead to cell death when ATP concentrations are sufficiently low [121]. Lapatinib inhibits Akt/mTOR signaling and activates AMPK, being both aspects related to anticancer effects in breast cancer cells [122]. SU6656, a Src kinase inhibitor, activates AMPK pathway by enhancing its phosphorylation by LKB1 independently of cellular energy state [119]. The inhibition of mTOR by AMPK activation induced by different TKI, such as Erlotinib, Imatinib, Lapatinib, Sorafenib, and other preclinical drugs such as SU6656 (Src) or AEE788 (VEGFR and ErbB2) is relevant for the antitumoral properties of the drugs. The antitumoral impact of mTOR inhibition in autophagy process is related to the cell type and drug target. All in all, targeting autophagy has also become an important drug discovery approach to increase cancer chemosensitivity (Fig. 4).

6. Regulation of PGC-1α during TKI

The peroxisome proliferator-activated receptor gamma coactivator 1 alpha (PGC-1α) regulates the activity of transcription factors and nuclear receptors that targets genes involved in mitochondrial biogenesis, oxidative metabolism, thermogenesis, anabolic pathways, glucose and lipid metabolisms, muscle fiber regeneration and antioxidant status [123–126]. The expression of PGC-1α is upregulated by p53 and the oncogenic melanocyte lineage-specification transcription factor (MITF), and downregulated by c-Myc and HIF-1 [127]. The activity of PGC-1α can be regulated by phosphorylation through AMPK, protein kinase A (PKA), Akt, and p38 MAPK, which modulates its transcription regulatory properties [128]. AMPK enhances mitochondrial biogenesis inducing PGC-1α transcription, and its phosphorylation ^{Thr177,Ser538}PGC-1α which promotes its co-transcriptional activity [129]. p38 MAPK activates PGC-1α by phosphorylation at Thr262, Ser265 and Thr298, increasing its half-life in cytoplasm [130]. By contrast, Akt inhibits PGC-1α activity through inducing its phosphorylation at ^{Ser570}PGC-1α [131]. In conditions of low cellular energy status, NAD-dependent deacetylase sirtuin-1 (SIRT1) deacetylates and activates PGC-1α. However, when the energy cellular status is high, histone acetylase GCN5 induces PGC-1α acetylation, that inhibits its activity [126]. In the context of HCC, the overexpression of SIRT1 was correlated with microvascular invasion, metastasis and predicted poor outcomes [132].

Opposite reports have been published assessing the expression of PGC-1α expression in tumors [133–136]. Although mitochondrial dysfunction is generally associated with the activation of glycolysis, many cancer cells possess intact mitochondrial respiration being some cancers subtypes dependent on mitochondrial respiration [127]. Mitochondrial biogenesis and metabolic reprogramming influence the phenotype of cancer cells and resistance to targeted therapy [137]. Interestingly, Hirpara et al. [138] showed that resistance to Gefitinib is associated with the upregulation of PGC1α and TFAM expression, and increased formation of supercomplexes I and II, oxygen consumption rate and mitochondrial mass in NSCLC cell line. Vemurafenib, an inhibitor of mutated serine/threonine kinase B-Raf, increases the MITF/PGC-1α signaling axis resulting in metabolic reprogramming towards oxidative phosphorylation and conferring cellular intrinsic resistance in melanoma cells [139]. Both studies identify OPB-51602 [138] and Gamitrinib [139] as targets of mitochondrial components to circumvent cellular resistance to TKI. The transient overexpression of SIRT1, as well as NAD repletion, decreases Sorafenib-induced apoptosis suggesting that SIRT1 could be an underlying mechanism of resistance to Sorafenib treatment in HCC [39].

7. Role of cell metabolism in cancer

The process of tumorigenesis and cancer progression involves alteration of cellular metabolism. During the last decades, numerous works have reported how metabolic reprogramming supports the anabolic requirements for cancer cell proliferation in terms of energetic demand for cell proliferation, increased macromolecules biosynthesis, new biomass building and tumor progression. Both genetic and microenvironmental factors are involved in the deregulation of tumor cells metabolism, which in turn are able to modulate the microenvironment inside the tumor driving cancer evolution, invasiveness or metastatic potential [140–142].

One of the hallmarks of cancer is the deregulation of cellular energetics towards aerobic glycolysis to generate ATP and metabolic intermediates even in presence of normal oxygen concentration, known as "Warburg effect" [143]. This effect is supported by tightly regulated molecular pathways including MAPK, PI3K, HIF-1, p53, c-Myc or AMPK pathways. Despite this shift from oxidative phosphorylation to glycolys for ATP production, mitochondria are required for tumor development and their regulation is a promising field for combined anticancer therapies. The activation of RTK/NRTK regulates PI3K-Akt-TSC1/2-Ras homolog enriched in brain (RHEB)-mTOR pathway in order to maintain a cellular balance between anabolism and catabolism. mTOR complex 1 regulates protein and nucleotide synthesis, lipogenesis and glycolysis. The stimulation of protein synthesis involves an increase of ribosome biogenesis and mRNA translation [144]. mTOR increases nucleotide synthesis by increasing ATF4-dependent expression of mitochondrial bifunctional enzyme methylenetetrahydrofolate dehydrogenase/cyclohydrolase, the key enzyme in mitochondrial tetrahydrofolate cycle, increasing the production of purine nucleotides [145]. mTOR augments lipogenesis in Sterol regulatory element-binding transcription factor 1 (SREBP1)-dependent pathway either through S6K1 phosphorylation [146] or by controlling the nuclear entry of lipin 1, a phosphatidic acid phosphatase, involved on SREBP1 gene regulation [147]. mTOR signaling also stimulates the expression of genes involved in nearly every step of glycolysis and pentose phosphate pathway (PPP) [146]. Several key enzymes of glucose metabolism, such as enolase 2 (ENO2), hexokinase II (HKII), lactate dehydrogenase (LDH) A, 6-phosphofructo-1-kinase (PFK1), and glucose transporter I (GLUT1) are described to be regulated by c-Myc [148], however, they are not upregulated in TSC-deficient cells [146].

7.1. Impact of TKIs in cancer metabolic pathways

TKIs can deregulate glycolysis in malignant tissue through its impact on EGFR, VEGFR, c-Met, Bcr-Abl, HER2 or ALK signaling in many different cancer types [149]. The inhibition of PDGFR, c-Kit and Bcr-Abl by Imatinib leads pyruvate entering into the tricarboxylic acid (TCA) cycle providing these cells with an alternative mechanism of glucose metabolism to compensate for the inhibition of glycolysis [150], and reduced GLUT1 in leukemic cell [151]. Thus, Imatinib induces a shift in the glucose metabolism between anaerobic glycolysis to aerobic mitochondrial TCA cycle depending on dosage (Fig. 5). In this sense, combined adjuvant therapies based on targeting mitochondrial metabolism are relevant to prevent treatment-acquired resistance [138,139].

Different studies using Erlotinib and Gefitinib, which specifically target EGFR, have shown that these drugs reduce extracellular acidification rate, lactate production and glucose consumption in lung adenocarcinoma cell lines [152]. These effects might be the consequence of c-Myc downregulation during EGFR inhibition [153]. Moreover, metabolomic analysis of TKI-treated cells shows a reduced presence of intermediate metabolites related to glucose metabolism [153].

The overexpression of EGFR and HER2 is associated with aggressive phenotypes and tumor progression in breast cancer. Lapatinib exerts a dual inhibition of EGFR and HER2, although its effects on HER2 appears to be more critical [154]. Among other interactions, Lapatinib blocks HER2 signaling inhibiting the phosphorylation of 6-phosphofructo-2-kinase/fructose-2,6-biphosphatase 2 (PFKFB2) in different cancer cell lines, decreasing the amount of intermediate metabolites in PPP and blocking the glucose-dependent EGFR/HER2 signaling [155]. Consequently, current studies are trying to determine how HER2 expression could be considered as a predictive biomarker of clinical prognosis.

The inhibition of c-Met reduces intracellular NADPH content which plays an essential role during lipid and nucleic acid biosynthesis, as well as by enzymatic systems regulating oxidative system [149]. In addition, c-Met inhibition modulates glucose metabolism preventing the expression of different mitochondrial proteins [156]. The increased tumor growth activity of Cabozantinib, that targets VEGFR, c-Met, Tie2, Axl, RET, c-Kit and Flt3 (Table 1), compared to Regorafenib is related to decreased glycolysis in a colon and rectum carcinoma (CRC) xenograft mouse model [157]. Cabozantinib significantly reduces glucose uptake and PI3K/mTOR-dependent signaling pathway in CRC098 and CRC162 cells [157]. Crizotinib, which targets c-Met and ALK, reduces the expression of phosphorylated pyruvate kinase isoenzyme type M2 (PKM2), lactate release, phosphorylated LDH and glucose uptake in lymphoma cells [158].

The administration of Sorafenib induces a glycolytic cell reprogramming that may represent a cellular resistance strategy potentially targetable by combination therapies. Sorafenib induces the expression of glucose transport 3 (GLUT3), ENO2, and PFK1 that are related to increased uptake of glucose and lactate production as a response to mitochondrial dysfunction [159] (Fig. 5). In addition, Sorafenib downregulates the expression of the mitochondrial enzyme pyruvate dehydrogenase E1 alpha 1 (PDHA1) [159].

The resistance to Axitinib treatment, which targets VEGFR, PDGFR and c-Kit, has been related to upregulation of cell surface exposure of GLUT1 and extracellular acidification rate, both reflecting an increased glycolytic rate [160]. Dovitinib, targeting VEGFR, FGFR, PDGFR, c-Kit, Flt3 and colony-stimulating factor receptor 1 (CSF-1R), is able to hinder glucose metabolism with combined downregulation of Akt-mTOR pathway [161]. Imatinib shifts glycolysis to mitochondrial glucose metabolism inducing a reduction of glucose uptake and an increment of cell energetic state [162]. The inhibition of EGFR- and/or c-Met-related pathways by Capmatinib, Gefitinib and Erlotinib reverts aerobic

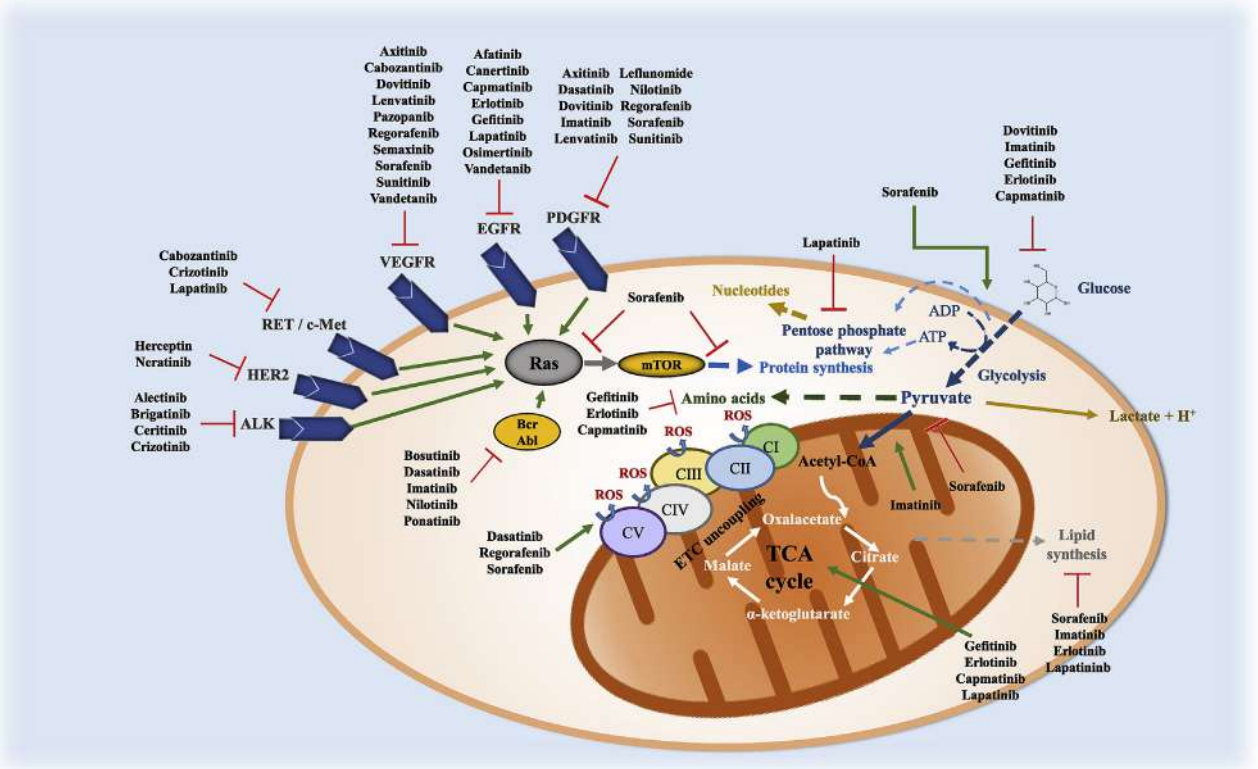

Fig. 5. Metabolic impact of tyrosine kinase inhibitor (TKI) administration. The inhibition of different receptor tyrosine kinase (RTK) alters all cancer hallmarks. Dovitinib, Imatinib, Gefitinib, Erlotinib and Capmatinib reduce glycolytic pathway, while Sorafenib promoted mitochondrial dysfunction. Lipid synthesis and protein synthesis were profoundly altered by TKIs. ETC; Electron transport chain.

glycolysis and reactivates mitochondrial oxidative phosphorylation in NSCLC through the concerted downregulation of HKII and phosphorylated PKM2, and upregulation of mitochondrial-dependent oxidative phosphorylation [163].

The contribution of reprogramming amino acids metabolism in malignant tissues is relevant for its requirement for protein synthesis. The impact of Sorafenib in mTOR and protein synthesis has also been already described [14]. Erlotinib, Gefitinb and Capmatinib have also been reported as negative regulators of amino acid levels [149]. Altered levels of lipids are widely related to carcinogenesis and cancer metastasis [164]. In fact, the levels of total cholesterol, triglycerides, HDL and LDL in plasma from breast cancer patients are significantly higher than those of control group [165]. Treatment of Bcr-Abl-positive cells with Imatinib decreases phosphocholine concentrations [162]. Erlotinib reduces the expression of fatty acid genes in MDA-MB-231 and Hs578T cells, while Capmatinib sensitizes MDA-MB-468 cells to knockdown of arachidonic and linoleic acid metabolism rate limiting enzymes [166]. The different response to TKI in sensitive or resistant cells is evidence that metabolic reprogramming is relevant to revert malignancy, and combined TKI-based strategies can be a very promising clinical tool for more effective targeted therapies to treat previously characterized subgroups of patients.

8. Induction of cell death by TKIs in cancer cells

The resistance to apoptosis is one of the main characteristics of tumor cells, characterized by their unlimited replicative potential, insensitivity to cellular stress, sustained angiogenesis, invasiveness and metastatic potential [167]. Apoptosis is a form of genetically programmed death process that can be mediated by ligand-dependent receptor activation (Type I) or mitochondrial outer membrane permeabilization (Type II), which could lead to an uncontrolled cell death process under limiting energy conditions termed necrosis, which involves cell swelling and sudden membrane rupture.

Sorafenib can induce apoptosis of cancer cells through regulation of multiple proapoptotic and antiapoptotic factors, including Bad, Bax, Bim, myeloid cell leukemia-1 (Mcl-1), and X-linked inhibitor of apoptosis protein (XIAP) [168]. The expression of these factors may be regulated at either transcriptional, translational, or posttranslational levels, and may involve mechanisms independent on ERK activity. The inhibition of Mcl-1 expression, which accounts for Sorafenib-induced apoptosis in multiple cancer types, has been found independent on Raf/MEK/ERK inhibition [169]. Recently, the proapoptotic factor Bim has been identified as an important factor in Sorafenib-induced apoptosis [14,170]. In fact, the progressive increase of ER stress and PERK-dependent CHOP expression, and reduction of ^{Thr308}Akt/Akt and ^{Ser473}Akt/Akt ratios are associated with the reduction of autophagic flux and an additional upregulation of BimEL expression and caspase-3 activity [14]. Small interfering-RNA (si-RNA) assays show that Bim, but not Bak and Bax, is involved in the induction of caspase-3 in Sorafenib-treated HepG2 cells [14]. The increase in Bad and decrease in Mcl-1 expression have also been shown to account for Sorafenib-induced apoptosis [171]. Bim exerts its proapoptotic activity through binding to several antiapoptotic Bcl-2 family members [172]. The mechanisms accounting for downregulation of Mcl-1 expression by Sorafenib may be cell type specific, and involve both ERK-dependent and ERK-independent mechanisms [173,174]. Sorafenib can also inhibit phosphorylation of eIF4B, which may lead to decreased translation of antiapoptotic factors such and Mcl-1 and cFLIP, and could also inhibit the nuclear translocation of the apoptosis-inducing factor (AIF) [175,176]. Beclin-1 contains a BH3 domain which binds to multiple antiapoptotic proteins belonging to the Bcl-2 family, such as Bcl-2, Bcl-xL, or Mcl-1 [177]. This interaction represses Beclin-1 activity and significantly reduces initiation of autophagy. When the BH3 domain is phosphorylated, there is a decrease in the binding affinity between these two proteins, resulting in Beclin-1 release and its subsequent activation [178]. Another significant signaling pathway related to reduced apoptotic cell death involves HIF-1α. HIF-1α levels are higher in Sorafenib-resistant HCC tissue samples than observed in Sorafenib-sensitive ones since, through HIF-1α resistant cells upregulate genes implicated in cell proliferation, angiogenesis, migration and autophagy [179]. Sorafenib reduces the expression of HIF-1α targets BCL2 Interacting Protein 3 (BNIP3) and BNIP3-like (NIX) that delay mitophagy, as revealed by their mitochondria and lysosomes colocalization and the autophagosome markers p62 and LC3-II [180].

The induction of apoptosis by Lenvatinib has also been related to reduction of tumor growth in a glioma-derived tumor bearing mice [181]. Lenvatinib significantly reduces Akt and ERK1/2

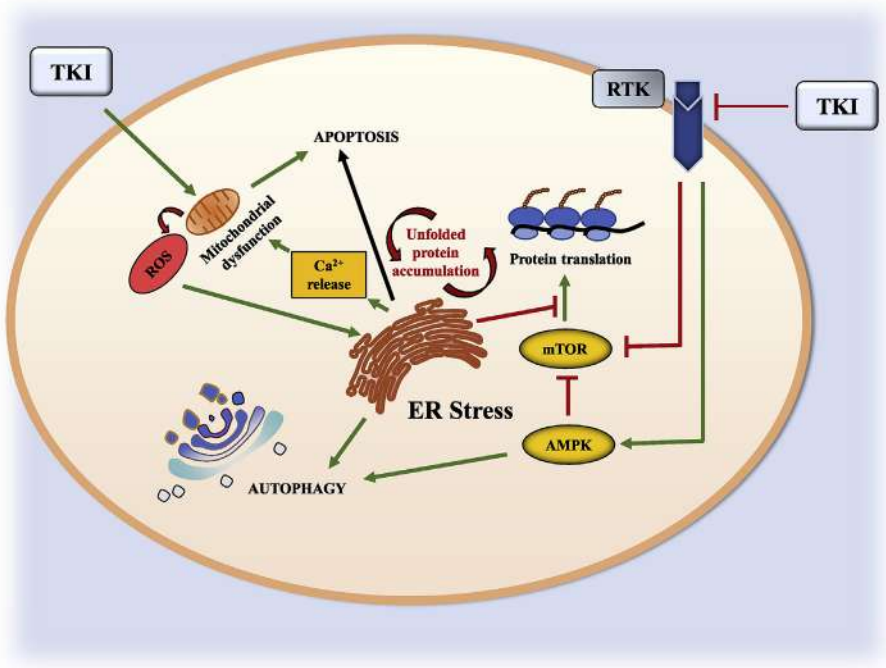

Fig. 6. Graphical Abstract. Tyrosine kinase inhibitor (TKI) induced endoplasmic reticulum (ER) stress promoting unfolded protein response (UPR), Ca^{2+} release, translation blockage, autophagy and apoptosis. Furthermore, other mechanisms of TKIs involve mitochondrial dysfunction, generation of reactive oxygen species (ROS), AMP-activated protein kinase (AMPK) activation and mammalian target of rapamycin (mTOR) inhibition. These cellular pathways are interconnected and result in the induction of autophagy and apoptosis.

phosphorylation, cyclin D1 expression and cell proliferation, as well as increases the percentage of apoptotic cells in cultured anaplastic thyroid cancer cells [181]. The induction of ER stress has also been associated with the induction of apoptosis, reduced cell migration and invasiveness in Lenvatinib-treated nasopharyngeal carcinoma cells [17].

The reduction of phospho-ERK and phospho-JNK by Regorafenib have been associated with decreased cell proliferation and induction of apoptosis in cultured liver cancer cells [182]. The induction of apoptosis by Sorafenib [183] and Regorafenib [184] is related to the activation of Src homology region 2 domain-containing phosphatase-1 (SHP-1) and inhibition of STAT3 phosphorylation. Analysis of Bcl-2 family members reveals dose- and time-dependent depletion of anti-apoptotic Mcl-1 in Regorafenib-treated HCT116 cells. A delayed and/or attenuated Mcl-1 degradation is observed in resistant Regorafenib-treated CRC [185]. Cabozantinib reduces cell proliferation and promotes apoptosis *in vitro* and *in vivo* in breast, lung, and glioma tumor cells [186]. Cabozantinib blocks hepatocyte growth factor (HGF)-stimulated c-Met pathway, and inhibits cell migration and invasiveness in cultured liver cancer cells, as well as reduces tumor growth and angiogenesis, and promotes apoptosis in xenograft-mouse model [187]. The reduced phosphorylation of c-Met RET and AXL is related to downregulation of PI3K/mTOR-dependent signaling pathway and increased ATG3, LC3 and Beclin-1 expression upon Cabozantinib treatment in CRC patient-derived tumor xenograft models [157].

9. Concluding remarks

Downregulation of RTK and NRTK by TKIs administration drastically alters cancer hallmarks involving cell survival/death, cellular stress, and metabolism. The alteration of TK-related signaling by TKIs involves the activation of ER stress and UPR that affect the expression of key proteins involved in mitochondrial function, PI3K/TSC/mTOR and AMPK that impact cell metabolism and death (Fig. 6). The balance between $O_2^{\cdot-}$ and H_2O_2 is tightly controlled, and proteins regulating redox status that change the activation/deactivation state of proteins involved in cellular signaling are altered during TKI treatment. The shift between pro- and antitumoral role of autophagy and mitochondria-related events can be involved in the resistance of cancer cells to treatments. In addition, the proximity of tumor cells to the apoptotic cliff promoted by TKI treatment can also limit the induction of cell death in cancer cells. In conclusion, the specific genetic pattern of cancer cells and the prevailing molecular signaling status upon drug pressure that drive resistance to cancer-related hallmarks, support the use of combined TKI treatments.

Acknowledgments

This study was funded by Institute of Health Carlos III (ISCiii) (PI16/00090, PI19/00838 and PI19/01266), Spanish Ministry of Economy and Competitiveness (BFU2016-80006-P), Andalusian Ministry of Economy, Innovation, Science and Employment (BIO-216 and CTS-6264), Andalusian Ministry of Equality, Health and Social Policies (PI-0198-2016) and Valencian Ministry of Education, Culture and Sports (PROMETEO/2019/027). P de la C-O was supported by FPU predoctoral fellowship (FPU17/00026) from Spanish Ministry of Education, Culture and Sports. E N-V was supported by the the predoctoral i-PFIS IIS-enterprise contract in science and technologies in health (IFI18/00014) from ISCiii. We thank the Biomedical Research Network Center for Cardiovascular Diseases (CIBERcv), and the Biomedical Research Network Center for Liver and Digestive Diseases (CIBERehd) founded by the ISCiii and co-financed by European Regional Development Fund (ERDF) "A way to achieve Europe" for their financial support.

References

[1] Q. Jiao, L. Bi, Y. Ren, S. Song, Q. Wang, Y.S. Wang, Advances in studies of tyrosine kinase inhibitors and their acquired resistance, Mol. Canc. 17 (2018) 36.
[2] M.A. Lemmon, J. Schlessinger, Cell signaling by receptor tyrosine kinases, Cell 141 (2010) 1117–1134.
[3] D. Woods, J.J. Turchi, Chemotherapy induced DNA damage response: convergence of drugs and pathways, Canc. Biol. Ther. 14 (2013) 379–389.
[4] M.E. Lomax, L.K. Folkes, P. O'Neill, Biological consequences of radiation-induced DNA damage: relevance to radiotherapy, Clin. Oncol. 25 (2013) 578–585.
[5] K.S. Bhullar, N.O. Lagaron, E.M. McGowan, I. Parmar, A. Jha, B.P. Hubbard, H.P.V. Rupasinghe, Kinase-targeted cancer therapies: progress, challenges and future directions, Mol. Canc. 17 (2018) 48.
[6] D.J. Lenihan, P.R. Kowey, Overview and management of cardiac adverse events associated with tyrosine kinase inhibitors, Oncologist 18 (2013) 900–908.
[7] Y. Togashi, H. Hayashi, K. Okamoto, S. Fumita, M. Terashima, M.A. de Velasco, K. Sakai, et al., Chronic nicotine exposure mediates resistance to EGFR-TKI in EGFR-mutated lung cancer via an EGFR signal, Lung Canc. 88 (2015) 16–23.
[8] M. Hojjat-Farsangi, Small-molecule inhibitors of the receptor tyrosine kinases: promising tools for targeted cancer therapies, Int. J. Mol. Sci. 15 (2014) 13768–13801.
[9] J.T. Hartmann, M. Haap, H.G. Kopp, H.P. Lipp, Tyrosine kinase inhibitors - a review on pharmacology, metabolism and side effects, Curr. Drug Metabol. 10 (2009) 470–481.
[10] T.A. Rapoport, B. Jungnickel, U. Kutay, Protein transport across the eukaryotic endoplasmic reticulum and bacterial inner membranes, Annu. Rev. Biochem. 65 (1996) 271–303.
[11] R.Y. Hampton, ER stress response: getting the UPR hand on misfolded proteins, Curr. Biol. 10 (2000) R518–R521.
[12] M. Liu, R. Zhou, X. Wu, X. Xu, M. Su, B. Yang, Clinicopathologic charcterization of sorafenib-induced endoplasmic reticulum stress in human liver cancer cells, J. Physiol. Pharmacol. 69 (2018).
[13] M. Rahmani, E.M. Davis, T.R. Crabtree, J.R. Habibi, T.K. Nguyen, P. Dent, S. Grant, The kinase inhibitor sorafenib induces cell death through a process involving induction of endoplasmic reticulum stress, Mol. Cell Biol. 27 (2007) 5499–5513.
[14] M.A. Rodriguez-Hernandez, R. Gonzalez, A.J. de la Rosa, P. Gallego, R. Ordonez, E. Navarro-Villaran, L. Contreras, et al., Molecular characterization of autophagic and apoptotic signaling induced by sorafenib in liver cancer cells, J. Cell. Physiol. 234 (2018) 692–708.
[15] P. Yi, A. Higa, S. Taouji, M.G. Bexiga, E. Marza, D. Arma, C. Castain, et al., Sorafenib-mediated targeting of the AAA(+) ATPase p97/VCP leads to disruption of the secretory pathway, endoplasmic reticulum stress, and hepatocellular cancer cell death, Mol. Canc. Therapeut. 11 (2012) 2610–2620.
[16] Q. Wang, G. Wu, X. Che, Q. Li, Z. Zhang, Q. Tang, Sorafenib induces renal cell carcinoma apoptosis via upregulating activating transcription factor 4, Pharmazie 73 (2018) 156–160.
[17] G. Wang, J. Zhuang, J. Ni, Y. Ye, S. He, W. Xia, Combined effects of Lenvatinib and iodine-131 on cell apoptosis in nasopharyngeal carcinoma through inducing endoplasmic reticulum stress, Exp. Ther. Med. 16 (2018) 3325–3332.
[18] K.S. Han, N. Li, P.A. Raven, L. Fazli, S. Frees, S. Ettinger, K.C. Park, et al., Inhibition of endoplasmic reticulum chaperone protein glucose-regulated protein 78 potentiates anti-angiogenic therapy in renal cell carcinoma through inactivation of the PERK/eIF2alpha pathway, Oncotarget 6 (2015) 34818–34830.
[19] P. Makhov, S. Naito, M. Haifler, A. Kutikov, Y. Boumber, R.G. Uzzo, V.M. Kolenko, The convergent roles of NF-kappaB and ER stress in sunitinib-mediated expression of pro-tumorigenic cytokines and refractory phenotype in renal cell carcinoma, Cell Death Dis. 9 (2018) 374.
[20] Y.C. Lin, M.H. Wu, T.T. Wei, Y.C. Lin, W.C. Huang, L.Y. Huang, Y.T. Lin, et al., Metformin sensitizes anticancer effect of dasatinib in head and neck squamous cell carcinoma cells through AMPK-dependent ER stress, Oncotarget 5 (2014) 298–308.
[21] P. Maione, C. Gridelli, T. Troiani, F. Ciardiello, Combining targeted therapies and drugs with multiple targets in the treatment of NSCLC, Oncologist 11 (2006) 274–284.
[22] Y.C. Wang, S.K. Kulp, D. Wang, C.C. Yang, A.M. Sargeant, J.H. Hung, Y. Kashida, et al., Targeting endoplasmic reticulum stress and Akt with OSU-03012 and gefitinib or erlotinib to overcome resistance to epidermal growth factor receptor inhibitors, Canc. Res. 68 (2008) 2820–2830.
[23] Z. Wang, T. Du, X. Dong, Z. Li, G. Wu, R. Zhang, Autophagy inhibition facilitates erlotinib cytotoxicity in lung cancer cells through modulation of endoplasmic reticulum stress, Int. J. Oncol. 48 (2016) 2558–2566.
[24] C. Mulder, N. Prust, S. van Doorn, M. Reinecke, B. Kuster, En van Bergen, P. Henegouwen, S. Lemeer, Adaptive resistance to EGFR-targeted therapy by calcium signaling in NSCLC cells, Mol. Canc. Res. 16 (2018) 1773–1784.
[25] O. Toman, T. Kabickova, O. Vit, R. Fiser, K.M. Polakova, J. Zach, J. Linhartova, et al., Proteomic analysis of imatinib-resistant CML-T1 cells reveals calcium homeostasis as a potential therapeutic target, Oncol. Rep. 36 (2016) 1258–1268.
[26] F. Weinberg, N.S. Chandel, Reactive oxygen species-dependent signaling regulates cancer, Cell. Mol. Life Sci. 66 (2009) 3663–3673.
[27] B. Van Houten, V. Woshner, J.H. Santos, Role of mitochondrial DNA in toxic responses to oxidative stress, DNA Repair 5 (2006) 145–152.
[28] F. Paech, C. Mingard, D. Grunig, V.F. Abegg, J. Bouitbir, S. Krahenbuhl, Mechanisms of mitochondrial toxicity of the kinase inhibitors ponatinib, regorafenib and sorafenib in human hepatic HepG2 cells, Toxicology 395 (2018) 34–44.

[29] Y. Will, J.A. Dykens, S. Nadanaciva, B. Hirakawa, J. Jamieson, L.D. Marroquin, J. Hynes, et al., Effect of the multitargeted tyrosine kinase inhibitors imatinib, dasatinib, sunitinib, and sorafenib on mitochondrial function in isolated rat heart mitochondria and H9c2 cells, Toxicol. Sci. 106 (2008) 153–161.

[30] T. Force, D.S. Krause, R.A. Van Etten, Molecular mechanisms of cardiotoxicity of tyrosine kinase inhibition, Nat. Rev. Canc. 7 (2007) 332–344.

[31] D.P. Jones, J.J. Lemasters, D. Han, U.A. Boelsterli, N. Kaplowitz, Mechanisms of pathogenesis in drug hepatotoxicity putting the stress on mitochondria, Mol. Interv. 10 (2010) 98–111.

[32] R.R. Shah, J. Morganroth, D.R. Shah, Hepatotoxicity of tyrosine kinase inhibitors: clinical and regulatory perspectives, Drug Saf. 36 (2013) 491–503.

[33] C. Mingard, F. Paech, J. Bouitbir, S. Krahenbuhl, Mechanisms of toxicity associated with six tyrosine kinase inhibitors in human hepatocyte cell lines, J. Appl. Toxicol. 38 (2018) 418–431.

[34] Z. Weng, Y. Luo, X. Yang, J.J. Greenhaw, H. Li, L. Xie, W.B. Mattes, et al., Regorafenib impairs mitochondrial functions, activates AMP-activated protein kinase, induces autophagy, and causes rat hepatocyte necrosis, Toxicology 327 (2015) 10–21.

[35] K.J. French, R.W. Coatney, J.P. Renninger, C.X. Hu, T.L. Gales, S. Zhao, L.M. Storck, et al., Differences in effects on myocardium and mitochondria by angiogenic inhibitors suggest separate mechanisms of cardiotoxicity, Toxicol. Pathol. 38 (2010) 691–702.

[36] J. Rimola, A. Diaz-Gonzalez, A. Darnell, M. Varela, F. Pons, M. Hernandez-Guerra, M. Delgado, et al., Complete response under sorafenib in patients with hepatocellular carcinoma: relationship with dermatologic adverse events, Hepatology 67 (2) (2018) 612–622.

[37] W. Ma, M. Liu, F. Liang, L. Zhao, C. Gao, X. Jiang, X. Zhang, et al., Cardiotoxicity of sorafenib is mediated through elevation of ROS level and CaMKII activity and dysregulation of calcium homoeostasis, Basic Clin. Pharmacol. Toxicol. 126 (2) (2020) 166–188.

[38] J. Bouitbir, A. Alshaikhali, M.V. Panajatovic, V.F. Abegg, F. Paech, S. Krahenbuhl, Mitochondrial oxidative stress plays a critical role in the cardiotoxicity of sunitinib: running title: sunitinib and oxidative stress in hearts, Toxicology 426 (2019) 152281.

[39] A. Garten, T. Grohmann, K. Kluckova, G.G. Lavery, W. Kiess, M. Penke, Sorafenib-induced apoptosis in hepatocellular carcinoma is reversed by SIRT1, Int. J. Mol. Sci. 20 (2019) 4048.

[40] R. Coriat, C. Nicco, C. Chereau, O. Mir, J. Alexandre, S. Ropert, B. Weill, et al., Sorafenib-induced hepatocellular carcinoma cell death depends on reactive oxygen species production in vitro and in vivo, Mol. Canc. Therapeut. 11 (2012) 2284–2293.

[41] M. Caraglia, G. Giuberti, M. Marra, R. Addeo, L. Montella, M. Murolo, P. Sperlongano, et al., Oxidative stress and ERK1/2 phosphorylation as predictors of outcome in hepatocellular carcinoma patients treated with sorafenib plus octreotide LAR, Cell Death Dis. 2 (2011) e150.

[42] J.F. Chiou, C.J. Tai, Y.H. Wang, T.Z. Liu, Y.M. Jen, C.Y. Shiau, Sorafenib induces preferential apoptotic killing of a drug- and radio-resistant Hep G2 cells through a mitochondria-dependent oxidative stress mechanism, Canc. Biol. Ther. 8 (2009) 1904–1913.

[43] G.M. Suddek, Sunitinib improves chemotherapeutic efficacy and ameliorates cisplatin-induced nephrotoxicity in experimental animals, Canc. Chemother. Pharmacol. 67 (2011) 1035–1044.

[44] J.G. Christensen, H.Y. Zou, M.E. Arango, Q. Li, J.H. Lee, S.R. McDonnell, S. Yamazaki, et al., Cytoreductive antitumor activity of PF-2341066, a novel inhibitor of anaplastic lymphoma kinase and c-Met, in experimental models of anaplastic large-cell lymphoma, Mol. Canc. Therapeut. 6 (2007) 3314–3322.

[45] H. Yan, J. Du, X. Chen, B. Yang, Q. He, X. Yang, P. Luo, ROS-dependent DNA damage contributes to crizotinib-induced hepatotoxicity via the apoptotic pathway, Toxicol. Appl. Pharmacol. (2019) 114768.

[46] K.R. Doherty, R.L. Wappel, D.R. Talbert, P.B. Trusk, D.M. Moran, J.W. Kramer, A.M. Brown, et al., Multi-parameter in vitro toxicity testing of crizotinib, sunitinib, erlotinib, and nilotinib in human cardiomyocytes, Toxicol. Appl. Pharmacol. 272 (2013) 245–255.

[47] B.J. Solomon, T. Mok, D.W. Kim, Y.L. Wu, K. Nakagawa, T. Mekhail, E. Felip, et al., First-line crizotinib versus chemotherapy in ALK-positive lung cancer, N. Engl. J. Med. 371 (2014) 2167–2177.

[48] H.R. Teppo, Y. Soini, P. Karihtala, Reactive oxygen species-mediated mechanisms of action of targeted cancer therapy, Oxid .Med. Cell Longev. 2017 (2017) 1485283.

[49] K.P. Orcutt, A.D. Parsons, Z.A. Sibenaller, P.M. Scarbrough, Y. Zhu, A. Sobhakumari, W.W. Wilke, et al., Erlotinib-mediated inhibition of EGFR signaling induces metabolic oxidative stress through NOX4, Canc. Res. 71 (2011) 3932–3940.

[50] A. Mukherjee, A.S. Dhadda, M. Shehata, S. Chan, Lapatinib: a tyrosine kinase inhibitor with a clinical role in breast cancer, Expet Opin. Pharmacother. 8 (2007) 2189–2204.

[51] K.M. Aird, J.L. Allensworth, I. Batinic-Haberle, H.K. Lyerly, M.W. Dewhirst, G.R. Devi, ErbB1/2 tyrosine kinase inhibitor mediates oxidative stress-induced apoptosis in inflammatory breast cancer cells, Breast Canc. Res. Treat. 132 (2012) 109–119.

[52] E. Buchdunger, C.L. Cioffi, N. Law, D. Stover, S. Ohno-Jones, B.J. Druker, N.B. Lydon, Abl protein-tyrosine kinase inhibitor STI571 inhibits in vitro signal transduction mediated by c-kit and platelet-derived growth factor receptors, J. Pharmacol. Exp. Therapeut. 295 (2000) 139–145.

[53] S.P. Chang, S.C. Shen, W.R. Lee, L.L. Yang, Y.C. Chen, Imatinib mesylate induction of ROS-dependent apoptosis in melanoma B16F0 cells, J. Dermatol. Sci. 62 (2011) 183–191.

[54] Z. Durackova, Some current insights into oxidative stress, Physiol. Res. 59 (2010) 459–469.

[55] S.G. Rhee, Y.S. Bae, S.R. Lee, J. Kwon, Hydrogen peroxide: a key messenger that modulates protein phosphorylation through cysteine oxidation, Sci. Signal. 2000 (2000) pe1–pe1.

[56] S. Pervaiz, M.V. Clement, Superoxide anion: oncogenic reactive oxygen species? Int. J. Biochem. Cell Biol. 39 (2007) 1297–1304.

[57] K. Schulze, S. Imbeaud, E. Letouze, L.B. Alexandrov, J. Calderaro, S. Rebouissou, G. Couchy, et al., Exome sequencing of hepatocellular carcinomas identifies new mutational signatures and potential therapeutic targets, Nat. Genet. 47 (2015) 505–511.

[58] G.M. DeNicola, F.A. Karreth, T.J. Humpton, A. Gopinathan, C. Wei, K. Frese, D. Mangal, et al., Oncogene-induced Nrf2 transcription promotes ROS detoxification and tumorigenesis, Nature 475 (2011) 106–109.

[59] J. Du, C. Sun, Z. Hu, Y. Yang, Y. Zhu, D. Zheng, L. Gu, et al., Lysophosphatidic acid induces MDA-MB-231 breast cancer cells migration through activation of PI3K/PAK1/ERK signaling, PloS One 5 (2010) e15940-e15940.

[60] A.R.M. Ruhul Amin, T. Senga, M.L. Oo, A.A. Thant, M. Hamaguchi, Secretion of matrix metalloproteinase-9 by the proinflammatory cytokine, IL-1beta: a role for the dual signalling pathways, Akt and Erk, Gene Cell. 8 (2003) 515–523.

[61] M. Hornsveld, T.B. Dansen, The hallmarks of cancer from a redox perspective, Antioxidants Redox Signal. 25 (2016) 300–325.

[62] Y.-W. Lou, Y.-Y. Chen, S.-F. Hsu, R.-K. Chen, C.-L. Lee, K.-H. Khoo, N.K. Tonks, et al., Redox regulation of the protein tyrosine phosphatase PTP1B in cancer cells, FEBS J. 275 (2008) 69–88.

[63] W.C. Barrett, J.P. DeGnore, S. König, H.M. Fales, Y.F. Keng, Z.Y. Zhang, M.B. Yim, et al., Regulation of PTP1B via glutathionylation of the active site cysteine 215, Biochemistry 38 (1999) 6699–6705.

[64] H. Murata, Y. Ihara, H. Nakamura, J. Yodoi, K. Sumikawa, T. Kondo, Glutaredoxin exerts an antiapoptotic effect by regulating the redox state of Akt, J. Biol. Chem. 278 (2003) 50226–50233.

[65] J. Kwon, S.R. Lee, K.S. Yang, Y. Ahn, Y.J. Kim, E.R. Stadtman, S.G. Rhee, Reversible oxidation and inactivation of the tumor suppressor PTEN in cells stimulated with peptide growth factors, Proc. Natl. Acad. Sci. Unit. States Am. 101 (2004) 16419–16424.

[66] C.H. Switzer, S.A. Glynn, R.Y. Cheng, L.A. Ridnour, J.E. Green, S. Ambs, D.A. Wink, S-nitrosylation of EGFR and Src activates an oncogenic signaling network in human basal-like breast cancer, Mol. Canc. Res. 10 (2012) 1203–1215.

[67] I.C. Low, T. Loh, Y. Huang, D.M. Virshup, S. Pervaiz, Ser70 phosphorylation of Bcl-2 by selective tyrosine nitration of PP2A-B56delta stabilizes its antiapoptotic activity, Blood 124 (2014) 2223–2234.

[68] Y. Du, H. Zhang, J. Lu, A. Holmgren, Glutathione and glutaredoxin act as a backup of human thioredoxin reductase 1 to reduce thioredoxin 1 preventing cell death by aurothioglucose, J. Biol. Chem. 287 (2012) 38210–38219.

[69] A.B. Fisher, The phospholipase A2 activity of peroxiredoxin 6, JLR (J. Lipid Res.) 59 (2018) 1132–1147.

[70] F. Wang, J.-L. Yang, K-k Yu, M. Xu, Y-z Xu, L. Chen, Y-m Lu, et al., Activation of the NF-kB pathway as a mechanism of alcohol enhanced progression and metastasis of human hepatocellular carcinoma, Mol. Canc. 14 (2015) 10-10.

[71] J.R. Matthews, N. Wakasugi, J.-L. Virelizier, J. Yodoi, R.T. Hay, Thioredoxin regulates the DNA binding activity of NF-$χ$B by reduction of a disulphid bond involving cysteine 62, Nucleic Acids Res. 20 (1992) 3821–3830.

[72] K. Hirota, M. Murata, Y. Sachi, H. Nakamura, J. Takeuchi, K. Mori, J. Yodoi, Distinct roles of thioredoxin in the cytoplasm and in the nucleus, J. Biol. Chem. 274 (1999) 27891–27897.

[73] J.E. Darnell, Validating Stat3 in cancer therapy, Nat. Med. 11 (2005) 595–596.

[74] E. Butturini, E. Darra, G. Chiavegato, B. Cellini, F. Cozzolino, M. Monti, P. Pucci, et al., S-Glutathionylation at Cys328 and Cys542 impairs STAT3 phosphorylation, ACS Chem. Biol. 9 (2014) 1885–1893.

[75] M.C. Sobotta, W. Liou, S. Stöcker, D. Talwar, M. Oehler, T. Ruppert, A.N.D. Scharf, et al., Peroxiredoxin-2 and STAT3 form a redox relay for H2O2 signaling, Nat. Chem. Biol. 11 (2015) 64–70.

[76] H.-M. Yun, K.-R. Park, M.H. Park, D.H. Kim, M.R. Jo, J.Y. Kim, E.-C. Kim, et al., PRDX6 promotes tumor development via the JAK2/STAT3 pathway in a urethane-induced lung tumor model, Free Radic. Biol. Med. 80 (2015) 136–144.

[77] S. Lamouille, J. Xu, R. Derynck, Molecular mechanisms of epithelial–mesenchymal transition, Nat. Rev. Mol. Cell Biol. 15 (2014) 178–196.

[78] D.Y. Rhyu, Y. Yang, H. Ha, G.T. Lee, J.S. Song, S.T. Uh, H.B. Lee, Role of reactive oxygen species in TGF-beta1-induced mitogen-activated protein kinase activation and epithelial-mesenchymal transition in renal tubular epithelial cells, J. Am. Soc. Nephrol. 16 (2005) 667–675.

[79] J.P. Thiery, J.P. Sleeman, Complex networks orchestrate epithelial-mesenchymal transitions, Nat. Rev. Mol. Cell Biol. 7 (2006) 131–142.

[80] L. Larue, A. Bellacosa, Epithelial-mesenchymal transition in development and cancer: role of phosphatidylinositol 3′ kinase/AKT pathways, Oncogene 24 (2005) 7443–7454.

[81] V. Helfinger, K. Schröder, Redox control in cancer development and progression, Mol. Aspect. Med. 63 (2018) 88–98.

[82] J. Dong, B. Zhai, W. Sun, F. Hu, H. Cheng, J. Xu, Activation of phosphatidylinositol 3-kinase/AKT/snail signaling pathway contributes to epithelial-mesenchymal transition-induced multi-drug resistance to sorafenib in hepatocellular carcinoma cells, PloS One 12 (2017) 1–16.

[83] G.S. Lu, M. Li, C.X. Xu, D. Wang, APE1 stimulates EGFR-TKI resistance by activating Akt signaling through a redox-dependent mechanism in lung adenocarcinoma, Cell Death Dis. 9 (2018) 1111.

[84] J. Wan, T. Liu, L. Mei, J. Li, K. Gong, C. Yu, W. Li, Synergistic antitumour activity of sorafenib in combination with tetrandrine is mediated by reactive oxygen species (ROS)/Akt signaling, Br. J. Canc. 109 (2013) 342–350.
[85] M.E. Irwin, B.P. Johnson, R. Manshouri, H.M. Amin, J. Chandra, A NOX2/Egr-1/Fyn pathway delineates new targets for TKI-resistant malignancies, Oncotarget 6 (2015) 23631–23646.
[86] S.W. Hong, N.S. Park, M.H. Noh, J.A. Shim, B.N. Ahn, Y.S. Kim, D. Kim, et al., Combination treatment with erlotinib and ampelopsin overcomes erlotinib resistance in NSCLC cells via the Nox2-ROS-Bim pathway, Lung Canc. 106 (2017) 115–124.
[87] L. Marcar, K. Bardhan, L. Gheorghiu, P. Dinkelborg, H. Pfäffle, Q. Liu, M. Wang, et al., Acquired resistance of EGFR-mutated lung cancer to tyrosine kinase inhibitor treatment promotes PARP inhibitor sensitivity, Cell Rep. 27 (2019) 3422–3432 e3424.
[88] A. Leone, M.S. Roca, C. Ciardiello, M. Terranova-Barberio, C. Vitagliano, G. Ciliberto, R. Mancini, et al., Vorinostat synergizes with EGFR inhibitors in NSCLC cells by increasing ROS via up-regulation of the major mitochondrial porin VDAC1 and modulation of the c-Myc-NRF2-KEAP1 pathway, Free Radic. Biol. Med. 89 (2015) 287–299.
[89] T. Yamadori, Y. Ishii, S. Homma, Y. Morishima, K. Kurishima, K. Itoh, M. Yamamoto, et al., Molecular mechanisms for the regulation of Nrf2-mediated cell proliferation in non-small-cell lung cancers, Oncogene 31 (2012) 4768–4777.
[90] C.C. Winterbourn, M.B. Hampton, Thiol chemistry and specificity in redox signaling, Free Radic. Biol. Med. 45 (2008) 549–561.
[91] M. Schieber, S. Chandel Navdeep, ROS function in redox signaling and oxidative stress, Curr. Biol. 24 (2014) R453–R462.
[92] A. Östman, J. Frijhoff, Å. Sandin, F.-D. Böhmer, Regulation of protein tyrosine phosphatases by reversible oxidation, J. Biochem. 150 (2011) 345–356.
[93] C.E. Paulsen, T.H. Truong, F.J. Garcia, A. Homann, V. Gupta, S.E. Leonard, K.S. Carroll, Peroxide-dependent sulfenylation of the EGFR catalytic site enhances kinase activity, Nat. Chem. Biol. 8 (2011) 57–64.
[94] M.J. Niederst, H. Hu, H.E. Mulvey, E.L. Lockerman, A.R. Garcia, Z. Piotrowska, L.V. Sequist, et al., The allelic context of the C797S mutation acquired upon treatment with third-generation EGFR inhibitors impacts sensitivity to subsequent treatment strategies, Clin. Canc. Res. : Off. J. Am. Assoc. Canc. Res. 21 (2015) 3924–3933.
[95] L. Wang, J. Liu, J. Liu, X. Chen, M. Chang, J. Li, J. Zhou, et al., GLRX inhibition enhances the effects of geftinib in EGFR-TKI-resistant NSCLC cells through FoxM1 signaling pathway, J. Canc. Res. Clin. Oncol. 145 (2019) 861–872.
[96] G. Powis, D.L. Kirkpatrick, Thioredoxin signaling as a target for cancer therapy, Curr. Opin. Pharmacol. 7 (2007) 392–397.
[97] A. Sadeghirizi, R. Yazdanparast, S. Aghazadeh, Combating trastuzumab resistance by targeting thioredoxin-1/PTEN interaction, Tumor Biol. 37 (2016) 6737–6747.
[98] W. Li, J. Shi, C. Zhang, M. Li, L. Gan, H. Xu, X. Yang, Co-delivery of thioredoxin 1 shRNA and doxorubicin by folate-targeted gemini surfactant-based cationic liposomes to sensitize hepatocellular carcinoma cells, J. Mater. Chem. B 2 (2014) 4901–4910.
[99] M.J. López-Grueso, R. González, J. Muntané, J.A. Bárcena, C.A. Padilla, Thioredoxin downregulation enhances sorafenib effects in hepatocarcinoma cells, Antioxidants 8 (2019) 501-501.
[100] Z. Guo, M. Cao, A. You, J. Gao, H. Zhou, H. Li, Y. Cui, et al., Metformin inhibits the prometastatic effect of sorafenib in hepatocellular carcinoma by upregulating the expression of TIP30, Canc. Sci. 107 (2016) 507–513.
[101] A.K. Murugan, A.K. Munirajan, N. Tsuchida, Genetic deregulation of the PIK3CA oncogene in oral cancer, Canc. Lett. 338 (2013) 193–203.
[102] N.R. Leslie, PTEN: an intercellular peacekeeper? Sci. Signal. 5 (2012) pe50.
[103] P.S. Mundi, J. Sachdev, C. McCourt, K. Kalinsky, AKT in cancer: new molecular insights and advances in drug development, Br. J. Clin. Pharmacol. 82 (2016) 943–956.
[104] T.W. Miller, J.M. Balko, C.L. Arteaga, Phosphatidylinositol 3-kinase and antiestrogen resistance in breast cancer, J. Clin. Oncol. 29 (2011) 4452–4461.
[105] J. Kim, M. Kundu, B. Viollet, K.L. Guan, AMPK and mTOR regulate autophagy through direct phosphorylation of Ulk1, Nat. Cell Biol. 13 (2011) 132–141.
[106] Z. Luo, A.K. Saha, X. Xiang, N.B. Ruderman, AMPK, the metabolic syndrome and cancer, Trends Pharmacol. Sci. 26 (2005) 69–76.
[107] Z. Wang, N. Wang, P. Liu, X. Xie, AMPK and cancer, Exper. Suppl. 107 (2016) 203–226.
[108] A.V. Budanov, M. Karin, p53 target genes sestrin1 and sestrin2 connect genotoxic stress and mTOR signaling, Cell 134 (2008) 451–460.
[109] D. Visnjic, V. Dembitz, H. Lalic, The role of AMPK/mTOR modulators in the therapy of acute myeloid leukemia, Curr. Med. Chem. 26 (2019) 2208–2229.
[110] P. Baumann, S. Mandl-Weber, B. Emmerich, C. Straka, R. Schmidmaier, Inhibition of adenosine monophosphate-activated protein kinase induces apoptosis in multiple myeloma cells, Anti Canc. Drugs 18 (2007) 405–410.
[111] E.Y. Chan, mTORC1 phosphorylates the ULK1-mAtg13-FIP200 autophagy regulatory complex, Sci. Signal. 2 (2009) pe51.
[112] D.N. Tripathi, R. Chowdhury, L.J. Trudel, A.R. Tee, R.S. Slack, C.L. Walker, G.N. Wogan, Reactive nitrogen species regulate autophagy through ATM-AMPK-TSC2-mediated suppression of mTORC1, Proc. Natl. Acad. Sci. U. S. A. 110 (2013) E2950–E2957.
[113] M. Zhao, D.J. Klionsky, AMPK-dependent phosphorylation of ULK1 induces autophagy, Cell Metabol. 13 (2011) 119–120.
[114] J. Liu, L. Fan, H. Wang, G. Sun, Autophagy, a double-edged sword in anti-angiogenesis therapy, Med. Oncol. 33 (2016) 10.
[115] A. Letai, Cell death and cancer therapy: don't forget to kill the cancer cell!, Clin. Canc. Res. 21 (2015) 5015–5020.
[116] J. Montero, K.A. Sarosiek, J.D. DeAngelo, O. Maertens, J. Ryan, D. Ercan, H. Piao, et al., Drug-induced death signaling strategy rapidly predicts cancer response to chemotherapy, Cell 160 (2015) 977–989.
[117] B.E. Fitzwalter, C.G. Towers, K.D. Sullivan, Z. Andrysik, M. Hoh, M. Ludwig, J. O'Prey, et al., Autophagy inhibition mediates apoptosis sensitization in cancer therapy by relieving FOXO3a turnover, Dev. Cell 44 (2018) 555–565 e553.
[118] N. Prieto-Dominguez, R. Ordonez, A. Fernandez, A. Garcia-Palomo, J. Muntane, J. Gonzalez-Gallego, J.L. Mauriz, Modulation of autophagy by sorafenib: effects on treatment response, Front. Pharmacol. 7 (2016) 151.
[119] F.A. Ross, S.A. Hawley, F.R. Auciello, G.J. Gowans, A. Atrih, D.J. Lamont, D.G. Hardie, Mechanisms of paradoxical activation of AMPK by the kinase inhibitors SU6656 and sorafenib, Cell Chem. Biol. 24 (2017) 813–824 e814.
[120] T. Hirao, M. Yamaguchi, M. Kikuya, H. Chibana, K. Ito, S. Aoki, Altered intracellular signaling by imatinib increases the anti-cancer effects of tyrosine kinase inhibitors in chronic myelogenous leukemia cells, Canc. Sci. 109 (2018) 121–131.
[121] E. Vakana, J.K. Altman, H. Glaser, N.J. Donato, L.C. Platanias, Antileukemic effects of AMPK activators on BCR-ABL-expressing cells, Blood 118 (2011) 6399–6402.
[122] X. Zhu, L. Wu, H. Qiao, T. Han, S. Chen, X. Liu, R. Jiang, et al., Autophagy stimulates apoptosis in HER2-overexpressing breast cancers treated by lapatinib, J. Cell. Biochem. 114 (2013) 2643–2653.
[123] K. Bhalla, B.J. Hwang, R.E. Dewi, L. Ou, W. Twaddel, H.B. Fang, S.B. Vafai, et al., PGC1alpha promotes tumor growth by inducing gene expression programs supporting lipogenesis, Canc. Res. 71 (2011) 6888–6898.
[124] F. Bost, L. Kaminski, The metabolic modulator PGC-1alpha in cancer, Am. J. Canc. Res. 9 (2019) 198–211.
[125] P. Puigserver, Z. Wu, C.W. Park, R. Graves, M. Wright, B.M. Spiegelman, A cold-inducible coactivator of nuclear receptors linked to adaptive thermogenesis, Cell 92 (1998) 829–839.
[126] J.T. Rodgers, C. Lerin, W. Haas, S.P. Gygi, B.M. Spiegelman, P. Puigserver, Nutrient control of glucose homeostasis through a complex of PGC-1alpha and SIRT1, Nature 434 (2005) 113–118.
[127] S. Vyas, E. Zaganjor, M.C. Haigis, Mitochondria and cancer, Cell 166 (2016) 555–566.
[128] P.J. Fernandez-Marcos, J. Auwerx, Regulation of PGC-1alpha, a nodal regulator of mitochondrial biogenesis, Am. J. Clin. Nutr. 93 (2011) 884S–890S.
[129] S. Jager, C. Handschin, J. St-Pierre, B.M. Spiegelman, AMP-activated protein kinase (AMPK) action in skeletal muscle via direct phosphorylation of PGC-1alpha, Proc. Natl. Acad. Sci. U. S. A. 104 (2007) 12017–12022.
[130] P. Puigserver, J. Rhee, J. Lin, Z. Wu, J.C. Yoon, C.Y. Zhang, S. Krauss, et al., Cytokine stimulation of energy expenditure through p38 MAP kinase activation of PPARgamma coactivator-1, Mol. Cell 8 (2001) 971–982.
[131] X. Li, B. Monks, Q. Ge, M.J. Birnbaum, Akt/PKB regulates hepatic metabolism by directly inhibiting PGC-1alpha transcription coactivator, Nature 447 (2007) 1012–1016.
[132] Y. Li, S. Xu, J. Li, L. Zheng, M. Feng, X. Wang, K. Han, et al., SIRT1 facilitates hepatocellular carcinoma metastasis by promoting PGC-1alpha-mediated mitochondrial biogenesis, Oncotarget 7 (2016) 29255–29274.
[133] J. Feilchenfeldt, M.A. Brundler, C. Soravia, M. Totsch, C.A. Meier, Peroxisome proliferator-activated receptors (PPARs) and associated transcription factors in colon cancer: reduced expression of PPARgamma-coactivator 1 (PGC-1), Canc. Lett. 203 (2004) 25–33.
[134] A. Cormio, F. Guerra, G. Cormio, V. Pesce, F. Fracasso, V. Loizzi, P. Cantatore, et al., The PGC-1alpha-dependent pathway of mitochondrial biogenesis is upregulated in type I endometrial cancer, Biochem. Biophys. Res. Commun. 390 (2009) 1182–1185.
[135] R. Liu, H. Zhang, Y. Zhang, S. Li, X. Wang, X. Wang, C. Wang, et al., Peroxisome proliferator-activated receptor gamma coactivator-1 alpha acts as a tumor suppressor in hepatocellular carcinoma, Tumour Biol. 39 (2017) 1010428317695031.
[136] J.B. Tennakoon, Y. Shi, J.J. Han, E. Tsouko, M.A. White, A.R. Burns, A. Zhang, et al., Androgens regulate prostate cancer cell growth via an AMPK-PGC-1alpha-mediated metabolic switch, Oncogene 33 (2014) 5251–5261.
[137] A. Lyons, M. Coleman, S. Riis, C. Favre, C.H. O'Flanagan, A.V. Zhdanov, D.B. Papkovsky, et al., Insulin-like growth factor 1 signaling is essential for mitochondrial biogenesis and mitophagy in cancer cells, J. Biol. Chem. 292 (2017) 16983–16998.
[138] J. Hirpara, J.Q. Eu, J.K.M. Tan, A.L. Wong, M.-V. Clement, L.R. Kong, N. Ohi, et al., Metabolic reprogramming of oncogene-addicted cancer cells to OXPHOS as a mechanism of drug resistance, Redox Biol. 25 (2019) 101076.
[139] R. Haq, J. Shoag, P. Andreu-Perez, S. Yokoyama, H. Edelman, G.C. Rowe, D.T. Frederick, et al., Oncogenic BRAF regulates oxidative metabolism via PGC1alpha and MITF, Canc. Cell 23 (2013) 302–315.
[140] G. Gentric, V. Mieulet, F. Mechta-Grigoriou, Heterogeneity in cancer metabolism: new concepts in an old field, Antioxidants Redox Signal. 26 (2017) 462–485.
[141] C.R. Justus, E.J. Sanderlin, L.V. Yang, Molecular connections between cancer cell metabolism and the tumor microenvironment, Int. J. Mol. Sci. 16 (2015) 11055–11086.
[142] N.N. Pavlova, C.B. Thompson, The emerging hallmarks of cancer metabolism, Cell Metabol. 23 (2016) 27–47.
[143] O. Warburg, On the origin of cancer cells, Science 123 (1956) 309.
[144] R.A. Saxton, D.M. Sabatini, mTOR signaling in growth, metabolism, and disease, Cell 168 (2017) 960–976.
[145] I. Ben-Sahra, G. Hoxhaj, S.J.H. Ricoult, J.M. Asara, B.D. Manning, mTORC1 induces purine synthesis through control of the mitochondrial tetrahydrofolate cycle, Science 351 (2016) 728–733.
[146] K. Duvel, J.L. Yecies, S. Menon, P. Raman, A.I. Lipovsky, A.L. Souza,

E. Triantafellow, et al., Activation of a metabolic gene regulatory network downstream of mTOR complex 1, Mol. Cell 39 (2010) 171–183.
[147] T.R. Peterson, S.S. Sengupta, T.E. Harris, A.E. Carmack, S.A. Kang, E. Balderas, D.A. Guertin, et al., mTOR complex 1 regulates lipin 1 localization to control the SREBP pathway, Cell 146 (2011) 408–420.
[148] R.C. Osthus, H. Shim, S. Kim, Q. Li, R. Reddy, M. Mukherjee, Y. Xu, et al., Deregulation of glucose transporter 1 and glycolytic gene expression by c-Myc, J. Biol. Chem. 275 (2000) 21797–21800.
[149] M. Poliaková, D.M. Aebersold, Y. Zimmer, M. Medová, The relevance of tyrosine kinase inhibitors for global metabolic pathways in cancer, Mol. Canc. 17 (2018) 27-27.
[150] F. Alvarez-Calderon, M.A. Gregory, C. Pham-Danis, D. DeRyckere, B.M. Stevens, V. Zaberezhnyy, A.A. Hill, et al., Tyrosine kinase inhibition in leukemia induces an altered metabolic state sensitive to mitochondrial perturbations, Clin. Canc. Res. : Off. J. Am. Assoc. Canc. Res. 21 (2015) 1360–1372.
[151] K. Barnes, E. McIntosh, A.D. Whetton, G.Q. Daley, J. Bentley, S.A. Baldwin, Chronic myeloid leukaemia: an investigation into the role of Bcr-Abl-induced abnormalities in glucose transport regulation, Oncogene 24 (2005) 3257–3267.
[152] S.-O. Lim, C.-W. Li, W. Xia, H.-H. Lee, S.-S. Chang, J. Shen, J.L. Hsu, et al., EGFR signaling enhances aerobic glycolysis in triple-negative breast cancer cells to promote tumor growth and immune escape, Canc. Res. 76 (2016) 1284–1296.
[153] H. Makinoshima, M. Takita, S. Matsumoto, A. Yagishita, S. Owada, H. Esumi, K. Tsuchihara, Epidermal growth factor receptor (EGFR) signaling regulates global metabolic pathways in EGFR-mutated lung adenocarcinoma, J. Biol. Chem. 289 (2014) 20813–20823.
[154] C. Oakman, M. Pestrin, E. Zafarana, E. Cantisani, A. Di Leo, Role of lapatinib in the first-line treatment of patients with metastatic breast cancer, Canc. Manag. Res. 2 (2010) 13–25.
[155] B. Ruprecht, E.A. Zaal, J. Zecha, W. Wu, C.R. Berkers, B. Kuster, S. Lemeer, Lapatinib resistance in breast cancer cells is accompanied by phosphorylation-mediated reprogramming of glycolysis, Canc. Res. 77 (2017) 1842.
[156] T. Guo, Y. Zhu, C.S. Gan, S.S. Lee, J. Zhu, H. Wang, X. Li, et al., Quantitative proteomics discloses MET expression in mitochondria as a direct target of MET kinase inhibitor in cancer cells, Mol. Cell. Proteomics : MCP 9 (2010) 2629–2641.
[157] A.J. Scott, J.J. Arcaroli, S.M. Bagby, R. Yahn, K.M. Huber, N.J. Serkova, A. Nguyen, et al., Cabozantinib exhibits potent antitumor activity in colorectal cancer patient-derived tumor xenograft models via autophagy and signaling mechanisms, Mol. Canc. Therapeut. 17 (2018) 2112–2122.
[158] S.R.P. McDonnell, S.R. Hwang, D. Rolland, C. Murga-Zamalloa, V. Basrur, K.P. Conlon, D. Fermin, et al., Integrated phosphoproteomic and metabolomic profiling reveals NPM-ALK-mediated phosphorylation of PKM2 and metabolic reprogramming in anaplastic large cell lymphoma, Blood 122 (2013) 958–968.
[159] V. Tesori, A.C. Piscaglia, D. Samengo, M. Barba, C. Bernardini, R. Scatena, A. Pontoglio, et al., The multikinase inhibitor Sorafenib enhances glycolysis and synergizes with glycolysis blockade for cancer cell killing, Sci. Rep. 5 (2015) 9149-9149.
[160] C.D. Hudson, T. Hagemann, S.J. Mather, N. Avril, Resistance to the tyrosine kinase inhibitor axitinib is associated with increased glucose metabolism in pancreatic adenocarcinoma, Cell Death Dis. 5 (2014) e1160-e1160.
[161] C. Fumarola, D. Cretella, S. La Monica, M.A. Bonelli, R. Alfieri, C. Caffarra, F. Quaini, et al., Enhancement of the anti-tumor activity of FGFR1 inhibition in squamous cell lung cancer by targeting downstream signaling involved in glucose metabolism, Oncotarget 8 (2017) 91841–91859.
[162] S. Gottschalk, N. Anderson, C. Hainz, S.G. Eckhardt, N.J. Serkova, Imatinib (STI571)-Mediated changes in glucose metabolism in human leukemia BCR-ABL-positive cells, Clin. Canc. Res. 10 (2004) 6661.
[163] V. De Rosa, F. Iommelli, M. Monti, R. Fonti, G. Votta, M.P. Stoppelli, S. Del Vecchio, Reversal of warburg effect and reactivation of oxidative phosphorylation by differential inhibition of EGFR signaling pathways in non–small cell lung cancer, Clin. Canc. Res. 21 (2015) 5110.
[164] J. Long, C.-J. Zhang, N. Zhu, K. Du, Y.-F. Yin, X. Tan, D.-F. Liao, et al., Lipid metabolism and carcinogenesis, cancer development, Am. J. Canc. Res. 8 (2018) 778–791.
[165] Y. Zhu, M.D. Aupperlee, Y. Zhao, Y.S. Tan, E.L. Kirk, X. Sun, M.A. Troester, et al., Pubertal and adult windows of susceptibility to a high animal fat diet in Trp53-null mammary tumorigenesis, Oncotarget 7 (2016) 83409–83423.
[166] N.J. Lanning, J.P. Castle, S.J. Singh, A.N. Leon, E.A. Tovar, A. Sanghera, J.P. MacKeigan, et al., Metabolic profiling of triple-negative breast cancer cells reveals metabolic vulnerabilities, Canc. Metabol. 5 (2017) 6-6.
[167] D. Hanahan, R.A. Weinberg, Hallmarks of cancer: the next generation, Cell 144 (2011) 646–674.
[168] W. Zhang, M. Konopleva, V.R. Ruvolo, T. McQueen, R.L. Evans, W.G. Bornmann, J. McCubrey, et al., Sorafenib induces apoptosis of AML cells via Bim-mediated activation of the intrinsic apoptotic pathway, Leukemia 22 (2008) 808–818.
[169] C. Yu, L.M. Bruzek, X.W. Meng, G.J. Gores, C.A. Carter, S.H. Kaufmann, A.A. Adjei, The role of Mcl-1 downregulation in the proapoptotic activity of the multikinase inhibitor BAY 43-9006, Oncogene 24 (2005) 6861–6869.
[170] M. Rahmani, T.K. Nguyen, P. Dent, S. Grant, The multikinase inhibitor sorafenib induces apoptosis in highly imatinib mesylate-resistant bcr/abl+ human leukemia cells in association with signal transducer and activator of transcription 5 inhibition and myeloid cell leukemia-1 down-regulation, Mol. Pharmacol. 72 (2007) 788–795.
[171] D.L. Ou, Y.C. Shen, J.D. Liang, J.Y. Liou, S.L. Yu, H.H. Fan, D.S. Wang, et al., Induction of Bim expression contributes to the antitumor synergy between sorafenib and mitogen-activated protein kinase/extracellular signal-regulated kinase kinase inhibitor CI-1040 in hepatocellular carcinoma, Clin. Canc. Res. 15 (2009) 5820–5828.
[172] L. Chen, S.N. Willis, A. Wei, B.J. Smith, J.I. Fletcher, M.G. Hinds, P.M. Colman, et al., Differential targeting of prosurvival Bcl-2 proteins by their BH3-only ligands allows complementary apoptotic function, Mol. Cell 17 (2005) 393–403.
[173] S.H. Kim, M.S. Ricci, W.S. El-Deiry, Mcl-1: a gateway to TRAIL sensitization, Canc. Res. 68 (2008) 2062–2064.
[174] Q. Ding, L. Huo, J.Y. Yang, W. Xia, Y. Wei, Y. Liao, C.J. Chang, et al., Down-regulation of myeloid cell leukemia-1 through inhibiting Erk/Pin 1 pathway by sorafenib facilitates chemosensitization in breast cancer, Canc. Res. 68 (2008) 6109–6117.
[175] R.R. Rosato, J.A. Almenara, S. Coe, S. Grant, The multikinase inhibitor sorafenib potentiates TRAIL lethality in human leukemia cells in association with Mcl-1 and cFLIPL down-regulation, Canc. Res. 67 (2007) 9490–9500.
[176] D.J. Panka, W. Wang, M.B. Atkins, J.W. Mier, The Raf inhibitor BAY 43-9006 (Sorafenib) induces caspase-independent apoptosis in melanoma cells, Canc. Res. 66 (2006) 1611–1619.
[177] M. Germain, A.P. Nguyen, J.N. Le Grand, N. Arbour, J.L. Vanderluit, D.S. Park, J.T. Opferman, et al., MCL-1 is a stress sensor that regulates autophagy in a developmentally regulated manner, EMBO J. 30 (2011) 395–407.
[178] W.T. Tai, C.W. Shiau, H.L. Chen, C.Y. Liu, C.S. Lin, A.L. Cheng, P.J. Chen, et al., Mcl-1-dependent activation of Beclin 1 mediates autophagic cell death induced by sorafenib and SC-59 in hepatocellular carcinoma cells, Cell Death Dis. 4 (2013) e485.
[179] L.P. Liu, R.L. Ho, G.G. Chen, P.B. Lai, Sorafenib inhibits hypoxia-inducible factor-1alpha synthesis: implications for antiangiogenic activity in hepatocellular carcinoma, Clin. Canc. Res. 18 (2012) 5662–5671.
[180] N. Prieto-Dominguez, C. Mendez-Blanco, S. Carbajo-Pescador, F. Fondevila, A. Garcia-Palomo, J. Gonzalez-Gallego, J.L. Mauriz, Melatonin enhances sorafenib actions in human hepatocarcinoma cells by inhibiting mTORC1/p70S6K/HIF-1alpha and hypoxia-mediated mitophagy, Oncotarget 8 (2017) 91402–91414.
[181] J.Z.C. Li, Z.M. Zhang, L.J. Lv, H.B. Qiao, X.J. Chen, A multi-targeted tyrosine kinase inhibitor lenvatinib for the treatment of mice with advanced glioblastoma, Mol. Med. Rep. 16 (5) (2017) 7105–7111.
[182] B.I. Carr, A. Cavallini, C. Lippolis, R. D'Alessandro, C. Messa, M.G. Refolo, A. Tafaro, Fluoro-Sorafenib (Regorafenib) effects on hepatoma cells: growth inhibition, quiescence, and recovery, J. Cell. Physiol. 228 (2013) 292–297.
[183] K.F. Chen, J.C. Su, C.Y. Liu, J.W. Huang, K.C. Chen, W.L. Chen, W.T. Tai, et al., A novel obatoclax derivative, SC-2001, induces apoptosis in hepatocellular carcinoma cells through SHP-1-dependent STAT3 inactivation, Canc. Lett. 321 (2012) 27–35.
[184] W.T. Tai, P.Y. Chu, C.W. Shiau, Y.L. Chen, Y.S. Li, M.H. Hung, L.J. Chen, et al., STAT3 mediates regorafenib-induced apoptosis in hepatocellular carcinoma, Clin. Canc. Res. 20 (2014) 5768–5776.
[185] J. Tong, S. Tan, F. Zou, J. Yu, L. Zhang, FBW7 mutations mediate resistance of colorectal cancer to targeted therapies by blocking Mcl-1 degradation, Oncogene 36 (2017) 787–796.
[186] F.M. Yakes, J. Chen, J. Tan, K. Yamaguchi, Y. Shi, P. Yu, F. Qian, et al., Cabozantinib (XL184), a novel MET and VEGFR2 inhibitor, simultaneously suppresses metastasis, angiogenesis, and tumor growth, Mol. Canc. Therapeut. 10 (2011) 2298–2308.
[187] Q. Xiang, W. Chen, M. Ren, J. Wang, H. Zhang, D.Y. Deng, L. Zhang, et al., Cabozantinib suppresses tumor growth and metastasis in hepatocellular carcinoma by a dual blockade of VEGFR2 and MET, Clin. Canc. Res. 20 (2014) 2959–2970.

ACS APPLIED BIO MATERIALS

www.acsabm.org Article

PDA-Based Glyconanomicelles for Hepatocellular Carcinoma Cells Active Targeting Via Mannose and Asialoglycoprotein Receptors

María Negrete,[#] Elena Romero-Ben,[#] Alicia Gutiérrez-Valencia, Cristian Rosales-Barrios, Eva Alés, Teresa Mena-Barragán, Juan A. Flores, M[a] Carmen Castillejos, Patricia de la Cruz-Ojeda, Elena Navarro-Villarán, Carmen Cepeda-Franco, Noureddine Khiar,*[,#] and Jordi Muntané*[,#]

Cite This: https://doi.org/10.1021/acsabm.0c01679 Read Online

ACCESS | Metrics & More | Article Recommendations | Supporting Information

ABSTRACT: Hepatocellular carcinoma (HCC) is the sixth most common neoplasia and the fourth most common cause of cancer-related mortality worldwide. Sorafenib is the first-line molecular therapy for patients in an advanced stage of HCC. However, the recommended clinical dose of Sorafenib is associated with several complications, which derive from its lack of cell specificity and its very low water solubility. To circumvent these drawbacks, in the present study we developed two sugar-coated polydiacetylene-based nanomicelles-Sorafenib carriers targeting mannose and asialoglycoprotein receptors (MR and ASGPR, respectively). The strategies allowed the inducement of apoptosis and reduction of cell proliferation at a nanomolar, instead of micromolar, range in liver cancer cells. The study showed that, contrary to literature data, Sorafenib included into the pMicMan (Man = mannose) vector (targeting MR) is more efficient than pMicGal (Gal = galactose) (targeting ASGPR). Indeed, pMicMan increased the endosomal incorporation with an increased intracellular Sorafenib concentration that induced apoptosis and reduced cell proliferation at a low concentration range (10−20 nM).

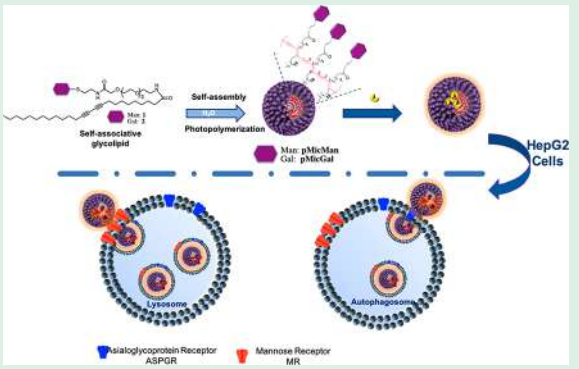

KEYWORDS: *active drug delivery, polydiacetylene-based nanomicelles, mannose receptor, asialoglycoprotein receptor, apoptosis, cell proliferation, cell trafficking, hepatocellular carcinoma*

INTRODUCTION

Hepatocellular carcinoma (HCC) is the sixth most common neoplasia in the world and the fourth most common cause of cancer-related mortality worldwide, causing 600 000 deaths per year.[1,2] HCC is the main primary malignancy in the liver, developing within the context of cirrhosis in 80−90% of cases, thereby influencing a therapy decision and outcome.[3,4] Transcatheter arterial chemoembolization is the standard care for patients within the intermediate stage having a well-preserved liver function, multinodular tumors but without vascular invasion or extrahepatic spread. However, the recommended treatment for patients with locally advanced/metastatic disease or vascular invasion is Sorafenib (SFB), which is a multikinase inhibitor reducing cell proliferation and angiogenesis.[5,6] Sorafenib administration is associated with several complications, such as tiredness, diarrhea, skin irritations, hand-foot syndrome (redness, pain, inflammation, and blisters on palms or soles), hypertension, bleeding, weight loss, infections, peripheral nerve sensory disorders, and laboratory abnormalities (hypophosphatemia, hyperamylasemia, lipase). These adverse side effects arise from its lack of cell specificity and water insolubility, making it necessary to administer high doses to ensure an effective treatment but which, in most cases, results in the reduction or suspension of the treatment.[7] Therefore, the search for alternative approaches that allow the use of Sorafenib with minimal or no toxic side effects is a standing area of interest in modern oncology. The advent of nanomedicine, whose ultimate aim is to transport a sufficient quantity of active substances across physiological barriers and to reach, selectively, target diseased tissues has had a significant impact in this field.[8−10]

A number of nano- and microparticle-based approaches are being developed for targeting Sorafenib to HCC. These include liposomes,[11] polymeric nanoparticles,[12,13] mesoporous nanoparticles,[14−16] core−shell microcapsules,[17,18] liquid crystalline nanoparticles,[19] solid lipid nanoparticles,[20−23] and neutral amphiphilic cyclodextrin-based nanocomposites.[24] However, molecular-based micelles loaded with Sorafenib

Received: December 31, 2020
Accepted: May 26, 2021

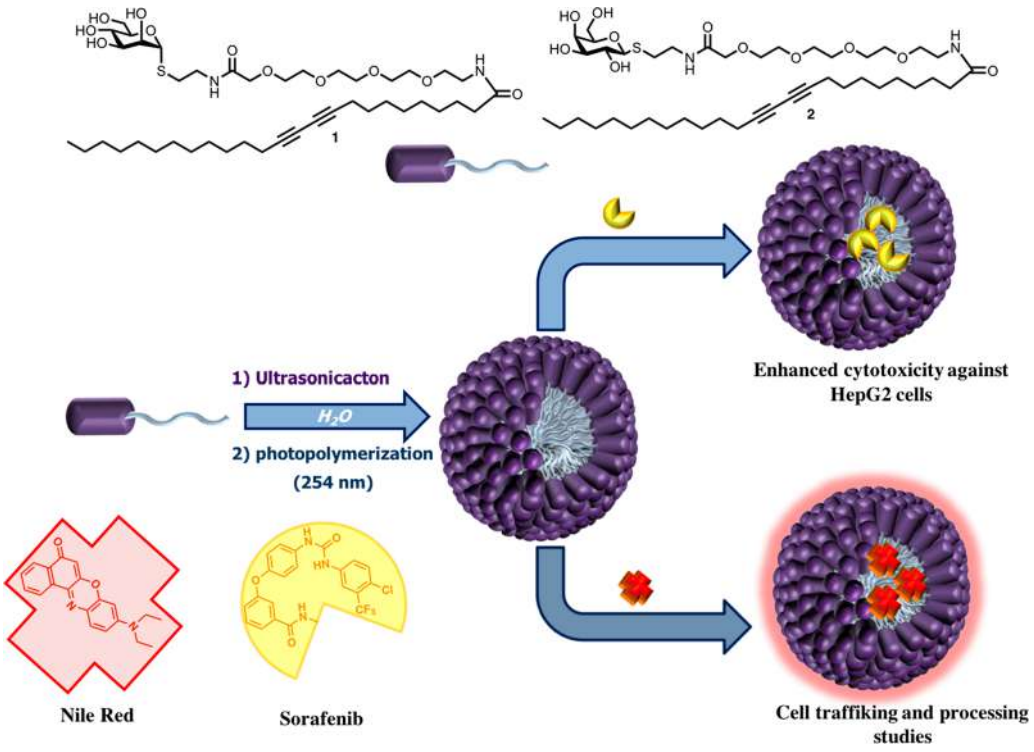

Figure 1. Schematic representation of the formation of photopolymerized (1) mannose- and (2) galactose-coated micelles with the capabilities of targeting mannose and asialoglycoprotein receptors present in HCC cells.

have not been investigated yet. Additionally, while most reported approaches are based on passive targeting, it has recently been shown that it is less adequate to reduce the side effects of antitumor compounds compared to active targeting, which is based on the programming of a nanoparticle by binding a ligand, which interacts selectively with cell surface receptors.[25] That is why finding new, specific, overexpressed biological targets with respect to normal cells, with a high endocytic efficiency and little tendency to suffer mutations, is of utmost importance in nanomedicine. One major receptor for such targeting is the asialoglycoprotein receptor (ASGPR),[26,27] which is found predominantly on hepatocytes and HCC and minimally in nonhepatic cells.[28] Notably, ASGPR belongs to the recycling receptor group and is endocytosed and recycled constitutively approximately every 15 min, with or without the ligands.[29] Another important receptor present on the hepatic cells is the mannose receptor (MR) (CD206), whose significance on the pathology of hepatic cancer is poorly understood. CD206, also a C-type lectin, is expressed on the surface of macrophages and some subsets of immature dendritic cells.[30] CD206 participates in antigen presentation and macrophage endocytosis and is considered a hallmark of tumor-associated macrophages.[31] A recent clinical study has shown an increased CD206 expression in liver cancer samples compared with healthy adjacent liver tissue and that increased MR expression was significantly associated with tumor size and metastasis, making MR an attractive receptor for targeting HCC.[32]

On the basis of these premises, we hypothesize that, beside ASPGR, MR may also be a significant target for targeting HCC. For this, the present study deals with the incorporation of Sorafenib into active drug delivery systems functionalized with mannose (Man) and galactose (Gal) ligands known for their selectivity toward MR and ASGPR, respectively. For the design of these nanocarriers, we took also into account the low affinity (generally in the millimolar range), which characterizes protein-carbohydrate interactions, by organizing the ligands into multivalent structures or glycoclusters,[33] known to enhance the affinity through the so-called "cluster glycoside effect".[34] Of the two strategies usually followed for the synthesis of functionalized multivalent nanosystems with varied morphologies, namely, the covalent and supramolecular approaches, we chose the latter due to its capacity to access multivalent nanosystems with a varied topology, composition, and assembly dynamics in a single step.[35]

Micelles, and more particularly polymeric micelles, are currently among the most efficient drug delivery systems; some of which have already been translated to the clinic, and others are at advanced clinical trials.[36] However, the use of micelles derived from amphiphilic derivatives with a low molecular weight has met little success because of their sensitivity to dilution. Consequently, the development of approximations that solve this problem are highly necessary for the use of these attractive nanomedicine systems. One solution would be, in the case of systems with an inadequate critical micelar concentration (CMC), to freeze the system by inhibiting the micelle-monomer equilibrium. Among the most designated compounds for this, diacetylene amphiphiles occupy a prominent place. Indeed, these compounds can be polymerized, via a 1,4-addition reaction, by a simple UV irradiation or thermal stimulus. This polymerization, which can take place within different supramolecular structures, has been used to obtain functional polydiacetylene nanomaterials (PDA),[37] including micelles,[38] with improved stability and interesting chromatic properties.[39]

Here, we report the synthesis of mannose and galactose-coated static micelles **pMicMan** and **pMicGal** from diacetylene-derived mannopyranosyl and galactopyranosyl glyco-

https://doi.org/10.1021/acsabm.0c01679
ACS Appl. Bio Mater. XXXX, XXX, XXX−XXX

Scheme 1. Synthesis of Self-Associative Galactose Amphiphile Monomer 2[a]

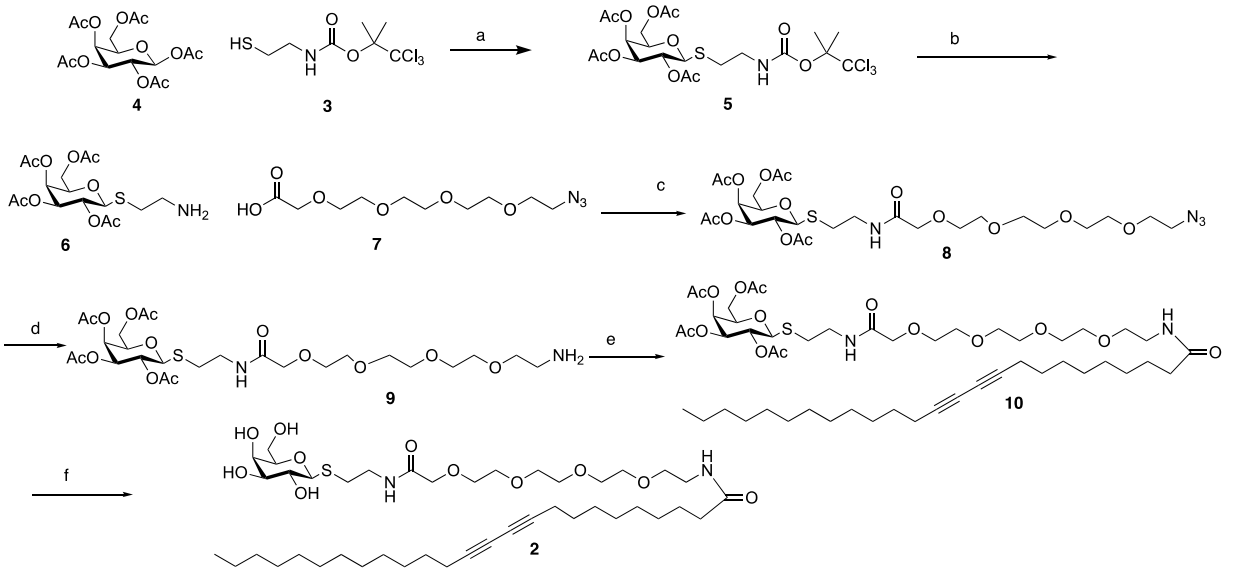

[a](a) $BF_3{\cdot}Et_2O$, CH_2Cl_2, 70%; (b) AcOH, Zn, CH_2Cl_2, 72%; (c) DIPEA, TBTU, DMF, 92%; (d) SnCl2, PhSH, NET_3, THF, 52%; (e) pentacosadiynoic acid, DIPEA, TBTU, DMF, 62%; (f) MeONa, MeOH, Amberlite IR 120 H+, quantitative yield.

lipids **1** and **2** (Figure 1), respectively. The first comparison of their ability as selective theranostic nanocarriers for HCC has been assessed. The structure and size of the obtained glyconanocarriers have been investigated by nuclear magnetic resonance (NMR), transmission electron microscopy (TEM), and dynamic light scattering (DLS). Next, we also addressed **pMicMan** and **pMicGal** trafficking through endosomes and autophagosomal processing and the impact of these micelles on the pro-apoptotic and antiproliferative properties of Sorafenib.

EXPERIMENTAL SECTION

Full details for the synthesis and characterization of the self-associative monomers **1** and **2** are given in the Supporting Information.

Synthesis of Nanomicelles pMicMan and pMicGal. The synthesis of the micelles was performed following a standard method.[38] Briefly, the self-associative monomer **1** or **2** was dissolved in milli-Q water at a higher concentration *n* than its CMC and sonicated with a sonication probe for 30 min in the total absence of light. The clear colloidal solution obtained was then subjected to irradiation at 254 nm for 1 h using a UV lamp, in order that the photopolymerization of the diyne derivatives to give the polydiacetylene adduct took place.

Incorporation of Sorafenib to Nanomicelles. **pMicMan** and **pMicGal** were loaded with Sorafenib at low and high concentrations leading to **pMicMan-SFB** and **pMicGal-SFB**. Convenient amounts of Sorafenib or Nile red (N3013, Sigma-Aldrich) were added to the polymerized micelles and left for 24 h under stirring at 54 °C. The amount of loaded Sorafenib was half that of the monomer in high-loaded nanovectors. The amount of drug was 10 times less than monomer in low-loaded nanovectors. After the completion of the procedure, excess of the drug was removed from micelles by centrifugation twice at 92*g* for 20 min. Supernatant containing loaded micelles was lyophilized and frozen at −80 °C.

Quantification of Sorafenib by HPLC. Sorafenib was quantified using a liquid chromatography-tandem mass spectrometry (LC-MS/MS) method.[40] Separation was performed on a Pursuit XRs Ultra C18 analytical column (2.8 μm, 100 mm × 2.0 mm) (546695, Agilent Technologies). The mobile phase consisted of a mixture of acetonitrile with 0.1% formic acid (1.59002.2500, EMD Millipore Corporation) (80/20 vol/vol organic/aqueous). [^{13}C, $^{2}H_3$] Sorafenib and [^{13}C, $^{2}H_3$] Sorafenib *N*-oxide standards were obtained from Alsachim (Shimadzu Group Company). The standard curves were highly linear over the range of 1−10.00 ng/mL.[40]

Assessment of Time-Course Spontaneous Sorafenib Release from pMicMan and pMicGal. The time-course drug release from Sorafenib-containing nanomicelles diluted in culture medium was assessed in a D-tube Dialyzer Midi (71506-3, EMD Millipore Corporation) in continuous agitation at 37 °C. The conditions were established in order to mimic an in vitro experimental environment. We collected samples at 0, 0.25, 0.5, 1, 6, 12, and 24 h. The remaining Sorafenib content was obtained after a treatment of nanomicelles with dimethyl sulfoxide (DMSO). The drug was extracted from the aqueous medium using acetonitrile.

Measurement of Endosomal Incorporation. Hepatocyte isolation was based on the two-step collagenase procedure.[41] FM 1−43 membrane probe is an excellent reagent for investigating the mechanisms of endocytic-dependent activity. Cells were incubated with FM1−43 (4 μM) (T3163, Thermo Fisher Scientific) for 30 min. The inhibition of endocytic activity was performed using cytochalasin D (8 μM) (C2618, Sigma-Aldrich) and dynasore (80 μM) (324410, Sigma-Aldrich) diluted in DMSO. The inhibitors were added 10 min before nanomicelles administration. The coverslips were washed for 5 min with a basal Locke solution containing 140 mM NaCl, 10 mM 4-(2-hydroxyethyl)-1-piperazineethanesulfonic acid (HEPES), 3 mM KOH, 2 mM $CaCl_2$, 1 mM $MgCl_2$, and 10 mM glucose. The pH of the solution was adjusted to 7.3 with NaOH. The fluorescence was measured with an Axiovert 200 inverted fluorescent microscope (Zeiss) equipped with a standard filter set for FM1−43 dye (XF115-2; Omega Optical). Images were captured with an ORCA-R2 CCD camera (Hamamatsu Photonics) controlled by HCImage software (Hamamatsu Photonics). Time-lapse images were acquired at a rate of 0.5 Hz, 1344 × 1024 pixels (binned 1 × 1), with an exposure time of 200 ms.

Measurement of pMicMan and pMicGal Trafficking. Nile red, which has been mainly used for studying lipid droplets, has also given useful information about the endosomal and lysosomal processing of Nile red-containing compounds. The presence of nanoparticles in different cellular compartments was evaluated using endosomal (anti-EEA1, E7659, Sigma-Aldrich), lysosomal (anti-Lamp1, L1418, Sigma-Aldrich), and autophagosome (anti-BECN-1, sc-48341, Santa Cruz Biotechnology) markers by an immunofluorescence costaining procedure. Cells were incubated with nanomicelles-containing Nile red for 6 h at 4 and 37 °C. The secondary antibodies used were Alexa

https://doi.org/10.1021/acsabm.0c01679
ACS Appl. Bio Mater. XXXX, XXX, XXX−XXX

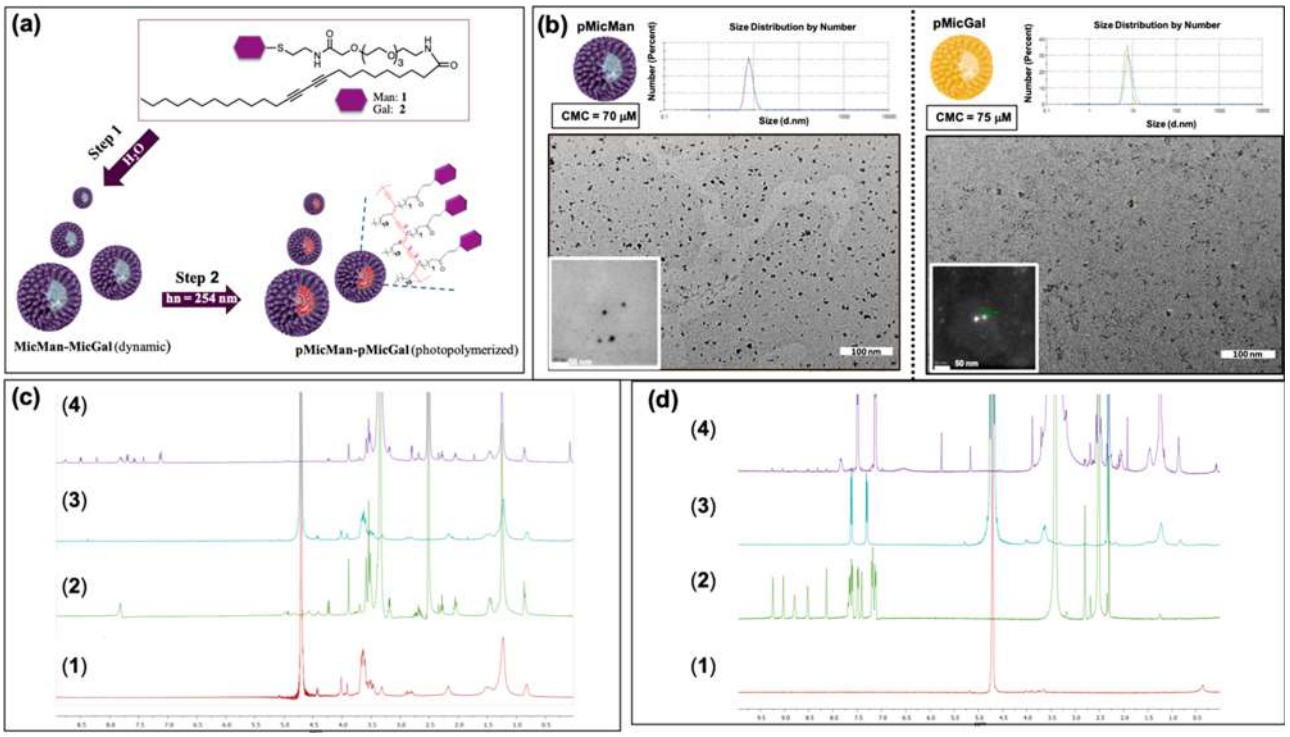

Figure 2. Micelle synthesis and structural and functional characterization. (a) Procedure for the synthesis of dynamic (**MicMan** and **MicGal**) and photopolymerized (**pMicMan** and **pMicGal**) nanomicelles. (Step 1) Sonication-promoted supramolecular self-assembly of the neoglycolipids into dynamic micelles (**MicMan** and **MicGal**) in water. (Step 2) Intermolecular photopolymerization of the neoglycolipid into homogeneous static micelles (**pMicMan** and **pMicGal**). (b) Size distribution of static micelles **pMicMan** and **pMicGal** determined by DLS and TEM; inside the TEM images are high-resolution STEM images. (c) ^{1}H NMR study of the inclusion of **SFB** within the sheltered hydrophobic part of **pMicGal**. (1) Empty **pMicGal** registered in D_2O, (2) **pMicGal** registered in DMSO-d_6, (3) inclusion complex **pMicGal-SFB** registered in D_2O, (4) inclusion complex **pMicGal** registered in DMSO-d_6. (d) ^{1}H NMR study of the inclusion of **SFBTs** within the sheltered hydrophobic part of **pMicMan**. (1) **SFBTs** registered in D_2O, (2) **SFBTs** registered in DMSO-d_6, (3) inclusion complex **pMicMan-SFBTs** registered in D_2O, (4) inclusion complex **pMicMan-SFBTs** registered in DMSO-d_6.

555 (A-21428, Thermo Fisher Scientific) and Alexa 488 (A-11001, Thermo Fisher Scientific). A mounting medium containing ProLong Gold antifade reagent with 4′,6-diamidino-2-phenylindole (DAPI) (P36935, Thermo Fisher Scientific) was used to stain the core. A Leica TCS-SP2 spectral laser scanning confocal microscope (Wetzlar) was used.

Inhibition of Autophagolysosomal Processing in pMicMan-SFB and pMicGal-SFB. The impact of the autophagolysosome processing of **pMicMan-SFB** and **pMicGal-SFB** was assessed using chloroquine (50 μM) (C6628, Sigma-Aldrich) that prevents the acidification of the lysosomes, and 3-methyladenine (3Me-A) (5 μM) (M9281, Sigma-Aldrich) that inhibits class I and III PI3K and autophagolysosome generation. The inhibitors were added 2 h before Sorafenib.

RESULTS AND DISCUSSION

Synthesis and Characterization of pMicMan and pMicGal Nanomicelles. The synthesis of the starting thiomannopyranoside monomer **1** was done in four synthetic steps as in our previously published method starting from 2-aminoethyl thiomannoside, itself obtained in one step from mannose pentaacetate.[38,42] For the synthesis of thiogalactopyranoside amphiphile **2**, a new route was developed. To ensure the needed β-stereoselectivity, we followed the method reported by Gildersleeve, Dahmén, and co-workers,[43] for the thioglycosylation step. The $BF_3{\cdot}Et_2O$-catalyzed thioglycosylation using 1,1-dimethyl-2,2,2-trichloroethyl *N*-(2-mercaptoethyl)carbamate **3** as a glycosyl acceptor and galactose penta-acetate **4** as a glycosyl donor afforded the corresponding β-thioglycoside **5** in 70% isolated yield. Next, the treatment of the chlorinated derivative **5** with zinc in the presence of acetic acid using dichloromethane as solvent yields the desired 2-aminoethylthioglycoside **6**, Scheme 1. Amide bond formation with the bifunctional spacer **7**, obtained in three steps from tetraethylene glycol (TEG), using 2-(1*H*-benzotriazole-1-yl)-1,1,3,3-tetramethylaminium tetrafluoroborate (TBTU) as an activating agent and *N*,*N*-diisopropylethylamine (DIPEA) as a base in dimethylformamide (DMF), afforded the azido derivative **8** in 92% yield. Subsequent reduction of the azido group with thiophenol and tin chloride, followed by an amide coupling of the resulting amine **9** with pentacosadiinoic acid (PCDA) gave the desired neoglycolipid **10** in good yield. A Zemplen deacetylation led to the desired galactose derivative **2** in quantitative yield (Scheme 1).

Once the monomers **1** and **2** were obtained and characterized by means of monodimensional (^{1}H, ^{13}C) and bidimensional (COSY and HETCOR) NMR and mass spectroscopies (see the Supporting Information), the corresponding CMCs were determined by fluorescence using pyrene as a probe (see the Experimental Section).[44] The CMC of **1** was determined as 70 ± 5 μM, while that of **2** was 75 ± 5 μM. Next, the spontaneous self-association of monomers **1** and **2** in water to form the corresponding micelles and their subsequent characterization were performed. The first step for the formation of the two designed directing systems consists in the dispersion of the starting monomers **1** and **2** in distilled water at concentrations higher than their

https://doi.org/10.1021/acsabm.0c01679
ACS Appl. Bio Mater. XXXX, XXX, XXX−XXX

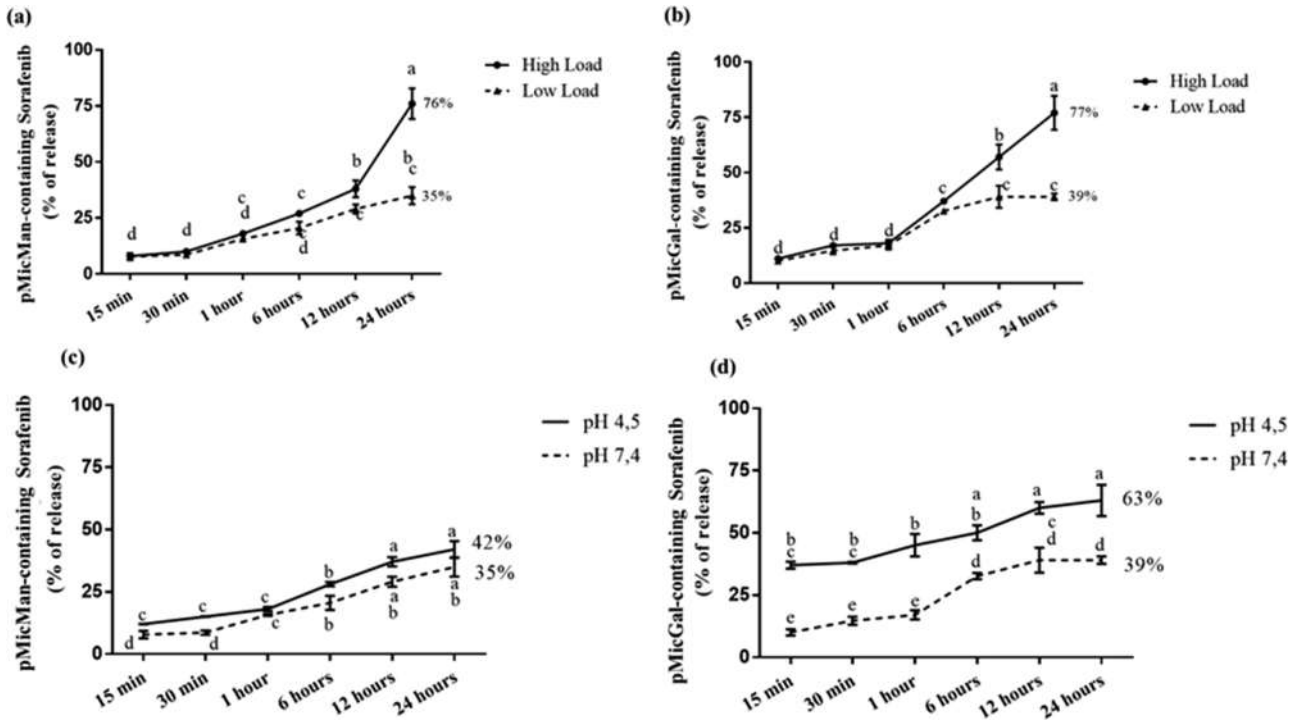

Figure 3. Kinetic in vitro release of Sorafenib at high and low loads of **pMicMan** (a) and **pMicGal** (b). At low load and at pH 7.4 vs 4.5 of **pMicMan** (c) and **pMicGal** (d). Sorafenib was measured by using LC-MS/MS. Data are expressed as mean ± standard error of measure of independent experiments (n = 6). The groups that were significantly different ($p \leq 0.05$) were indicated with different letters (a, b, c, or d).

CMCs, followed by probe sonication. The dynamic systems **MicMan** and **MicGal** thus obtained (Figure 2a) were then dialyzed against deionized water for 48 h in order to remove the unassociated monomers **1** and **2**. The second step of the synthetic sequence consists in the UV irradiation (254 nm) for 3 h, which allows the photopolymerization of self-organized monomers giving rise to the final polydiacetylenic-based micelles (**pMicMan** and **pMicGal**). This polymerization, the exact mechanism of which is not yet fully known, is due to the ability of amphiphilic diacetylenic derivatives to associate spontaneously in a highly ordered manner. As a result of this photopolymerization and the subsequent formation of the conjugated polydiacetylenic backbone, the obtained micelles are no longer in dynamic equilibrium and are, therefore, more stable toward external conditions such as dilution, for example. In addition, and unlike other nanometric systems obtained by polymerization, which require the use of a generally toxic and difficult to remove catalyst, the nanomicelles **pMicMan** and **pMicGal** are obtained in a pure manner without the need of further purification steps. Once obtained, the determination of their sizes and morphologies were performed by DLS and TEM measurements (Figure 2b). The size distribution histogram determined by DLS in an aqueous solution gives a multimodal distribution with hydrodynamic diameters of 8 and 8.2 nm for **pMicMan** and **pMicGal**, respectively, with a narrow size distribution (polydispersion index (PDI) less than 0.3, Figure 2b). The results of the analysis of the morphology of **pMicMan-pMicGal**, visualized by TEM, confirms that the neoglycolipids **1** and **2** self-assemble in water into spherical micelles whose sizes are adequate for an effective intracellular drug delivery (vide infra) and deep penetration within the tumor.

Sorafenib's Loading Capacity and Efficiency of pMicMan and pMicGal Nanomicelles. The obtained **pMicMan** and **pMicGal** micelles are endowed with a hydrophobic cavity, which can acts as a refuge for scarcely water-soluble molecules such as Sorafenib. For the formation of the inclusion complexes, we followed the method of stirring and heating without adding any organic solvent. After centrifugation and lyophilization, the amount of Sorafenib incorporated was determined by the difference in mass between the loaded micelle and the empty micelle, as well as by high-performance liquid chromatography (HPLC). The drug loading capacity (DLC) and drug loading efficiency (DLE) of both nanocarriers were calculated from the following eqs 1 and (2).

$$\mathrm{DLC}(\%) = \frac{\text{weight of loaded SFB}}{(\text{weight of Mic} + \text{weight of loaded SFB})} \times 100 \quad (1)$$

$$\mathrm{DLE}(\%) = \frac{\text{weight of loaded SFB}}{\text{weight of input SFB}} \times 100 \quad (2)$$

pMicMan presents a maximum DLC of 63% and a DLE of 50% for Sorafenib. Similarly, **pMicGal** presents a maximum DLC of 42% and DLE of 43%. However, we found that a sustainable controlled release can be achieved using a lower loading capacity, 18% for **pMicMan** and 13% for **pMicGal**. An additional confirmation that the drugs are actually encapsulated by the micelles was obtained by a ^{1}H NMR analysis, as shown in Figure 2c using **pMicGal** as a sheltered hydrophobic nanocarrier. ^{1}H NMR spectra of empty **pMicGal** micelles, loaded **pMicGal-SFB** micelles, and free Sorafenib were recorded in D_2O and in deuterated dimethyl sulfoxide (DMSO-d_6) (Figure 2c). As shown in Figure 2c1,c2, the spectra of the empty micelles in D_2O and DMSO-d_6 contain basically the signals, corresponding to the self-associated

https://doi.org/10.1021/acsabm.0c01679
ACS Appl. Bio Mater. XXXX, XXX, XXX−XXX

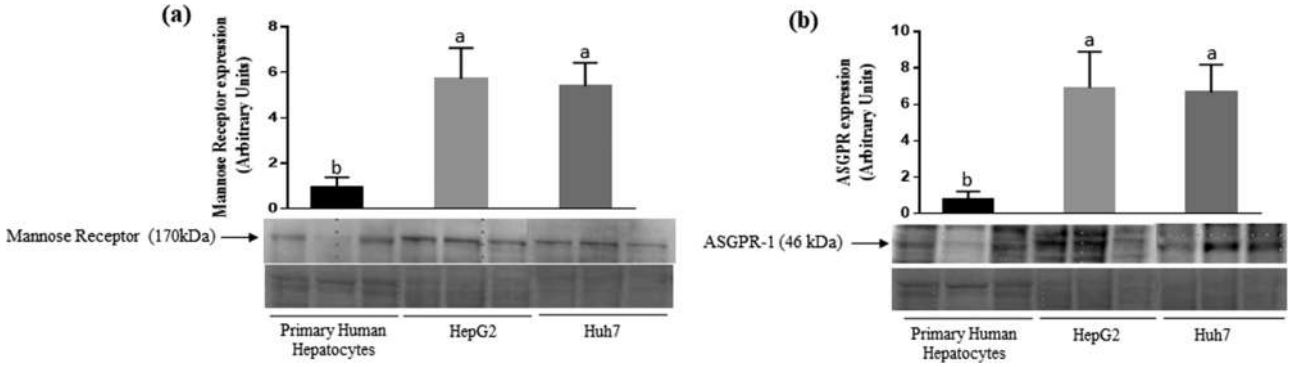

Figure 4. Expression of mannose (a) and asialoglycoprotein (b) receptors (MR and ASGPR, respectively) in primary human hepatocytes and HepG2 cells. Three independent cell batches of human primary hepatocytes and HepG2 were used. The expression of MR and ASGPR was evaluated by a western blot analysis as described in the Material and Methods. Protein expression was normalized to total protein content following Stain-Free technology. Data are expressed as mean ± standard error of measure of independent experiments (n = 3). The groups significantly different ($p \leq 0.05$) were indicated with different letters (a or b).

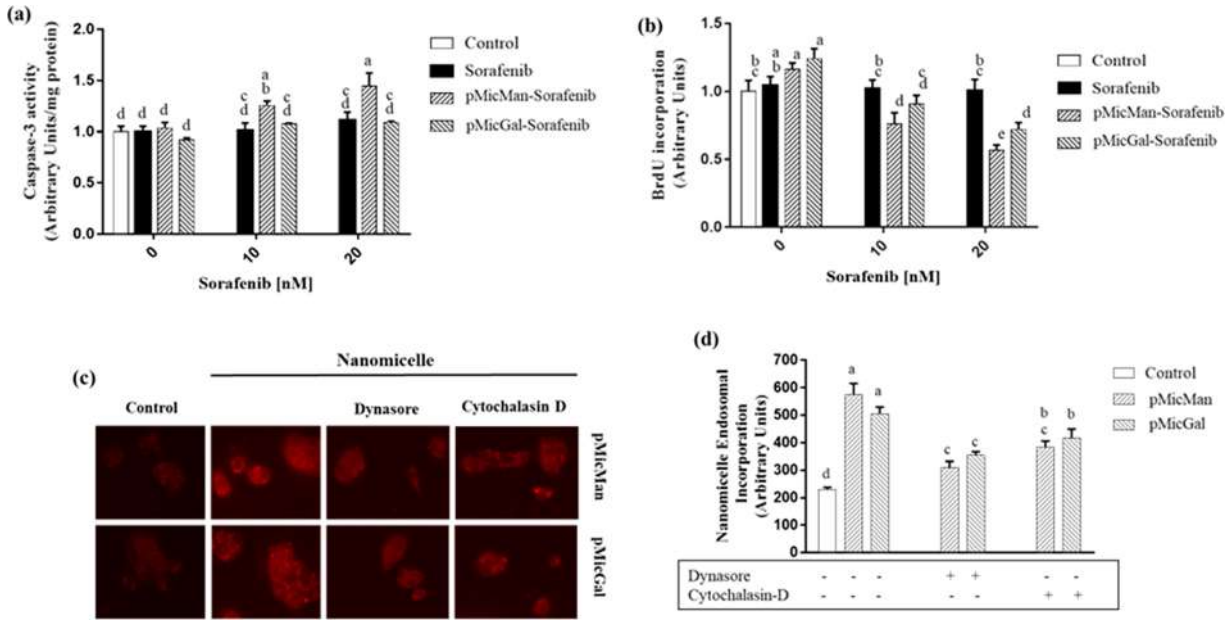

Figure 5. Apoptosis of HepG2 cells and intracellular incorporation of nanomicelles. Induction of caspase-3 (a) and reduction of cell proliferation (b) by nonvectorized Sorafenib and pMicMan- and pMicGal-containing Sorafenib in HepG2 cells. (c) Endosomal incorporation of pMicMan and pMicGal by immunofluorescence using FM 1−43-containing nanomicelles. (d) Endosomal incorporation was reduced using dynasore (80 μM) or cytochalasin D (8 μM) preincubation for 10 min. Data are expressed as mean ± standard error of measure of independent experiments (n = 8). The groups significantly different ($p \leq 0.05$) were indicated with different letters (a, b, c, or d).

monomer **2**. The spectrum of the micelles loaded with Sorafenib **pMicGal-SFB** registered in D_2O is very similar to that of the empty micelles (Figure 2c3), without any characteristic signal of Sorafenib. However, when recording the spectrum of the micelles charged with Sorafenib in DMSO-d_6 (Figure 2c4), additional signals in the aromatic zone that match the spectrum of Sorafenib were observed along with the signals from the micelle. Even more indicative of the capacity of these nanomicelles to encapsulate Sorafenib were the experiments performed with Sorafenib tosylate (**SFTs**) with both vectors. As an illustrative example, Figure 2d collects the results with the nanovector **pMicMan** and **SFTs**. The difference observed in this case compared with that of the inclusion of Sorafenib in **pMicGal** is the appearance of an AB system in the aromatic zone when the spectrum is taken in deuterated water (compare Figure 2c3,d3). This system, which corresponds to the aromatic protons of the tosyl group, clearly indicates that the micelles are capable of dissociating SFB from the tosylate counterions. Taken all together, these results clearly show the ability of micelles to function as nanocontainers to store highly hydrophobic compounds inside their sheltered hydrophobic area.

Stability Studies and Sorafenib Release Capacity in Culture Medium at Different pH of pMicGal and pMicMan Nanomicelles. One of the main drawbacks in using micelles formed by a self-association of low molecular weight monomers, as DDS, is their instability in general and toward dilution in particular. Stability studies conducted on **pMicGal** and **pMicMan** have shown that these micelles remain stable for at least one week in deionized water and in diluted solutions (Figures S8 and S9 in the Supporting Information). The micelles are also stable in physiological medium (Dulbecco's Modified Eagle's Medium (DMEM) 10% fetal bovine serum (FBS)), generally used to emulate stability in

https://doi.org/10.1021/acsabm.0c01679
ACS Appl. Bio Mater. XXXX, XXX, XXX−XXX

vivo, with a slight increase in size from 8.2 to 9.5 nm in the case of **pMicGal** (Figure S9 in the Supporting Information). Release studies in a culture medium conducted on **pMicMan-SFB** with high and low loading show that these micelles released 76% and 35%, respectively, of their cargo after 24 h (Figure 3a). In the same conditions, the **pMicGal-SFB** samples were able to release 77% and 39% of their drug content to the culture medium (Figure 3b). We previously showed that the induction of endoplasmic reticulum (ER) stress by Sorafenib (10 μM) was related to an increase in apoptosis and reduced cell proliferation in HepG2 cells.[45] Thus, we conducted a Sorafenib release study in an acidic medium (at pH = 4.5) of **pMicMan-SFB** and **pMicGal-SFB**. In these conditions, which emulate the expected acidity in the autophagolysosomes, an increase of Sorafenib release was observed (Figure 3c,d, respectively).

Expression of Mannose and Asialoglycoprotein Receptors on Primary Hepatocytes and HepG2 Cells. As stated before, while there are a number of DDS targeting liver cancer through the asialoglycoprotein, no studies have evaluated mannosylated DDSs against HCC cells.[46] Besides, the incidence of the MR in liver diseases is generally poorly known, suggesting a weak expression of this receptor on liver cells. Therefore, before testing our mannosylated and galactosylated nanomicelles, we, first, conduct a quantification study on the expression of ASGPR and MR on primary hepatocytes and HepG2 cells. This study confirmed that MR (Figure 4a) and ASGPR (Figure 4b) are expressed in primary human hepatocytes and HepG2 cells. Interestingly, the expression of MR appeared greater than ASGPR expression in HepG2 versus primary human hepatocytes.

Proapoptotic and Antiproliferative Studies. The proapoptotic and antiproliferative studies of the prepared nanopharmaceuticals were conducted with a low loading of **pMicMan-SFB** and **pMicGal-SFB** by measuring the induction of caspase-3 and the reduction of cell proliferation, Figure 5. Satisfyingly, the administration of **pMicMan-SFB**, but not **pMicGal-SFB**, at 10 and 20 nM was able to increase caspase-3 (Figure 5a) or reduce cell proliferation (Figure 5b) in HepG2. Interestingly enough, nonvectorized Sorafenib did not increase cell death or alter cell proliferation in the nanomolar range in HepG2 cells ($p \leq 0.05$). It is worth mentioning that, in most studies reported, vectorized Sorafenib is active at a much higher concentration, that is, in the micromolar range. The major activity of the **pMicMan**-incorporated Sorafenib was related to increased endosomal incorporation (Figure 5c,d).

In view of these results, the scope of the sugar-coated micelles targeting other hepatic cells was evaluated. For this purpose, we submitted Huh7 cells to the same protocol and determined the caspase-3 activity under Sorafenib (10 and 20 nM) treatment either alone or incorporated to pMicMan or pMicGal, Table 1. As shown in Table 1, the administration of Sorafenib in **pMicMan** exerts a more potent proapoptotic effect than when incorporated to **pMicGal**. Interestingly, these results are in accordance with those obtained with HepG2 cells and support the HCC cell-targeting efficiency of the reported sugar-coated micelles.

Trafficking of pMicMan and pMicGal in HepG2 Cells. Cells are able to take up macromolecules from the surrounding medium by endocytosis either through a receptor-mediated endocytosis in clathrin-coated pits, generating clathrin-coated vesicles (CCV), or through clathrin-independent endocytosis pathways based on the invaginations at caveolae.[46] The

Table 1. Caspase-3 Activity Induced by Sorafenib (10 and 20 nM) Either Alone or Incorporated to pMicMan or pMicGal Vectors[a]

	0 nM	10 nM	20 nM
control	1.00 ± 0.090^{c}		
Sorafenib	1.01 ± 0.080^{c}	1.00 ± 0.010^{c}	1.03 ± 0.080^{c}
pMicMan-SFB	1.04 ± 0.090^{c}	1.20 ± 0.010^{b}	1.34 ± 0.012^{a}
pMicGal-SFB	1.06 ± 0.045^{c}	1.070 ± 0.011^{c}	1.09 ± 0.012^{c}

[a]Caspase-3 (Arbitrary Units/mg protein) was measured as described in Material and Methods. Data are expressed as mean ± standard error of measure of independent experiments (n = 8). The groups significantly different ($p \leq 0.05$) were indicated with different letters (a, b, or c).

formation and internalization of clathrin-coated pits involves the participation of F-actin cytoskeleton,[47] and the process of CCV formation is energy-dependent and requires multiple guanosine triphosphate (GTP)-binding proteins such as dynamin.[48] The endosomal incorporation of **pMicMan** and **pMicGal** in HepG2 cells was performed by immunofluorescence using FM 1−43-containing nanomicelles (Figure 5c). The inhibition of the internalization mechanism of endocytosis was assessed by dynasore and cytochalasin D. These studies show that **pMicMan** and **pMicGal** were actively incorporated through endosomal mechanisms, their incorporation being more affected by a dynamin inhibition using dynasore than inhibition of actin polymerization using cytochalasin D (Figure 5d). The incorporation of **pMicMan** and, at lesser extent, **pMicGal** is highly affected by the use of dynasore and cytochalasin D suggesting that CCV is involved in the process of nanomicelle internalization (Figure 5).

The early endosome sorts the endocytosed material into material that will be either recycled back to the plasma membrane, secreted, or degraded by fusion with the lysosome in later steps. The incorporation of Nile Red to nanomicelles allows the evaluation of their cellular incorporation and trafficking to specific compartments using endosomal (anti-EEA1), lysosomal (anti-Lamp1), and autophagosomal (anti-BECN1) markers by immunofluorescence procedures. The endosomal incorporation of **pMicMan** and **pMicGal** was prevented at 4 °C when compared to that observed at 37 °C (Figure 6a). In addition, results showed that **pMicMan** was extensively colocalized at endosomal and lysosome levels, while **pMicGal** was extensively colocalized at an autophagolysosomal level in relation to the corresponding counterparts (6 h) in HepG2 (Figure 6b).

Impact of Lysosomal-Dependent Processing of pMicMan-SFB and pMicGal-SFB in Their Proapoptotic Properties. The effects of chloroquine on caspase-3 activity was assayed in Sorafenib (20 nM)-containing nanomicelles (Figure 7). Chloroquine prevents the acidification of the lysosomes and consequently protein degradation,[49] which can additionally involve the blockage of the late step of macroautophagy. Interestingly, it has been proposed that this blockage is at the basis of the inhibitory effect of chloroquine and hydroxychloroquine on the severe acute respiratory syndrome coronavirus 2 (SARS-CoV2) coronavirus, responsible of the current coronavirus disease of 2019 (COVID-19) pandemic.[50] The obtained data showed that chloroquine increased the caspase-3 activity (Figure 7) in cells treated with **pMicMan-SFB** and **pMicGal-SFB** (20 nM). These data suggest that both nanovectors are active intracellularly and

https://doi.org/10.1021/acsabm.0c01679
ACS Appl. Bio Mater. XXXX, XXX, XXX−XXX

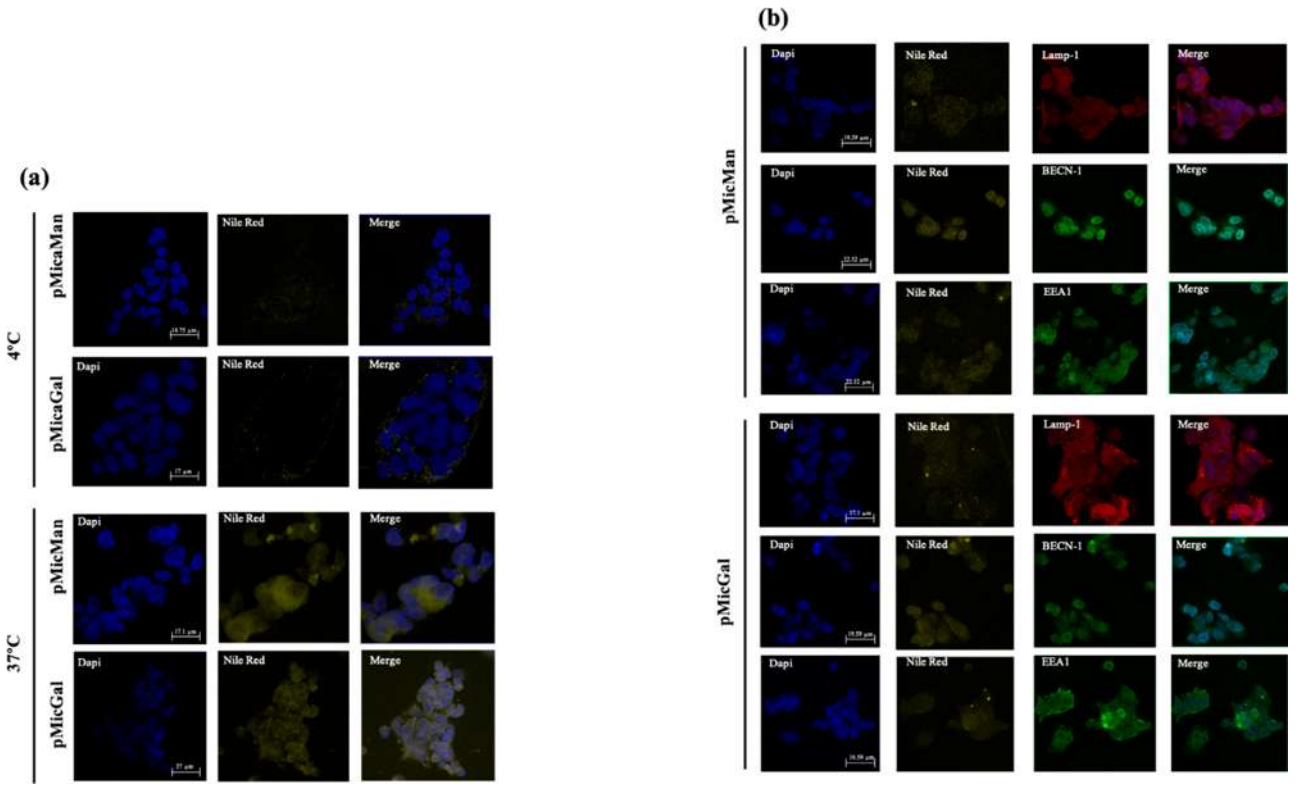

Figure 6. Trafficking of **pMicMan** and **pMicGal**. Nile red was used to give information regarding endosomal and lysosomal processing. The incubation of cells at 4 °C blocked nanomicelle incorporation (a). The presence of nanoparticles in different cellular compartments were evaluated using endosomal, lysosomal, and autophagosome markers by immunofluorescence costaining procedures (b). The procedures for probe incorporation and immunofluorescence are described in the Experimental Section. Images are representative of six independent experiments (n = 5). Magnification ×60.

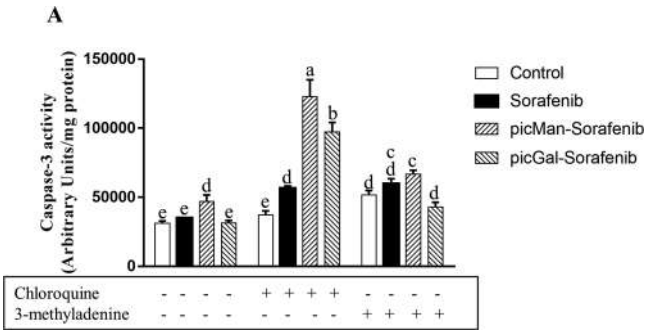

Figure 7. Role of lysosome in **pMicMan** and **pMicGal** processing through caspase-3 activity. Cells were incubated with chloroquine (50 μM) 2 h before the administration of **pMicMan** and **pMicGal** containing Sorafenib (20 nM). Caspase-3 activity was determined as described in Material and Methods. Data are expressed as mean ± standard error of measure of independent experiments (n = 6). The groups significantly different ($p \leq 0.05$) were indicated with different letters (a, b, c, or d).

degraded in HepG2 cells. The transference of nanovector-containing drugs to perinuclear lysosomes promotes an acceleration of increased rate of drug intracellular release.[51] In this sense, the reduction of pH from 7.4 to 4.5 induced the in vitro release of Sorafenib in **pMicMan** and **pMicGal** (Figure 3c,d).

CONCLUSION

In summary, we have reported the synthesis of two glycosylated nanomicelles coated with mannose and galactose designed for the active targeting of Sorafenib to HCC through MR and ASGPR. The presence of a diyne group in the hydrophobic tail of the starting self-associative neoglycolipids allows the stabilization of the nanomicelles facing dilution, by simple irradiation at 254 nm, without the need for any catalyst or initiator, facilitating the purification of the nanovectors. The spherical-static nanomicelles obtained have shown a great capacity for trapping Sorafenib, thus considerably increasing its solubilization in water, one of the current problems in the clinical application of this drug. Studies have confirmed that both systems are capable of internalizing into HepG2 hepatic cells by endocytosis, releasing their cytotoxic load in the cytoplasm and producing cell death by apoptosis. Interestingly, our study has shown, for the first time, that the incorporation of Sorafenib into a nanovector targeting MR, **pMicMan**, gives better results than its incorporation into a nanovector targeting the ASGPR generally used to target nano drugs to the HCC cells. Indeed, **pMicMan-SFB** increases the endosomal incorporation and the intracellular concentration of Sorafenib, which promotes apoptosis and reduces cell proliferation at a low concentration (10−20 nM). At the same concentration (10−20 nM), nonvectorized Sorafenib was inactive when administered in HepG2 cells. The study also showed that a release at an acidic pH could lead to the degradation or hydrolysis of Sorafenib—a urea-based compound—and reduce the efficiency of the nanosystems. Therefore, it could be that a low incorporation and rapid lysosomal degradation affect the efficacy of **pMicGal-SFB**. Although more studies are needed, our results constitute a proof of principle on the use of MR as an attractive entry to target liver disease and mannose-coated

https://doi.org/10.1021/acsabm.0c01679
ACS Appl. Bio Mater. XXXX, XXX, XXX−XXX

nanomicelles as excellent nanovectors to do so. In addition, the ease of synthesis of the reported nanomicelles will allow their production on a large scale, while their small size will facilitate their deep penetration into cancerous tissue.

■ ASSOCIATED CONTENT

Supporting Information

The Supporting Information is available free of charge at https://pubs.acs.org/doi/10.1021/acsabm.0c01679.

Experimental details for the synthesis and characterization of compounds **1** and **2**. Characterization of the nanoparticles, ^{1}H and ^{13}C NMR spectra of **1** and **2**, TEM and STEM images of the empty and charged micelles, stability studies of the micelles, NMR study of the sorafenib tosylate inclusion in **PMicMan**, blot and gel for the quantification of MR and ASPGR (PDF)

■ AUTHOR INFORMATION

Corresponding Authors

Noureddine Khiar − *Institute of Chemical Research, CSIC/University of Seville, Seville, Spain*; orcid.org/0000-0003-4211-7138; Phone: +34 954489559; Email: khiar@iiq.csic.es

Jordi Muntané − *Hospital University "Virgen del Rocío"/CSIC/University of Seville, Institute of Biomedicine of Seville, Seville, Spain; Networked Biomedical Research Center Hepatic and Digestive Diseases, Madrid, Spain; Department of Medical Physiology and Biophysics, University of Seville, Seville, Spain*; Phone: +34-955923122; Email: jmuntane-ibis@us.es; Fax: +34-955923002

Authors

María Negrete − *Hospital University "Virgen del Rocío"/CSIC/University of Seville, Institute of Biomedicine of Seville, Seville, Spain*

Elena Romero-Ben − *Institute of Chemical Research, CSIC/University of Seville, Seville, Spain*

Alicia Gutiérrez-Valencia − *Hospital University "Virgen del Rocío"/CSIC/University of Seville, Institute of Biomedicine of Seville, Seville, Spain*

Cristian Rosales-Barrios − *Institute of Chemical Research, CSIC/University of Seville, Seville, Spain*

Eva Alés − *Department of Medical Physiology and Biophysics, University of Seville, Seville, Spain*

Teresa Mena-Barragán − *Institute of Chemical Research, CSIC/University of Seville, Seville, Spain*

Juan A. Flores − *Department of Medical Physiology and Biophysics, University of Seville, Seville, Spain*

Mª Carmen Castillejos − *Institute of Chemical Research, CSIC/University of Seville, Seville, Spain*

Patricia de la Cruz-Ojeda − *Hospital University "Virgen del Rocío"/CSIC/University of Seville, Institute of Biomedicine of Seville, Seville, Spain; Networked Biomedical Research Center Hepatic and Digestive Diseases, Madrid, Spain; Department of Medical Physiology and Biophysics, University of Seville, Seville, Spain*

Elena Navarro-Villarán − *Hospital University "Virgen del Rocío"/CSIC/University of Seville, Institute of Biomedicine of Seville, Seville, Spain; Networked Biomedical Research Center Hepatic and Digestive Diseases, Madrid, Spain; Department of Medical Physiology and Biophysics, University of Seville, Seville, Spain*

Carmen Cepeda-Franco − *Department of General Surgery, Hospital University "Virgen del Rocío"/CSIC/University of Seville/IBiS, Seville, Spain*

Complete contact information is available at: https://pubs.acs.org/10.1021/acsabm.0c01679

Author Contributions

N.K. and J.M. conceived the project. N.K. designed and supervised the synthetic part of the research and wrote the manuscript. J.M. supervised the biological assays of the manuscript and help in the redaction of the manuscript. M.N., E.N.-V., and P. de la C.-O. conducted the in vitro experiments, including the measurement of MR and AGPR expression, measurement of cell proliferation and death. E.R. and C.R. conducted the synthesis and characterization of nanovectors. C.B.-B., J.M.A.-M., A.C., and C.C.-F. were involved in the isolation and culture of primary human hepatocytes. A.G.-V. and M.N. measured Sorafenib in nanomicelles and conducted the in vitro experiments for the preparation, quantification, and release of Sorafenib in nanovectors. M.N., E.A., and J.A.F. designed the experiment for the trafficking of nanoparticles in HepG2. T.M.B. and C.C. conducted the synthesis and characterization of the self-associative monomers. All authors have given approval to the final version of the manuscript.

Author Contributions

[#](M.N., E.R.-B., N.K., and J.M.) These authors contributed equally.

Notes

The authors declare no competing financial interest.

■ ACKNOWLEDGMENTS

Financial support was provided by the Spanish Ministry of Economy and Competitiveness (CTQ2016-78580-C2-1-R, PID2020-119949RB-I00 to N.K.) and the Institute of Health Carlos III (ISCIII) (PI13/00021, PI16/00090, and PI19/01266 to J.M.) both cofinanced by the European Regional Development Fund (ERDF) from FEDER and the European Social Fund (ESF), as well by the Andalusian Ministry of Economy, Science and Innovation (P07-FQM-2774 to N.K., CV20-04221 to N.K.) and CTS-6264 to J.M.), the PAIDI Program from the Andalusian Government (FQM-313 to N.K., CV20-04221 to N.K., and CTS-0664 to J.M.), the Andalusian Ministry of Health (PI-00025-2013, and PI-0198-2016 to J.M.), and the CSIC (CSIC−COV19-047). We thank the Biomedical Research Network Center for Liver and Digestive Diseases founded by the ISCIII and cofinanced by FEDER "A way to achieve Europe" and ERDF for their financial support. The COST action CA-18132 "Functional Glyconanomaterials for the Development of Diagnostic and Targeted Therapeutic Probe" is also acknowledged. E.R.B., C.C.A., and P. de la C.-O. were supported by FPU predoctoral fellowship (FPU15/04267, FPU17/00190, and FPU17/00026) from Spanish Ministry of Education, Culture and Sports. E.N.-V. was supported by the predoctoral i-PFIS IIS-enterprise contract in science and technologies in health (IFI18/00014) from ISCiii. We thank the Centre of Research Technology and Innovation of the University of Seville for the use of TEM, AFM, and NMR facilities.

https://doi.org/10.1021/acsabm.0c01679
ACS Appl. Bio Mater. XXXX, XXX, XXX−XXX

REFERENCES

(1) Bray, F.; Ferlay, J.; Soerjomataram, I.; Siegel, R. L.; Torre, L. A.; Jemal, A. Global Cancer Statistics 2018: GLOBOCAN Estimates of Incidence and Mortality Worldwide for 36 Cancers in 185 Countries. *Ca-Cancer J. Clin.* **2018**, *68* (6), 394−424.

(2) El-Serag, H. B.; Rudolph, K. L. Hepatocellular Carcinoma: Epidemiology and Molecular Carcinogenesis. *Gastroenterology* **2007**, *132* (7), 2557−2576.

(3) Fattovich, G.; Stroffolini, T.; Zagni, I.; Donato, F. Hepatocellular Carcinoma in Cirrhosis: Incidence and Risk Factors. *Gastroenterology* **2004**, *127* (5), S35−S50.

(4) Sanyal, A. J.; Yoon, S. K.; Lencioni, R. The Etiology of Hepatocellular Carcinoma and Consequences for Treatment. *Oncologist* **2010**, *15* (S4), 14−22.

(5) Llovet, J. M.; Ricci, S.; Mazzaferro, V.; Hilgard, P.; Gane, E.; Blanc, J. F.; de Oliveira, A. C.; Santoro, A.; Raoul, J. L.; Forner, A.; et al. Sorafenib in Advanced Hepatocellular Carcinoma. *N. Engl. J. Med.* **2008**, *359* (4), 378−390.

(6) Cheng, A. L.; Kang, Y. K.; Chen, Z.; Tsao, C. J.; Qin, S.; Kim, J. S.; Luo, R.; Feng, J.; Ye, S.; Yang, T. S.; et al. Efficacy and Safety of Sorafenib in Patients in the Asia-Pacific Region with Advanced Hepatocellular Carcinoma: A Phase III Randomised, Double-Blind, Placebo-Controlled Trial. *Lancet Oncol.* **2009**, *10* (1), 25−34.

(7) Rimola, J.; Diaz-Gonzalez, A.; Darnell, A.; Varela, M.; Pons, F.; Hernandez-Guerra, M.; Delgado, M.; Castroagudin, J.; Matilla, A.; Sangro, B.; et al. Complete Response under Sorafenib in Patients with Hepatocellular Carcinoma: Relationship with Dermatologic Adverse Events. *Hepatology* **2018**, *67*, 612−622.

(8) Lu, J.; Wang, J.; Ling, D. Surface Engineering of Nanoparticles for Targeted Delivery to Hepatocellular Carcinoma. *Small* **2018**, *14*, 1−25.

(9) Sun, Y.; Ma, W.; Yang, Y.; He, M.; Li, A.; Bai, L.; Yu, B.; Yu, Z. Cancer Nanotechnology: Enhancing Tumor Cell Response to Chemotherapy for Hepatocellular Carcinoma Therapy. *Asian J. Pharm. Sci.* **2019**, *14*, 581−594.

(10) Chew, S. A.; Moscato, S.; George, S.; Azimi, B.; Danti, S. Liver Cancers: Current and Future Trends Using Biomaterials. *Cancers* **2019**, *11*, 2026.

(11) Liu, J.; Boonkaew, B.; Arora, J.; Mandava, S. H.; Maddox, M. M.; Chava, S.; Callaghan, C.; He, J.; Dash, S.; John, V. T.; Lee, B. R. Comparison of Sorafenib-Loaded Poly (Lactic/Glycolic) Acid and DPPC Liposome Nanoparticles in the in Vitro Treatment of Renal Cell Carcinoma. *J. Pharm. Sci.* **2015**, *104* (3), 1187−1196.

(12) Kim, D. H.; Kim, M. D.; Choi, C. W.; Chung, C. W.; Ha, S. H.; Kim, C. H.; Shim, Y. H.; Jeong, Y. I.; Kang, D. H. Antitumor Activity of Sorafenib-Incorporated Nanoparticles of Dextran/Poly(Dl-Lactide-Co-Glycolide) Block Copolymer. *Nanoscale Res. Lett.* **2012**, *7*, 91.

(13) Mieszawska, A. J.; Kim, Y.; Gianella, A.; van Rooy, I.; Priem, B.; Labarre, M. P.; Ozcan, C.; Cormode, D. P.; Petrov, A.; Langer, R.; et al. Synthesis of Polymer-Lipid Nanoparticles for Image-Guided Delivery of Dual Modality Therapy. *Bioconjugate Chem.* **2013**, *24* (9), 1429−1434.

(14) Zhao, R.; Li, T.; Zheng, G.; Jiang, K.; Fan, L.; Shao, J. Simultaneous Inhibition of Growth and Metastasis of Heptacellular Carcinoma by Co-Delivery of Ursolic Acid and Sorafenib Using Lactobionic Acid Modified and PH-Sensitive Chitosan-Conjugated Mesoporus Silica Nanocomplex. *Biomaterials* **2017**, *143*, 1−17.

(15) Guan, Q.; Guo, R.; Huang, S.; Zhang, F.; Liu, J.; Wang, Z.; Yang, X.; Shuai, X.; Cao, Z. Mesoporus Polydopamine Carrying Sorafenib and SPIO Nanoparticles for MRI-Guided Ferroptosis Cancer Therapy. *J. Controlled Release* **2020**, *320*, 392−403.

(16) Wang, C. F.; Makila, E. M.; Kaasalainen, M. H.; Liu, D.; Sarparanta, M. P.; Airaksinen, A. J.; Salonen, J. J.; Hirvonen, J. T.; Santos, H. A. Copper-Free Azide-Alkyne Cycloaddition of Targeting Peptides to Porous Silicon Nanoparticles for Intracellular Drug Uptake. *Biomaterials* **2014**, *35* (4), 1257−1266.

(17) Pascalau, V.; Tertis, M.; Pall, E.; Suciu, M.; Marinca, T.; Pustan, M.; Merie, V.; Rus, I.; Moldovan, C.; Topala, T. Bovine Serum Albumin Gel/Polyelectrolyte Complex of Hyaluronic Acid and Chitosan Based Microcarriers for Sorafenib Targeted Delivery. *Applied Polym. Sc.* **2020**, *137* (34), 1−16.

(18) Chen, J.; Sheu, A. Y.; Li, W.; Zhang, Z.; Kim, D. H.; Lewandowski, R. J.; Omary, R. A.; Shea, L. D.; Larson, A. C. Poly(Lactide-Co-Glycolide) Microspheres for MRI-Monitored Transcatheter Delivery of Sorafenib to Liver Tumors. *J. Controlled Release* **2014**, *184*, 10−17.

(19) Thapa, R. K.; Choi, J. Y.; Poudel, B. K.; Hiep, T. T.; Pathak, S.; Gupta, B.; Choi, H. G.; Yong, C. S.; Kim, J. O. Multilayer-Coated Liquid Crystalline Nanoparticles for Effective Sorafenib Delivery to Hepatocellular Carcinoma. *ACS Appl. Mater. Interfaces* **2015**, *7* (36), 20360−20368.

(20) Zhang, H.; Zhang, F. M.; Yan, S. J. Preparation, in Vitro Release, and Pharmacokinetics in Rabbits of Lyophilized Injection of Sorafenib Solid Lipid Nanoparticles. *Int. J. Nanomed.* **2012**, *7*, 2901−2910.

(21) Zhang, Z.; Niu, B.; Chen, J.; He, X.; Bao, X.; Zhu, J.; Yu, H.; Li, Y. The Use of Lipid-Coated Nanodiamond to Improve Bioavailability and Efficacy of Sorafenib in Resisting Metastasis of Gastric Cancer. *Biomaterials* **2014**, *35* (15), 4565−4572.

(22) Grillone, A.; Riva, E. R.; Mondini, A.; Forte, C.; Calucci, L.; Innocenti, C.; de Julian Fernandez, C.; Cappello, V.; Gemmi, M.; Moscato, S. Active Targeting of Sorafenib: Preparation, Characterization, and In Vitro Testing of Drug-Loaded Magnetic Solid Lipid Nanoparticles. *Adv. Healthcare Mater.* **2015**, *4* (11), 1681−1690.

(23) Benizri, S.; Ferey, L.; Alies, B.; Mebarek, N.; Vacher, G.; Appavoo, A.; Staedel, C.; Gaudin, K.; Barthélémy, P. Nucleoside-Lipid-Based Nanocarriers for Sorafenib Delivery. *Nanoscale Res. Lett.* **2018**, *13*, 17.

(24) Bondi, M. L.; Scala, A.; Sortino, G.; Amore, E.; Botto, C.; Azzolina, A.; Balasus, D.; Cervello, M.; Mazzaglia, A. Nanoassemblies Based on Supramolecular Complexes of Non-Ionic Amphiphilic Cyclodextrin and Sorafenib as Effective Weapons to Kill Hunman HCC Cells. *Biomacromolecules* **2015**, *16*, 3784−3791.

(25) Kamaly, N.; Xiao, Z.; Valencia, P. M.; Radovic-Moreno, A. F.; Farokhzad, O. C. Targeted Polymeric Therapeutic Nanoparticles: Design, Development and Clinical Translation. *Chem. Soc. Rev.* **2012**, *41*, 2971−3010.

(26) Li, Y.; Huang, G.; Diakur, J.; Wiebe, L. I. Targeted Delivery of Macromolecular Drugs: Asialoglycoprotein Receptor (ASGPR) Expression by Selected Hepatoma Cell Lines Used in Antiviral Drug Development. *Curr. Drug Delivery* **2008**, *5*, 299−302.

(27) D'Souza, A. A.; Devarajan, P. V. Asialoglycoprotein Receptor Mediated Hepatocyte Targeting-Strategies and Applications. *J. Controlled Release* **2015**, *203*, 126−139.

(28) Spiess, M. The Asialoglycoprotein Receptor: A Model for Endocytic Transport Receptors. *Biochemistry* **1990**, *29*, 10009−10018.

(29) Schwartz, A.; Fridovich, S.; Lodish, H. Kinetics of Internalization and Recycling of the Asialoglycoprotein Receptor in a Hepatoma Cell Line. *J. Biol. Chem.* **1982**, *257*, 4230−4237.

(30) Staines, K.; Hunt, L. G.; Young, J. R.; Butter, C. Evolution of an Expanded Mannose Receptor Gene Family. *PLoS One* **2014**, *9* (11), No. e110330.

(31) Lee, S. H.; Charmoy, M.; Romano, A.; Paun, A.; Chaves, M. M.; Cope, F. O.; Ralph, D. A.; Sacks, D. L. Mannose Receptor High, M2 Dermal Macrophages Mediate Nonhealing Leishmania Major Infection in a Th1 Immune Environment. *J. Exp. Med.* **2018**, *215*, 357−375.

(32) Fan, W.; Yang, X.; Huang, F.; Tong, X.; Zhu, L.; Wang, S. Identification of CD206 as a Potential Biomarker of Cancer Stem-like Cells and Therapeutic Agent in Liver Cancer. *Oncol. Lett.* **2019**, *18*, 3218−3226.

(33) Muller, C.; Despras, G.; Lindhorst, T. K. Organizing Multivalency in Carbohydrate Recognition. *Chem. Soc. Rev.* **2016**, *45*, 3275−3302.

(34) Lundquist, J. J.; Toone, E. J. The Cluster Glycoside Effect. *Chem. Rev.* **2002**, *102* (2), 555−578.

https://doi.org/10.1021/acsabm.0c01679
ACS Appl. Bio Mater. XXXX, XXX, XXX−XXX

(35) Barnard, A.; Smith, D. K. Self-Assembled Multivalency: Dynamic Ligand Arrays for High Affinity Binding. *Angew. Chem., Int. Ed.* **2012**, *51*, 6572−6581.
(36) Cabral, H.; Miyata, K.; Osada, K.; Kataoka, K. Block Copolymer Micelles in Nanomedicine Applications. *Chem. Rev.* **2018**, *118*, 6844−6892.
(37) Assali, M.; Cid, J.-J.; Fernández, I.; Khiar, N. Supramolecular Diversity through Click Chemistry: Switching from Nanomicelles to 1D Nanotubes and Tridimensional Hydrogels. *Chem. Mater.* **2013**, *25*, 4250−4261.
(38) Romero-Ben, E.; Mena Barragán, T.; García De Dionisio, E.; Sánchez-Fernández, E. M.; Garcia Fernández, J. M.; Guillén-Mancina, E.; López-Lázaro, M.; Khiar, N. Mannose-Coated Polydiacetylene (PDA)-Based Nanomicelles: Synthesis, Interaction with Concanavalin A and Application in the Water Solubilization and Delivery of Hydrophobic Molecules. *J. Mater. Chem. B* **2019**, *7* (39), 5930−5946.
(39) Qian, X.; Städler, B. Recent Developments in Polydiacetylene-Based Sensors. *Chem. Mater.* **2019**, *31*, 1196−1222.
(40) Bobin-Dubigeon, C.; Heurgue-Berlot, A.; Bouche, O.; Amiand, M. B.; Le Guellec, C.; Bard, J. M. A New Rapid and Sensitive LC-MS Assay for the Determination of Sorafenib in Plasma: Application to a Patient Undergoing Hemodialysis. *Ther. Drug Monit.* **2011**, *33* (6), 705−710.
(41) Pichard, L.; Raulet, E.; Fabre, G.; Ferrini, J.; Ourlin, J.; Maurel, P. Human Hepatocyte Culture. *Methods Mol. Biol.* **2005**, *320*, 283−293.
(42) Pernía Leal, M.; Assali, M.; Cid, J. J.; Valdivia, V.; Franco, J. M.; Fernández, I.; Pozo, D.; Khiar, N. Synthesis of 1D-Glyconanomaterials by a Hybrid Noncovalent-Covalent Functionalization of Single Wall Carbon Nanotubes: A Study of Their Selective Interactions with Lectins and with Live Cells. *Nanoscale* **2015**, *7* (45), 19259.
(43) Manimala, J. C.; Roach, T. A.; Li, Z.; Gildersleeve, J. C. High-Throughput Carbohydrate Microarray Analysis of 24 Lectins. *Angew. Chem., Int. Ed.* **2006**, *45*, 3607−3610.
(44) Basu Ray, G.; Chakraborty, I.; Moulik, S. P. Pyrene Absorption Can Be a Convenient Method for Probing Critical Micellar Concentration (Cmc) and Indexing Micellar Polarity. *J. Colloid Interface Sci.* **2006**, *294*, 248−254.
(45) Rodriguez-Hernandez, M. A.; Gonzalez, R.; de la Rosa, A. J.; Gallego, P.; Ordonez, R.; Navarro-Villaran, E.; Contreras, L.; Rodríguez-Arribas, M.; González-Gallego, J.; Álamo-Martínez, J. M.; et al. Molecular Characterization of Autophagic and Apoptotic Signaling Induced by Sorafenib in Liver Cancer Cells. *J. Cell. Physiol.* **2019**, *234* (1), 692−708.
(46) Ziello, J. E.; Huang, Y.; Jovin, I. S. Cellular Endocytosis and Gene Delivery. *Mol. Med.* **2010**, *16* (5−6), 222−229, DOI: 10.2119/molmed.2009.00101.
(47) Yarar, D.; Waterman-Storer, C. M.; Schmid, S. L. Dynamic Actin Cytoskeleton Functions at Multiple Stages of Clathrin-Mediated Endocytosis. *Mol. Biol. Cell* **2005**, *16* (2), 964−975, DOI: 10.1091/mbc.e04-09-0774.
(48) Damke, H. Dynamin and Receptor-Mediated Endocytosis. *FEBS Lett.* **1996**, *389* (1), 48−51.
(49) Ahlberg, J.; Berkenstam, A.; Henell, F.; Glaumann, H. Degradation of Short and Long Lived Protein in Isolated Rat Liver Lysosomes. Effects of PH, Temperature, and Proteolytic Inhibitors. *J. Biol. Chem.* **1985**, *260* (9), 5847−5854.
(50) Klionsky, D. J.; Abdelmohsen, K.; Abe, A.; Abedin, M. J.; Abeliovich, H.; Acevedo Arozena, A.; Adachi, H.; Adams, C. M.; Adams, P. D.; Adeli, K.; et al. Guidelines for the Use and Interpretation of Assays for Monitoring Autophagy (3rd Edition). *Autophagy* **2016**, *12* (1), 1−222.
(51) Guo, W.; Deng, L.; Yu, J.; Chen, Z.; Woo, Y.; Liu, H.; Li, T.; Lin, T.; Chen, H.; Zhao, M. Sericin Nanomicelles with Enhanced Cellular Uptake and PH-Triggered Release of Doxorubicin Reverse Cancer Drug Resistance. *Drug Delivery* **2018**, *25* (1), 1103−1116.

https://doi.org/10.1021/acsabm.0c01679
ACS Appl. Bio Mater. XXXX, XXX, XXX−XXX